

**DETERMINATION OF ROLLING TYRE
CHARACTERISTICS AND
STRUCTURE BORNE VEHICLE INTERIOR NOISE**

A THESIS

submitted by

P. SAKTHIVEL

for the award of the degree

of

DOCTOR OF PHILOSOPHY



**DEPARTMENT OF ENGINEERING DESIGN
INDIAN INSTITUTE OF TECHNOLOGY MADRAS
CHENNAI-600 036**

FEBRUARY 2016

THESIS CERTIFICATE

This is to certify that the thesis entitled "**DETERMINATION OF ROLLING TYRE CHARACTERISTICS AND STRUCTURE BORNE VEHICLE INTERIOR NOISE**" submitted by **P. SAKTHIVEL** to the Indian Institute of Technology Madras, Chennai for the award of the degree of **Doctor of Philosophy** is bonafide record of research work carried out by him under my supervision. The contents of this thesis, in full or in parts, have not been submitted and will not be submitted to any other Institute or University for the award of any degree or diploma.

Research Guide

Dr. R. Krishna Kumar
Professor
Department of Engineering Design
Indian Institute of Technology Madras
Chennai - 600 036
India

Chennai 600 036

Date: February 2016

Dedicated

to

my parents, wife, daughter and my beloved students

ACKNOWLEDGEMENTS

First and foremost I would like to express my sincere thanks and deep sense of gratitude to my research guide Prof. R. Krishna Kumar for his invaluable guidance, continuous encouragement and keen involvement in my research work. I have understood the meaning of dedication looking at my guide. Today, I feel enriched with the skill set and confident to march forward to work further in the field of Automotive NVH is because of my guide. He has always been a mentor and the source of inspiration to me. I thank God for giving me this opportunity to work as a student with my professor from whom I have learnt in all these years. I wish to develop my personality like my professor.

I express my profound gratitude to Dr. K. V. Narasimha Rao, Deputy General Manager, RPSCOE for Tyre & Vehicle Mechanics, JK Tyre and Industries Ltd., for his continuous observation and encouragement shown to my research work. His friendly approach and the concern gave me immense energy level to work longer hours every day in order to pursue my research without much of the difficulties. He never said 'no' for any resource utilization of the research centre. I feel he has always been my well wisher.

I am very much thankful to J. K. Tyre & Industries Ltd., for providing a complete research facility of RPSCOE which was established with IIT Madras under the esteemed leadership of Prof. R. Krishna Kumar. The computational and experimental facilities provided throughout the period of research work was important in the completion of this thesis.

I am indebted to Prof. Nilesh Jayantilal Vasa, Head, Department of Engineering Design and the members of my doctoral committee, Prof. A. Meher Prasad, Head, Department of Civil Engineering, Prof. C. Sujatha, Department of Mechanical Engineering, Prof. Shankar Ram C S and Prof. Sankara J Subramanian, Department of Engineering Design for their positive insightful comments and motivating suggestions during various stages of this research work.

I thank all my fellow lab mates for their cordial relationship. Special thanks to Prasanth, Rajesh, Dr. Prasenjit Ghosh, Dr. Jaiganesh, Vijay Alagappan, Saravanan, Apoorva, Jagadish, Sabarinath, Hem, Vinid, Yagnanarayanan and Kashif. Sincere thanks to Govindabalan and Anand Suresh Kumar for participating in stimulating discussions during laboratory experiments and thesis writing. My very special thanks to V. Balasubramaniam (Balu sir), who extended not only a fatherly attachment to me but also helped me in conducting road

tests, which played a vital role in the construction of this thesis. I also extend by thanks to Dr. K. Paranjothi, Department of Engineering Design, Dr. G. Balaganesan, Mr. M. Gajendran, and Mr. D. Muthurajan, Central Workshop, IIT Madras for their support during my experimental work.

I am grateful to Prof. Bhaskar Ramamurthi, Director, IIT Madras and Prof. A. K. Mishra, Dean Academic Research, IIT Madras for the wonderful opportunity given to me to pursue my research from one of the prestigious institutes of our country.

I would like to express my sincere gratitude and hearty thanks to the core group members Dr. G. Viswanathan, Chancellor, Dr. Anand A Samuel, Vice Chancellor, Dr. S. Narayanan, Pro-Vice Chancellor and Dr. V. Raju, Pro-Vice Chancellor of VIT University, Vellore for sponsoring me to pursue my PhD degree. Also convey my sincere thanks to the Vice Presidents of VIT University and a special thanks to Prof. A. Senthil Kumar, Director, Centre for Engineering Design, Automotive and Manufacturing Engineering, VIT University for his concern shown during my research work.

The unconditional love and the support rendered by my dear wife Vijayalakshmi and my sweet heart daughter Valarmathi made me to focus completely on my research work from the beginning. The quiet understanding and support of my parents, my in-laws, my sister, my brother and their family members offered me continuous encouragement. I just cannot say only the word 'thanks' to all of them. I thank and pray God for having them with me.

Finally, I thank one and all who have either directly or indirectly helped me during the period of my research work at IIT Madras.

P. Sakthivel

ABSTRACT

KEYWORDS: *Rolling tyre modal analysis, Tyre dynamic behavior, Explicit Finite Element Analysis, Operational Modal Analysis, Experimental Modal Analysis, Experimental Transfer Path Analysis, Structure borne vehicle interior noise, Local structural Frequency Response Functions (FRFs), Noise transfer functions (NTFs), Operational accelerations, Tyre/Road interaction, Road input excitation, FRF based sub-structuring*

The term automotive NVH refers to Noise, Vibration and Harshness characteristics of a vehicle which determine its comfort standard. Competition has compelled passenger car manufacturers to attract their customers by providing vehicles with lower vibration and quieter cabin without compromising on the performance and safety aspects of the vehicle. This is achieved by conducting a subjective and objective evaluation of the vehicle's NVH characteristics. Jury tests are conducted to predict NVH characteristics from the driver's subjective perception whereas analytical and experimental techniques developed by researchers are used to carry out the objective analysis for more meaningful quantitative results.

The pneumatic tyres are one of the important sources of noise and vibration in a vehicle. Modern vehicles have implemented good preventive and control measures for power unit and aerodynamic NVH. Hence, the tyre/road interaction becomes a dominant source at moderate speeds and contributes to the interior and exterior noise in a vehicle. The interior noise consists of two components; a low frequency structure borne component (below 500 Hz) and a mid and high frequency air borne component (above 500 Hz), which are named after the mediums through which the energy transfer takes place i.e. from the source to the target response location. In order to address various noise generation mechanisms and noise propagation phenomena of a tyre, it is necessary to study the tyre dynamic behavior in terms of their modal parameters. These mechanisms are mainly influenced by the resonance characteristics of the rolling tyre. The low frequency belt vibrations influence the tyre and wheel dynamics and form the basis for energy transfer through its structural paths resulting in structure borne vehicle interior noise. The noise radiation due to the mid and high frequency

vibration of the tread and sidewall acoustically excite the vehicle body resulting in air borne interior noise.

Rolling tyre modal parameters are complex in nature and challenging to predict. The main objective of this thesis is to understand the rolling tyre modal behavior and its role in contributing to the structure borne vehicle interior noise. This thesis enumerates a novel method of finding the modal parameters of a rolling tyre using Explicit Finite Element Analysis (EFEA) and Operational Modal Analysis (OMA). ABAQUS/Explicit, a commercial Finite Element (FE) code has been used to simulate the phenomena of a tyre rolling over a straight and inclined semi-circular cleat. The acceleration responses obtained from these simulations are used as input for OMA. LMS test lab has been used for carrying out the OMA. The modal results obtained from OMA are compared with the FE modal results of a stationary unloaded, stationary loaded and Steady State Transport rolling tyre. Further using this established FEA-OMA procedure, the influence of design parameters and operational conditions of rolling tyre such as inflation pressure and static preload are studied. The influence of tyre dimensions and boundary conditions on modal parameters are further investigated through Experimental Modal Analysis (EMA).

Experimental Transfer Path Analysis(classical TPA) is successfully employed to synthesize the structure borne vehicle interior noise due to the tyre/road interaction. Numerous laboratory experiments are conducted on a passenger car with and without tyre/wheel assembly to determine structural Frequency Response Functions (FRFs) and Noise Transfer Functions (NTFs). The operational measurements are obtained from road test for varying vehicle speeds with engine on and engine off conditions. The operational loads at rim spindle interface as well as at tyre contact patch are estimated from these operational acceleration responses and the local structural FRFs using matrix inverse method. These operational loads are further combined with corresponding NTFs to synthesize the structure borne vehicle interior noise.

Component based TPA techniques are used to integrate the vehicle and tyre/wheel characteristics to synthesize the structure borne vehicle interior noise. Additional experiments are conducted on the tyre in 'in-situ' and 'free' condition to determine its characteristics. Road loads (estimated using matrix inverse method) and structural FRFs (of

tyre/wheel assembly) are combined to get operational accelerations at rim spindle interface virtually, without an actual road test. These are further used to estimate the equivalent operational loads at rim spindle interface. These equivalent operational loads are combined with corresponding NTFs to determine the structure borne noise components inside the vehicle. This component based TPA procedure is used to study the influence of a new set of tyres over the synthesized interior noise.

Two procedures have been established and presented in this thesis. First one is FEA-OMA technique used for the determining the modal parameters of a rolling tyre which essentially depicts the belt vibration that forms the basis for an important mechanism of noise transfer to the vehicle. A second procedure is established based on component based TPA techniques with a relatively easier method compared to the classical matrix inverse method in order to predict the structure borne vehicle interior noise due to belt vibration during tyre/road interaction. A significant reduction in the product development cycle time and cost can be achieved by applying these procedures.

TABLE OF CONTENTS

	Page No.
ACKNOWLEDGEMENTS.....	i
ABSTRACT.....	iii
LIST OF TABLES.....	xi
LIST OF FIGURES.....	xii
ABBREVIATIONS.....	xxi
NOTATION.....	xxii
CHAPTER 1 INTRODUCTION	
1.1 Introduction.....	1
1.2 Literature background.....	2
1.3 Research objective and contributions.....	3
1.4 Organization of the thesis.....	4
CHAPTER 2 TYRE MODAL CHARACTERISTICS AND ROAD NOISE	
2.1 Introduction.....	6
2.2 Radial Tyre construction and its requirements.....	6

Table of Contents (continued)		Page No.
2.3	Tyre Materials.....	8
2.4	Noise generation mechanisms.....	8
2.4.1	Vibrational mechanisms.....	9
2.4.2	Aerodynamical mechanisms.....	12
2.4.3	Amplification and reduction mechanisms.....	14
2.5	Tyre modal characteristics.....	16
2.5.1	Experimental setup and procedure.....	18
2.5.2	Estimation of modal parameters.....	20
2.5.3	Parametric study.....	23
2.6	Structure borne vehicle interior noise.....	28
2.6.1	Introduction to road noise models.....	29
2.6.2	Introduction to road noise tests.....	29
2.6.3	Techniques followed by researchers.....	30
2.7	Summary.....	31

CHAPTER 3 DETERMINATION OF ROLLING TYRE MODAL PARAMETERS

3.1	Introduction.....	32
3.2	Procedure for extraction of mode shape.....	34
3.2.1	Explicit Finite Element Analysis and Operational Modal Analysis....	34
3.2.2	Steady state transport analysis of rolling Tyre.....	43

Table of Contents (continued) Page No.

3.3	Validation of Results.....	44
3.3.1	Description of Structural tyre model of Kindt et al. (2009).....	44
3.3.2	Comparison of rolling tyre modal results.....	46
3.4	Results and Discussion.....	47
3.4.1	Comparison of mode shapes obtained by different methods.....	54
3.5	Summary.....	58

**CHAPTER 4 EXPERIMENTAL TRANSFER PATH ANALYSIS FOR
STRUCTURE BORNE VEHICLE INTERIOR NOISE**

4.1	Introduction.....	59
4.2	Mechanism of structure borne interior noise.....	59
4.3	Experimental set up and measurements.....	60
4.3.1	Laboratory tests.....	60
4.3.2	Road tests.....	68
4.4	Experimental Transfer path analysis.....	70
4.5	Results and Discussion.....	74
4.6	Summary.....	80

**CHAPTER 5 IMPLEMENTATION OF TRANSFER PATH ANALYSIS
TECHNIQUES**

5.1	Introduction.....	81
5.2	TPA Techniques.....	82
5.3	Road loads.....	84
5.3.1	Road load estimation for TPA	85
5.4	Implementation of various TPA methods.....	87
5.4.1	Matrix inverse method.....	87
5.4.2	In-situ method.....	88
5.4.3	Free velocity method.....	91
5.5	Results and discussions.....	94
5.6	Summary.....	116

**CHAPTER 6 EXPERIMENTAL REPEATABILITY FOR MULTI
REFERENCE TRANSFER PATH ANALYSIS**

6.1	Introduction.....	117
6.2	Principal component analysis for TPA.....	117
6.3	Repeatability of laboratory experiments.....	119
6.4	Repeatability of road tests.....	121
6.5	Summary.....	126

CHAPTER 7 CONCLUSION AND FUTURE WORK

7.1	Contributions.....	127
7.2	Conclusions.....	128
7.3	Scope of future work.....	130
APPENDIX I.....		131
APPENDIX II.....		150
REFERENCES.....		153
LIST OF PUBLICATIONS.....		158

LIST OF TABLES

Table	Title	Page No.
2.1	Generation mechanism of tyre/road noise and related phenomena (Sandberg and Ejsmont,2002).....	9
2.2	Typical frequencies for Tread and Texture impact mechanisms (Sandberg and Ejsmont,2002).....	11
2.3	Tyre modal frequencies for different size tyres.....	24
2.4	Tyre modal frequencies for different boundary conditions.....	26
3.1	Hyperelastic Material Definition in SI units.....	35
3.2	Correlation study for selection of reference point.....	41
3.3	Comparison of Experimental and FEA-OMA Rolling Tyre Results	46
3.4	Frequency of tyre rolling speed as function of speed.....	53
3.5	Operational modal frequencies for speed of 28.3kmph as function of Inflation Pressure.....	53
3.6	Comparison of circumferential and cross sectional modes and the effect of loading and rolling over natural frequencies of a tyre.....	56
4.1	Laboratory Experiment for Local Structural FRFs and NTFs.....	69
4.2	Operational Measurement.....	70
5.1	Summary of TPA framework of various methods.....	83
5.2	Vector contribution analysis of principal component no. 1(PRCM:0001:S) at 121 Hz.....	110
5.3	Vector contribution analysis of principal component no. 1(PRCM:0001:S) at 261 Hz.....	111

LIST OF FIGURES

Figure	Title	Page No.
1.1	Contribution of structure borne and air borne component of vehicle interior noise (Hartleip and Roggenkamp, 2005).....	1
2.1	Components of radial tyre (Gent and Walter, 2005).....	7
2.2	Vibrational Mechanisms (Peter Kindt,2009).....	10
2.3	Aerodynamical and amplification mechanisms (Peter Kindt,2009)....	13
2.4	Typical tyre dispersion curves (Kim and Bolton, 2004).....	15
2.5	First and second acoustic cavity resonance modes (Peter Kindt, 2009)	16
2.6	Labelling of tyre structural modes (n,a) (Peter Kindt, 2009).....	18
2.7	Circumferential and cross sectional modes of an unloaded free boundary condition tyre.....	18
2.8	Experimental Modal Analysis test setup.....	19
2.9	Stabilization Curve for mode selection.....	20
2.10	Circumferential modes of tyre for free spindle condition.....	21
2.11	Cross sectional modes of tyre for free spindle condition.....	22
2.12	Rigid and acoustical mode of tyre for free spindle condition.....	22
2.13	Spindle fixed condition of unloaded tyre for experimental modal analysis.....	23
2.14	Variation of circumferential modes as function of tyre size.....	25
2.15	Variation of cross sectional modes as function of tyre size.....	25
2.16	Variation of circumferential modes for different spindle boundary conditions.....	27
2.17	Variation of cross sectional modes for different spindle boundary conditions.....	27

List of Figures (continued)	Page No.
2.18 Vehicle interior noise components (Riegel and Wiedemann,2008).....	28
3.1a Section details of 205/55R16 radial passenger car tyre.....	34
3.1b Tyre FE model.....	34
3.2a Contact pressure of stationary loaded tyre.....	36
3.2b Contact pressure of rolling tyre just before straight cleat.....	37
3.2c Contact pressure during straight cleat impact.....	37
3.2d Contact pressure of rolling tyre just before 45 ° inclined cleat.....	37
3.2e Contact pressure during 45° inclined cleat impact.....	37
3.3a Tyre rolling over straight cleat road.....	37
3.3b Tyre rolling over 45 ⁰ inclined cleat road.....	38
3.4 Vertical Spindle Force due to straight cleat impact excitation.....	39
3.5 Acceleration measurement nodes of finite element tyre model.....	39
3.6 Modal model geometry for operational modal analysis.....	40
3.7 Crosspower sum.....	41
3.8a Stabilization diagram and pole selection by AMPS.....	42
3.8b Comparison of operational and synthesized crosspower.....	42
3.9 Fully assembled tyre-wheel model (Cavity mesh is not shown) P Kindt, 2009).....	45
3.10a Straight cleat impact excitation.....	47
3.10b PSD of spindle force due to straight cleat impact.....	48
3.11a 45 ⁰ Inclined cleat impact excitation.....	48
3.11b PSD of spindle force due to 45° inclined cleat impact.....	49
3.12 Operational modal parameters obtained from straight cleat impact test.....	50
3.13 Operational modal parameters obtained from 45 ⁰ inclined cleat impact test..	51

List of Figures (continued)	Page No.
3.14	Variation of rolling frequency with vehicle speed..... 52
3.15	Variation of rolling frequency with Inflation Pressure for 28.3 kmph..... 52
3.16	Cross sectional bending modes due to 45 ⁰ inclined cleat impact test..... 53
3.17	Mode shape comparison among various tyre conditions..... 55
3.18a	Comparison of dispersion curves of circumferential modes..... 57
3.18b	Comparison of dispersion curves of cross sectional modes..... 57
4.1	Laboratory experimental set up for TPA..... 61
4.2	Position of accelerators..... 61
4.3	Position of interior microphones..... 62
4.4	Drive point coherences and local structural FRFs for vehicle..... 63
4.5	Variation of NTFs between all paths and driver's right ear position and the corresponding coherence functions as function of frequency... 64
4.6a	Variation of local structural FRFs between all path indicators and Riminterface_FL:X and the corresponding coherence functions as function of frequency..... 65
4.6b	Variation of local structural FRFs between all path indicators and Riminterface_FR:X and the corresponding coherence functions as function of frequency..... 66
4.6c	Variation of local structural FRFs between all path indicators and Riminterface_RR:X and the corresponding coherence functions as function of frequency..... 67
4.6d	Variation of local structural FRFs between all path indicators and Riminterface_RL:X and the corresponding coherence functions as function of frequency..... 68
4.7	Formulation of multi reference experimental Transfer Path Analysis.. 71
4.8	Principal components of virtual reference spectra of path indicator Spindle FL:X..... 72
4.9	Operational path loads at wheel rim spindle interface..... 73

List of Figures (continued)	Page No.
4.10 Individual path contribution to the total structure borne interior noise at driver's right ear position.....	74
4.11 Comparison of TPA results with measurements of driver's ear target..	75
4.12 Comparison of engine on and engine off results of driver's ear target..	76
4.13 Path contribution results from matrix inverse method for sub system V: vertical bars at the top represents the contribution from principal components and horizontal acoustic color map represents the contribution from physical references.....	77
4.14 Contribution of principal components to the chosen critical path 'Riminterface_FL: Z' from matrix inverse method for sub system V: vertical bars at the top represents the contribution from physical references and horizontal acoustic color map represents the contribution of individual principal components.....	78
4.15a Vector contribution results from matrix inverse method for sub system V at 121 Hz frequency.....	78
4.15b Vector contribution results from matrix inverse method for sub system V at 261 Hz frequency.....	79
5.1 Nomenclature of vehicle measurement points.....	84
5.2 Laboratory experimental set up for full vehicle system (TV).....	85
5.3 Amplification and isolation of road excitation at the front left contact patch in the longitudinal direction.....	87
5.4 Experimental set up of front tyre wheel assembly for tyre transfer characteristics by in-situ method.....	89
5.5a Front right wheel structural FRFs and Coherences in the longitudinal direction (in-situ method).....	90
5.5b Front right wheel structural FRFs and Coherences in the lateral direction (in-situ method).....	90
5.5c Front right wheel structural FRFs and Coherences in the vertical direction (in-situ method).....	91
5.6 Position of accelerometers for free velocity method.....	92

List of Figures (continued)	Page No.
5.7a Front right wheel structural FRFs and Coherences in the longitudinal direction (free velocity method).....	93
5.7b Front right wheel structural FRFs and Coherences in the lateral direction (free velocity method).....	93
5.7c Front right wheel structural FRFs and Coherences in the vertical direction (free velocity method).....	94
5.8a Comparison of operational loads in the longitudinal direction at rim spindle interface for all wheel from various methods.....	95
5.8b Comparison of operational loads in the lateral direction at rim spindle interface for all wheel from various methods.....	96
5.8c Comparison of operational loads in the vertical direction at rim spindle interface for all wheel from various methods.....	97
5.9a Variation of condition number of structural FRFs in different TPA methods.....	98
5.9b Truncation of condition number and the corresponding variation of rank of structural FRF matrix as function of frequency in 'in-situ' method.....	98
5.9c Truncation of condition number and the corresponding variation of rank of structural FRF matrix as function of frequency in 'in-situ' method.....	99
5.10a Individual path contribution analysis of Riminterface_FL:+Z to driver ear's target by matrix inverse method (subsystem V).....	100
5.10b Individual path contribution analysis of Riminterface_FL:+Z to driver ear's target by in-situ method.....	101
5.10c Individual path contribution analysis of Riminterface_FL:+Z to driver ear's target by free velocity method.....	102
5.11a Path contribution results from matrix inverse method for assembly TV: vertical bars represents the contribution from principal components and horizontal acoustic color map represents the contribution from physical references.....	104

List of Figures (continued)**Page No.**

5.11b	Contribution of principal components to the chosen critical path 'Tyre_FL:Z' from matrix inverse method for assembly TV: vertical bars at the top represents the contribution from physical references and horizontal acoustic color map represents the contribution of individual principal components.....	104
5.11c	Variation of NTFs the between all tyre contact patch centre and driver's ear position and the corresponding coherence functions as function of frequency.....	105
5.11d	Path contribution results from matrix inverse method for vehicle subsystem V: vertical bars represents the contribution from principal components and horizontal acoustic color map represents the contribution from physical references.....	106
5.12a	Path contribution results from in-situ method: vertical bars represents the contribution from principal components and horizontal acoustic color map represents the contribution from physical references.....	106
5.12b	Contribution of principal components to the chosen critical path 'Riminterface_FL:Z' from in-situ method: vertical bars at the top represents the contribution from physical references and horizontal acoustic color map represents the contribution of individual principal components.....	107
5.13a	Path contribution results from free velocity method: vertical bars represents the contribution from principal components and horizontal acoustic color map represents the contribution from physical references.....	107
5.13b	Contribution of principal components to the chosen critical path 'Riminterface_FL:Z' from free velocity method: vertical bars at the top represents the contribution from physical references and horizontal acoustic color map represents the contribution of individual principal components.....	108
5.14	Comparison of total sound pressure levels obtained from various methods.....	109
5.15a	Vector contribution results at 121 Hz from matrix inverse for assembly TV.....	112
5.15b	Vector contribution results at 121 Hz from in-situ method.....	112
5.15c	Vector contribution results at 121 Hz from free velocity method.....	113

List of Figures (continued)	Page No.	
5.15d	Vector contribution results at 261Hz from matrix inverse for assembly TV.....	113
5.15e	Vector contribution results at 261 Hz from in-situ method.....	114
5.15f	Vector contribution results at 261 Hz from free velocity method.....	114
5.16	Comparison of sound pressure level obtained from different methods with measurements of driver's ear target.....	115
6.1	Details of experiments and methodology for various TPA methods.....	118
6.2	Measurement setup used for each run.....	119
6.3	Repeatability of spectral testing.....	121
6.4	Repeatability of interior noise measurements: Driver ear's sound pressure level.....	122
6.5	Repeatability of interior noise measurements: Co-passenger ear's sound pressure level.....	122
6.6	Repeatability of interior noise measurements: Rear right microphone's sound pressure.....	123
6.7	Repeatability of interior noise measurements: Rear left microphone's sound pressure.....	123
6.8	Microphone positions for near field exterior noise measurement.....	124
6.9	Test vehicle with operational measurement sensors.....	124
6.10	Repeatability of operational acceleration measurement.....	126
A1.1	Variation of NTFs between all paths and co-passenger's left ear position and the corresponding coherence functions as function of frequency.....	131
A1.2	Variation of NTFs between all paths and rear left passenger's left ear position and the corresponding coherence functions as function of frequency.....	132
A1.3	Variation of NTFs between all paths and rear right passenger's right ear position and the corresponding coherence functions as function of frequency.....	133

List of Figures (continued)	Page No.
A1.4 Variation of local structural FRFs between all path indicators and Riminterface_FL:Y and the corresponding coherence functions as function of frequency.....	134
A1.5 Variation of local structural FRFs between all path indicators and Riminterface_FR:Y and the corresponding coherence functions as function of frequency.....	135
A1.6 Variation of local structural FRFs between all path indicators and Riminterface_RR:Y and the corresponding coherence functions as function of frequency.....	136
A1.7 Variation of local structural FRFs between all path indicators and Riminterface_RL:Y and the corresponding coherence functions as function of frequency.....	137
A1.8 Variation of local structural FRFs between all path indicators and Riminterface_FL:Z and the corresponding coherence functions as function of frequency.....	138
A1.9 Variation of local structural FRFs between all path indicators and Riminterface_FR:Z and the corresponding coherence functions as function of frequency.....	139
A1.10 Variation of local structural FRFs between all path indicators and Riminterface_RR: Z and the corresponding coherence functions as function of frequency.....	140
A1.11 Variation of local structural FRFs between all path indicators and Riminterface_RL:Z and the corresponding coherence functions as function of frequency.....	141
A1.12 Individual path contribution to the total structure borne interior noise at copassenger's right ear position.....	142
A1.13 Individual path contribution to the total structure borne interior noise at rear right passenger's right ear position.....	142
A1.14 Individual path contribution to the total structure borne interior noise at rear left passenger's left ear position.....	143
A1.15 Comparison of TPA results with measurements of co-passenger's left ear target.....	144
A1.16 Comparison of TPA results with measurements of rear right passenger's right ear target.....	145

List of Figures (continued)

Page No.

A1.17	Comparison of TPA results with measurements of rear left passenger's left ear target.....	146
A1.18	Comparison of 'engine on' and 'engine off' results of co-passenger's left ear target for measurements and TPA separately.....	147
A1.19	Comparison of 'engine on' and 'engine off' results of rear right passenger's right ear target for measurements and TPA separately.....	148
A1.20	Comparison of 'engine on' and 'engine off' results of rear left passenger's left ear target for measurements and TPA separately.....	149

ABBREVIATIONS

BEM	Boundary Element Method
DOF	Degree of freedom
EFEA	Explicit Finite Element Analysis
EMA	Experimental Modal Analysis
FE	Finite Element
FEA	Finite Element Analysis
FRFs	Frequency Response Functions
FBS	FRF based sub-structuring technique
FEMA	Finite Element Modal Analysis
FRFs	Frequency Response Functions
IEM	Infinite Element Method
LAN	Local Area Network
ODS	Operational Deflection Shape
OMA	Operational Modal Analysis
PCA	Principal Component Analysis
PCs	Principal components
PSD	Power Spectral Density
RMS	Root mean square
SVD	Singular Value Decomposition
SPL	Sound Pressure Level
TPA	Transfer Path Analysis
NVH	Noise, Vibration and Harshness
NTFs	Noise Transfer Functions

NOTATION

f_1	Road input
f_2^{eq}	Equivalent force at the rim spindle interface
g_2^V	Operational load at rim spindle interface
$G'_{xx}(f)$	Virtual autopower matrix
$G_{yx}'(f)$	Virtual crosspowers between the principal components and indicator responses
horiz.	Horizontal
n	Circumferential mode index
m	axial bending mode index
p	Interior target sound pressure
u_2	Rim spindle interface acceleration estimated
u_3	Target response
u_2^{free}	Rim spindle acceleration estimated from free velocity method
u_4	Indicator accelerations
vert.	Vertical
ω_{n1}	Resonance frequency of backward travelling wave
ω_{n2}	Resonance frequency of forward travelling wave
X'	Principal components
Y'	Referenced virtual spectra
Y_{21}^{TV}	Structural FRFs between tyre contact patch and rim spindle interface (with tyre wheel assembly TV)

Notation (continued)

Y_{21}^T	Structural FRFs between tyre contact patch and rim spindle interface for free tyre wheel
Y_{22}^T	Structural FRFs at rim spindle interface for free tyre wheel
Y_{22}^V	Structural FRFs at rim spindle interface on vehicle side (without tyre wheel assembly)
Y_{31}^{TV}	Noise transfer functions between tyre contact patch and target interior position for vehicle (with tyre wheel assembly TV)
Y_{32}^V	Noise transfer functions between rim spindle interface and target interior position for vehicle (without tyre wheel assembly V)
Y_{41}^{TV}	Local structural FRFs between tyre contact patch and indicator points at spindle, suspension and lower arm (for vehicle with tyre wheel assembly TV)
Y_{42}^{TV}	Local structural FRFs between rim spindle interface and indicator points at spindle, suspension and lower arm (for vehicle with tyre wheel assembly TV)

CHAPTER 1

INTRODUCTION

1.1 INTRODUCTION

The pneumatic tyre, which forms one of the most important component of the vehicle is also an important sources of noise and vibration in a vehicle. Modern vehicles have implemented good preventive and control measures for power unit and aerodynamic noise, making the study of tyre noise important. Vehicle interior noise due to tyre/road interaction consists of two components, namely structure borne noise caused due to low frequency excitation (below 500 Hz) and air borne components, which are due to mid and high frequency excitation (above 500 up to 2000 Hz). Figure 1.1, due to Hartleip and Roggenkamp, 2005, shows this composition clearly. Variation of A-weighted total sound pressure level and its components are described as a function of 1/3rd octave frequency bands while driving on a rough road surface. The modes of a rolling tyre make significant contributions to tyre/road interaction noise. To address various noise generating mechanisms and noise propagation phenomena of a tyre, it is necessary to study the tyre dynamic behavior in terms of its modal parameters. The mechanism of noise generation, experimental procedure and theoretical underpinning are well documented in the tyre/road noise reference book. (Sandberg and Ejsmont, 2002).

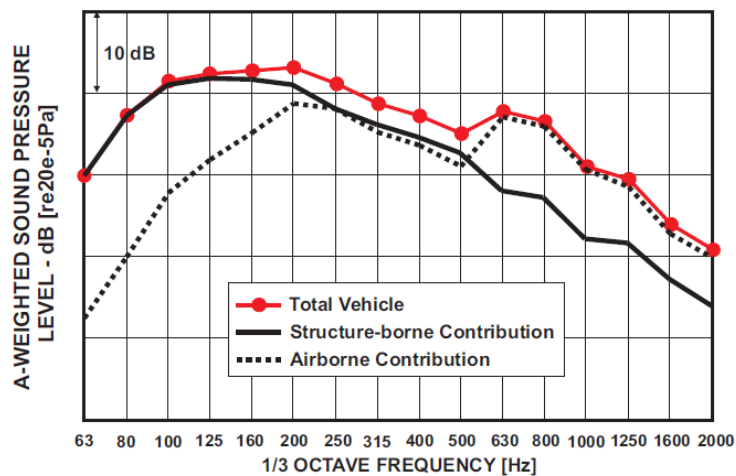


Figure 1.1 Contribution of structure borne and air borne component of vehicle interior noise (Hartleip and Roggenkamp, 2005)

1.2 LITERATURE BACKGROUND

Experimental Modal Analysis (EMA) and/or Finite Element Modal Analysis (FEMA) are the well established methods to find the tyre modal results with basic assumption of linearity and reciprocity of time invariant systems (Allemang,1999). Though these results give an overall idea about the tyre mode shapes, they do not address the effect of operational conditions on a rolling tyre. There are techniques developed by researchers to measure rotating tyre vibrations. Burroughs and Dugan (2003) used embedded accelerometers, which were placed into the tread block to measure the tyre vibration responses, as it rotates through the contact patch. This technique has not become popular due to the frequent failure of the embedded accelerometer. Contrary to the direct measurement techniques, contactless measurement technique was used by Peter Kindt, (2009) to measure the rotating tyre vibration. They used Laser Doppler Vibrometer and multi-axial wheel hub dynamometer with an inbuilt encoder in a tyre on tyre arrangement during the measurement. Rolling tyre modal data are directly used in Boundary Element Method (BEM) and Infinite Element Method (IEM) based tyre models. Nakajima et al.(1993) have used the tyre modal results to define the surface vibration boundary conditions in order to predict air borne noise fields. Constant et al. (2001) have studied the vibro-acoustic interaction between tyre and car subsystems and have identified the main suspension parts affecting the structure borne interior noise. Operational Deflection Shapes (ODS) of tyre wheel subsystem were used by Ichiro Kido and Sagiri Ueyama (2005) to quantify the force transmitted through suspension sub-system to the vehicle body to address the structure borne interior noise of the vehicle.

Transfer path analysis (TPA) is a proven technique (LMS International, 1998) that has been used by NVH engineers, on a regular basis in automotive industry; especially in troubleshooting of noise and vibration issues. Using this technique the source strength can be identified and the contribution of individual paths to the target response can be synthesized. The application of TPA to the vehicle requires both laboratory and on-road test measurements. Jin Chang et al.(2010) have considered three translational degrees of freedom at each spindle of the vehicle as noise transfer paths to identify critical paths using TPA. In their work, emphasis was given to the vehicle characteristics rather than the contact patch at tyre/road interaction. To characterize the coupled operating force at the spindle, it is

necessary to understand various noise generation mechanism of tyre/road interaction (Sandberg and Ejsmont, 2002). The low frequency excitation of the spindle is mainly attributed by the belt package vibration of the treadband. According to Pinnington and Briscoe (2002) vibration of a rolling tyre exhibits complex modal behavior in the low frequency range i.e. below 400Hz. When the natural frequencies of these complex modes coincide with the road excitation frequencies, the tyre belt resonance occurs and due to this, high amplitude low frequency excitation is felt at the spindle.

It is evident from the literature background, that the pneumatic tyres play a vital role in the NVH characteristics of a vehicle. The tyre is very reactive to the road input excitation. On one hand, it isolates the higher frequency excitation forces entering from the road to the vehicle, through structural paths on the other, it amplifies, due to belt vibrations, low frequency excitation components. Tyre belt package has its natural frequencies corresponding to the rigid body translational and rotational modes along with the flexural modes in the low frequency range. In this research work, tyre vibration due to tyre/road interaction is considered to be the main noise source. Procedures have been established to predict the rolling tyre modal parameters and study the influence of tyre design and their characteristics over the structure borne vehicle interior noise.

1.3 RESEARCH OBJECTIVE AND CONTRIBUTIONS

The objective of the research work is to understand the dynamic characteristics of the rolling tyre and to synthesize the structure borne vehicle interior noise of a passenger car through numerical and experimental techniques.

Following tasks are undertaken to accomplish the objective.

1. To conduct a virtual cleat test on a rolling tyre using FEA.
2. To obtain the rolling tyre modal parameters using OMA.
3. To understand the influence of operating conditions over the rolling tyre modal results through a parametric study.

4. To determine the local structural Frequency Response Functions (FRFs) and Noise Transfer Functions (NTFs) of a passenger car.
5. To measure operational accelerations and the interior noise from on-road tests.
6. To implement the experimental TPA for structure borne vehicle interior noise.
7. To estimate road input excitation using laboratory and on-road test measurements.
8. To combine vehicle and tyre wheel transfer characteristics in order to get the overall transfer characteristics from tyre contact patch using FRF based sub-structuring technique (FBS).
9. To establish a procedure for virtual operational acceleration measurements without actual road test for the proposed TPA.

The main contribution of the research work is that, the established FEA-OMA based procedure for determining the rolling tyre modal parameters can be extended to study the influence of operating conditions of a tyre on the modal results. And the proposed TPA procedure, can be used to study the effect of new tyre design over the synthesized structure borne vehicle interior noise without further actual road tests.

1.4 ORGANIZATION OF THE THESIS

This chapter gives an overview of the available literature and work done in the field of tyre modal analysis and tyre/road interaction noise prediction. The tasks required to fulfill the objective are also listed. In Chapter 2 a literature survey is reported on the tyre modal characteristics and its significance in contributing to the tyre/road interaction noise. Further, it highlights the Experimental Modal Analysis (EMA) results of tyre modal characteristics to study the influence of boundary conditions and tyre size. Chapter 3 discusses the FEA-OMA based procedure to determine the rolling tyre modal characteristics and a parametric study that has been carried out to understand the influence of operating conditions over rolling tyre modal parameters. Also the assessment of rolling tyre modal results are reported with the modal results of tyre under various conditions such as unloaded stationary, loaded stationary and steady state transport rolling tyre. Chapter 4 explains the successful implementation of

experimental Transfer Path Analysis (TPA) to synthesize the structure borne vehicle interior noise. Chapter 5 explains the application of TPA for the estimation of road loads. Further, it explains the implementation aspects of component based TPA methods to establish a procedure to study and understand the influence of tyre over structure borne vehicle interior noise. This procedure replaces an actual road test and estimates the required operational acceleration responses from these estimated road loads. Additional experiments conducted for this procedure that predicts tyre characteristics are also discussed. Chapter 6 presents the experimental repeatability observed during the laboratory and on-road tests that supports the reliability of experimental data. Chapter 7 summarizes the work done and the contributions of the research work.

CHAPTER 2

TYRE MODAL CHARACTERISTICS AND ROAD NOISE

2.1 INTRODUCTION

Tyre/road interaction is an important source in automotive NVH. In the study of vehicle dynamics, a pneumatic tyre is observed to behave in three different forms. Below 100 Hz it acts as lumped mass and spring, that affects the vehicle handling and ride vibration behaviour (Kropp, 1989). From 100 Hz to 400 Hz, it exhibits a modal behaviour that is responsible for vibrational energy transfer through various mechanical structural paths. This results in a structure borne vehicle interior noise known as road noise. Beyond 400 Hz, it does not show modal behaviour and the structural waves originates from the point of excitation corresponding to higher frequencies (above 400 Hz) die out faster due to the tyre damping characteristics and refer to tyre non modal behaviour. However, during operational condition, at this frequency range (above 400 Hz), the vibration of tyre near the contact patch (leading and trailing end) and sidewall disturbs the surrounding air, thereby radiating the acoustic energy in the form of the exterior noise known as tyre noise. This thesis focuses on studying the tyre modal behaviour and the resulting structure borne vehicle interior noise. This chapter describes the construction of a radial tyre, its materials and its noise generation mechanisms followed by experimental modal analysis of the tyre. This chapter also highlights the conventional techniques followed by NVH engineers for predicting vehicle interior noise.

2.2 RADIAL TYRE CONSTRUCTION AND ITS REQUIREMENTS

A pneumatic tyre in which the plies are arranged in a radial manner is called as a radial ply tyre which is commonly used in passenger cars. Figure 2.1 shows various components of radial tyre. Chapter 1 'An overview of tire technology' written by Lindenmuth (2006) of 'The Pneumatic Tire' (Gent and Walter, 2005) referred to understand the overview of tyre technology in particular about radial tyres and summarized in this section.

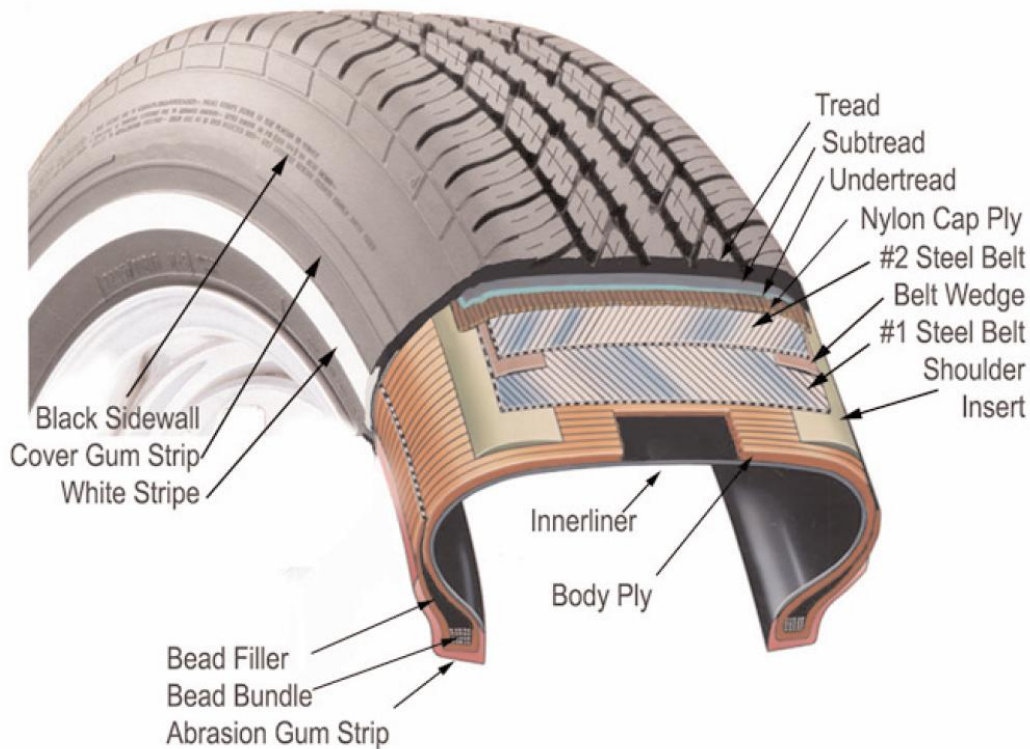


Figure 2.1 Components of radial tyre (Gent and Walter, 2005)

The function of inner liner is to improve the air retention capability of a tyre. The body plies are wrapped around the bead bundle and provide strength to contain the inflation pressure and provide impact resistance to the sidewall. The bead bundles act to anchor the inflated tyre to the wheel rim. Abrasion gum strip also called gum chafer or gum toe guard is a layer of rubber that provides airtight seal between the tyre and the rim under all operating conditions. Bead filler, also known as the apex, is placed on top of the bead bundles. It fills the void between the inner body plies and the turned up body ply. The sidewall rubber serves to protect the body plies from abrasion, impact and fatigue. There are two steel belts placed at opposite angles between the tread and the body plies. The belt widths and belt angles influences the vehicle ride and handling characteristics. The belts resist expansion of the body ply chords and stabilize the tread area and provide impact resistance. The belt ends are separated from body plies by contoured shoulder inserts. The tread pattern is designed to provide uniform wear, to channel water out of the footprint, and to minimize pattern noise on different road surfaces. The necessary function of tread is to provide better grip or traction for driving, braking and cornering. The tread material is made of a special compound that provides a balance between wear, traction, handling and rolling resistance. The subtread exhibits lower hysteresis losses thereby reducing the tyre's rolling resistance. The under tread

is a thin layer of rubber normally placed below the sub-tread to boost adhesion of the tread to the stabilizer plies during assembly. It also covers the cut ends of the belts.

2.3 TYRE MATERIALS

A tyre is a composite structure consisting of three groups of materials (Mark, Erman and Roland, 2013). They are tyre reinforcement materials, rubber compounds and additives. The reinforcement materials are steel, nylon, aramid fiber, rayon, fiber glass, polyester and kevlar. These materials are used to reinforce the rubber and primarily act as a load carrying component within the tyre. Rubber compounds are formulated by four basic components: the polymer network, the filler or particulate reinforcing system, the stabilizer system, and the vulcanization system. The additives are the secondary materials which includes reinforcing chemicals (carbon black, silica, resins), anti-degradants (antioxidants/ozonants paraffin waxes), curatives (cure accelerators, activators, sulfur) and processing aids (oils, softeners).

Elastomers used in radial tyres are basically of four types (Mark, Erman and Roland 2013):

1. Natural rubber
2. Styrene-butadiene copolymer
3. Polybutadiene
4. Butyl rubber (poly isobutylene with approximately 2 % isoprene) and halogenated butyl rubber.

A typical passenger car tyre contains an average of 30 different types of synthetic rubber compounds, 8 different types of natural rubber compounds, 8 types of carbon black, steel cords, polyester, nylon and 40 different kinds of chemicals, waxes, oils, pigments, silica and clays. (Anne and Russ Evans, 2006)

2.4 NOISE GENERATION MECHANISMS

Tyre/road interaction noise has been studied for several decades. The mechanism of noise generation, experimental procedure and theoretical underpinning are well documented in the 'tyre/road noise reference book' (Sandberg and Ejsmont, 2002). The tyre/road noise

generation, amplification and reduction phenomena are classified into two groups: vibrational and aerodynamical phenomena. The classification of these groups are summarized in Table 2.1. The noise generation due to these mechanisms and their relative importance depends on the operating conditions of the tyre. When a tyre is excited at the treadband, structural waves such as bending waves, shear waves and longitudinal waves propagate along the tyre's circumference. The frequencies of these waves are below 3000 Hz (Larsson and Kropp (2002) and Pinnington and Briscoe (2002)). The tyre dynamic behaviour is determined by the propagation and interaction characteristics of these structural waves. Modal frequencies, damping and mode shapes describe the dynamic behaviour of the tyre and form the basis for one of the important mechanisms of noise generation. Hence, there is a need to understand these generation mechanisms and evaluate the modal results of the rolling tyre.

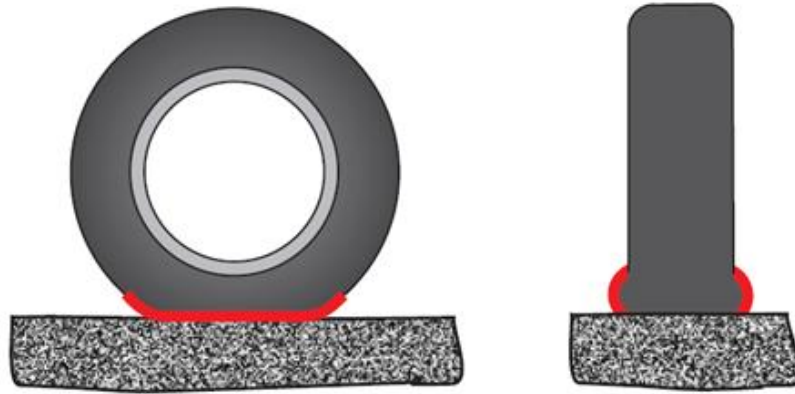
Table 1 Generation mechanism of tyre/road noise and related phenomena (Sandberg and Ejsmont, 2002)

Generation mechanisms	Vibrational	1. Impact mechanisms (mostly radial)	1.a Running deflection 1.b Tread impact (300-1500 Hz) 1.c Texture impact (800-1250 Hz)
		2. Adhesion mechanisms (mostly tangential)	2.a Stick/slip (> 1000 Hz) 2. b Stick/snap (1000-2000 Hz)
	Aerodynamical	3. Air displacement mechanisms	3.a Air turbulence (300 Hz) 3.b Air pumping (> 1000 Hz) 3.c Pipe resonances (900-2000 Hz) 3.d Helmholtz resonances (1000-2500 Hz)
Amplification or Reduction mechanisms	4. Horn effect (600-2000 Hz) pass by measurements		
	5. Tire resonances	5.a Belt resonances (600 - 1300 Hz) 5.b Torus cavity resonance (200 - 250 Hz)	
	6. Mechanical impedance effect	The road surface gives more or less reaction to tire block impacts depending on tire/road stiffness	
	7. Acoustical impedance effect	7.a Porous surfaces affect the source strength 7.b Porous surfaces affect the sound propagation to far field receiver	

2.4.1 Vibrational mechanisms

Radial forces and the momentary distortion created at the trailing and leading edges due to running deflection are the causes of free and forced vibration of tread and sidewall of a rotating tyre. Figure 2.2 summarises the vibrational mechanisms. It shows the tyre running

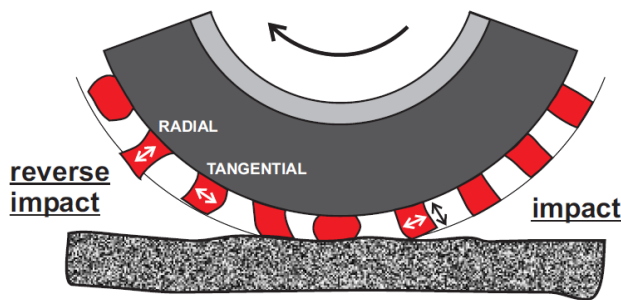
deflections in a slick tyre. The tread and belts undergo radial deformation and sidewall undergoes lateral deformation. The non uniformities in the tyre stiffness causes additional variations in running deflection. This creates structural waves that propagate along the tread and sidewalls.



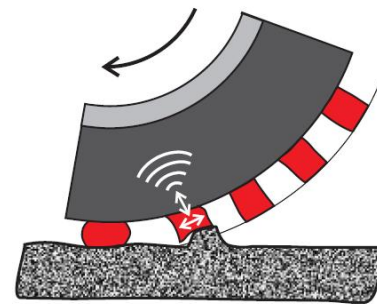
Tyre running deflections

(a) Tread and belt radial deformation

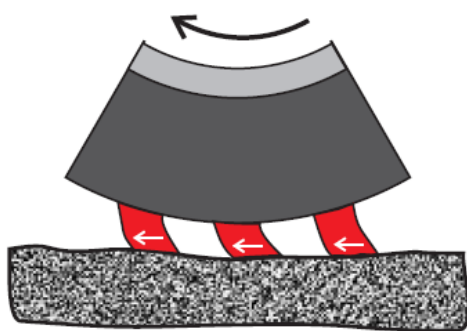
(b) Sidewall lateral deformation



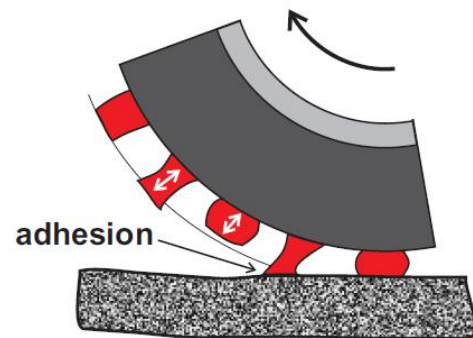
(c) Tread element impact



(d) Road texture impact



(e) Stick-slip adhesion



(f) Stick-snap adhesion

Figure 2.2 Vibrational Mechanisms (Peter Kindt, 2009)

Tread impact mechanism is due to the impact of the tread on the rigid surface which forces the tread band to undergo deformation and this resulting deflection induces vibrations in the radial and tangential directions as shown in figure 2.2. If the tread block size is uniform it excites in a periodical manner which results in a tonal noise while rolling at a constant speed. This noise is called tread whine (Peter Kindt, 2009). The texture impact mechanism illustrated in figure 2.2 is similar to that of tread impact mechanism but in this case the road surface asperities strike against the tyre. At the leading edge of the contact patch, the asperities of the texture impacts against the tread and at the trailing edge, the texture releases from the tread. In texture impact mechanism the excitation frequency is dependent on the wavelength of the texture and rolling speed of the tyre. This excitation from the texture is neither perpendicular to the road nor radial to the tyre. As a result the tyre vibrates both radially and tangentially.

Equation 2.1 gives the value of excitation frequencies of these mechanisms.

$$f = \frac{v}{\lambda} \quad 2.1$$

Where, f = excitation frequency, v = vehicle velocity and λ = block length (tread impact) or distance between major road asperities (texture impact).

Table 2.2 gives the typical values of excitation frequencies for tread impact and texture impact mechanisms for various rolling speed.

Table 2.2 Typical frequencies for Tread and Texture impact mechanisms(Sandberg and Ejsmont,2002)

λ [mm]		Speed [km/h]				
		30	50	70	90	110
Tread impact mechanism						
20-40	Excitation frequency	420-210	700-350	970-490	1250-625	1540-770
30	Excitation frequency	275	465	650	830	1025
Texture impact mechanism						
8-20	Excitation frequency	1040-420	1740-700	2430-970	3125-1250	3825-1540
14	Excitation frequency	600	990	1390	1790	2180

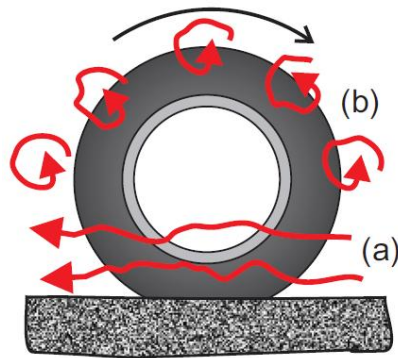
The stick/slip and the stick/snap adhesion mechanisms are also described in figure 2.2. Stick/slip mechanism appears during the vehicle's acceleration, braking and cornering scenarios. The tread element sticks to the road surface and accumulates potential energy as it

enters the contact patch, until the tangential forces exceed the frictional forces. At this instant, the tread block slips back to its impending state at which the friction forces are large enough to keep the block in place. This induces a vibration as the phenomena continues during operation. Stick/snap mechanism occurs mostly on winter tyres. On a clean road, when the operating temperatures are high, the tyre surface becomes sticky and adheres to the road surface. This adhesion of tyre block releases additional forces. Before the release, the rubber tread block is stretched a bit and after release, it vibrates as it regains its rest position. This mechanism is mostly realised in the laboratory tests on clean drums rather than a dirt filled road surface.

2.4.2 Aerodynamic mechanisms

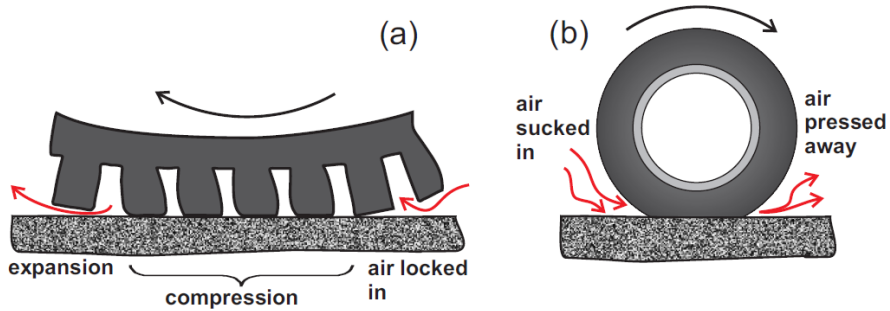
Figure 2.3 summaries the aerodynamic and amplification mechanisms. Air turbulence refers to the motion of air created around the tyre during rotation of the wheel. The motion of air can be longitudinal due to tyre translation and it creates displacement turbulence noise. The motion of air can also be dragged around the rotating tyre's external surface there by creating rotational turbulence noise. This air turbulence noise generation mechanism is illustrated in figure 2.3. However, the noise contribution due to these air turbulence mechanisms are significant only at higher speeds than normal urban speed limits.

Noise generation due to the compression of air cavities between the tread pattern grooves and fine porosities of road surface texture at the contact patch results in air pumping mechanism as shown in figure 2.3. The air is compressed and pressed away at the beginning of the contact patch and expanded and sucked into the cavities at the rear. Figure 2.3 also depicts the pipe resonance aerodynamical phenomena. Pipe resonance refers to the acoustic resonators formed by the contact patch pipes. These pipes are tread pattern grooves trapped in the contact patch which either have both ends open or just one open end. These pipe resonators amplify the air vibration caused by the air pumping mechanisms.



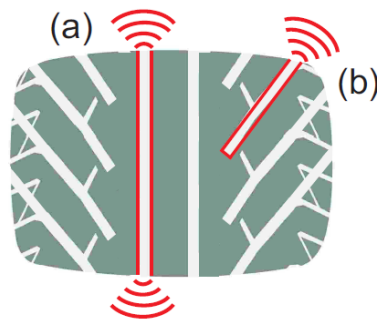
Air turbulence

(a) displacement turbulence (b) rotational turbulence



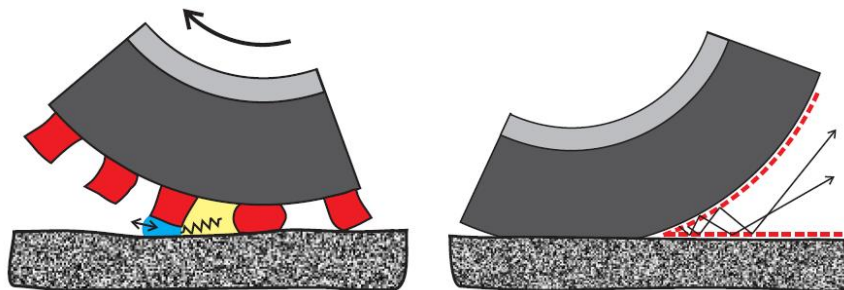
Air pumping

(a) air displacement in the tread (b) air displacement near contact patch



Pipe resonance

(a) open pipe resonator (b) half open pipe resonator



Helmholtz resonator

Horn effect

Figure 2.3 Aerodynamical and amplification mechanisms (Peter Kindt, 2009)

As the tyre rolls, closed cavities are formed between the tread pattern and the road surface. If one considers the volume of cavity leaving the contact with the road surface as a spring and the air present between the tread and the road to be mass, Helmholtz resonance occurs and these unclosed cavities are called Helmholtz resonators, as shown in Figure 2.3. This resonance is suddenly realized, the moment when the cavity opens at the rear of the contact patch. As the cavity further moves away from the trailing edge, the volume and thus the mass of the air immediately outside the cavity increase. Hence the resonance frequency changes during the cavity movement with decreasing amplitude. This means that there is a tone burst associated with each cavity leaving the contact patch, starting at a high amplitude and medium frequency while fading-off at higher frequencies.

2.4.3 Amplification and reduction mechanisms

A narrow throat formation at the leading and trailing edges at the contact patch creates horn effect. The throat begins to widen as it moves away from the edges. This geometric change causes throat impedance and the ambient acoustical impedance to coincide. Hence the noise generated at the throat is further amplified due to this horn effect and it is observed up to 20 dB. (Graf et. al., 1999). This horn effect is due to horn-shaped region, which is formed between the tyre tread surface and the road surface as shown in figure 2.3.

The deformation of the tyre tread near the contact patch creates radial and tangential stress discontinuities, which induce vibrational modes in the carcass and the belt. The flexural waves propagate from the contact patch in both directions around the tyre, merge and create standing waves. There are two types of waves: slow bending waves (60-80 m/s) and fast longitudinal waves (120 -180 m/s) as reported by Kim & Bolton, 2001. Figure 2.4 shows typical tyre dispersion curves for these two waves. The fast modes are considered to be efficient radiators. Apart from these wave modes, air column vibration of the tyre cavity can resonate at a certain frequency which depends on the tyre and rim size, speed of sound in the medium that inflates the tyre. Typical first tyre cavity resonance frequencies for passenger car tyres are in a range of 230-280 Hz ($n=1$) and contribute to structure borne vehicle interior noise (Sakata et al.,1990). Similar to structural waves, at certain frequencies the pressure waves travelling in opposite circumferential direction interfere constructively. The resulting

acoustic pressure distribution in the air cavity forms a standing wave pattern. Figure 2.5 shows the pressure distribution inside the air cavity for the first two acoustic resonances in the circumferential direction.

A simplified equation for the cavity resonance frequency is given by equation 2.2

$$f = \frac{c}{l} = \frac{2 \cdot n \cdot c}{\pi \cdot (D+d)} \text{ [Hz]} \quad 2.2$$

where, c - speed of sound in the gas inflating the tyre [m/s]

l - length of the cavity [m]

D - outer diameter of the cavity [m]

d - inner diameter of the cavity [m]

n - integer

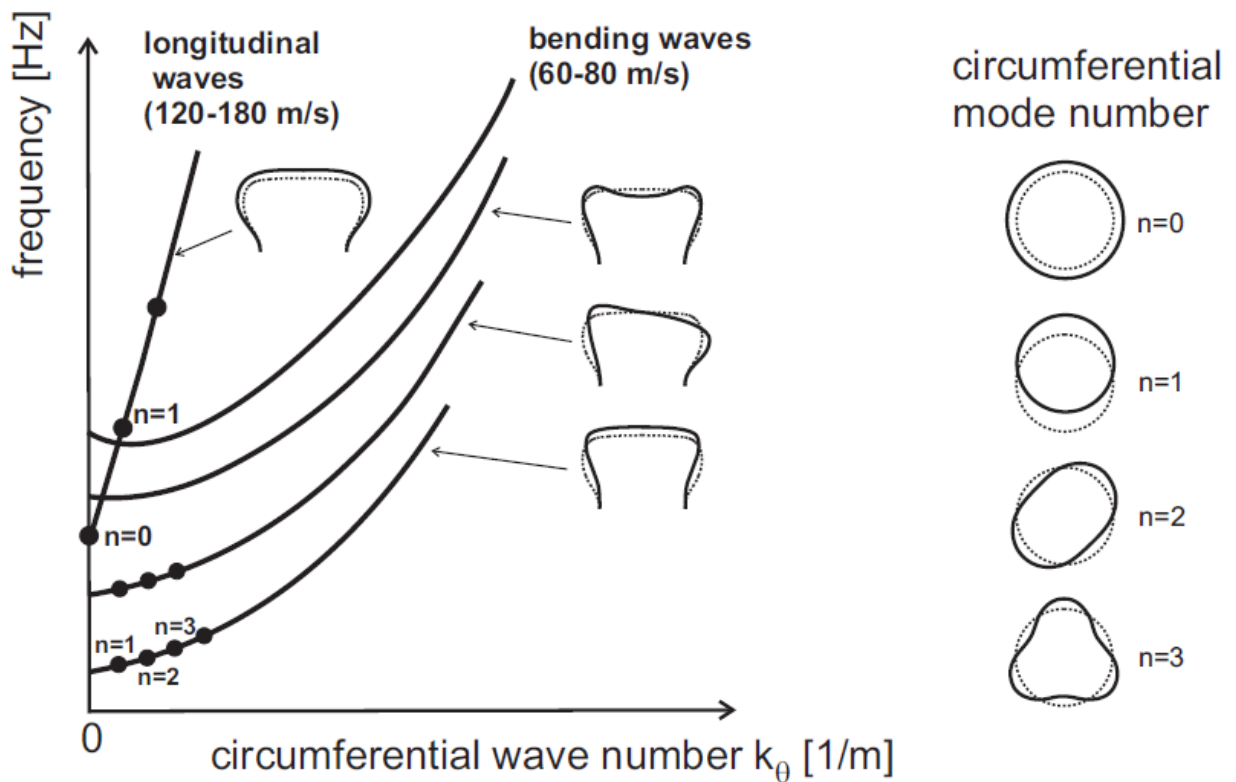


Figure 2.4 Typical tyre dispersion curves (Kim and Bolton, 2004)

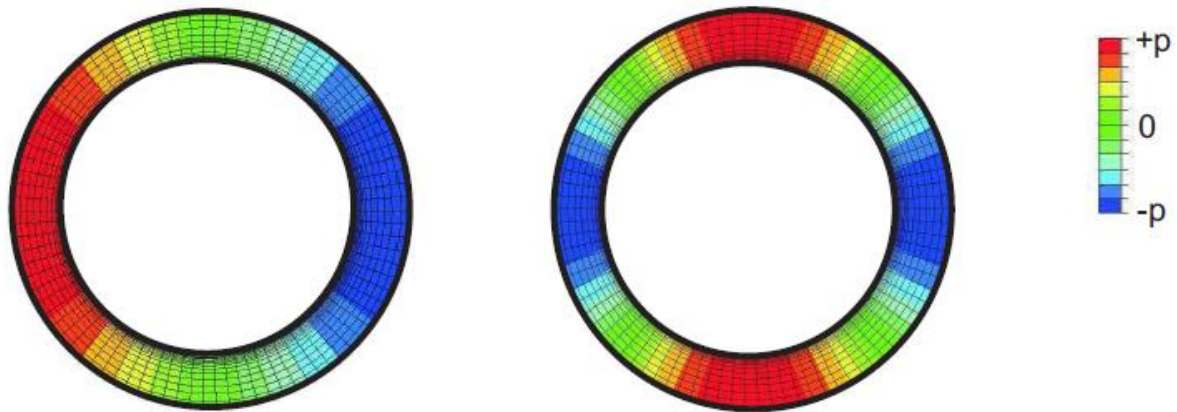


Figure 2.5 First and second acoustic cavity resonance modes (Peter Kindt, 2009)

From the mechanisms discussed in section 2.4, tyre vibration can be induced by individual mechanisms or a combination of different mechanisms. It is difficult to understand their relative importance. Apart from tyre cavity resonance, all the other mechanisms contribute majorly to the exterior noise of the vehicle. A part of this radiated noise contributes to vehicle's interior as air borne components, but tyre belt resonance characteristics and tyre/wheel dynamics formulate the basic mechanism for the structure borne vehicle interior noise.

2.5 TYRE MODAL CHARACTERISTICS

Tyre modal characteristics are important to mitigate tyre/road interaction noise. Tyre modes are classified into rigid modes and flexible modes. Rigid modes refer to translational and rotational motion of tyre tread band and flexible modes show the deformation of the tread band. Peter Willem Anton Zegelaar,(1998) studied the tyre's in plane vibrations. First he studied dynamic behaviour of a rigid ring tyre model in the frequency range of 0-80 Hz and validated experimentally through cleat and brake test. He has also carried out experimental modal analysis of tyre with different boundary conditions: a free unloaded tyre in horizontal position, a tyre with its spindle axis fixed and a tyre loaded on the road in vertical direction. These experimental results are compared with modes of flexible ring model.

Tyre construction and rotational velocity affects the tyre modes (Zegelaar, 1998). The construction of a radial tyre provides stiff treadband and it exhibits eight modes in the

frequency range of 0- 300 Hz whereas for bias ply tyre, only the two lowest modes are observed. The tyre rotation causes centrifugal acceleration and Coriolis acceleration. The pre-tension of the treadband increases as the centrifugal force increases, and this causes increased flexible mode frequencies. However, the rigid body frequencies are significantly lower at higher velocities. Moreover, to model the rotating tyre vibration, transformations are to be specified between the rotating and fixed coordinate systems. Also, Zegelaar (1998) reported the influence of spindle boundary conditions and contact patch boundary conditions.

There are four spindle boundary conditions: (1) A free wheel, (2) a pinned wheel (vertical and horizontal motion of the spindle are constrained, but the wheel rotates freely), (3) a fixed wheel (spindle fixed) and (4) the wheel in an actual vehicle suspension. Only the rigid body modes of the tyre are affected by 'fixed spindle' boundary condition. The contact patch boundary condition refers to the loaded tyre and in this condition the tyre symmetry vanishes and it becomes difficult to express the circumferential modes by harmonic functions. The non-symmetry causes the splitting of resonance frequency peaks into double peaks. This explains the limitations of modelling a loaded tyre vibration analytically.

Further, experimental modal analysis was carried out to study the influence of different tyre dimensions (175/65R14, 205/60R16 and 235/65R17) and boundary conditions (free and fixed spindle conditions). Tyre modes are labelled in this thesis according to the mode nomenclature followed by Peter Kindt (2009). Figure 2.6 describes the mode labelling, where 'n' represents circumferential index and 'a' represents belt cross sectional index. (2,a)0 represents and (2,a)extr. represents the example of loaded tyre modes. The additional labels '0' and 'extr.' refer to the zero and extreme radial displacement along the cross section located in the middle of the tyre/road contact patch respectively. Figure 2.7 shows the tyre modes obtained from FE modal analysis of 205/55R16 tyre in an unloaded free spindle boundary condition. FE modal analysis is explained for various conditions of tyre in order to make an assessment of a rolling tyre modal frequencies in the following chapter.

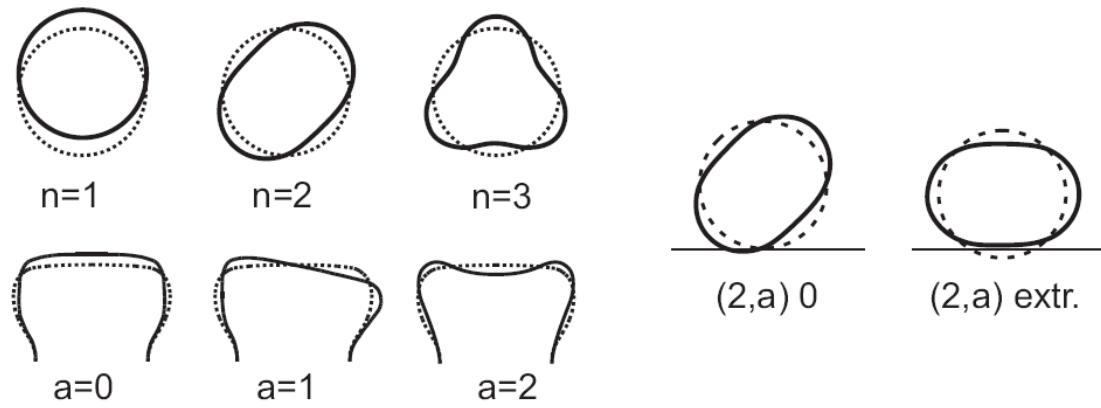


Figure 2.6 Labelling of tyre structural modes (n,a) (Peter Kindt, 2009)

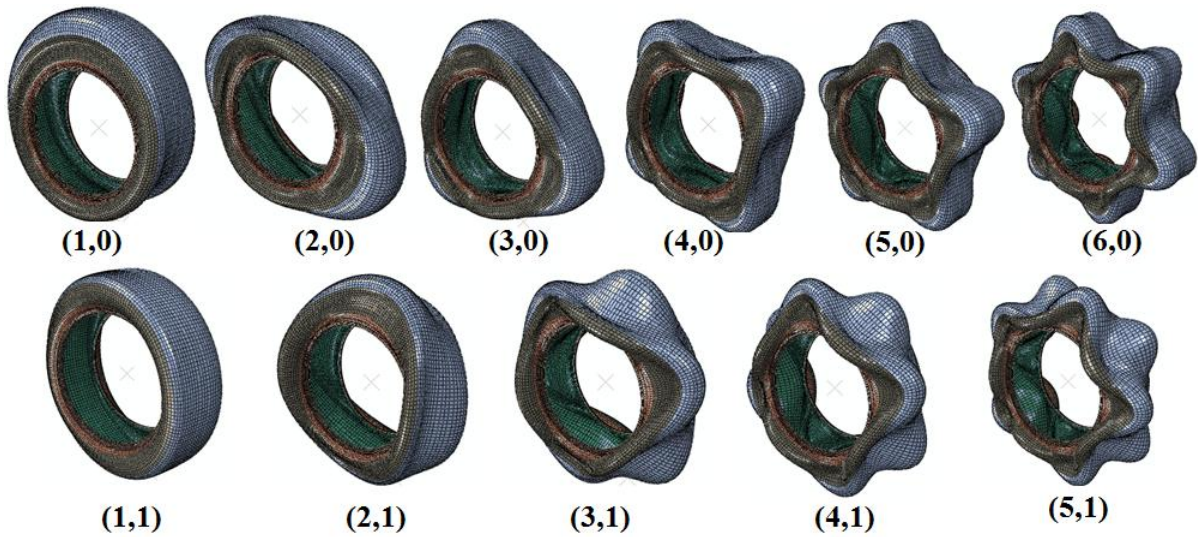


Figure 2.7 Circumferential and cross sectional modes of an unloaded free boundary condition tyre

2.5.1 Experimental setup and procedure

Figure 2.8 shows the experimental set up for experimental modal analysis of a tyre. This test environment typically includes a test rig where the tyre is hung with use of bungee cords to get the free boundary condition. The test tyre is first cleaned and labelled for response measurement points. There are 120 points in total on six circles each of 20 points, considered. An aluminium block is glued to the tyre firmly as shown for the purpose of excitation in all three directions (radial, tangential and lateral). An impact hammer instrument is used to give an impulse excitation. Three tri-axial accelerometers were used to measure the acceleration

responses. The rowing accelerometer procedure is followed. LMS SCADAS Mobile data acquisition with 16 channel along with the LMS Test Lab spectral Testing module is used for signal acquisition and processing. Total of 1080 acceleration responses were obtained for three directional excitation.

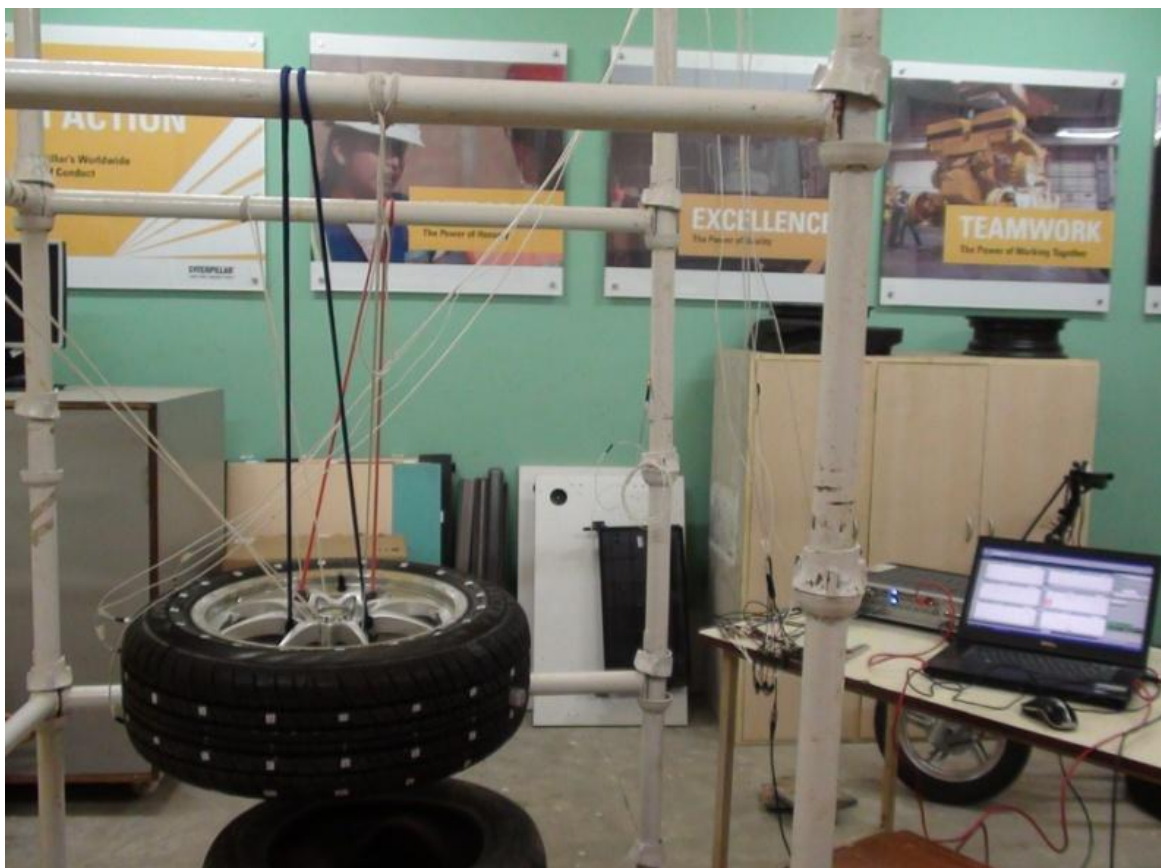


Figure 2.8 Experimental Modal Analysis test setup

During this experiment, for each measurement, an average of ten responses were collected for each degree of freedom, to improve signal to noise ratio. The duration of each impact excitation was two seconds at 1024 Hz sampling frequency. The coherence function during each run was verified to evaluate the validity of each measurement.

2.5.2 Estimation of Modal parameters

The frequency response functions were calculated for each response with three input excitation (three references in radial, tangential and lateral and 1080 responses were considered). The FRF sum of all measurement degrees of freedom is obtained for stabilisation curve fit as shown in figure 2.9.

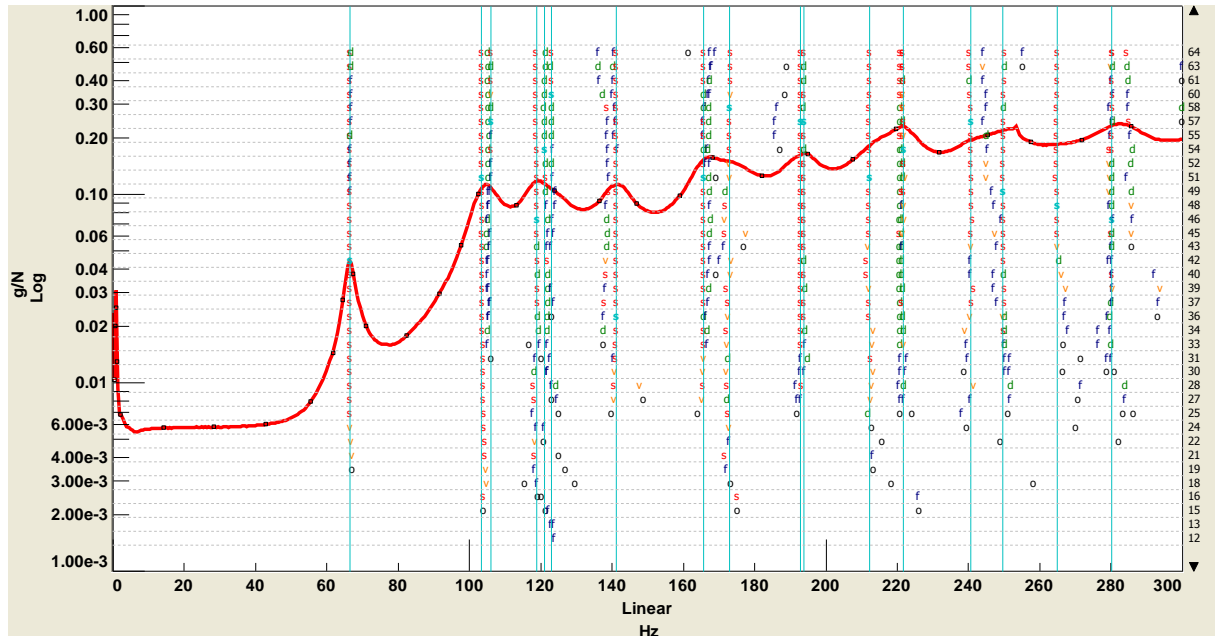
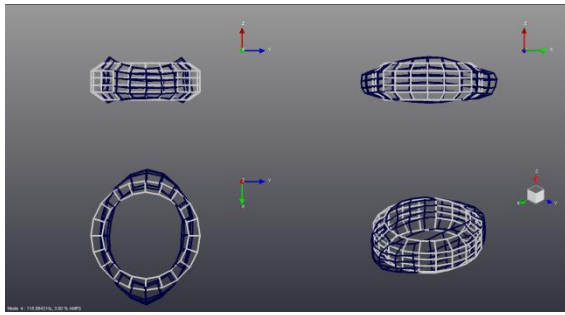
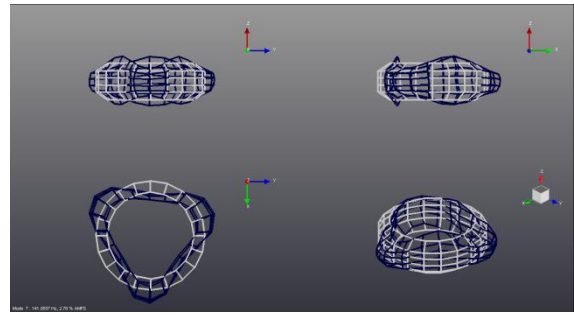


Figure 2.9 Stabilization Curve for mode selection

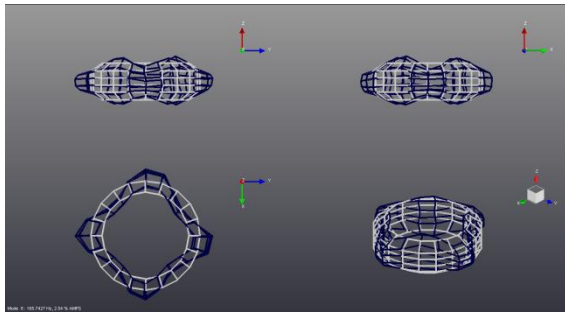
The peaks of this curve correspond to the modes obtained for the tyre. The modal results and the corresponding frequencies are shown in figure 2.10, figure 2.11 and figure 2.12. The rigid body modes (torsional, pitch and axial) and flexible modes, both circumferential bending and axial bending modes were obtained.



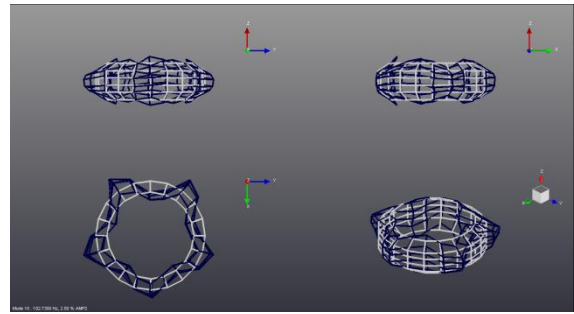
Mode (2,0)



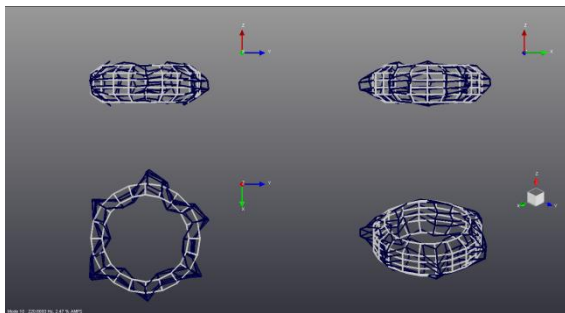
Mode (3,0)



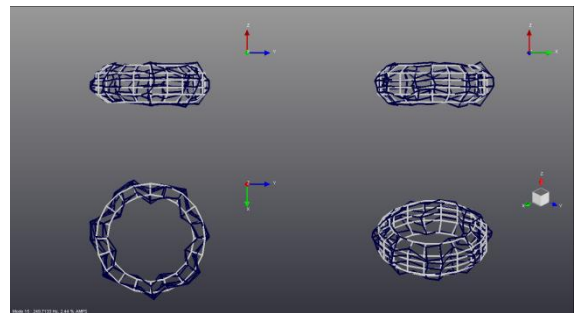
Mode (4,0)



Mode (5,0)



Mode (6,0)



Mode (7,0)

Figure 2.10 Circumferential modes of tyre for free spindle condition

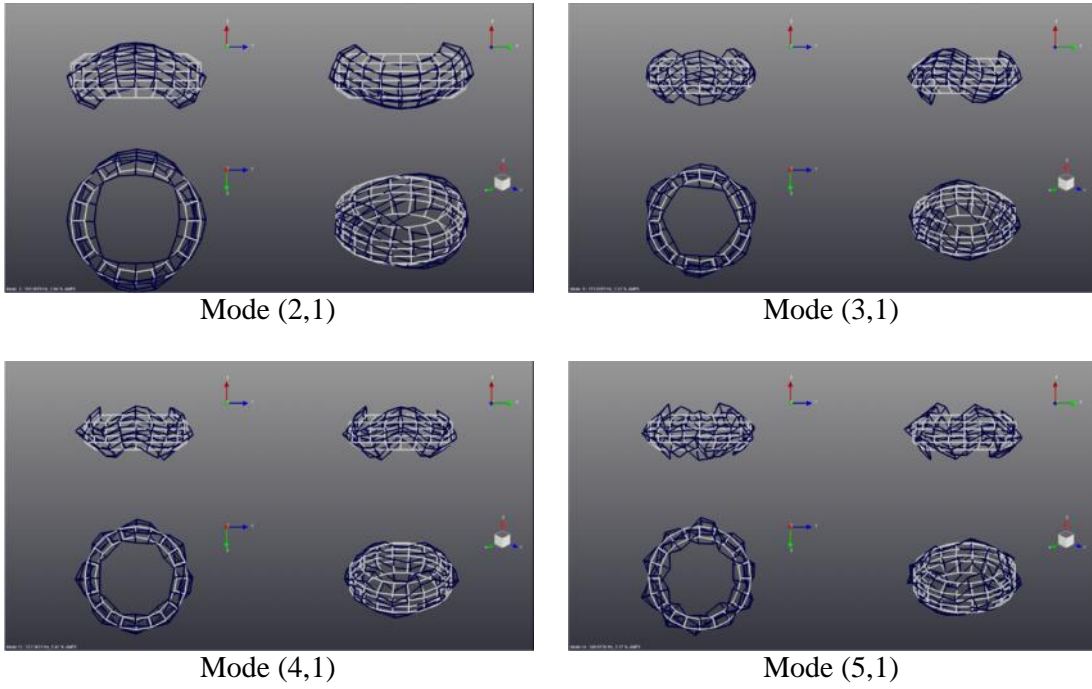


Figure 2.11 Cross sectional modes of tyre for free spindle condition

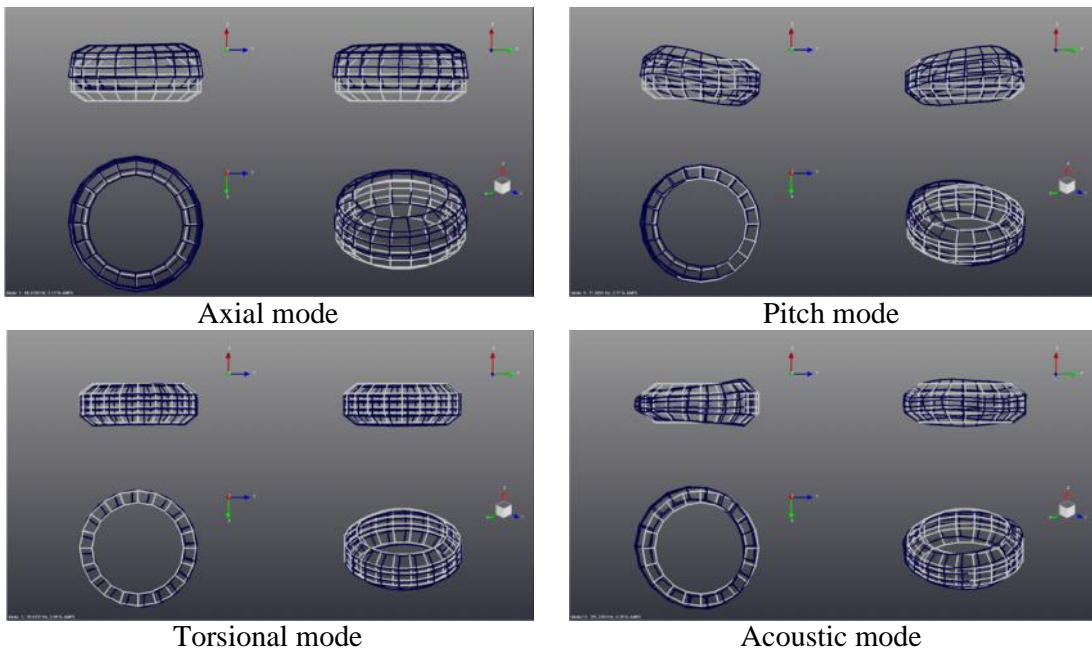


Figure 2.12 Rigid and acoustical mode of tyre for free spindle condition

2.5.3 Parametric study

A parametric study is carried out to observe the variation of modal frequencies due to tyre size and boundary condition. Three different tyre sizes have been chosen and experimental modal analysis is carried out. Table 2.3 compares the modal frequencies obtained for these tyres. The influence of spindle boundary condition is studied on 175/65R14 JK Tornado tyre.



Figure 2.13 Spindle fixed condition of unloaded tyre for experimental modal analysis

Figure 2.13 shows the test tyre with vehicle. The spindle fixed condition is obtained by locking the wheel and lifting the vehicle axle. Figure 2.14 and Figure 2.15 compare the circumferential and cross sectional modes for different tyre sizes. It is observed that as the tyre size increases the modal frequencies decreases for a fixed mode. This variation appears linear for circumferential modes whereas for cross sectional modes it becomes non linear.

Table 2.3 Tyre modal frequencies for different size tyres

Modes	Free Free condition : Frequencies (Hz)		
	Tornado 175/65R14	Vectra 205/60R16	Elanzo NXT 235/65R17
Mode(2,0)	118.88	111.9	87.91
Mode(3,0)	141.06	133.72	102.15
Mode(4,0)	165.74	158.07	119.26
Mode(5,0)	192.73	184.16	138.42
Mode(6,0)	220.67	211.83	158.02
Mode(7,0)	249.70	241.08	178.05
Mode(8,0)	280.23	--	--
Mode(2,1)	103.37	104.51	71.66
Mode(3,1)	173.04	162.03	124.88
Mode(4,1)	212.34	200.26	155.07
Mode(5,1)	240.67	228.33	162.93
Mode(6,1)	264.83	253.90	--
Axial Mode	66.52	69.85	44.01
Pitch Mode	105.99	--	78.24
Acoustic Mode	253.8	225.25	--
Mode (1,0)	121	109.3	98.39

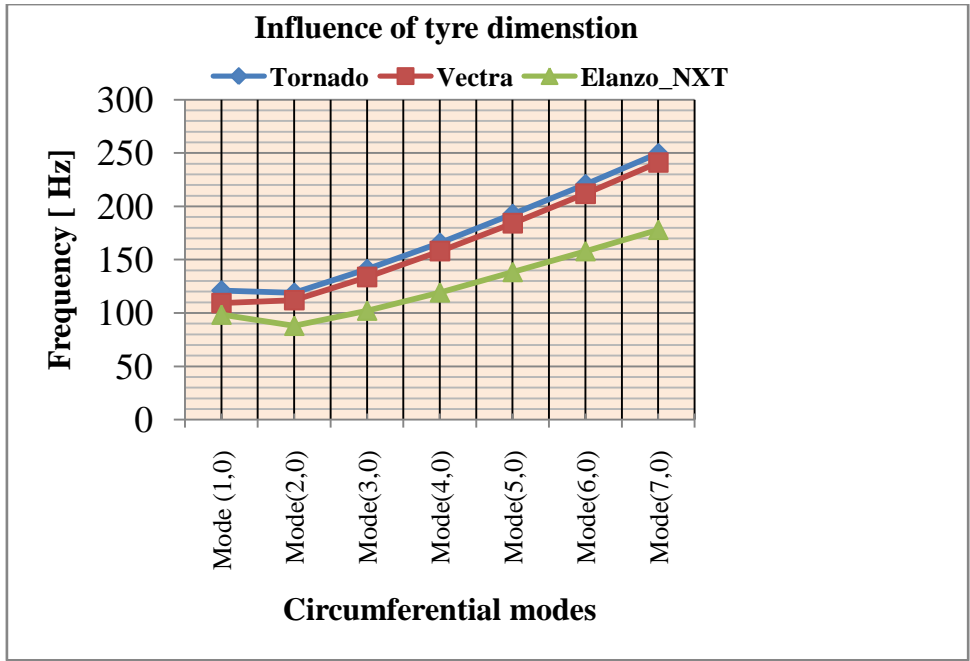


Figure 2.14 Variation of circumferential modes as function of tyre size

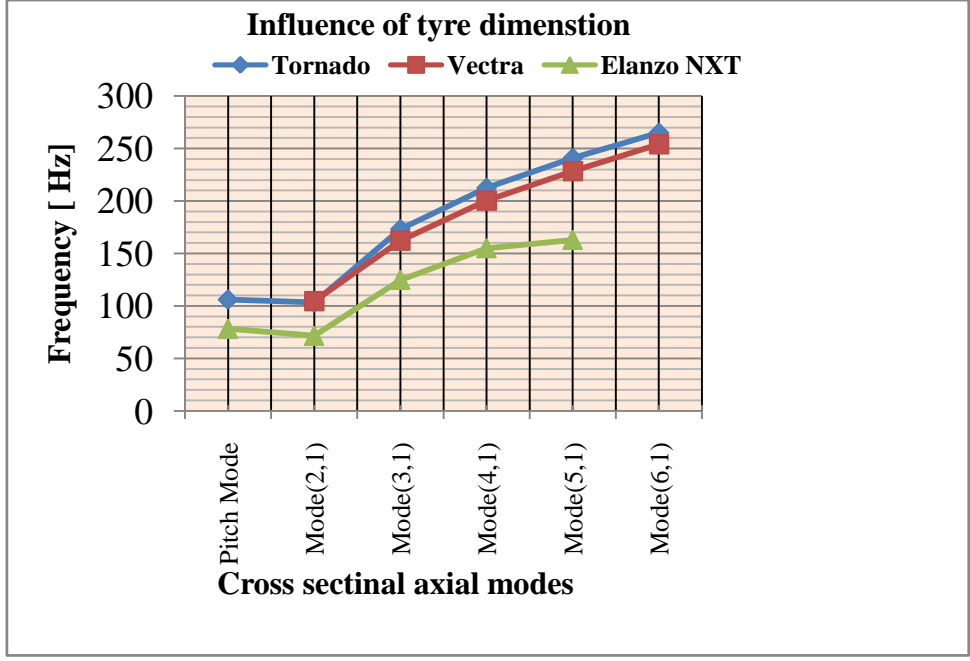


Figure 2.15 Variation of cross sectional modes as function of tyre size

Table 2.4 compares the results of free spindle condition with the fixed spindle condition. It is observed that only the rigid modes are influenced by the fixed spindle condition, as can be observed from Figs 2.16 and 2.17. This is in accordance with the observation made by Zegelaar (1998). There is no change in flexible mode for different spindle conditions, whereas axial mode frequency increases for fixed boundary condition. The torsional modes were not excited as the spindle was fixed.

Table 2.4 Tyre modal frequencies for different boundary conditions

Modes	Frequencies (Hz)	
	Free Free	Spindle Fixed
Mode(2,0)	118.88	121.63
Mode(3,0)	141.06	142.50
Mode(4,0)	165.74	167.52
Mode(5,0)	192.73	194.64
Mode(6,0)	220.67	222.86
Mode(7,0)	249.70	253.34
Mode(8,0)	280.23	284.89
Mode(2,1)	103.37	101.00
Mode(3,1)	173.04	171.96
Mode(4,1)	212.34	214.68
Mode(5,1)	240.67	245.86
Mode(6,1)	264.83	273.64
Axial Mode	66.52	47.83
Torsional Mode	--	35.83
Pitch Mode	105.99	71.96
Acoustic Mode	253.8	251
Mode (1,0)	121	108.88

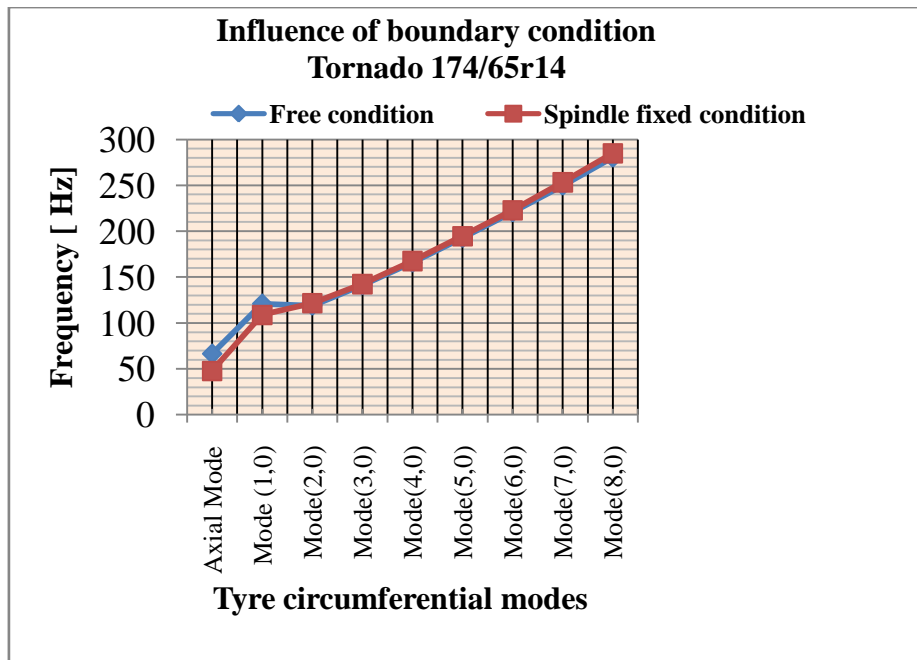


Figure 2.16 Variation of circumferential modes for different spindle boundary conditions

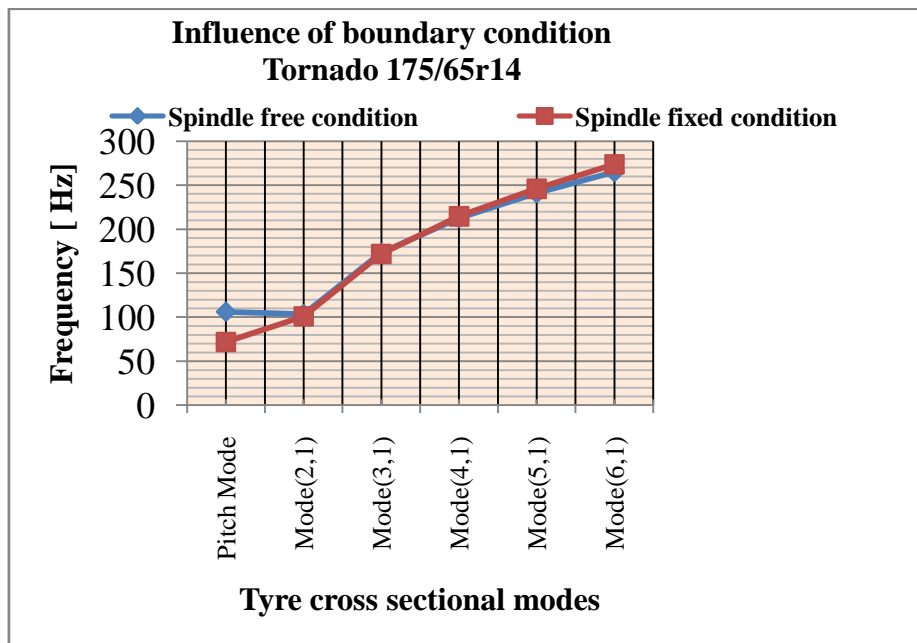


Figure 2.17 Variation of cross sectional modes for different spindle boundary conditions

2.6 STRUCTURE BORNE VEHICLE INTERIOR NOISE

Engine vibration, vehicle aerodynamics and tyre/road interaction are the main sources of vehicle interior noise. Significant research contributions have been made on reducing engine vibration (power unit noise) and vehicle aerodynamics noise (wind noise). However, relatively less effort has gone to address vehicle interior noise induced due to tyre/road interaction. For urban speeds, the interior noise is contributed mainly due to tyre/road interaction. Riegel and Wiedemann, (2008) have studied and reported contributions by various sources to total vehicle interior noise. Figure 2.18 shows these contributions for a standard class vehicle on an asphalt road at 70 kmph. Both structure borne and air borne components of tyre/road noise dominate other sources throughout the range except engine noise at around 60 to 80 Hz. Wind noise due to vehicle aerodynamics dominates only at higher speeds(>120 kmph) By comparison, engine noise is less intrusive at cruise conditions (Bangyi Dong et al. 1995)

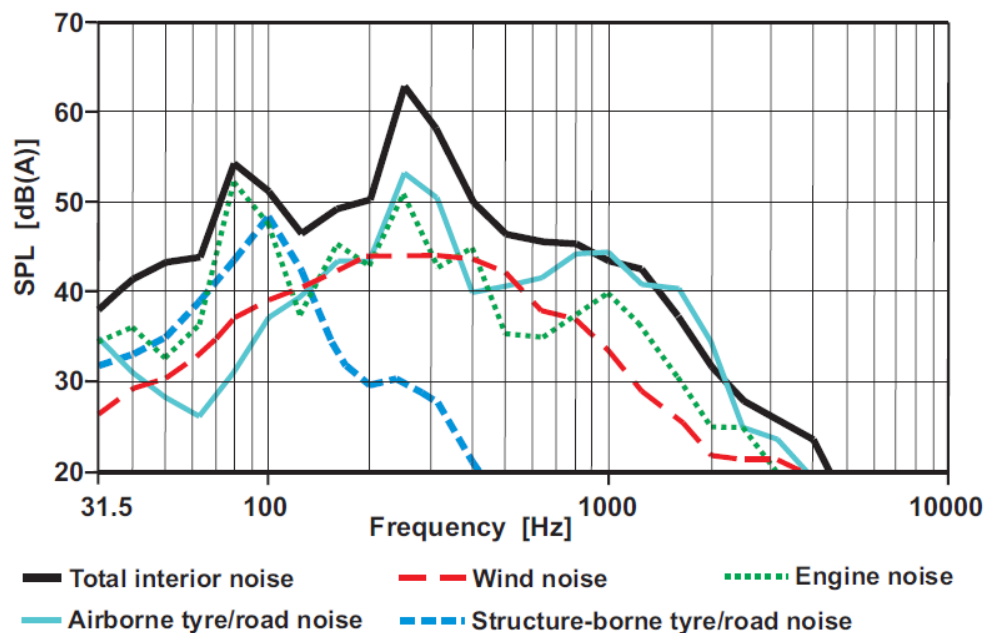


Figure 2.18 Vehicle interior noise components (Riegel and Wiedemann, 2008)

2.6.1 Introduction to road noise models

This thesis focuses on the structure borne vehicle interior noise generated due to complex tyre/road interaction. From literature, it is understood that road noise mainly involves the study of various mechanisms responsible for energy transfer from the source (contact patch) to the target locations (passenger compartment). The energy transfer that happens through the medium 'air' constitutes the mechanism for air borne vehicle interior noise and if it happens through the structure (system consists of tyre/wheel, suspension and chassis and floor and vehicle body), it constitutes the mechanism for structure borne vehicle interior noise. Understanding and predicting the component and system level behaviour is an important step to synthesize structure borne vehicle interior noise. This can be achieved by both simulation and experimental techniques. Filip De Coninck, (2007) stated that "Component characteristics can be predicted and measured with reasonable accuracy, whereas system level behaviour is subjected to more uncertainty in the component interfaces and measurement set-up". There are various models available in literature to predict road noise. They can be grouped as Physical models, Parametric models, Finite element models, Multi-body models, Modal models, Frequency models and Hybrid models. Except modal and frequency models other models are able take up non-linear behaviour of the components or the system.

2.6.2 Introduction to road noise tests

Road noise tests are conducted either on proving ground or on road drums dynamometers in the laboratory. Both objective and subjective measurements are made on proving ground tests. Laboratory test set-up requires semi-anechoic room, hammer and electromagnetic shakers. The advent of controller hardware for high power applications like electric and hydraulic actuators brought in the use of complex installations such as road noise dynamometers for measurement of interior noise, kinematics and compliance rigs for the study of suspension behaviour, four poster test rigs and multi degree shaker tables for vehicle ride, comfort and durability evaluation. This thesis presents the TPA technique to synthesize structure borne vehicle interior noise in chapter 4. Both laboratory and on road test measurements were made for this purpose.

2.6.3 Techniques followed by researchers

Scott et al. (1993) have developed automotive suspension models using component mobility technique. This technique basically involves determination of the FRFs between two points. They have considered the front suspension of a vehicle sub components to find mobility matrix and coupled them to get the suspension mobility model for prediction of vehicle interior noise. Bangyi Dong et al.(1995) have developed road noise model using Statistical Energy Analysis (SEA). They derived tyre noise source functions from acoustic and vibration measurements by conducting numerous experiments in the laboratory chassis dynamometer road. The accuracy of their SEA model was reported to be within 2-4 dB for a wide frequency bandwidth of 200 - 3000 Hz. Renata and Paulo, (2003) have investigated sub system contribution to in a pick-up truck for boom noise power unit vibration. They developed an in-house software called INCAWIN (Interior Noise Contribution Analysis for Windows) using hybrid method based on noise path analysis to simulate interior noise.

Byung and Kyoung, (2005) have used Noise Path Analysis (NPA) to address road noise reduction by modifying the identified critical path. They have used stiffness based method to estimate the operational loads at suspension bushes. They further carried out Panel Contribution Analysis with the measured acoustic transfer function. Charles et al.(2005) have followed a hybrid approach, where finite element suspension and drive train models are coupled with a test based Frequency Response Function (FRF) model of the trimmed body. They have used FRF based sub-structuring technique to couple the FE suspension model with the vehicle trimmed body. In this process they have developed a full vehicle model to evaluate the road induced noise and vibration response for a given suspension and steering column design. However, they have not considered the actual road contact patch forces instead estimated the operational loads at the knuckle by matrix inversion method.

Nicolas and Jean, 2007 have studied the booming noise problem due to engine vibration and suspension characteristics. They worked to reduce this structure borne noise using high damping foam technology and proposed vibration barrier concept, using this high damping foam. They demonstrated FEA design of this vibration barrier, with full car body model and

interior acoustic cavity. Luca et al. (2007) have used reciprocal measurement technique to determine the Noise Transfer Functions, which is a metric for quantifying the vehicle performance for structure borne interior noise components due to power train noise. This procedure uses the volume source and excites the cabin cavity for the required frequencies of interest; and the acceleration responses were measured at the engine mount points. Johan and Luca, (2009) used low frequency and mid frequency volume sources to excite the cabin cavity to get the noise transfer function between suspension and cabin cavity and the tyre surface and cabin cavity by using accelerometer and microphone respectively without application of hammer or shaker excitation by reciprocal measurement. Van der Auweraer et al. (2007) have formulated a fast, hybrid and operational path analysis to determine the critical path for vehicle NVH refinement process. This Operational Path Analysis (OPA) takes an advantage of working with only operational data and does not require the estimation of operational loads which is required for implementation of experimental TPA.

2.7 SUMMARY

In this chapter various noise generation mechanisms of tyre/road interaction are explained. Also it is stated that not all the discussed mechanisms directly contribute to the vehicle's interior noise. The tyre treadband / belt vibration and the whole wheel dynamics play a vital role in contributing to vehicle interior noise. Then, experimental modal analysis procedure is explained to predict modal frequencies and mode shapes. The influence of spindle boundary conditions and tyre size have also been addressed. Finally, the chapter includes a literature review of structure borne vehicle interior noise in order to understand the various techniques followed by the researchers. The following chapter discusses determination of rolling tyre modal parameters.

CHAPTER 3

DETERMINATION OF ROLLING TYRE MODAL PARAMETERS

3.1 INTRODUCTION

In order to address various noise generation mechanisms and noise propagation phenomena of a tyre, it is necessary to study the tyre dynamic behaviour in terms of modal parameters. This chapter enumerates a novel method for finding the modal parameters of a rolling tyre using FEA and Operational Modal Analysis (OMA). Commercial Explicit FE codes have been used to simulate the experiment of a tyre rolling over a semi-circular straight and inclined cleat. The acceleration responses obtained from these simulations are used as input to the OMA. LMS test. lab has been used for carrying out the OMA. The modal results are compared with the published results of Kindt et al.(2009) and validated. Also, the modal results obtained from OMA are compared with FE modal results of stationary unloaded, stationary loaded and Steady State Transport rolling tyre.

Traditionally, tyre modal parameters are found from Experimental Modal Analysis (EMA) and/or FE analysis of a non-rolling tyre with the basic assumption of system linearity and reciprocity, obtained from the estimation of Frequency Response Functions (FRFs) for a known dynamic excitation force. But, for a rolling tyre, it is difficult to measure the excitation force at the tyre road interface. Hence, OMA is preferred, as this technique does not require input excitation force. OMA makes use of the crosspower sum of the output responses with a suitable reference for modal parameter extraction (Mehdi Batel, 2002).

Zegelaar (1998) showed that the modes of vibration of a tyre strongly depend on tyre construction, rotational velocity, spindle boundary conditions and contact patch boundary conditions. Yam et al. (2000) have obtained three dimensional mode shapes (radial, tangential and lateral directional modal parameters) of a tyre using EMA. Lauwagie et al. (2006) have done a comparative study of modal parameter extraction procedure viz., OMA and EMA, either individually or in combination, in a small hydraulic crane modal analysis

study. Rao et al.(2003) have used a FE tyre model based on a hyperelastic material that included all the reinforcements, to study cornering, braking and cornering cum braking dynamic behaviour of tyre. This approach is adapted to develop a FE model of tyre for the current research work of structure borne vehicle interior noise due to tyre/road interaction. Determination of mode shapes of a rolling tyre is a challenging problem. Experiments are difficult to perform. Apart from the novel work of Kindt et al. (2009) there has been no other experimental work to determine the mode shape of a rolling tyre.

Finite Element Analysis has been a popular technique to determine the mode shapes of a stationary tyre, both as a free body and under load with contact. Recently, steady state transport algorithms have been used as a basis for extracting mode shapes (Brinkmeier and Nackenhorst, 2008). Contact condition has been used for tyre road contact. Contact definition for mode shape determination is a practical approach, but has theoretical limitation. This can easily be seen in the mode shapes published and in this work as well.

Finally, there have been several attempts to understand and determine modal parameters analytically (Bolton and Kim, 2000,2003). Here again, these models are limited by the inability to solve the actual loaded tyre, rolling on a road. Hence, it is felt that a new approach is required to capture the mode shapes. The difficult experimental determination of deformation of a rolling tyre, is replaced by numerical experiments, using an explicit finite element analysis. A pneumatic tyre is made to roll over a cleat, and the ensuing deformations are captured. (Abaqus, Documentation R.12, 2011). These deformations are used as inputs to a commercial OMA codes from LMS (LMS Test. Lab, OMA documentation, 2009) that uses the popular polyreference least square complex exponential frequency domain approach.

The FE procedure and further processing with OMA are discussed in section 3.2 and the obtained rolling tyre modal parameters are compared with experimental results reported by Kindt et al.(2009) in section 3.3. Also, to make an assessment of this procedure, the results obtained, are compared with the mode shapes and resonance frequencies of stationary unloaded, stationary loaded and steady state transport rolling tyre in section 3.4. Finally, the conclusions are highlighted in section 3.5.

3.2. PROCEDURE FOR EXTRACTION OF MODE SHAPE

3.2.1 Explicit Finite Element Analysis and Operational Modal Analysis

Passenger car radial tyre of size 205/55R16 has been chosen to construct a Finite Element model. The size is the same as that used by Kindt et al. (2007) in their study. Figure 3.1(a) and Figure 3.1(b) show the details of the tyre section and a smooth full tyre model that has been developed. Various colours in the tyre section describe the various components and constructional details of the tyre. The tyre includes two belts and a ply and a protection ply. The details of material and reinforcement definition are given in the Table 3.1. Yeoh model (1993) has been used to define strain energy potential. Table 3.1 gives the material constants used for hyperelastic material definition for various components of the tyre. Rebar elements are defined for both the belts and ply for reinforcement assignment. Nonlinear geometric effects are included in the simulation.

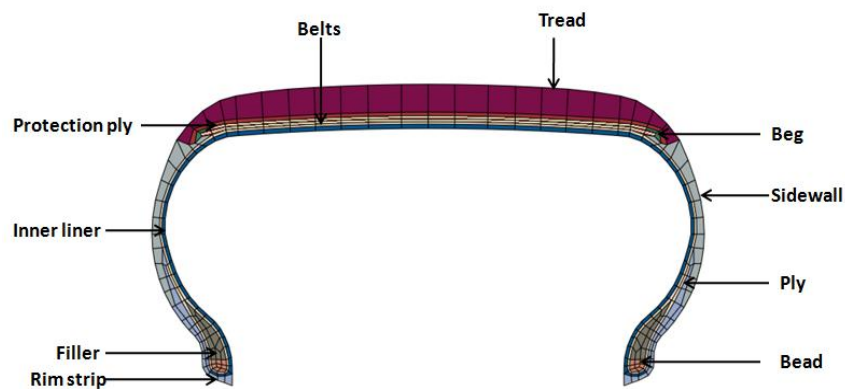


Figure 3.1(a) Section details of 205/55R16 radial passenger car tyre



Figure 3.1(b) Tyre FE model

Table 3.1 Hyperelastic Material Definition in SI units

Components	Density	Yeoh Model Material Constants			
		C10	C20	C30	D1
Inner liner	1050	3.14470e5	-1.10385e5	2.65448e4	1.58998e-7
Ply	1050	3.72454e5	-9.69403e4	2.43385e4	1.34244e-7
Wing Tip	1050	2.98750e5	-8.25992e4	1.90295e4	1.67364e-7
Protection Ply	1050	8.96732e5	-2.80203e4	7.88071e4	5.57580e-8
Belt	1050	8.96732e5	-2.80203e4	7.88071e4	5.57580e-8
Beg	1050	1.21927e6	-4.85253e5	1.96638e5	4.10082e-8
Tread	750	6.16047e5	-1.90709e5	4.75049e4	8.11627e-8
Sidewall	1050	4.87666e5	-1.41343e5	3.86106e4	1.02529e-7
Rimstrip	1050	1.13364e6	-4.43953e5	1.18935e5	4.41059e-8
Filler	1050	8.76048e5	-2.93303e5	7.93587e4	5.70745e-8
		Young's Modulus		Poisson's ratio	
Bead	7800	2.06399e11		0.3	
Reinforcement definition for continuum elements					
Ply	1070	4.715258e9		0.49	
Protection Ply	940.5	2.19652e9		0.49	
Belt	7800	1.74652e11		0.3	
Reinforcement definition of geometry					
	Cross sectional area of rebar (m2)	Spacing between rebar (m)		Orientation angle(degree)	
Ply	3.52565e-7	9.056e-4		-1	
Belt1	1.41196e-7	1.581e-3		60	
Belt2	1.41196e-7	1.593e-3		-60	
Protection Ply1	2.29031e-7	1.016e-3		90	

Explicit dynamic rolling of this model over a semi-circular cleat of 25 mm radius has been carried out for the following operating conditions: inflation pressure of 250 kPa, static preloading of 3300 N and speed of 28.3 kmph to have an equivalent numerical experiment as that of tyre on tyre experimental arrangement of Kindt et.al (2009). The minimum cleat dimension of 25 mm is chosen so as to provide a higher energy level to the rolling tyre.

The contact conditions can be invoked by considering the two bodies to be deformable or one to be deformable and the other to be rigid. The contact is defined between two surfaces. Here, the contact is between the deformable tread, defined through its outer surface and the rigid

road surface defined through an analytical expression. The definition is through surface interaction. During inflation and loading, the coefficient of friction is assigned to be zero and in the next step during rolling its value is 1. In case of tyre rolling over inclined cleat, contact pair is defined between tread outer surface and road discrete rigid surface that is created based on the outer surface definition of the road elements.

First, the tyre foot print analysis is carried out and its shape is compared with the well-established contact pressure distribution in the literature (Rao et al.(2003) and Clark (2006)).The tyre foot print analysis represents inflation and loading steps of the FE model. During the explicit analysis, inflation and loading steps are carried out simultaneously. Loading is done by displacement boundary condition applied to the road. The contact pressure at the end of this step shows an increase in the shoulder region of the tyre, shown in figure 3.2(a) and in the next step explicit rolling of the tyre has been carried out. The contact pressures are observed before and at the time of cleat impact across the treadband. Figure 3.2(b) shows that the pressure distribution is symmetric across the contact patch that ensures flat contact of tyre during straight rolling as it approaches the cleat. The line contact shown in figure 3.2(c) ensures impulse excitation across the treadband, which is responsible for flat excitation spectrum. Analogue plots of figure 3.2(b) and figure 3.2(c), are described in figure 3.2(d) and figure 3.2(e) respectively for 45° inclined cleat simulation.

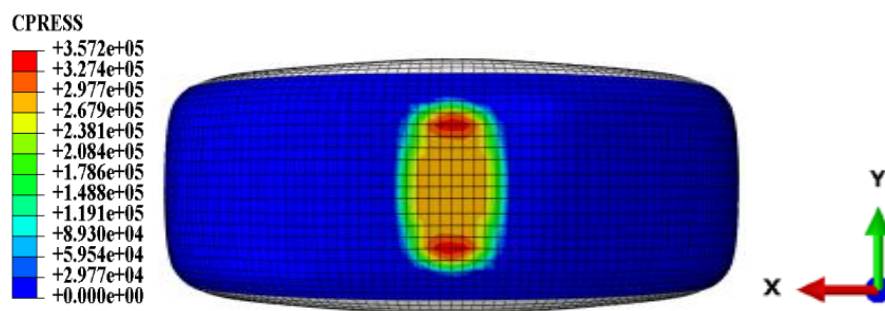


Figure 3.2(a) Contact pressure of stationary loaded tyre

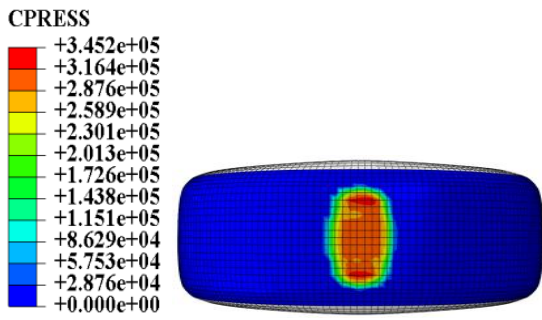


Figure 3.2(b) Contact pressure of rolling tyre just before straight cleat

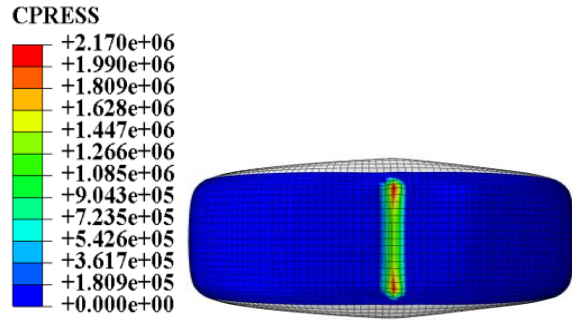


Figure 3.2(c) Contact pressure during straight cleat impact

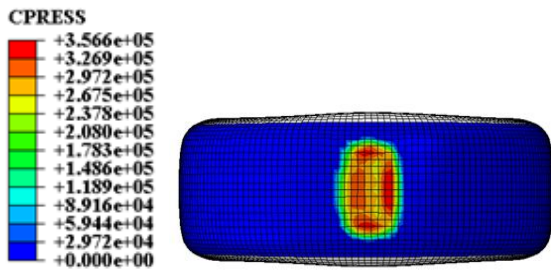


Figure 3.2(d) Contact pressure of rolling tyre just before 45° inclined cleat

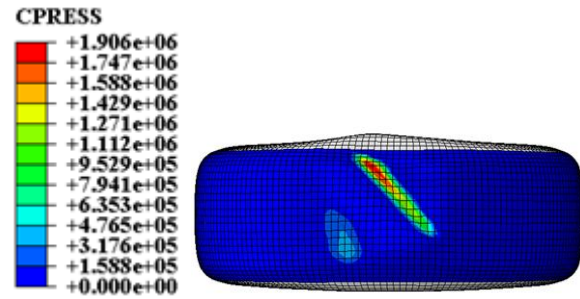


Figure 3.2(e) Contact pressure during 45° inclined cleat impact

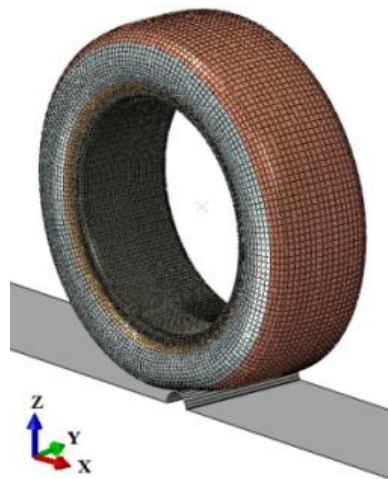


Figure 3.3(a) Tyre rolling over straight cleat road

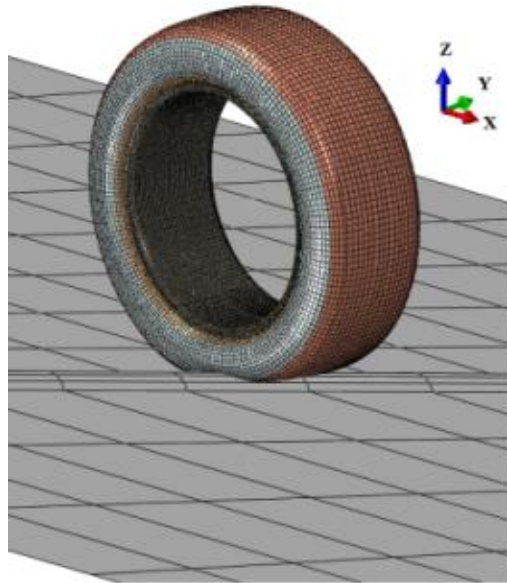


Figure 3.3(b) Tyre rolling over 45° inclined cleat road

Figure 3.3(a) and Figure 3.3(b) represent the simulation trials for the same operating conditions, over straight and 45° inclined cleats. The 45° inclined cleat is chosen to have equal excitation in longitudinal and lateral direction of the rolling tyre. The rim is modelled by rigid element outer surface definition and road modelled as rigid surface. The focus of the current research work is to predict structure borne vehicle interior noise due to tyre road interaction. One of the main noise source is the low frequency (<500 Hz) belt vibrations that contribute to the typical wheel rim dynamics in this region that transfer road excitation to the spindle. Above 500 Hz, the tyre vibration contribute significantly to the exterior noise (Sandberg and Ejsmont, 2002). Kiho Yum et al. (2007) used wave number decomposition method to study the influence of tyre size and shape on sound radiation in mid frequency range (500 Hz - 800 Hz) and reported that these frequency components can be transferred to vehicle interior by structural and air-borne path simultaneously. The sidewall vibration contribute more in the mid frequency range whereas tread vibration due to texture and tread impact contribute to the exterior noise in the frequency range between 800 Hz to 1500 Hz. Also tread pattern grooves in the tyre lead to other noise generation mechanisms such as pipe resonance, horn effect and so on. Hence smooth tyre is considered to eliminate the influence of tread pattern vibrations and tread groove resonances over the whole tyre vibrations. The spindle force and tyre structural vibration responses are obtained from the simulation results.

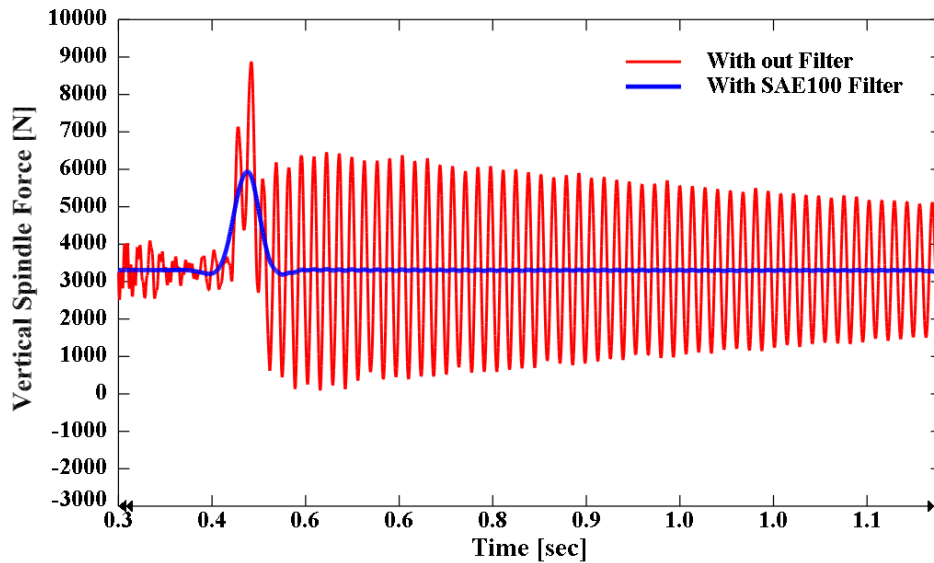


Figure 3.4 Vertical Spindle Force due to straight cleat impact excitation

During explicit rolling of tyre, the tread nodes are subjected to repeated impact as they come into contact with the road. The vertical force obtained at the spindle contains high frequency numerical noise components. Such oscillations are common in explicit analyses. Abaqus SAE100 Filter has been used to remove the noise. Figure 3.4 compares the variation of spindle force with and without the filter. It is clear that the peak at 0.5 sec is due to the impulse excitation of the cleat. The acceleration and vertical spindle force measurements are made with a sampling frequency of 2048 Hz. The acceleration responses in x, y and z directions with respect to the fixed global Cartesian references and time are obtained.

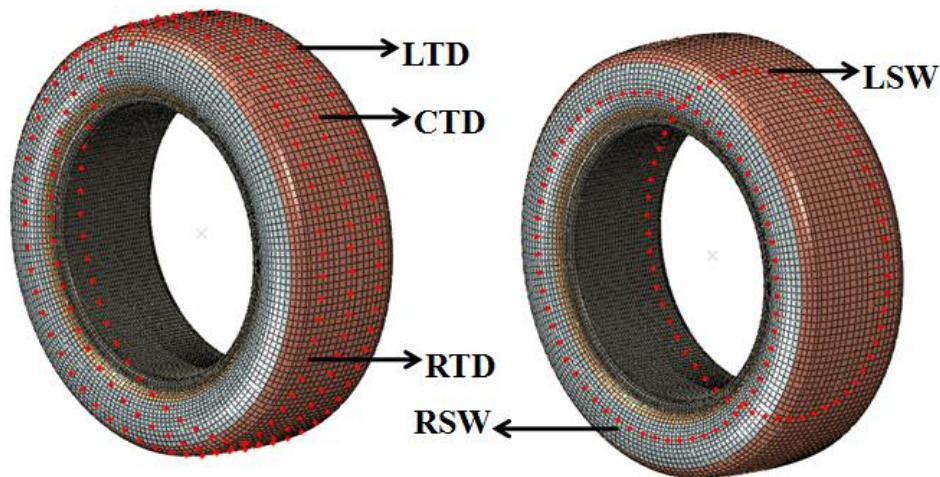


Figure 3.5 Acceleration measurement nodes of finite element tyre model

The measurements points are shown in Figure 3.5. RTD, CTD and LTD represent right, centre and left tread points whereas RSW and LSW represent right and left sidewall measurement points respectively. A wave can be represented with sufficient geometrical resolution if six or more points are measured per wavelength (Kindt, 2009). In the frequency range of interest (<500 Hz), in order to get higher circumferential mode number, a total of 300 points in five circles around the circumference of the tyre are considered for acceleration response measurements (60 nodes on each circle of the tyre). These output responses in x, y and z direction result in 900 signals. They are considered for further signal processing.

Secondly, these output responses are communicated to LMS Test Lab software, as if they have been acquired from 300 tri-axial accelerometers through a data acquisition system. Figure 3.6 shows the modal model geometry used for modal extraction where all these 900 signals are mapped to this model. As the energy content of the travelling wave is more in the leading edge than the trailing edge, three sets of reference signals (x, y and z direction signals) are chosen at the leading edge node point RTD60074.

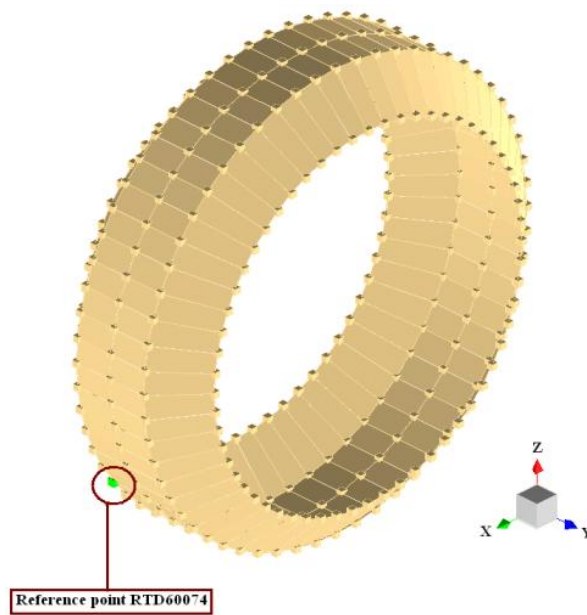


Figure 3.6 Modal model geometry for operational modal analysis

Table 3.2 represents the correlation of these reference signals with the response signals at the top of the tyre (CTD9041) and it is observed that vertical and longitudinal acceleration responses have good correlation with other measurement points and hence the point

(RTD60074) responses are considered to be reference signals for crosspower sum calculation. It is also confirmed that this point selection gives good cross correlation with other response signals in vertical and longitudinal directions. Representative data are shown in the Table 3.2. The amplitude and the phase of the crosspower sum are shown in figure 3.7 as a function of frequency up to 500 Hz.

Table 3.2 : Correlation study for selection of reference point

Reference	Response	Correlation (%)	Error (%)
RTD60074x	CTD9041x	91.58	9.21
	CTD9041y	66.39	50.62
	CTD9041z	92.76	7.84
RTD60074y	CTD9041x	70.19	42.48
	CTD9041y	32.48	207.90
	CTD9041z	68.22	46.59
RTD60074z	CTD9041x	90.78	10.19
	CTD9041y	80.45	24.31
	CTD9041z	95.36	4.86

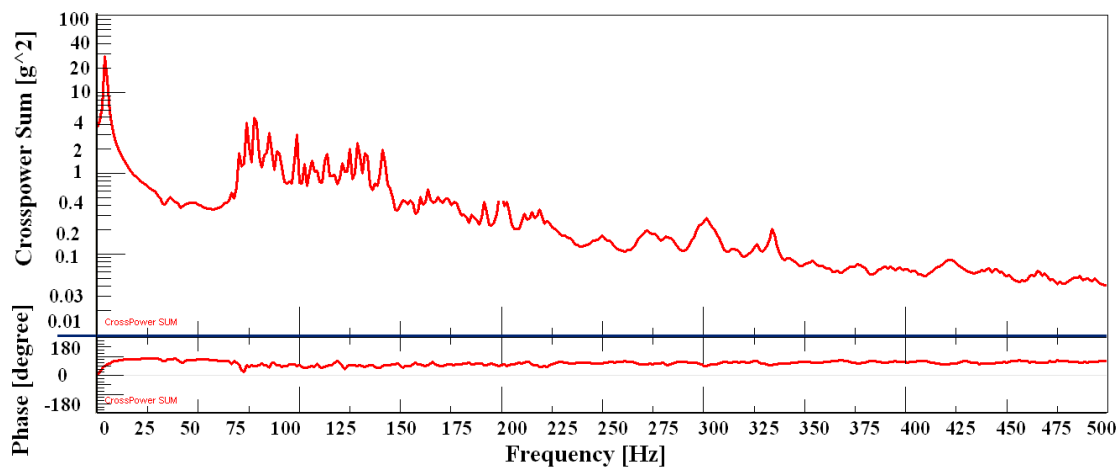


Figure 3.7 Crosspower sum

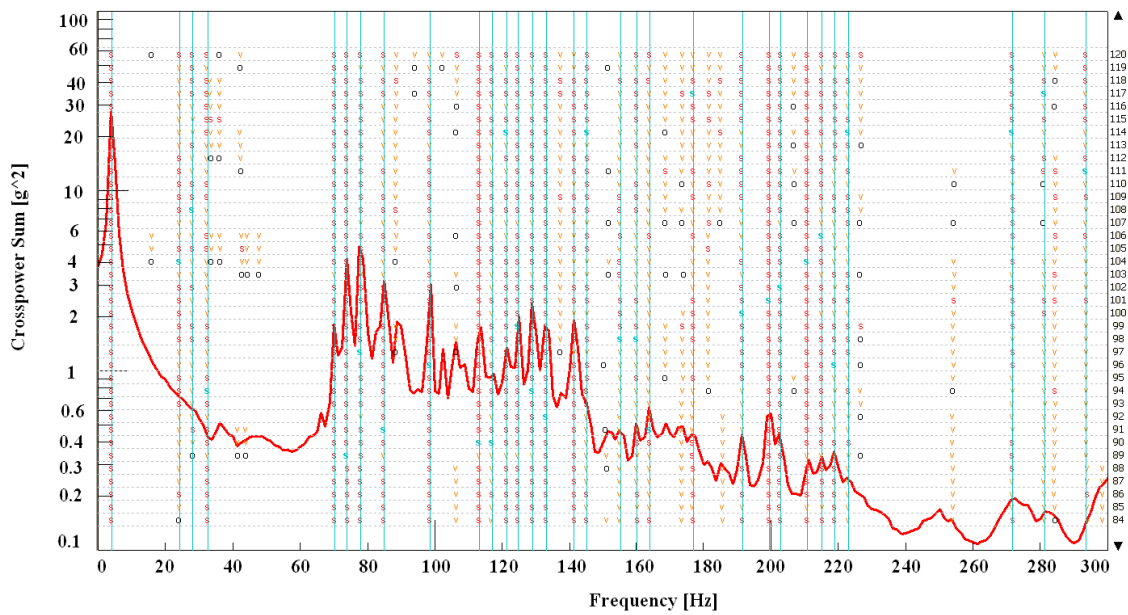


Figure 3.8(a) Stabilization diagram and pole selection by AMPS

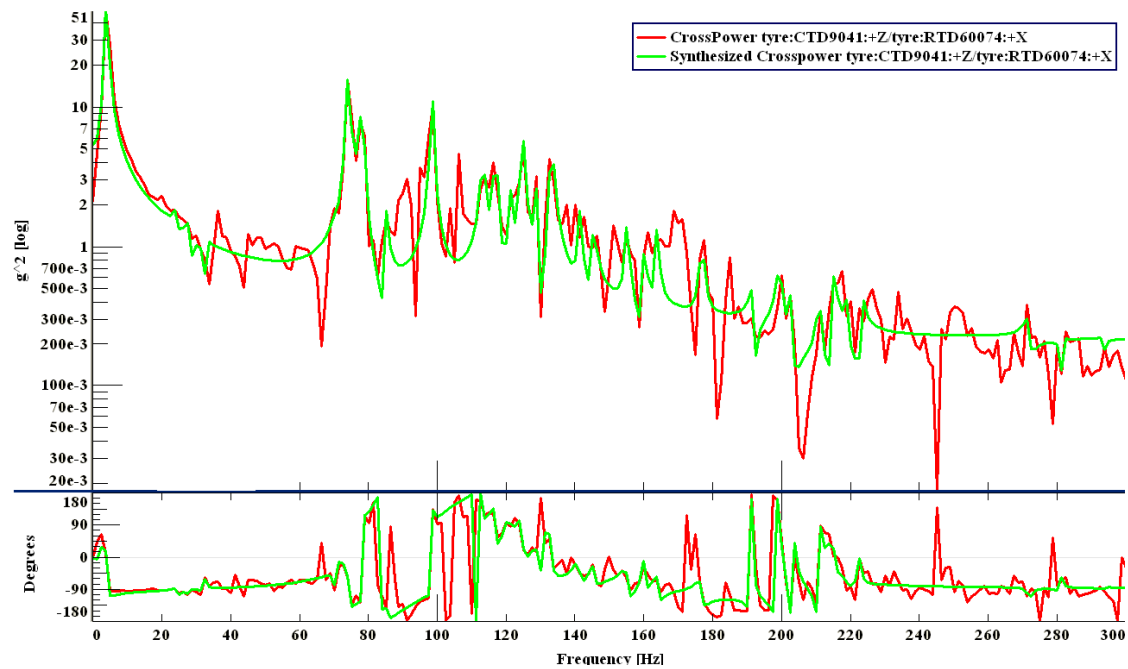


Figure 3.8(b) Comparison of operational and synthesized crosspower

The Polyreference least square complex exponential frequency domain algorithm (Guillaume,2003 and Peeters,2004) of LMS Test Lab software is used for modal extraction. The stabilization curve fit for crosspower sum of all spectrums is shown in Figure 3.8(a).The agreement between the operational and synthesised crosspower of the chosen reference with

the response for the physical modes obtained is good and the comparison of this operational and synthesised crosspower between the representative reference and response signal is shown in figure 3.8(b). It validates the modal frequency extraction procedure. Using Automatic Modal Parameter Selection (AMPS) tool, the physical modes are picked from the stabilization curve from which the modal frequencies, damping and mode shapes are obtained. In this procedure, the FE simulation model does not include the viscoelastic material property and the damping values obtained do not match with those reported by Kindt et al. (2007); however, the mode shapes and resonance frequencies closely match their results.

3.2.2 Steady State Transport Analysis of Rolling Tyre

Generally FE Modal analysis is carried out in order to validate the modal parameters obtained from EMA or vice versa. These methods were developed based on the important assumption that the system is linear, time invariant, observable and obeys reciprocity principle (Allemang, 1999). These results are useful to understand the standing wave pattern depicted by the mode shapes. Linear perturbation analysis of unloaded tyre gives repeated eigen values, called double poles. To understand the effect of loading, an eigen value analysis is performed on the inflated, loaded tyre which is fully constrained at wheel spindle interface of the rim. Loading of the tyre is achieved by displacing the road reference node towards the tyre. The established contact between the tyre tread surface and road surface induce large deformations at the treadband. The modal frequencies obtained are no more double poles; they split into two single poles due to loading. However, these large deformations along with the hyperelastic material definition, introduces non-linearity into the system. Also, it is questionable to use contact algorithms for eigen value extraction.

A relative kinematic theory was developed by Nackenhorst (1993) based on Arbitrary Lagrangian Eulerian (ALE) description. This theory is applied to solve large deformation rolling contact problem of elastic bodies using FE analysis. Readers can refer the paper published by Nackenhorst (1993) for theoretical foundation of ALE and application of FE method to solve rolling contact problem of elastic bodies (Nachenhorst, 2004). In this study, the commercial finite element code ABAQUS has been used for the steady state transport

analysis. The frictional and inertia effects are also accounted for in this analysis (Abaqus Technology Brief, 2011).

The steady state transport rolling analysis requires both rotational spinning velocity and translating ground velocity of the tyre. First, free rolling angular velocity is determined. A free rolling tyre generally travels farther in one revolution than the value determined by its centre height, but it is less than the value obtained from the radius of the unloaded tyre. The free rolling solution refers to an equilibrium solution for a rolling tyre that has zero torque applied around the axis of the tyre. An equilibrium solution with a non-zero torque is referred to either as braking or as traction depending on the sense of the torque. If the resultant torque opposes the direction of angular velocity of free rolling solution the state is referred to as braking and if the resultant torque acts in the same direction as the angular velocity of free rolling solution it is referred to as traction. Full braking or traction occurs when all the contact points between the tyre and the road are in a state of slip (Abaqus Documentation 6-12, 2011). Hence, from the unloaded and loaded tyre radius, the angular velocities for braking state and traction state are determined for the ground velocity of 28.3 kmph.

Then for the fixed ground velocity, a series of steady state solutions are obtained between the state of braking and the state of traction, by gradually increasing the angular velocity. Thus the free rolling angular velocity is found to be 25.3 rad/s, corresponding to the zero tangential reaction force at the contact interface. Finally, the steady state transport analysis is performed, and complex eigen frequencies are extracted for a free rolling tyre, using Lanczos solver for the frequency range up to 300 Hz (Abaqus Technology Brief, 2011).

3.3. VALIDATION OF RESULTS

3.3.1 Description of Structural tyre model of Kindt et al. (2009)

Kindt et al. (2009) have developed a Finite Element structural tyre model shown in figure 3.9 based on flexible ring on an elastic foundation for the prediction of structure borne interior vehicle noise that validate up to 300Hz (i.e. below (n,2)modes).

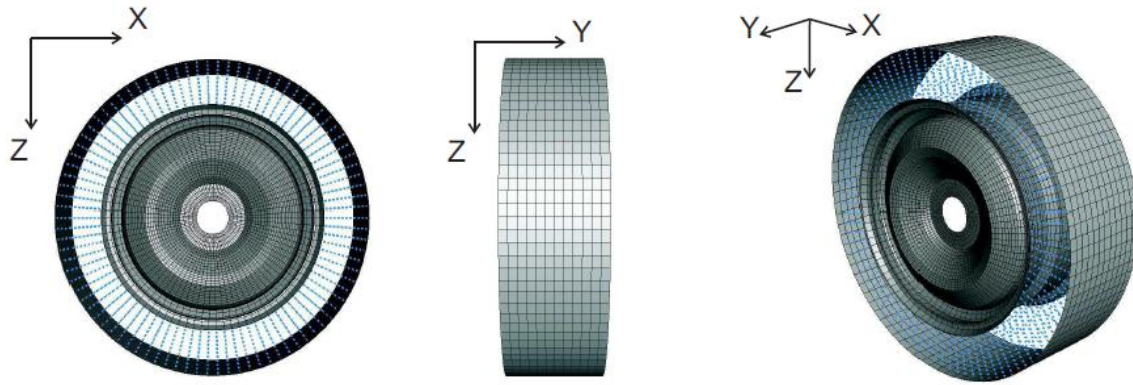


Figure 3.9 Fully assembled tyre-wheel model
(Cavity mesh is not shown) P Kindt,(2009)

This model includes wheel, treadband ring, and tyre sidewall and air cavity sub models. However, this model is not a complete fundamental FE tyre model and the characterization of the sidewall is done through an analytical approach. Isotropic material property is used for the treadband ring. The sidewall is represented by spring elements. The equivalent sidewall mass is divided into two halves and added to the treadband and wheel rim. The radial, tangential and axial stiffness parameters of sidewall spring are determined from the natural frequencies of (1, 0) mode, torsional mode and axial mode respectively. These modes were obtained from experimental modal analysis (EMA). The Young's modulus was tuned by adjusting its value in order to reduce the error on the predicted natural frequencies of the model. Also, they have considered orthotropic material model definition and found that this has a higher influence on cross sectional modes (n, 1), compared to the circumferential modes (n, 0). The difference between the resonance frequencies of the model with isotropic and orthotropic treadband becomes larger as the index 'n' increases. They used the results obtained from this tyre model with isotropic material definition to compare the experimental modal analysis results of unloaded and loaded tyre to study dynamic behaviour of loaded tyre. However the rolling tyre modal results of the model were not reported. They determined the rolling tyre modal parameters from the cleat impact test from their state-of-the-art, experimental set up of tyre-on- tyre arrangement followed by Operational Modal Analysis (OMA). They have observed circumferential modes up to (5, 0) and only one cross sectional mode (2, 1). The experimental results reported by them have been taken to compare the rolling tyre modal parameters obtained from the procedure reported in this thesis.

3.3.2 Comparison of rolling tyre modal results

In this work, the tire considered is very similar to that used by Kindt et al. (2009), though the exact tyre used is not available. As the tyre does not have tread blocks and the construction of the tyres in this range is standard and the results may not vary drastically.

Table 3.3 represents the comparison of determined rolling tyre modal frequencies with the experimental results reported by Kindt et al. From the straight cleat simulation only circumferential modes are obtained and from inclined cleat simulation, in addition to the circumferential modes, cross sectional modes (2, 1) and (3, 1) are also obtained. Table 3.3 shows a comparison between the experimental results and the results obtained from the procedure followed in this thesis. A deviation of the current simulation results from the experiment is within 0.6 % to 12 %. This clearly shows that the values obtained by the current procedure compares very well with the published experimental results.

Table 3.3 Comparison of Experimental and FEA-OMA Rolling Tyre Results

Resonance frequencies in Hz			
Modes	P. Kindt et. al.[30] Experiment-OMA	Finite Element -OMA	Percentage Deviation
(1,0) hor.	--	84.90	--
(1,0)vert.	81.83	74.18	9.35
(2,0)0	102.98	98.51	4.34
(2,0)extr.	113.94	113.24	0.61
(3,0)0	124.09	109.37	11.86
(3,0)extr.	139.33	125.40	10.00
(4,0)0	151.76	141.39	6.83
(4,0)extr.	167.52	159.27	4.92
(5,0)0	182.70	160.25	12.29
(5,0)extr.	198.88	176.94	11.03
*(2,1)0	96.09	*88.88	7.50
*(2,1)extr.	91.29	*80.45	11.87
*(3,1)0	--	*135.36	--
*(3,1)extr.	--	*119.96	--

-- not identified modes * obtained from inclined cleat test

3.4. RESULTS AND DISCUSSION

It is necessary to excite the rolling tyre sufficiently in order to invoke complete modal behaviour. Figure 3.10(a) and 3.10(b) show the spindle force excitation and power spectral density functions (PSD) in longitudinal, lateral and vertical directions. Straight cleat impact simulation adequately excites all the circumferential bending modes of the tyre belt vibration. As the tyre rolls over the cleat, the observed excitation is neither longitudinal nor vertical, but a combination of both. The longitudinal and vertical spindle force excitation energy is significant till 300 Hz. As observed by Kindt et al.(2009), the oscillations of the spindle forces in the longitudinal direction are damped. The frequency of 32.54 Hz corresponds to the torsional tyre mode. It can also be noted that circumferential modes, up to (7, 0) are excited. Also, it is clear that no significant excitation takes place in the lateral direction during the impact. Hence, another simulation with 45° inclined cleat has been carried out to achieve lateral excitation.

Figure 3.11(a) (spindle force excitation) and Figure 3.11(b) (power spectral density functions) show significant lateral excitation, offered by an inclined cleat. In this case, as seen from 3.11(b), some of the cross sectional bending modes of the tyre are obtained in the frequency range between 270Hz and 340 Hz. Also cross sectional rotational modes (2,1)0, (2,1)extr, (3,1)0, and(3,1)extr are excited. However, circumferential modes (4, 0)0, (6,0)extr and (7,0)0 that are identified from straight cleat test, are not excited.

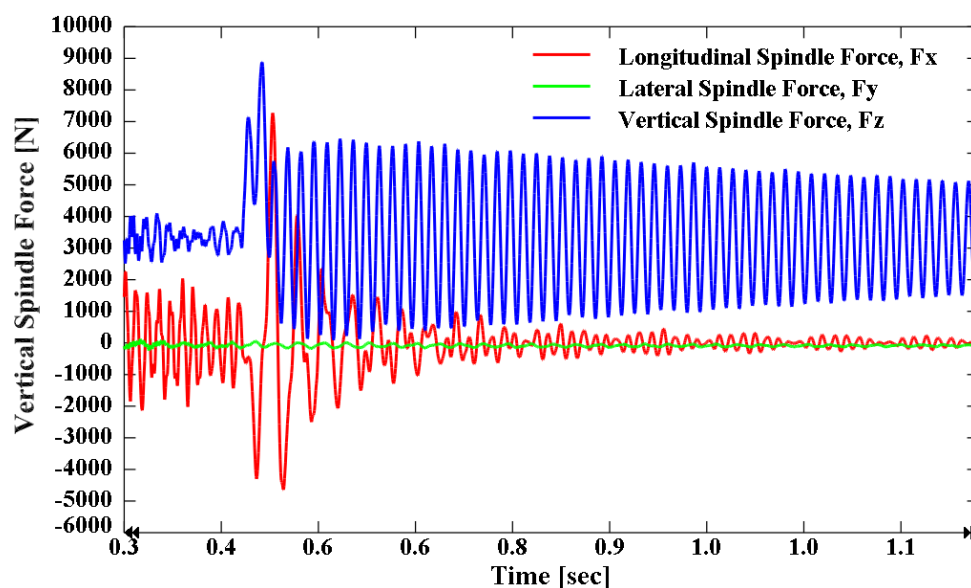


Figure 3.10(a) Straight cleat impact excitation

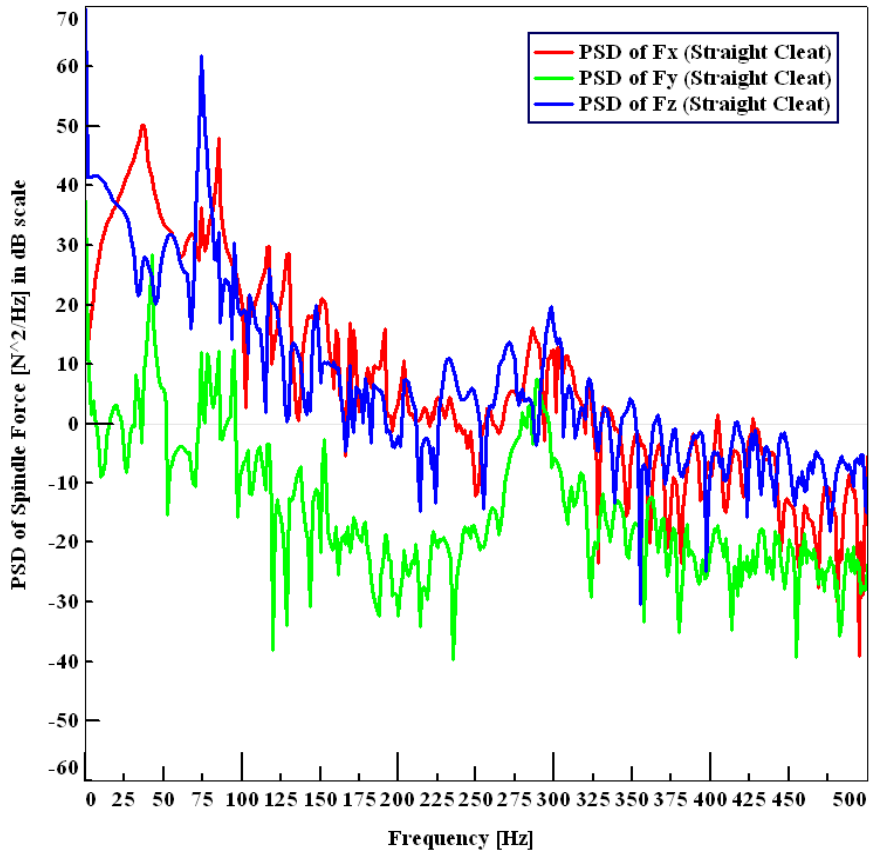


Figure 3.10(b) PSD of spindle force due to straight cleat impact

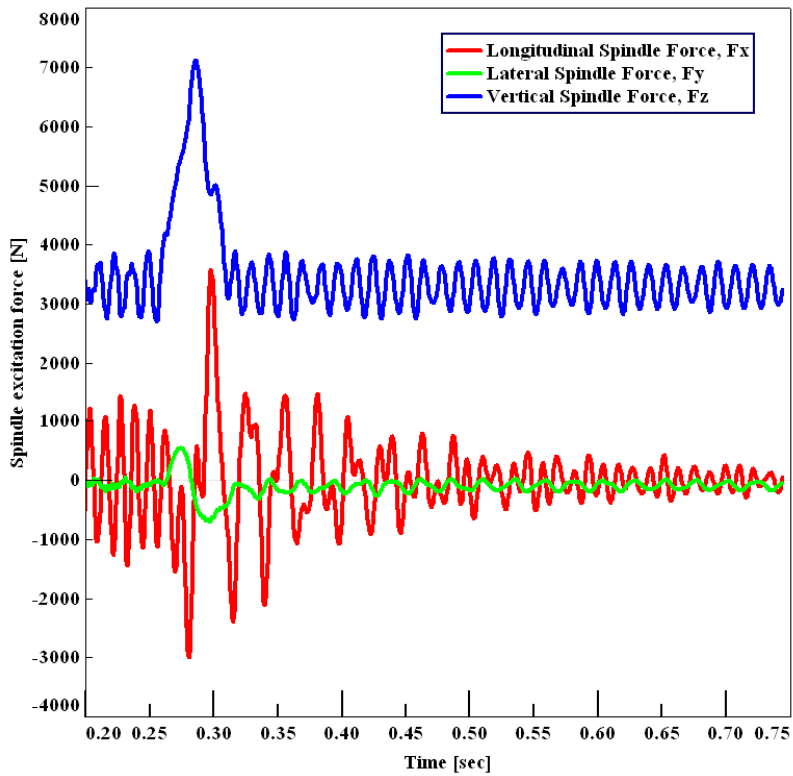


Figure 3.11(a) 45° Inclinced cleat impact excitation

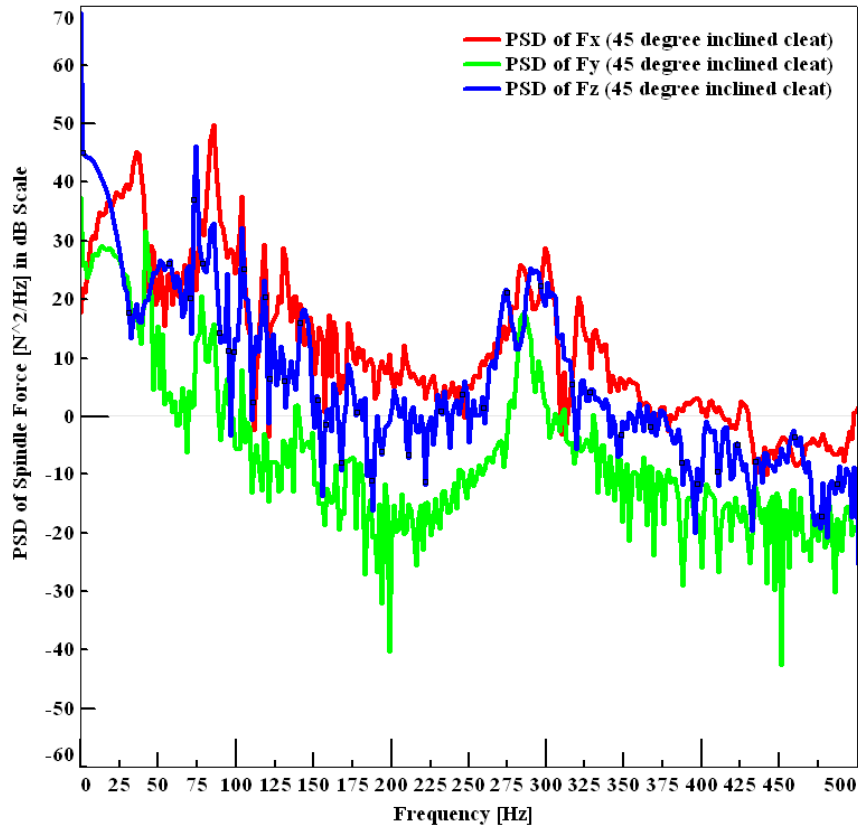


Figure 3.11(b) PSD of spindle force due to 45° inclined cleat impact

Figure 3.12 and Figure 3.13 show mode shapes and the corresponding resonance frequencies obtained from these straight and inclined cleat tests. Modes are represented by (n,m); 'n' - refers to circumferential mode index and 'm' refers to axial bending mode index. According to Kindt et al.,(2009), it is clear that breathing mode refers to first longitudinal mode at n= 0; and this appears for m=1,2 which is normally observed at higher frequencies. This breathing mode is not captured and a "mode (0, 0)", is identified at 4 Hz and is due to the rolling speed of the tyre model. This "mode" is hardly reported in the literature. Also it is verified, for different speeds the existence of this mode.

Figure 3.14 shows the corresponding rolling speed frequencies and these frequencies are tabulated in Table 3.4. Further it is supported from Figure 3.15, that the rolling speed frequency is independent of inflation pressure. Except rolling speed frequency other modal frequencies vary as a function of inflation pressure as observed in Table 3.5. The (1,0) vertical mode at 74 Hz indicates that the belt behaves as a rigid surface and moves in the vertical direction in the wheel plane. The (2,0) mode at 100 Hz is the first deformation belt mode.



Figure 3.12 Operational modal parameters obtained from straight cleat impact test

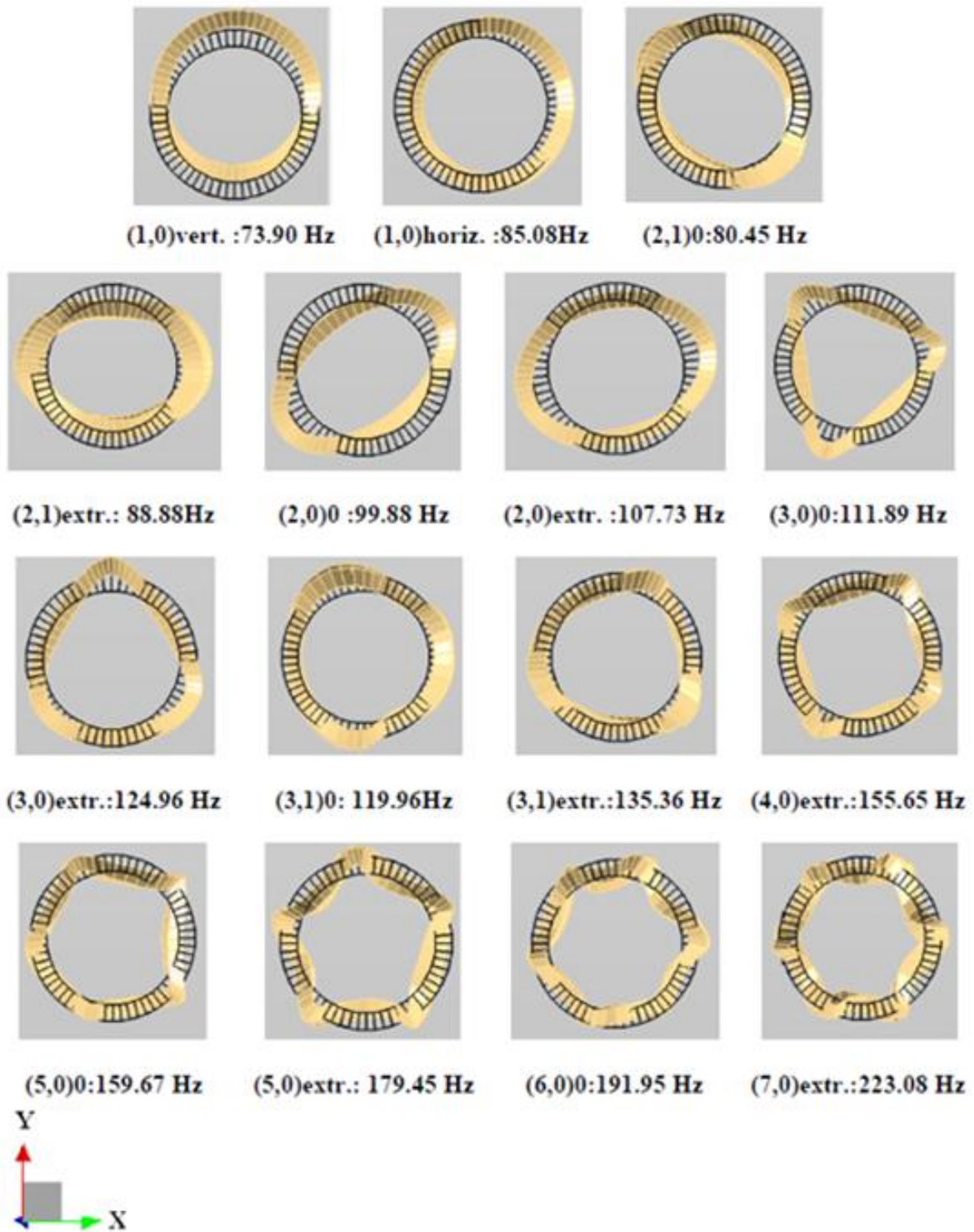


Figure 3.13 Operational modal parameters obtained from 45° inclined cleat impact test

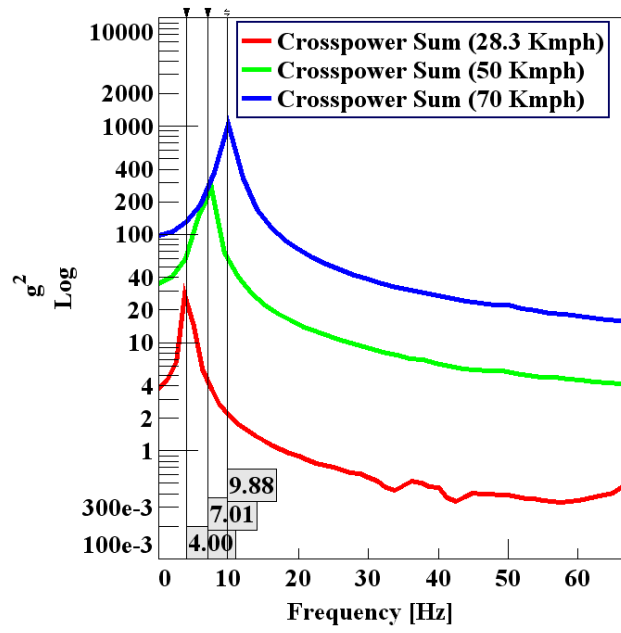


Figure 3.14 Variation of rolling frequency with vehicle speed

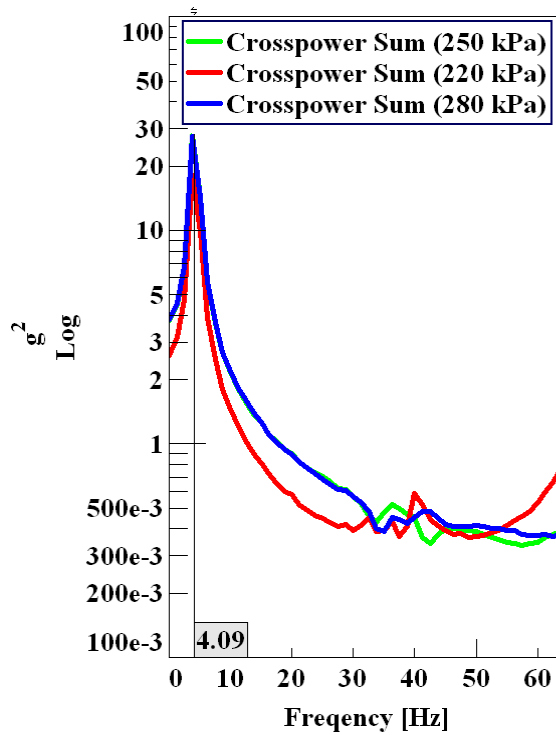


Figure 3.15 Variation of rolling frequency as function with inflation pressure for 28.3 kmph

Table 3.4 Frequency of tyre rolling speed as function of speed

Rolling Frequency (Hz)	Vehicle Speed					
	28.3 kmph		50 kmph		70 kmph	
	Calculated	From OMA	Calculated	From OMA	Calculated	From OMA
	3.93	4	6.95	7.01	9.78	9.88

Table 3.5 Operational modal frequencies for speed of 28.3kmph as function of Inflation Pressure

Mode Shape (OMA results)	Inflation Pressure		
	220 kPa	250 kPa	280 kPa
Mode(1,0)vert.	71.05	74.18	76.93
Mode(1,0)horiz.	81.65	84.89	88.09
Mode(2,0)0	94.87	98.51	104.70
Mode(2,0)extr	-	113.24	-
Mode(3,0)0	107.14	109.37	116.66
Mode(3,0)extr	119.32	125.40	130.59
Mode(4,0)0	123.53	141.39	151.27
Mode(4,0)extr	148.72	159.27	163.41

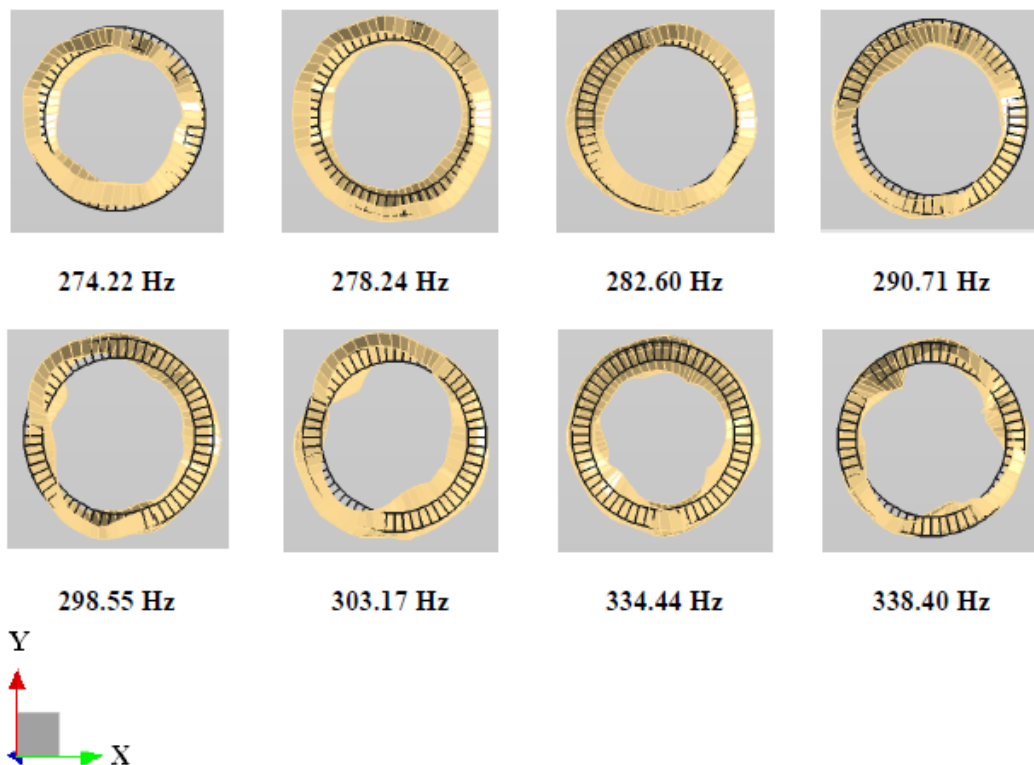


Figure 3.16 Cross sectional bending modes due to 45° inclined cleat impact test

Figure 3.16 shows the cross sectional bending modes (n,2), obtained from the inclined cleat test. Kindt et al.(2009) have reported that in general, the start of cross sectional bending modes is approximately 300 Hz. The actual frequency, at which the first (n,2) mode appears, needless to say, depends on the tyre. However, for most tyres the onset of this mode appears in the frequency range of the (10,0) mode. The first (n,2) mode is seen at 274 Hz. The modal parameter results except for the damping values are similar to the findings of Kindt et al.(2009). It is observed from their results that sidewall dynamic behaviour depends on the tread dynamic behaviour up to 300Hz.

3.4.1 Comparison of Mode Shapes obtained by different methods

The results obtained from operational modal analysis are compared with the mode shapes obtained from stationary unloaded , stationary loaded , steady state transport rolling tyre. Figure 3.17 summaries the circumferential bending modes of the tyre model at different conditions. It is observed that, except for the unloaded stationary tyre's mode shapes, two different frequencies exist for the same mode shape. This is due to the effect of loading and rolling of the tyre.

Comparison of only the (n,0) modes (circumferential bending modes) is shown in figure 3.17. These modes are the predominant modes and are excited during rolling of the tyre. These modes are obtained by straight cleat impact test simulation, which excites the belt along its entire width. Moreover, (n,1) modes (cross sectional modes) might not have been excited. However, for other procedures, in addition to the circumferential bending modes, cross sectional tilting and bending modes viz., (n,1) and (n,2) modes are also obtained. In reality, during operational conditions all these modes may or may not be excited but the obtained modes give a complete idea about the modal behaviour of the tyre.

The effect of loading and rolling makes all the circumferential mode number 'n' larger than zero, to split into two resonance frequencies and that refers to (ω_{n1}) backward travelling wave, travelling in the opposite direction to the tyre rotation and (ω_{n2}) forward travelling wave that travels in the same direction as of the tyre rotation. In this modal simulation, travelling waves are observed with respect to a fixed reference system, where in $\omega_{n1} < \omega_{n2}$ is

observed and this effect is known as Doppler shift. In addition to the difference in eigen values marked by Doppler shift, frequency veering is contributed by the Coriolis effect. It is evidently seen even in case of an unloaded rotating tyre in the co-rotating and stationary reference frame. The Coriolis effect contributes to the frequency veering (Kindt,2009). Table 3.6 gives the effect of loading and rolling of the tyre with respect to their unloaded double poles.



Figure 3.17 Mode shape comparison among various tyre conditions

Table 3.6: Comparison of circumferential and cross sectional modes and the effect of loading and rolling over natural frequencies of a tyre

Modal frequencies are in Hz

Modes	FEA Unloaded	FEA Loaded	SST Rolling	OMA Rolling
Mode(1,0)	71.29	56.71	56.84	74.18
		76.57	76.30	84.90
Mode(2,0)	99.93	92.68	91.10	98.51
		108.89	105.13	113.24
Mode(3,0)	127.53	122.58	--	109.37
		138.71	119.74	125.40
Mode(4,0)	155.53	149.75	132.74	141.39
		167.72	145.84	159.27
Mode(5,0)	183.06	185.95	--	160.25
		195.28	161.52	176.94
Mode(6,0)	209.02	209.94	--	191.55
		219.62	177.74	202.80
Mode(7,0)	232.22	231.39	189.83	215.26
		239.36	198.13	223.08
Mode (2,1)	93.4	95.46	99.16	*88.88
		80.96	78.22	*80.45
Mode (3,1)	138.82	138.24	--	*135.36
		127.76	120.33	*119.96
Mode (4,1)	170.14	168.98	150.45	--
		160.90	142.62	--
Mode (5,1)	193.78	192.09	183.67	--
		184.05	163.30	--

-- not identified modes

* obtained from inclined cleat test

Figure 3.18a and 3.18b show the dispersion curves of circumferential and cross sectional modes respectively, for different conditions of the tyre modal results obtained from FE modal analysis and OMA.

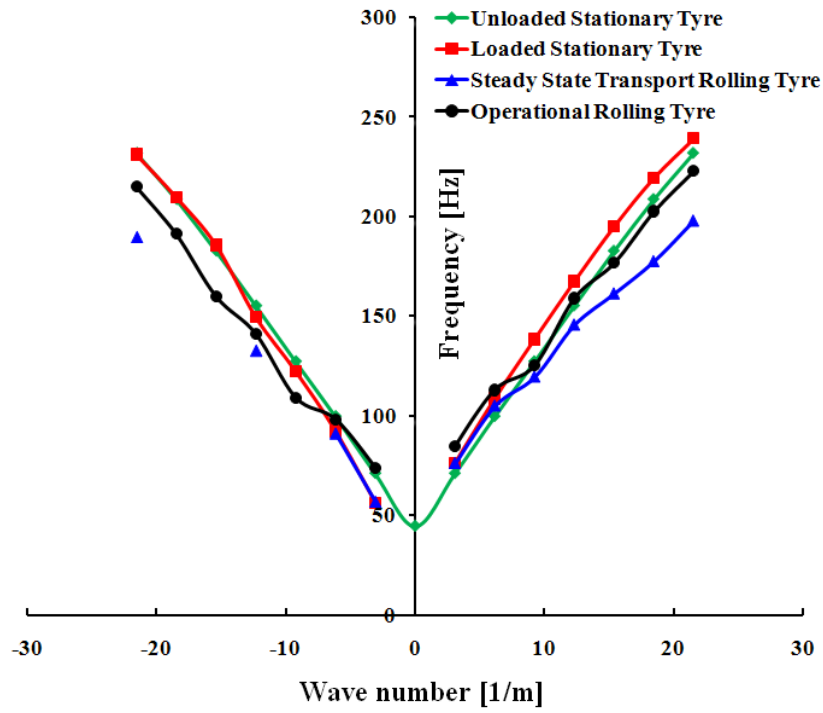


Figure 3.18a Comparison of circumferential modes dispersion curves

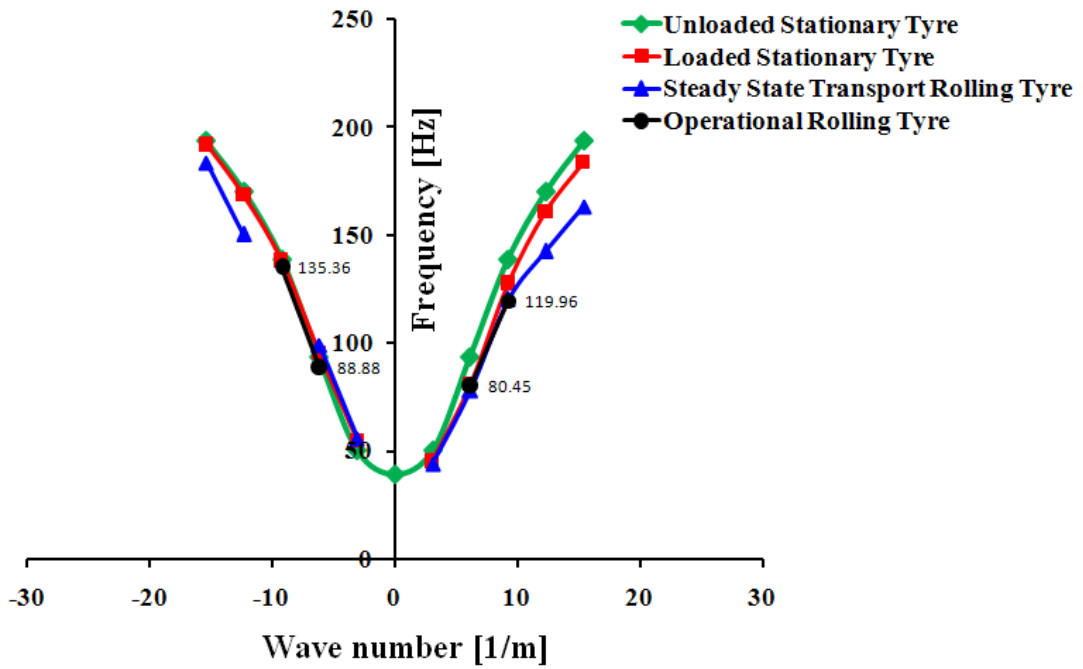


Figure 3.18b Comparison of cross sectional modes dispersion curves

The dispersion curve of unloaded stationary tyre is symmetric due to double poles ($\omega_{n1} = \omega_{n2}$). The loading of the tyre causes splitting of real valued eigen modes into forward and backward waves travelling with a complex valued eigen modes. The shift in natural frequency of forward travelling wave is more than the backward travelling wave when compared to its standing wave natural frequency. In a similar way, a procedure is followed to describe the effect of rolling on the tyre modal behaviour. It predicts a clear splitting of standing wave into two travelling waves as reported by Kindt et al.(2009).

3.5. SUMMARY

Integration of vibration results from cleat impact simulation of a FE rolling tyre model, with OMA technique has been accomplished successfully. Circumferential bending modes are obtained from straight cleat impact simulation. Additionally, cross sectional bending modes are obtained from 45° inclined cleat simulations. Modal frequencies extracted from OMA clearly show the splitting of real eigen modes of an unloaded stationary tyre into two opposite travelling complex eigen mode waves. The results are compared with the published experimental results and a good comparison has been noted. This established procedure can be applied to study dynamic behaviour of tyre under various operation conditions in order to understand the vehicle interior and exterior noise due to tyre/road interaction.

CHAPTER 4

EXPERIMENTAL TRANSFER PATH ANALYSIS FOR STRUCTURE BORNE VEHICLE INTERIOR NOISE

4.1 INTRODUCTION

Modern vehicles have implemented good preventive and control measures for power unit and aerodynamic NVH. Hence, the tyre/road interaction has become a dominant source. Riegel and Wiedemann (2008) reported the dominance of tyre/road interaction over engine and wind sources, in contributing to the vehicle interior noise. Hamet, Klein and Lelong (2005) made the following observations: “vehicle noise emission starts with the power unit noise, and as the speed increases so does the tyre/road interaction noise”. The speed at which the vehicle tyre/road interaction noise dominates over the power unit noise is called as cross-over speed. This cross-over speed ranges from 15kmph to 20 kmph for cruising and 30 to 45 kmph for accelerating passenger cars respectively. As mentioned earlier, vehicle interior noise due to tyre/road interaction consists of two components, namely structure borne noise and air borne noise. Transfer Path Analysis (TPA) is a tool to identify whether the source or transmission path needs to be altered for reducing the cabin noise. This chapter describes the successful implementation of experimental TPA to synthesize structure borne vehicle interior noise due to tyre/road interaction on a sedan class passenger car.

4.2 MECHANISM OF STRUCTURE BORNE INTERIOR NOISE

During tyre/road interaction, road undulations cause excitation at the tyre contact patch. This excitation is a time varying force of a wide spectrum. The energy of this force spectrum enters into the tyre wheel assembly and further transmitted through the suspension and the lower arm to the vehicle body, which in turn vibrates the body structure and windows of the vehicle. This vibration excites the cabin cavity and thus creates a low frequency annoying

structure borne interior noise known as road noise. The low frequency excitation to the spindle is mainly due to belt package vibration of the treadband. According to Pinnington and Briscoe (2002) rolling tire vibration exhibits complex modal behavior in the low frequency range i.e. below 400Hz. When the natural frequencies of these travelling waves of complex modes coincide with the road excitation frequencies, the tyre belt resonance occurs and due to this, high amplitude low frequency excitation is imparted to the spindle.

4.3 EXPERIMENTAL SET UP AND MEASUREMENTS

4.3.1 Laboratory tests

Figure 4.1 shows the test vehicle and laboratory experimental set up for TPA. Tata Indigo, a sedan class passenger car with radial tyres is used for testing. A three ton capacity lift post is used to lift the vehicle. All the four tyre wheel assembly are removed and the necessary safety precautions are taken. The sensors mount points are cleaned. After installing the microphones inside the vehicle at target positions, all doors and windows were closed to ensure leak proof cabin. The translational degrees of freedom (DOF) of all the four wheel rim-spindle interface points are considered to be the energy transfer paths and thus the twelve structural path indicators for the vehicle have been defined. It is recommended that, a minimum of (Application Note Transfer path analysis, LMS International,1998) two additional indicator points for each path is required to ensure good quality estimation of operational forces. Hence two additional points with three translational DOF per point has been included. One sensor is mounted at the suspension bracket while the other is attached to the lower arm. In the laboratory set up, the acceleration responses are measured at these indicator points (wheel rim spindle interface, suspension bracket and lower arm) by exciting the paths (rim spindle interface) using an instrumented hammer. Figure 4.2 and Figure 4.3 show the accelerometers and microphone positions respectively during the laboratory tests. Three translational excitations per wheel spindle interface are given at one of the bolt heads, which is fastened rigidly at the rim spindle interface as shown in Figure 4.2.



Figure 4.1 Laboratory experimental set up for TPA

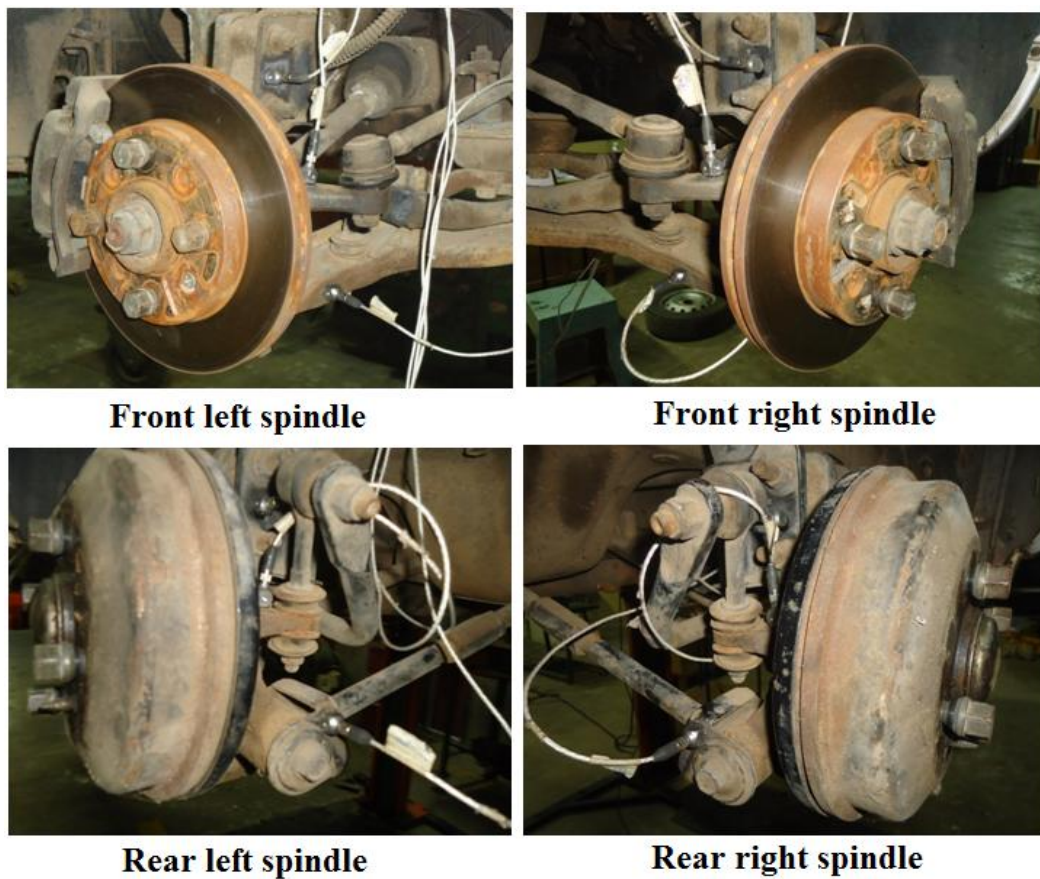


Figure 4.2 Position of accelerators

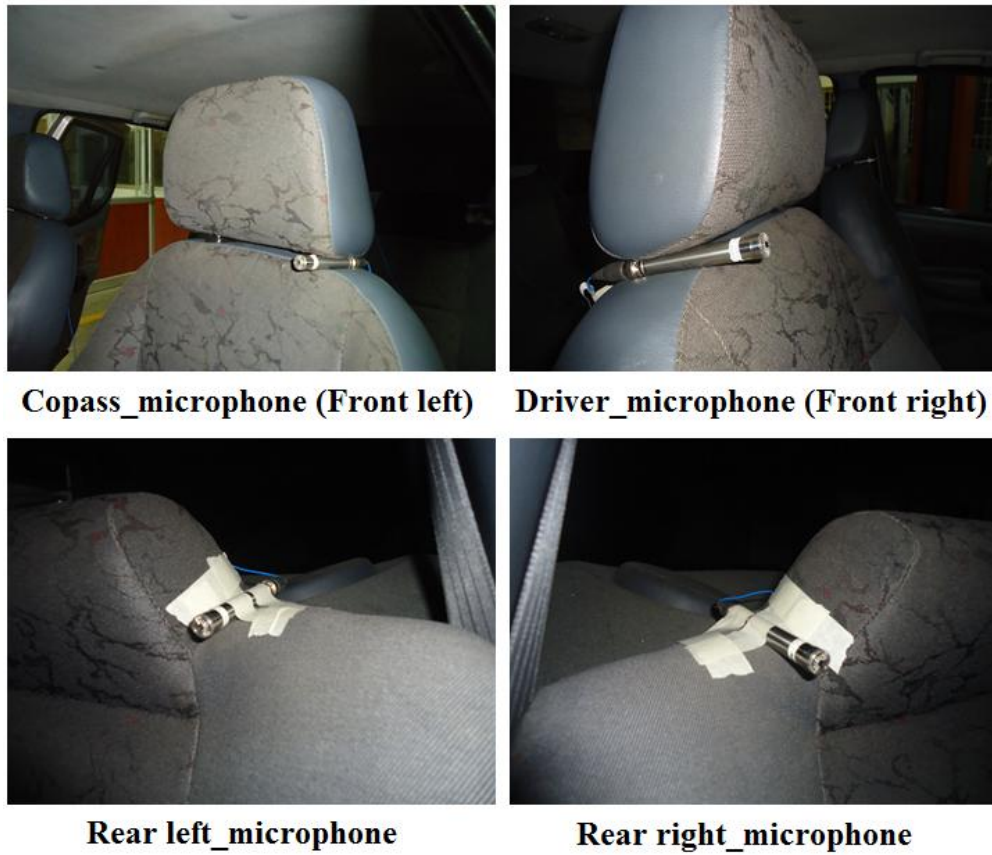


Figure 4.3 Position of interior microphones

From these measurements, the local structural FRFs matrix $[Y_{42}^V]$, among the path indicators and between the paths and the additional indicators are determined. Simultaneously, the Noise Transfer Functions (NTFs) $[Y_{32}^V]$ between the paths and target microphone's position at driver's right ear, co-passenger left ear, rear right and rear left passenger's window sides are also calculated from the interior pressure measurement for the same impulse excitations at the path indicators. Figure 4.4 shows the drive point coherences along with the local structural FRFs of all the path indicators. This ensures that the responses measured at the path and additional indicators are due to the given input impulse excitations. Figure 4.5 shows the NTFs and the corresponding coherence values between driver's right ear microphone position and all the twelve paths. The coherence values are close to one corresponding to the peaks observed in the NTFs. The NTFs of other target locations and the corresponding coherence values are given in Appendix I. Figures 4.6a to 4.6d, represent a sample of local structural FRFs of all the twelve path indicators due to the excitation in the longitudinal direction at front left, front right, rear right and rear left rim spindle interface bolt head points. From Figures (4.6a and 4.6b), the existence of partial coherence between front left and front right spindle can be observed. It means the excitation at front left rim spindle interface correlate to

the responses measured at front right indicators. Hence, either side excitation at vehicle front spindles give good coherence values, where as they do not correlate well with the rear spindle responses. Similarly, from Figures (4.6c and 4.6d), the existence of partial coherence between rear right and rear left spindle can be observed and they do not correlate well with the vehicle's front spindle responses.

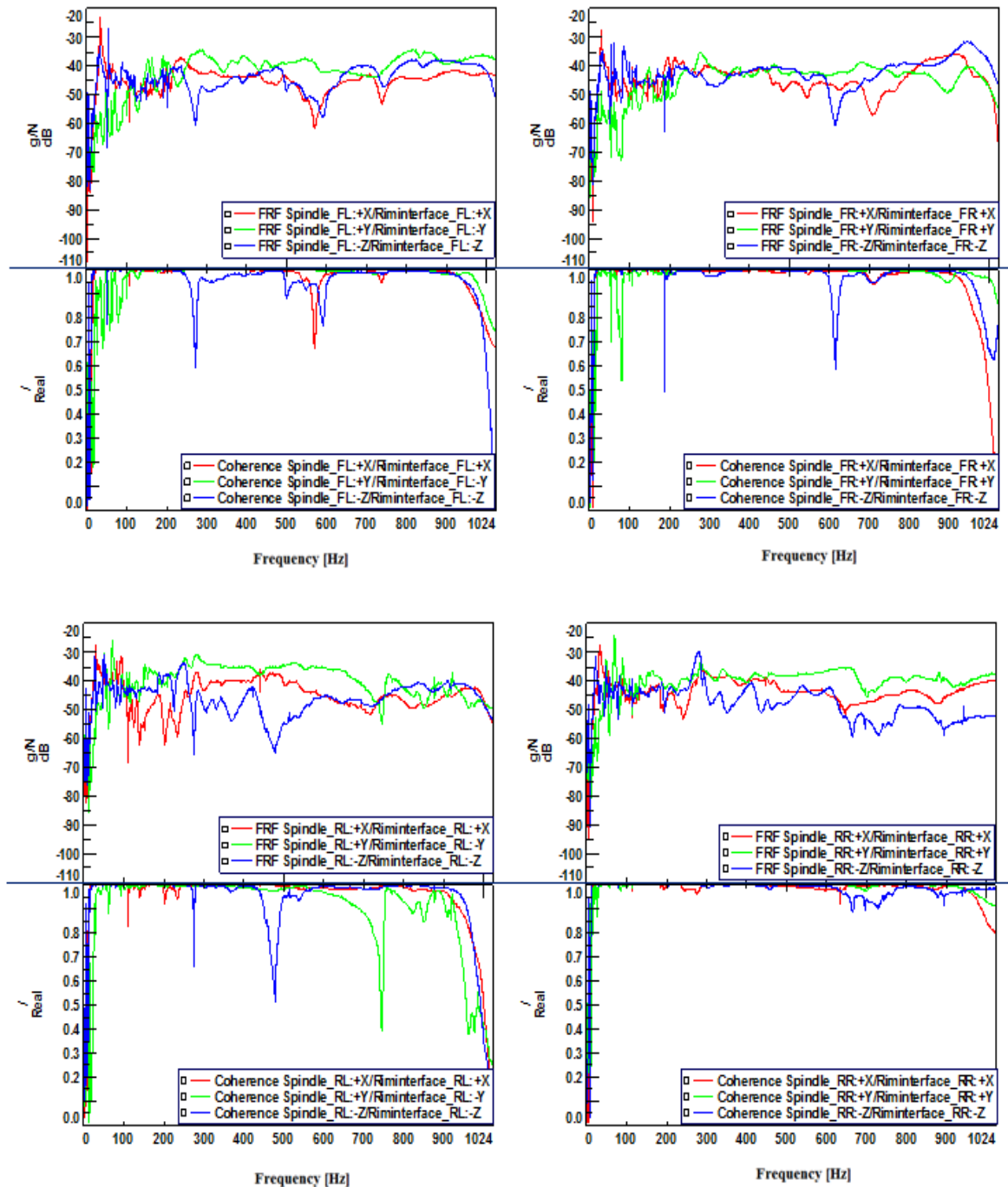


Figure 4.4 Drive point coherences and local structural FRFs for vehicle

Similar observations are verified for the given excitation in the lateral and the vertical direction at front left, front right, rear right and rear left rim spindle interface bolt head points and these are reported in the Appendix I. This necessitates the use of multi reference TPA problem. The mathematical background of multi reference TPA followed in this thesis work for prediction of road noise is explained in the Appendix II

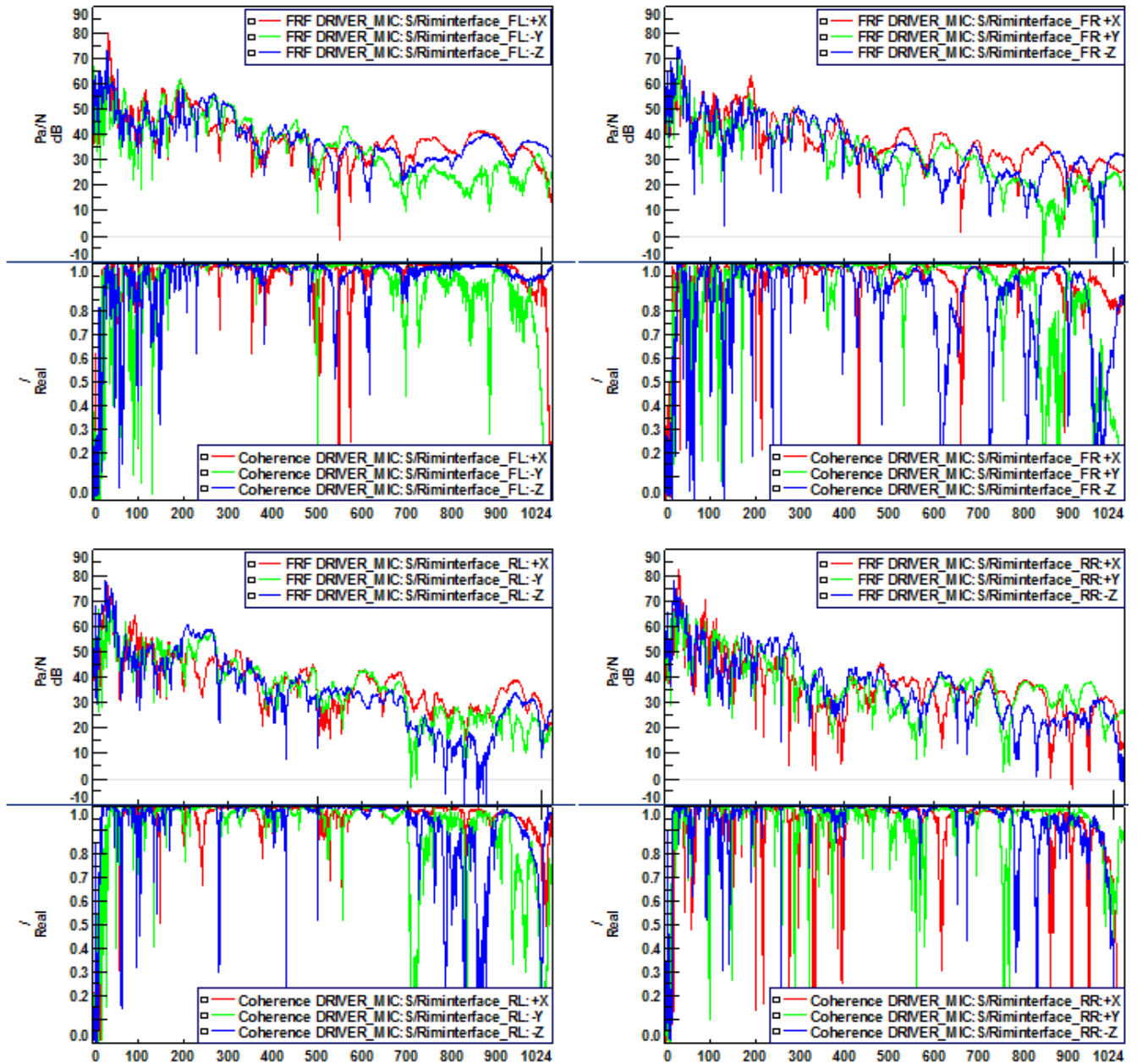


Figure 4.5 Variation of NTFs between all paths and driver's right ear position and the corresponding coherence functions as function of frequency

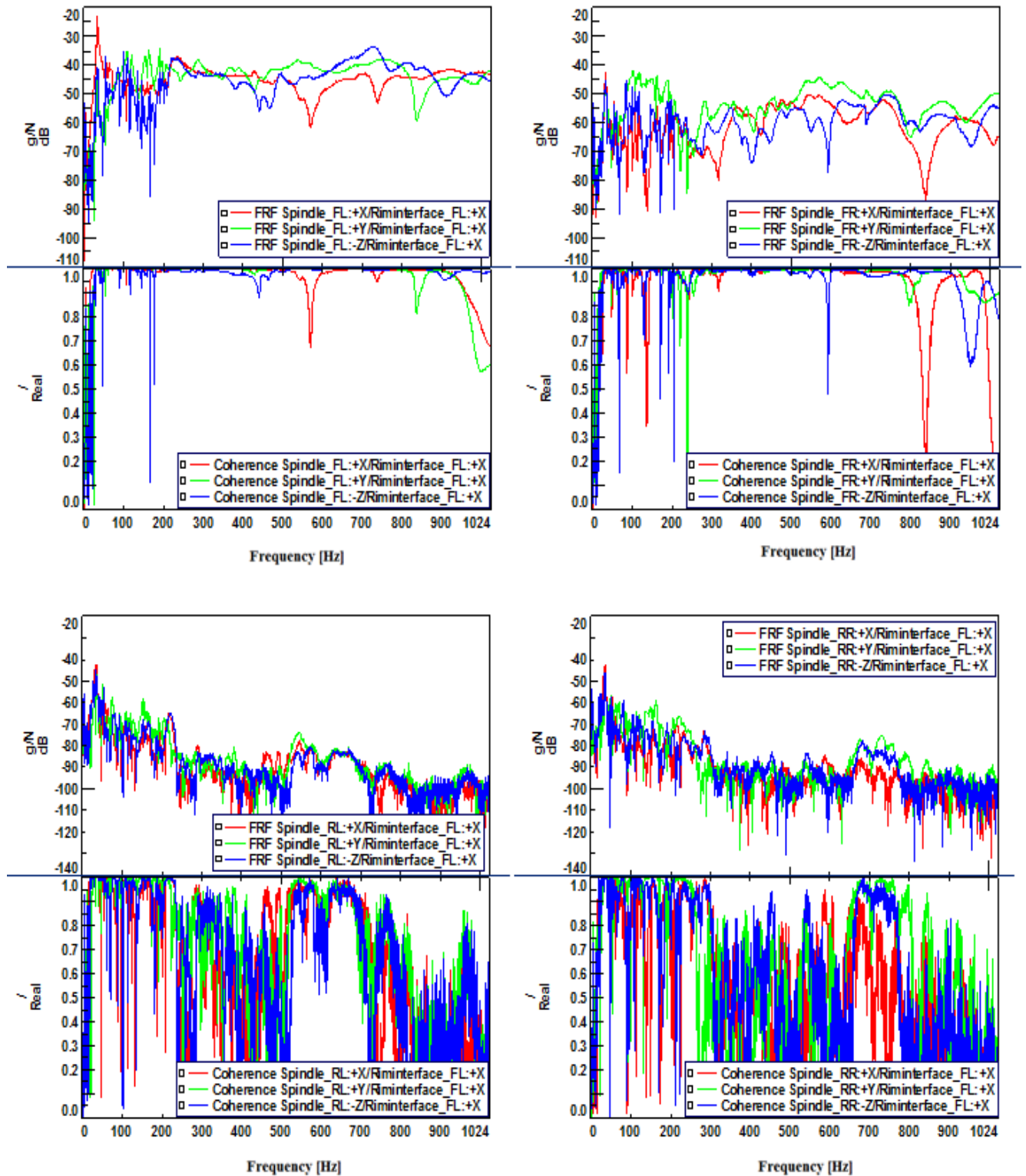


Figure 4.6a Variation of local structural FRFs between all path indicators and Riminterface_FL:X and the corresponding coherence functions as function of frequency

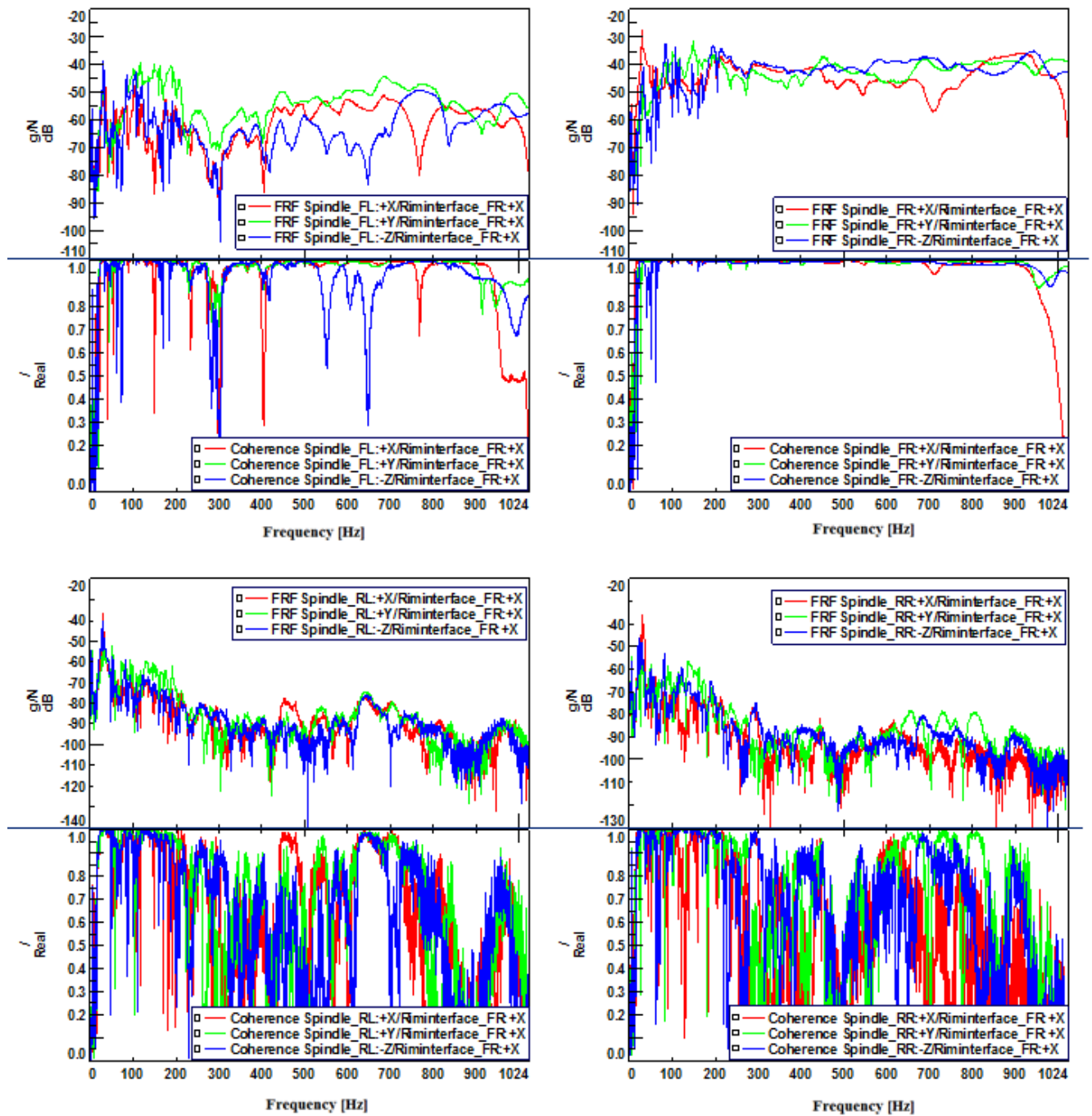


Figure 4.6b Variation of local structural FRFs between all path indicators and Riminterface_FR:X and the corresponding coherence functions as function of frequency

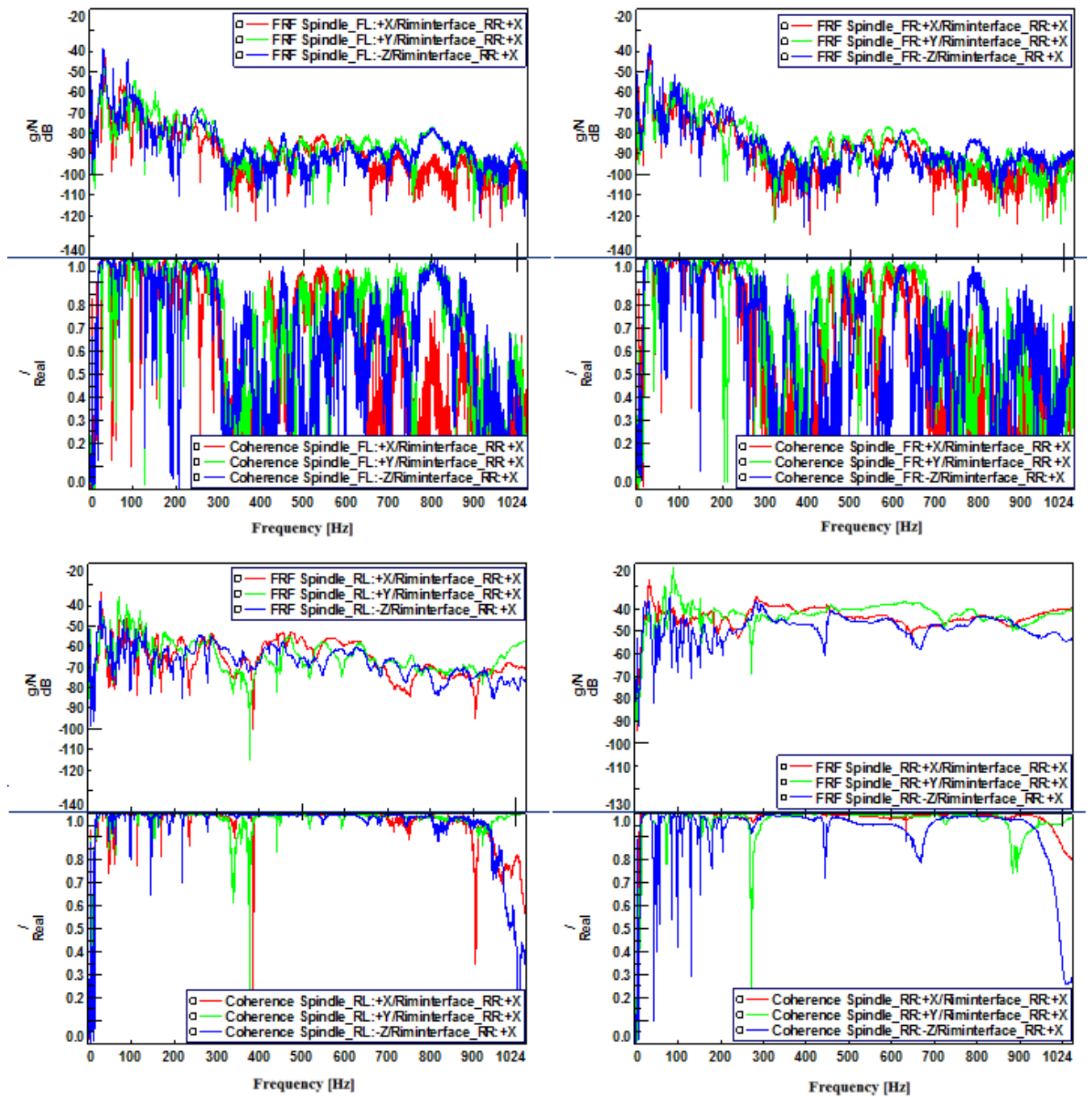


Figure 4.6c Variation of local structural FRFs between all path indicators and Riminterface_RR:X and the corresponding coherence functions as function of frequency

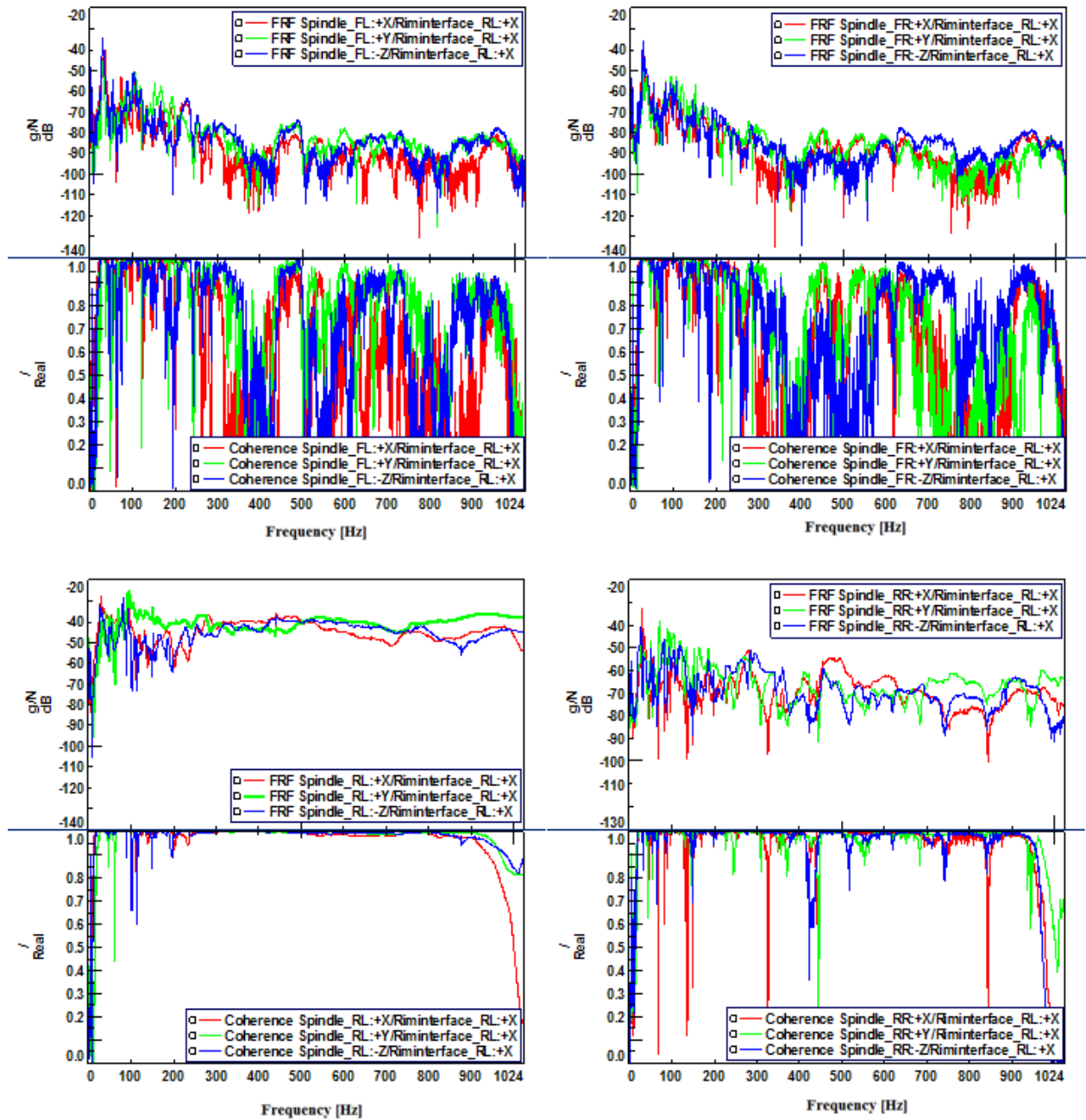


Figure 4.6d Variation of local structural FRFs between all path indicators and Riminterface_RL:X and the corresponding coherence functions as function of frequency

4.3.2 Road tests

Following the laboratory experiments, road tests were conducted. The operational accelerations of all indicators and the target interior sound pressures are measured at the same positions considered during the laboratory experiment on a straight asphalt road for engine

'on' and 'off' (coast- by) conditions with varying vehicle speeds. Tables 4.1 and 4.2 describe the details of the laboratory and on-road tests respectively. In Table 4.1 columns represent the path indicators considered at the rim spindle interface and rows represent the measured acceleration responses of all indicators. The shaded rows and columns indicate the existence of correlation between front right and front left spindles; rear right and rear left spindles respectively which were confirmed through the observation of coherence values as discussed earlier from the Figures 4.6a to 4.6d.

Table 4.1 Laboratory Experiment for Local Structural FRFs and NTFs

Local structural FRF and NTFs Measurements												
Accelerometer position	Excitation at transfer paths											
	FL_X	FL_Y	FL_Z	FR_X	FR_Y	FR_Z	RR_X	RR_Y	RR_Z	RL_X	RL_Y	RL_Z
Spindle_FL_X												
Spindle_FL_Y												
Spindle_FL_Z												
Spindle_FL1_Sus_X												
Spindle_FL1_Sus_Y												
Spindle_FL1_Sus_Z												
Spindle_FL2_LA_X												
Spindle_FL2_LA_Y												
Spindle_FL2_LA_Z												
Spindle_FR_X												
Spindle_FR_Y												
Spindle_FR_Z												
Spindle_FR1_Sus_X												
Spindle_FR1_Sus_Y												
Spindle_FR1_Sus_Z												
Spindle_FR2_LA_X												
Spindle_FR2_LA_Y												
Spindle_FR2_LA_Z												
Spindle_RR_X												
Spindle_RR_Y												
Spindle_RR_Z												
Spindle_RR1_Sus_X												
Spindle_RR1_Sus_Y												
Spindle_RR1_Sus_Z												
Spindle_RR2_LA_X												
Spindle_RR2_LA_Y												
Spindle_RR2_LA_Z												
Spindle_RL_X												
Spindle_RL_Y												
Spindle_RL_Z												
Spindle_RL1_Sus_X												
Spindle_RL1_Sus_Y												
Spindle_RL1_Sus_Z												
Spindle_RL2_LA_X												
Spindle_RL2_LA_Y												
Spindle_RL2_LA_Z												

Note: during all the hammer test four interior microphone position fixed for measurement of NTFs

Table 4.2 Operational Measurement

Operational acceleration and interior noise measurement				
Accelerometer position	Road condition	Vehicle condition	Runs and Vehicle Speed (Kmph)	
Spindle_Front left	Asphalt road	Engine on	run 1 30	run 2 35
		Engine off	run 3 30	run 4 35
Spindle_Front right	Asphalt road	Engine on	run 5 30	run 6 35
		Engine off	run 7 30	run 8 35
Spindle_Rear right	Asphalt road	Engine on	run 9 30	run 10 35
		Engine off	run 11 30	run 12 35
Spindle_Rear left	Asphalt road	Engine on	run 13 30	run 14 35
		Engine off	run 15 30	run 16 35

4.4 EXPERIMENTAL TRANSFER PATH ANALYSIS

Figure 4.7 represents the methodology followed to carry out the experimental Transfer Path Analysis (TPA). The operational loads exerted at the spindle, quantifies the energy that enters from the road through tyre/wheel assembly to the vehicle. To estimate these operational loads, matrix inversion method is used which requires local structural FRFs and operational accelerations. These are obtained from the laboratory and road tests respectively. In the TPA formulation, the vibration of tyre/wheel assembly has been taken as an active part rather than the contact patch to estimate the operational loads at the paths (rim-spindle interface).

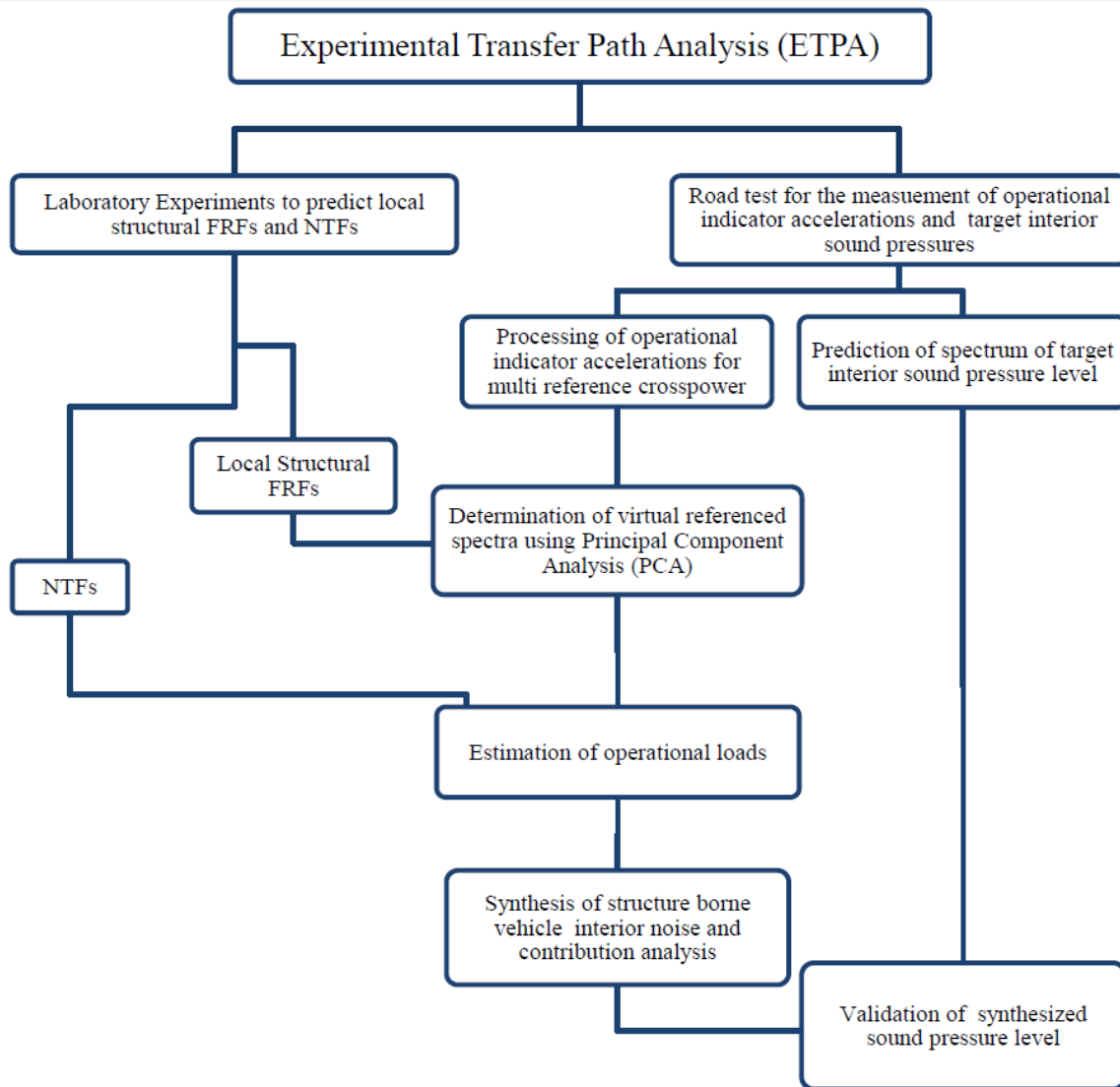


Figure 4.7 Formulation of multi reference experimental Transfer Path Analysis

Subsequent to the determination of local structural FRFs the operational loads are estimated at the rim spindle interface (g_2^V). Due to the existence of partial coherence among the twelve physical path references, as well as among the indicator responses, the multi reference TPA is performed. Hence for the estimation of operational loads, the referenced virtual spectra, (Y') of all operational indicator signals are to be calculated. This referenced virtual spectra consists of the contribution of the Principal Components (PCs), (X'). The PCs are obtained from the orthogonal transformation of the physical references. Then the virtual crosspowers, $[G_{yx'}(f)]$ between the PCs and the other indicator acceleration responses are obtained. The referenced virtual spectra (Y'), is calculated from the virtually referenced crosspower matrix $[G_{yx'}(f)]$ and the virtual autopower matrix of PCs $[G'_{xx}(f)]$ as given in Equation 4.1.

$$Y'_{i,j} = \frac{G_{Y_i X'_j}}{\sqrt{G_{X'_j X'_j}}} \dots\dots\dots(4.1)$$

Referenced virtual spectra obtained from Equation 4.1 are used in the operational load estimation. Figure 4.8 shows the principal components of virtual referenced spectra of the path 'Front left: X' (translational degree of freedom at front left spindle in longitudinal direction). Similarly, using the principal components, the corresponding virtual referenced spectra of all indicators are determined. The next step is the estimation of the operational spindle rim interface loads by multiplying the inverted local structural FRF matrix with these virtual referenced spectra. Figure 4.9 shows the root mean square (RMS) sum of the estimated operational path loads (spindle forces) for all the paths. All NTFs are multiplied by the respective operational path loads to obtain the partial contributions and are summed to get the synthesized total structure borne vehicle interior noise. This synthesized TPA results are compared with spectrum of the actual sound pressure measurements made during the road tests. This procedure is repeated for both the engine 'on' and 'off' condition to observe the independent contribution.

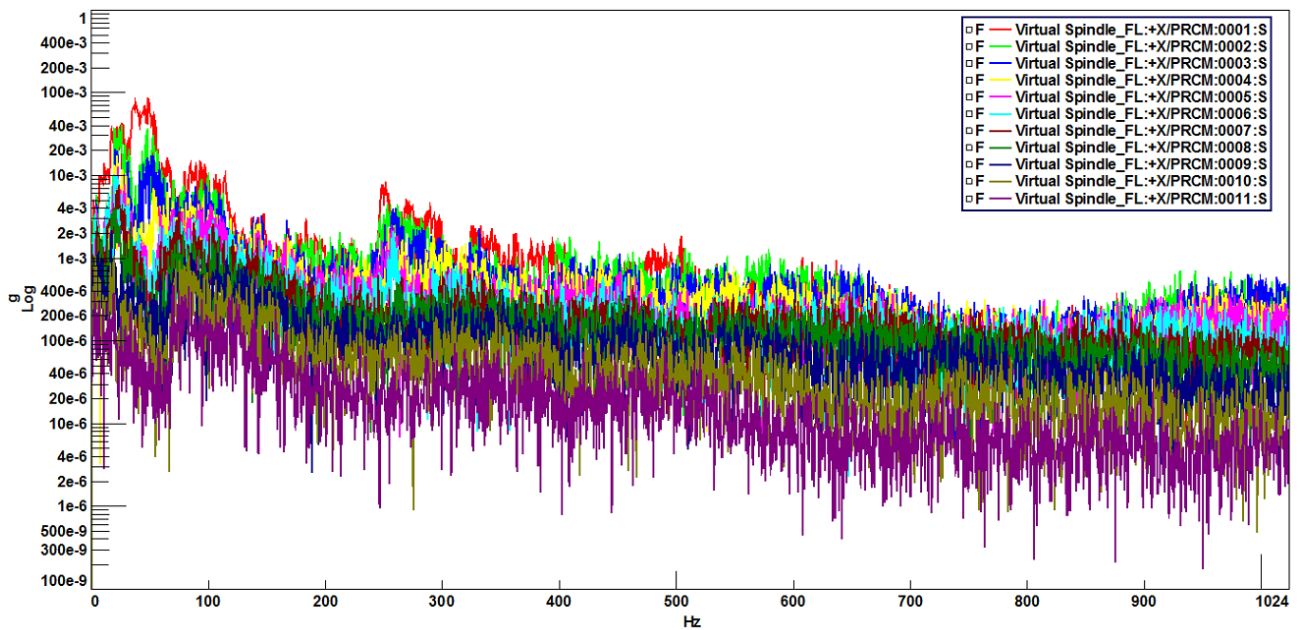


Figure 4.8 Principal components of virtual reference spectra of path indicator Spindle FL:X

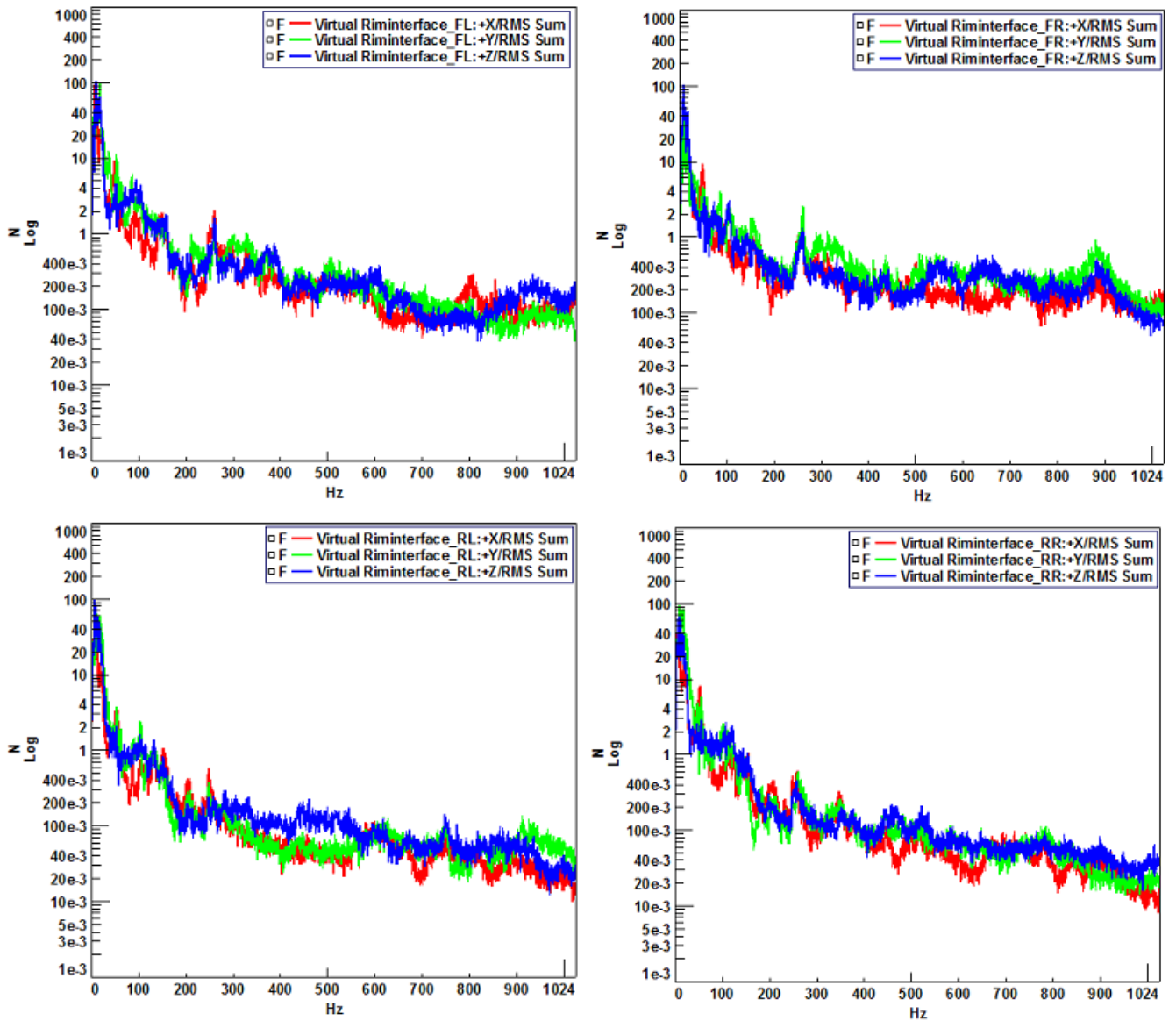


Figure 4.9 Operational path loads at wheel rim spindle interface

Figure 4.10 shows the individual path contribution to the total structure borne interior noise at driver's right ear position. Similar to Figure 4.10, the individual path contribution to the other target positions (copassenger's left ear, rear right and rear left) are given in Appendix I

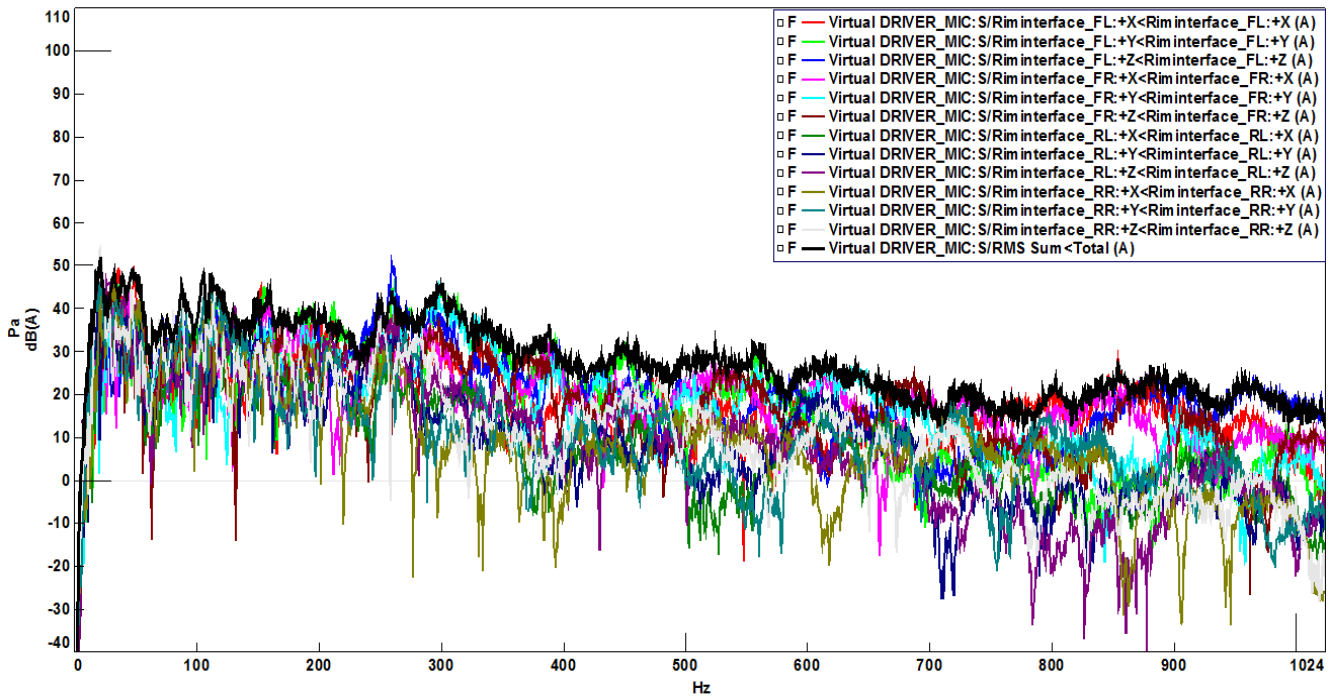


Figure 4.10: Individual path contribution to the total structure borne interior noise at driver's right ear position

4.5 RESULTS AND DISCUSSIONS

The test runs corresponding to the speed of 30 kmph with engine 'on' and 'off' conditions are considered for the discussion. Figure 4.11 compares the 1/3 octave sound pressure level (SPL) of the synthesized TPA results of the actual measurements for engine 'on' and 'off' conditions. Barring the low frequency bands, the comparison between TPA and the actual measurements seems to be reasonable. Figure 4.12 gives the comparison of sound pressure level of engine 'on' and 'off' condition for the actual measurements and synthesized TPA results separately. At 50 Hz central frequency band and beyond 400 Hz central frequency the engine 'on' condition shows higher sound pressure level than engine off condition in actual measurements and as well as the synthesized TPA. This shows that the higher sound pressure level at 50 Hz central frequency for 'engine on' condition, is due to the power train noise source and not due to tyre road interaction. The target responses for the remaining interior target responses are given in Appendix I. Contribution analysis shows that the major contributing paths for the critical frequencies, i.e. 121 Hz and 261 Hz, correlate with the high amplitude operational load at wheel rim spindle interface and is shown in Figure 4.9. The

path contribution analysis and the vector contribution analysis results at these peak frequencies are further discussed.

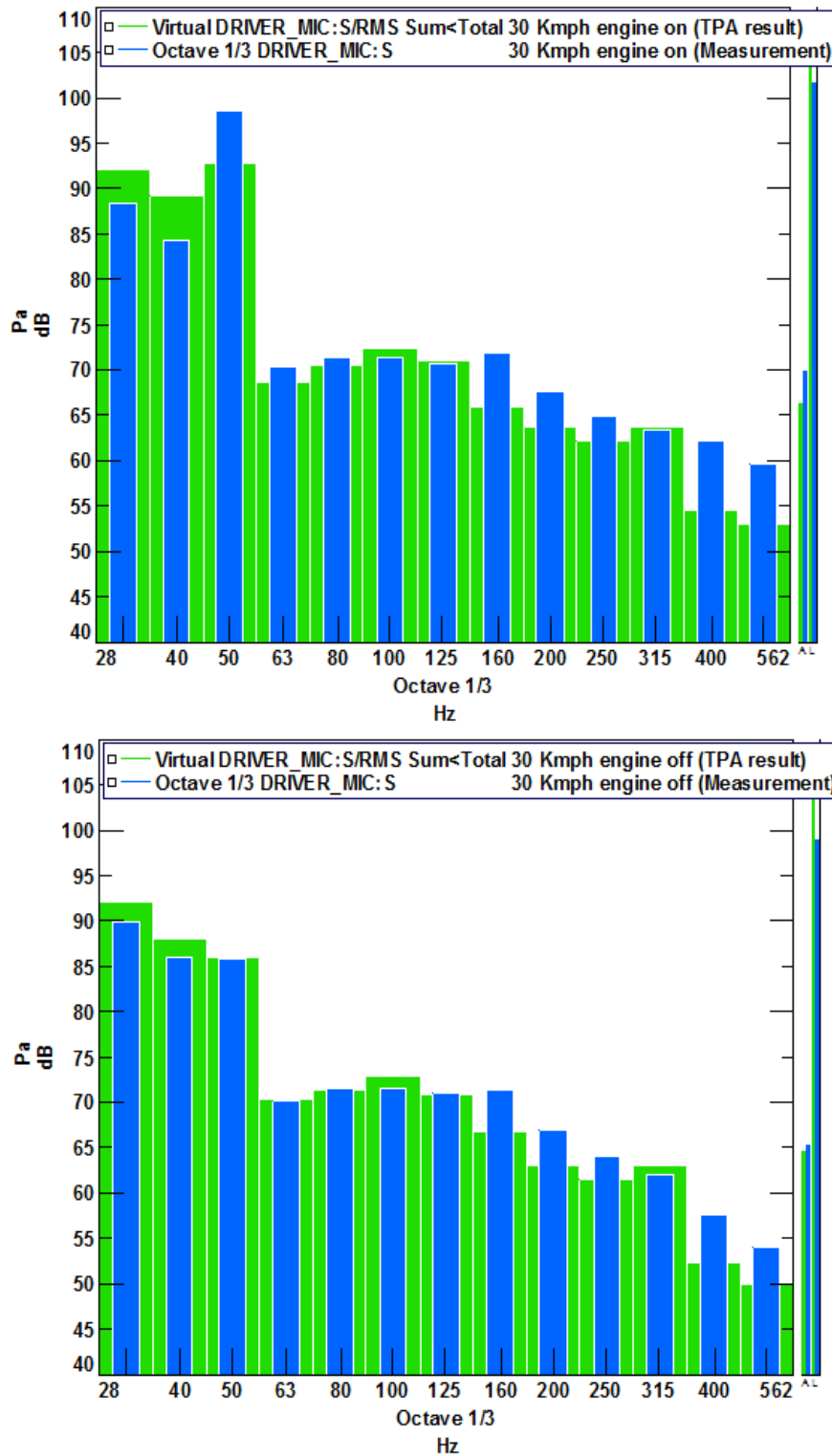


Figure 4.11 Comparison of TPA results with measurements of driver's ear target

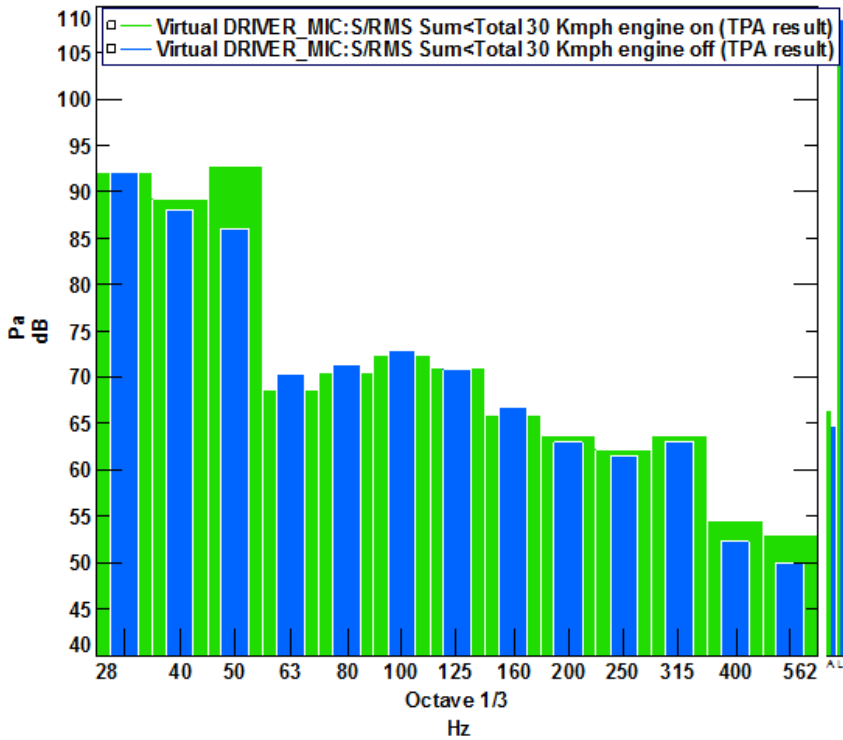
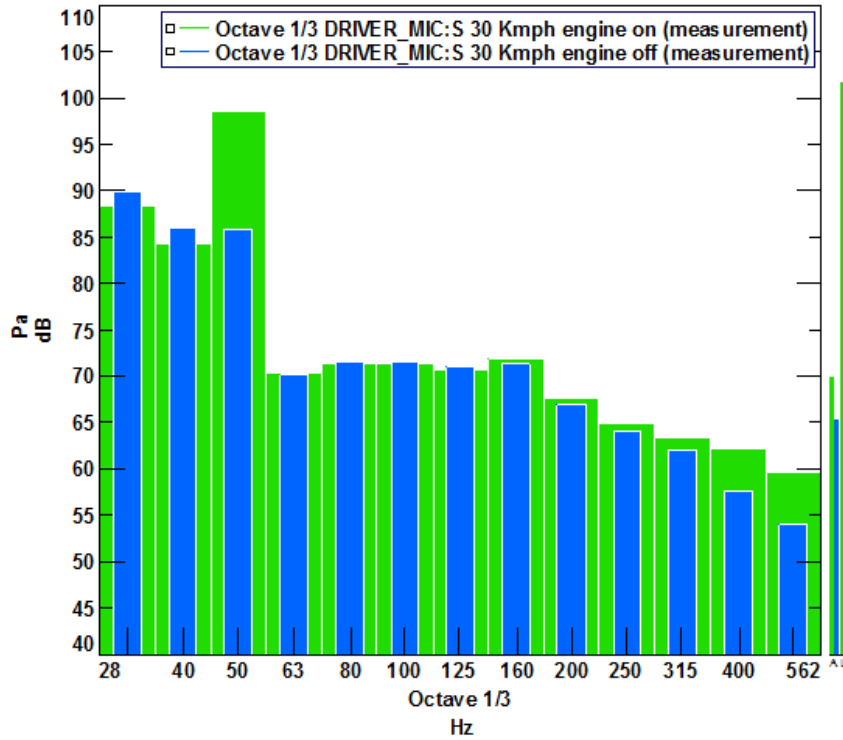


Figure 4.12 Comparison of engine on and engine off results of driver's ear target

Figure 4.13 shows the results of the path contribution analysis. The partial contributions of all paths (physical references represented by horizontal acoustic color bands) are below 400 Hz, as is usually the case with structure-borne noise. This contribution plot gives the ranking of individual paths for the total RMS sound pressure level (SPL). The vertical bars represents

the total sound pressure level in terms of principal components (virtual references). It is readily observed from figure 4.13 that, at 121 Hz the contribution from Front Left 'Y' and 'Z' directions, Front Right 'Z' direction and Rear Right 'Y' and 'Z' directions are significant compared to other paths and for 261 Hz the Front Left 'X' and 'Z' directions, Front Right 'X' and 'Y' directions and Rear Left 'Y' and 'Z' directions are important. Hence, the path contribution analysis is used to identify major contributing paths at different critical frequencies based on the RMS values. But the limitation of this plot is that it does not show the phase relationship between the noise contributing paths with respect to the total interior noise. The total sound pressure level can also be expressed in terms of principal components (virtual references). Figure 4.14 represents the analogous plot to path contributions with the virtual references given by horizontal acoustic color bands and the physical references by vertical bar graph. Riminterface_FL:Z path is chosen. It is observed that the contribution from principal component no.12 (Spectrum: PRCM: S) is insignificant compared to the others PCs. Another plot called the vector contribution plot can be drawn at any given frequency, which gives the phase relationship of transfer paths with total interior noise. Principal component no. 1 (Spectrum: PRCM: S) shows the significant contribution among all and consider further for vector contribution analysis.

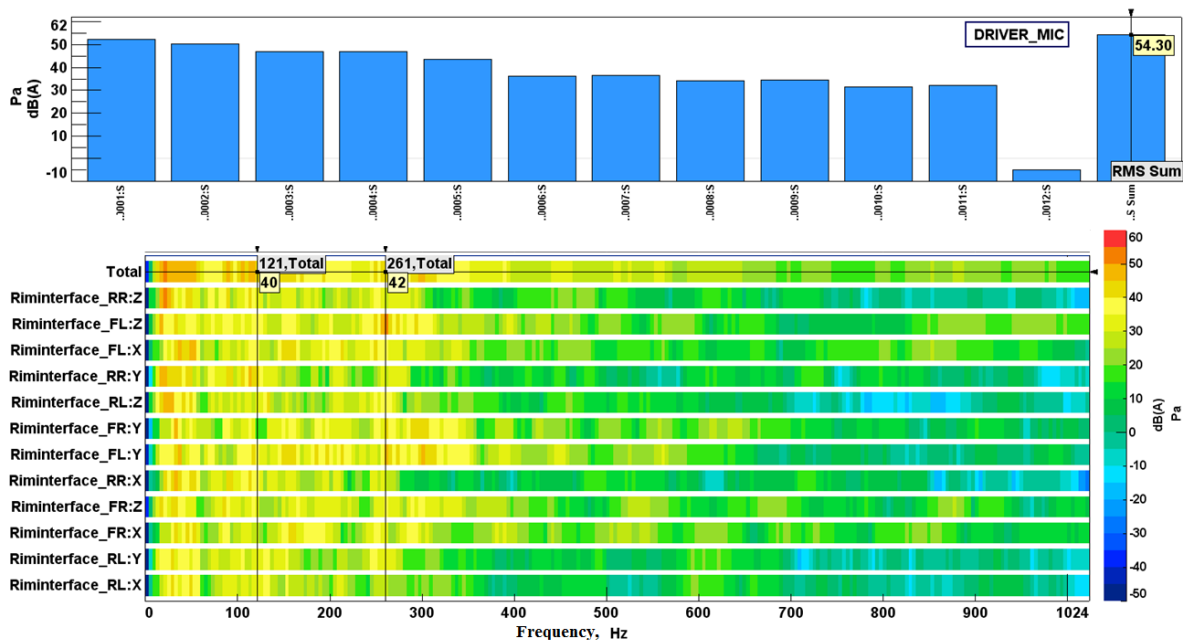


Figure 4.13 Path contribution results from matrix inverse method for sub system V: vertical bars at the top represents the contribution from principal components and horizontal acoustic color map represents the contribution from physical references

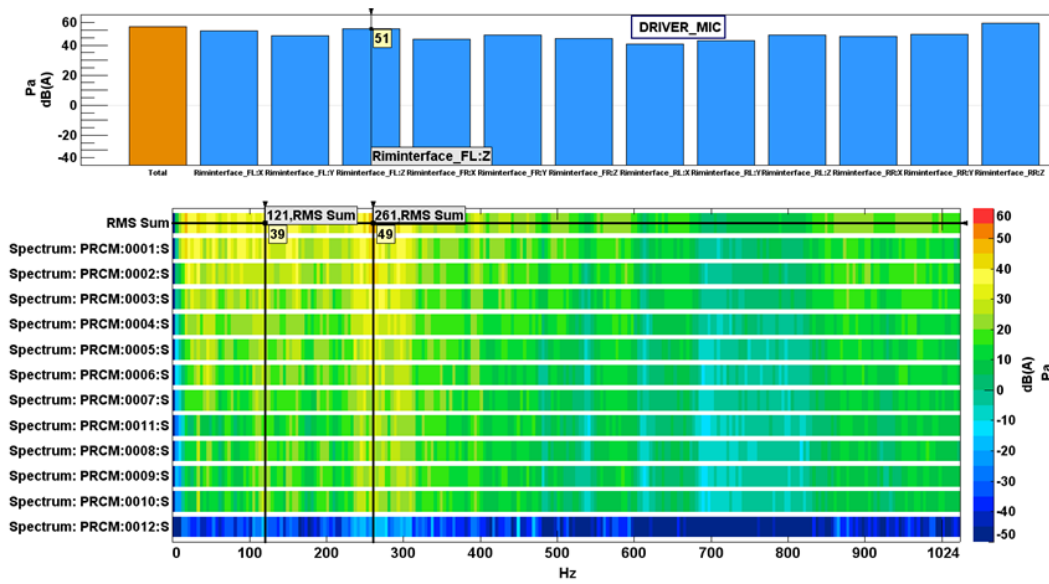


Figure 4.14 Contribution of principal components to the chosen critical path 'Riminterface_FL: Z' from matrix inverse method for sub system V: vertical bars at the top represents the contribution from physical references and horizontal acoustic color map represents the contribution of individual principal components.

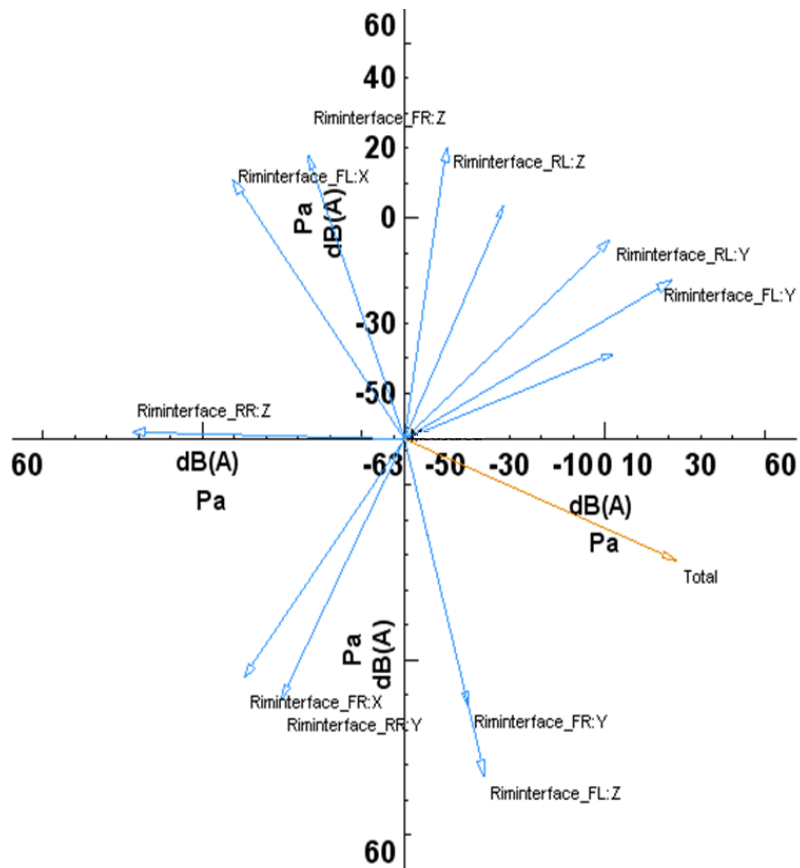


Figure 4.15a Vector contribution results from matrix inverse method for sub system V at 121 Hz frequency

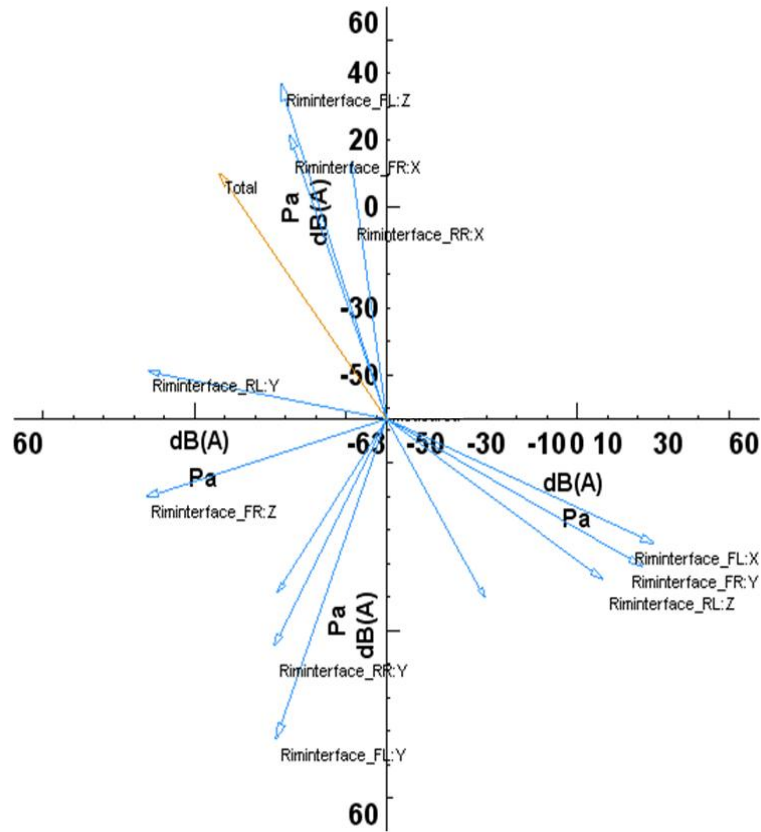


Figure 4.15b Vector contribution results from matrix inverse method for sub system V at 261 Hz frequency

Figure 4.15a and 4.15b show, the results of the vector contribution analysis for spectrum PRCM: 0001: S at the critical frequencies (121 Hz and 261 Hz). At 121 Hz, the total sound pressure level vector is placed in the fourth quadrant. The observed major contributing paths from the path contribution analysis are placed in different quadrants. Out of these, the critical paths 'Riminterface_FL:Z' and 'Riminterface_FR:Y' are in the fourth quadrant along with the total sound pressure level vector. This implies that the increase in contribution of these directions adds to the total Sound Pressure Level (SPL), whereas the remaining major contributing paths placed in second quadrant are not in phase with total sound pressure level. The increase of vector magnitude in these paths direction reduces the total SPL. The vector 'Riminterface_RR:Y' is almost 90 degrees out of phase with the total SPL vector, implying that this path is insignificant. Similarly, from figure 4.15b and at 261 Hz frequency, it can be seen that the vectors are in phase with the total SPL vector in the second quadrant. The traditional approach is to use this diagram for noise reduction. The problem with this approach are highlighted in the next chapter.

4.6 SUMMARY

TATA Indigo, a sedan class passenger car's structure borne interior noise is synthesized at four interior positions successfully, using multi-reference transfer path analysis. The critical paths are identified through path and vector contribution analysis for chosen frequencies. Variation in sound pressure level between the synthesized and the road test measurements are found to be minimum. Coherence analysis and repeatability check for all the experiments were carried out and the quality of the measured data was ensured. The procedure explained in this chapter is an application of direct ETPA to predict the structure borne vehicle interior noise, where actual road input excitations are not explicitly found but forces are estimated at the vehicle wheel rim spindle interfaces. Hence a modified procedure is proposed in this thesis and explained in the next chapter that determines the road excitation forces at the contact patch by indirect use of TPA. The proposed procedure can be used for different set of tyres without conducting actual road tests.

CHAPTER 5

IMPLEMENTATION OF TRANSFER PATH ANALYSIS TECHNIQUES

5.1 INTRODUCTION

The Noise, Vibration and Harshness (NVH) characteristics of a vehicle are predicted and enhanced during the product development cycle itself by various techniques. Frequency response function Based Sub-structuring technique (FBS) and Transfer Path Analysis (TPA) are the important techniques widely used by researchers and engineering professionals to study the dynamic behaviour of complex mechanical systems such as automobiles, locomotives, aircrafts, submarines, etc. The FBS technique is basically applied on complex mechanical systems made of two or more sub-assemblies in order to predict its dynamic characteristics. It divides the whole system into sub components, hence the name sub-structuring and then predicts the Frequency Response Functions (FRFs) of the individual components. Further these FRFs are combined to get the overall force transfer characteristics of the whole structure. TPA is a rigorous test based method that quantifies the flow of vibro-acoustic energy from a source, through a set of structure borne and air borne paths to a chosen target/receiver's location. A typical TPA model divides the global system into active and passive parts. Active part is the source, whereas the passive part contains the indicators, and target points where the responses are measured.

One of the major concerns of subsystem manufacturers is to test the system without resorting to the whole structure. In other words, the subsystem manufacturers would like to carry out measurements in a test bench and integrate it into the overall system dynamics. Such a procedure, called component transfer path analysis, was adopted for a gear box by D. de Klerk & Rixen (2010) and Kim & Kang (2011) for the case of an engine. Though there have been several studies on FBS and TPA technique, such as Tsai & Chou (1988), Ren & Beard (2001), Liu & Ewins (2002), Lee & Hwang (2007), and Gehringer (2005) a broad framework has been put forward for TPA by van der Seijs et. al (2016). The next section explains this

framework and helps the positioning of this work. The terminologies used to explain the work are also derived from this reference.

5.2 TPA TECHNIQUES

Recent publication by van der Seijs et. al.(2016) has given a thorough review on the historical development and the theoretical background of various TPA techniques on a general framework that can be employed for vibrational and/or noise problem, that occurs due to the transmission of vibrations in a complex mechanical systems. In the TPA framework the complex system considered is divided into two subsystems. One subsystem is an active part that describes the source and the other is the passive part where the indicator and the target locations of responses are defined. There are eleven techniques summarized in the TPA framework, and are classified into three families, namely classical, component based, and transmissibility based TPA methods. This chapter describes the adaptation and implementation of three methods from these families.

The definitions for terms such as source, interface, receiver, indicator points etc. are defined in this paper. Consider an assembled system such as the tyre T and the vehicle body V. Our interest is the determination of sound pressure, p at a certain locations inside the car due to the road input, \mathbf{f} . In tune with this paper let subscript "1" indicate the excitation point, the road, "2" indicates the interface which in this case is the mounting location and subscript "3" the measurement location of the output. This is shown in Figure 1.

First one is the 'matrix inverse' method from classical TPA family and the other two are 'in-situ' and 'free velocity' methods from component based TPA family. First the matrix inverse technique is employed by considering tyre wheel assembly (T) as the source and the interface operational forces (g_2^V) are estimated to characterize the source, further used on the passive side of the vehicle (V) with the NTFs (Y_2^V) to predict the structure borne vehicle interior noise. Secondly, the matrix inverse technique is used to quantify the road input excitation (f_1) at the contact patch considering the full vehicle (TV) on a passive side of TPA framework. This characterizes the road, further used with the NTFs (Y_{31}^V) to predict the noise. Subsequently, 'in-situ' and 'free velocity' methods are employed. These two methods propose

a procedure to virtually predict the operational acceleration at the wheel-rim interface without an actual road test and facilitates the study of influence of the tyre design over structure borne vehicle interior noise.

Table 5.1 summaries the application of these methods in the TPA framework in terms of the required operational measurements and source characterization those are to be applied on the NTFs to predict the structure borne vehicle interior noise (p) for a passenger car. The active subsystem (tire wheel assembly) is referred by 'T', the passive subsystem (vehicle without tyre wheel assembly) is referred by 'V' and the full vehicle is referred by 'TV'.

Table 5.1 Summary of TPA framework of various methods

Family	Method	Operational measurement		Source characterization		Apply to
		Quantity	On system	Quantity	Using	NTFs
Classical TPA	Matrix inverse	Indicator accelerations (u_4)	TV	Interface force (g_2^V)	Structural FRFs (Y_{42}^V)	NTFs (Y_{32}^V)
	Matrix inverse	Indicator accelerations (u_4)	TV	Road input (f_1)	Structural FRFs (Y_{41}^{TV})	NTFs (Y_{31}^{TV})
Component Based TPA	In-situ	Interface acceleration estimated* $u_2 = Y_{21}^{TV} \{f_1\}$	TV	Equivalent force (f_2^{eq})	Structural FRFs (Y_{22}^{TV})	NTFs (Y_{32}^V)
	Free velocity	Interface acceleration estimated* $\{u_2^{free}\} = [Y_{21}^T]^{-1} f_1$	T (free)	Equivalent force (f_2^{eq})	Structural FRFs ($Y_{22}^T + Y_{22}^V$)	NTFs (Y_{32}^V)

* not measured during road test

Figure 5.1 gives the nomenclature of vehicle measurement points represented by subscript of measurements. Point '1' represents the center of contact patch where the road input loads act. Point '2' refers the interface between the sub systems 'T' and 'V'. Point '3' is the interior target response location and the point '4' refers to the indicators at spindle, suspension and lower arm locations.



- 1 - Tire road interaction contact patch point
- 2 - Rim interface point
- 3 - Cabin interior
- 4 - Spindle, Suspension and Lower arm points

Figure 5.1 Nomenclature of vehicle measurement points

5.3 ROAD LOADS

Road loads describes road randomness and the excitation characteristics of the road that influences the road noise. Though there have been multi axial road reproduction experiments by Filip De Coninck (2007), in this work road data is characterized by a single value, acting at the center of the contact patch. Though more sophisticated road input is possible, this work concentrates on a design procedure to validate tyre designs. In other words, the current procedure can be used to compare various tyre designs. Hence road data is calculated through TPA. Once the road excitation forces are obtained readily at the contact patch due to road profile and/or texture, it is easy to determine the equivalent operational loads at the wheel rim spindle interface through TPA. It further requires the operational accelerations at the rim spindle interface. Measurement of accelerations at the rim spindle interface ' $\{u_2\}$ ' (at bolt location) is not possible during road test as it is impractical to mount the accelerometer at the interface. The in-situ and the free velocity methods offer a procedure to determine operational acceleration at the interface from the road loads estimated from matrix inverse method.

5.3.1 Road Load Estimation for TPA

There are two experiments conducted for direct experimental TPA (Classical TPA) explained in the previous chapter. The first one was the laboratory experiment to determine the local structural FRFs ($[Y_{42}^V]$) and the NTFs ($[Y_{32}^V]$) on the passive side (V) of the TPA model. The tyre/wheel assemblies (T) were removed as they are considered as sources and constituted the active side (T) of the model. The second experiment was the road test conducted for the indicator's operational accelerations and the target's operational sound pressure measurements. The experimental TPA is cumbersome and time consuming to repeat for studying the influence of new tyre replacement. In order to study the effect of replacement of the tyres, and to observe the corresponding variation in the TPA results, the TPA model is modified to account for the entire vehicle on the passive part of the model while the tyre contact patch acts as the interface between the passive part side and the active part side of road loads (sources). In order to estimate the operational road loads, a third laboratory experiment is conducted to determine the local structural FRFs ($[Y_{41}^{TV}]$) between the contact patch and the passive side indicator points. These indicators are the same points that were considered during the first experiment. In this experiment the tire/wheel assembly is not removed from the vehicle, but an instrumented hammer in three translational directions excites the centre of the contact patch. A small aluminium cube at the centre of contact patch is fixed for the excitation. Along with the structural FRFs ($[Y_{41}^{TV}]$) the NTFs ($[Y_{31}^{TV}]$) are also determined.



Figure 5.2 Laboratory experimental set up for full vehicle system (TV)

Figure 5.2 describes the experimental set up for the third experiment. The operational road loads are estimated by combining these structural FRFs ($[Y_{41}^{TV}]$) and the virtual referenced spectra of operational accelerations $\{u_4\}$ measured from the road test (second experiment).

The equation 5.1 gives the indicator's operational acceleration in terms of the structural FRFs between road contact and indicator points $[Y_{41}^{TV}]$ and the road loads $\{f_1\}$ estimated using matrix inversion method given in equation 5.2.

$$\{u_4\} = [Y_{41}^{TV}]\{f_1\} \dots \dots \dots (5.1)$$

$$\{f_1\} = [Y_{41}^{TV}]^{-1}\{u_4\} \dots \dots \dots (5.2)$$

The structural FRF sets obtained from the first (without tyre wheel assembly (V)) and third (with tyre wheel assembly (TV)) experiments in the laboratory for the same indicator points exciting at the interface and contact patch respectively. The spindle force (g_2^V) and road loads (f_1) can be related through a transmissibility function Y_{21}^{TV} as given by equation 5.3.

$$g_2^V = Y_{21}^{TV} f_1 \dots \dots \dots (5.3)$$

At low frequency range (below 400 Hz), tyre exhibits the modal behavior. This is due to belt vibration. The magnitude of road excitation corresponding to the frequencies that match with these resonance frequencies of tyre belt vibration are amplified and the magnitudes other than these frequencies are isolated (filtered). Figure 5.3 describes the tyre behavior as an amplifier at low frequencies and a filter at high frequencies. The estimated road load at the front left contact patch in the longitudinal direction as function of frequency is considered for discussion and shown in green. The force exerted due to this road load at the front left spindle in the longitudinal direction is shown in red. The transmissibility function of this force transfer through tyre wheel assembly is given in blue which is obtained by dividing g_2^V by f_1 . This calculated transmissibility function in Figure 5.3 depicts tyre behavior from the amplified road excitation force (red) below 420 Hz, and filtered excitation force (green) beyond 420 Hz. The similar tyre behaviour is observed for the remaining eleven road input loads estimated at their translational degree of freedoms at the center of contact patch. The belt frequencies were determined in the earlier chapter 3.

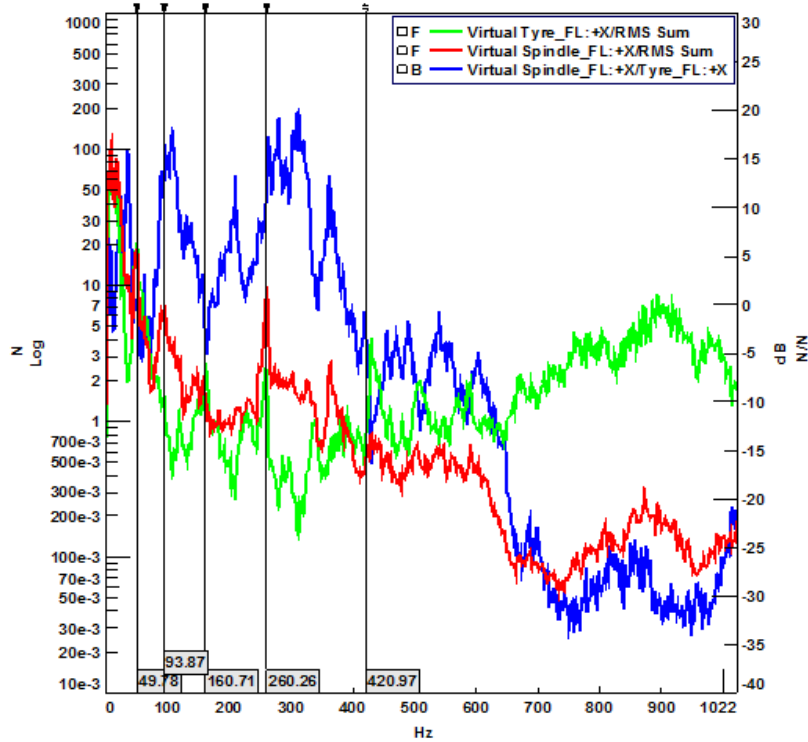


Figure 5.3 Amplification and isolation of road excitation at the front left contact patch in the longitudinal direction

5.4 IMPLEMENTATION OF VARIOUS TPA METHODS

This section describes the mathematical frame work of three methods (van der Seijs et. al. (2016)) and their implementation aspects. Additional experiments conducted for component based TPA methods are also explained.

5.4.1 Matrix inverse method

This method represents a classical TPA procedure discussed in the previous chapter 4. The name 'matrix inverse' is because of the inversion of structural FRFs for the estimation of operational loads. Equation 5.4 represents the target interior sound pressure that can be obtained by the product of NTFs of the vehicle passive subsystem (V) and operational

interface loads given by Equation 5.5. The $\{u_4\}$ are obtained from the road test under coast by condition.

$$u_3 = Y_{32}^V g_2^V \dots\dots\dots(5.4)$$

where,

g_2^V is the interface forces given by

$$g_2^V = [Y_{42}^V]^{-1} \{u_4\} \dots\dots\dots(5.5)$$

Further, the road loads estimated by Equation 5.2 is used with the NTFs obtained for the full vehicle system (TV) from the experiment no.3 explained earlier. Equation 5.6 gives the corresponding interior sound pressure of the full vehicle.

$$\{u_3\} = [Y_{31}^{TV}] \{f_1\} \dots\dots\dots(5.6)$$

Equation 5.4 and 5.6 are mathematically equivalent, except that the explicit use of road loads with NTFs in case of Equation 5.6. The limitation of this method is that it requires repetition of road test and laboratory tests to study the influence of tyre design.

5.4.2 In-situ method

This method is implemented for the full vehicle system. It requires the structural FRFs for an individual tyre for the given contact patch excitation as it is assembled in the vehicle (TV). The vehicle is raised using a hydraulic jack at the front right side with the tyre wheel assembly until the contact between tyre and floor disappeared. An aluminium cube is fixed at the centre of the tread at the wheel plane to represent the centre of the contact patch as shown in Figure 5.4.



Figure 5.4 Experimental set up of front tyre wheel assembly for tyre transfer characteristics by in-situ method

The excitation in all three translational direction are given at aluminium cube and acceleration responses are measured at two points, one at a point nearer to the contact patch and the other at a point nearer to the rim spindle interface using tri-axial accelerometers mounted as shown in Figure 5.4. Similarly excitation is given at rim spindle interface at the bolt head and the responses are measured. This resulted in estimation of $[Y_{11}^{TV}]$, $[Y_{21}^{TV}]$ and $[Y_{22}^{TV}]$. These structural FRFs are used for the remaining tyre/wheel assemblies also.

Figure 5.5a to 5.5c show the structural FRFs obtained for the front right tyre wheel assembly. The drive point structural FRFs $[Y_{11}^{TV}]$ and $[Y_{22}^{TV}]$ at the contact patch (Tyre_FR) and at the rim spindle interface (Riminterface_FR) are represented in red and blue respectively and the tyre structural FRFs between contact patch (Tyre_FR) and the rim spindle interface (Riminterface_FR) $[Y_{21}^{TV}]$ is represented in green as a function of frequency in the top half of the graph. The corresponding coherence functions for all structural FRFs with the corresponding colors are given in the bottom half of the graph. The coherence function for $[Y_{21}^{TV}]$ shown in green and the corresponding FRFs indicate the effect of belt vibration below 400 Hz. This was explained in Chapter 3. Above 400 Hz, the FRF is almost flat, indicating the lack of contribution due to structure in noise propagation. Additionally, the structural FRFs $[Y_{11}^{TV}]$ and $[Y_{22}^{TV}]$ shows good coherence values even beyond 400 Hz that ensures the good quality of the experimental measurements.

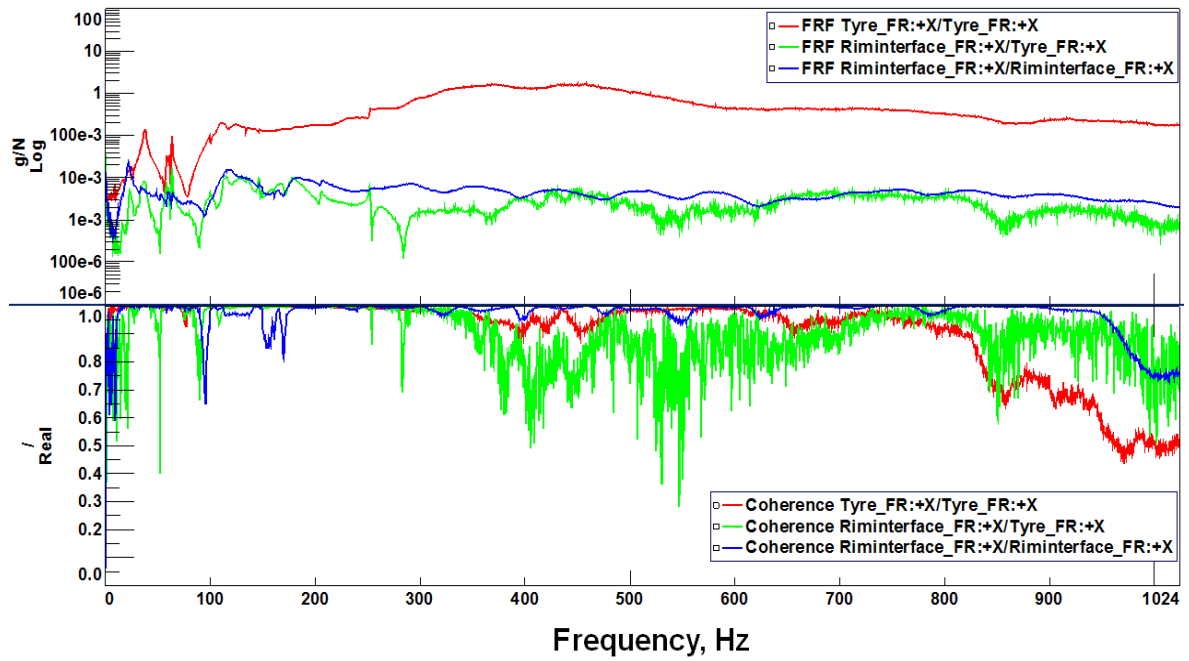


Figure 5.5a Front right wheel structural FRFs and Coherences in the longitudinal direction (in-situ method)

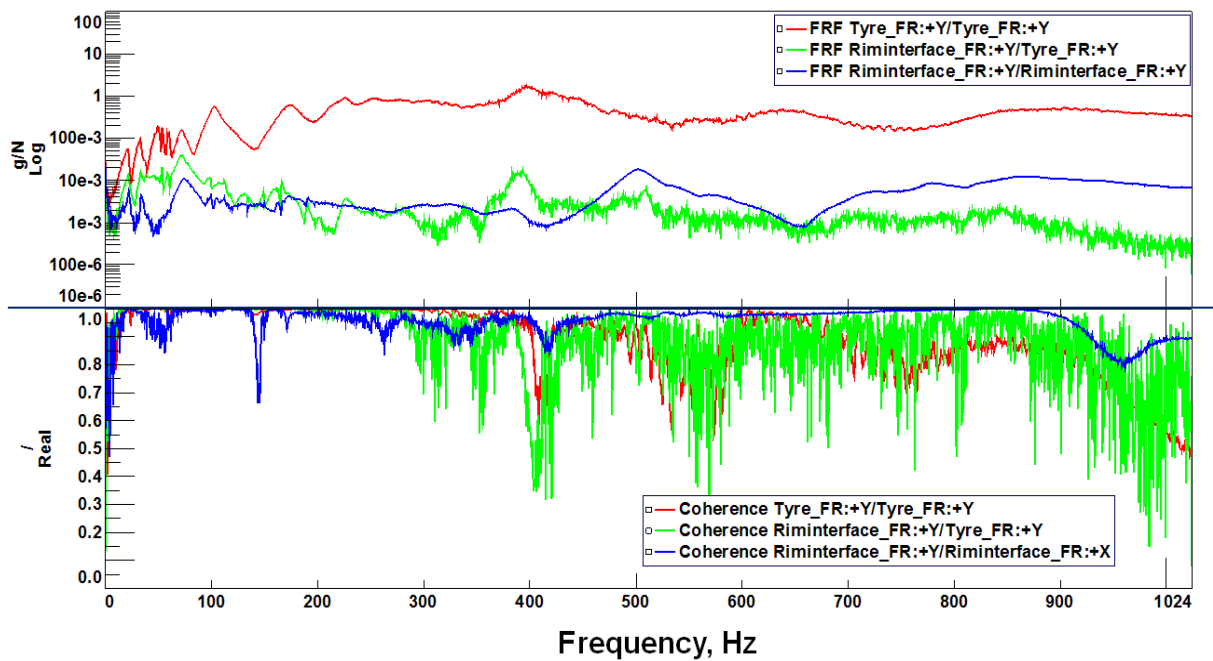


Figure 5.5b Front right wheel structural FRFs and Coherences in the lateral direction (in-situ method)

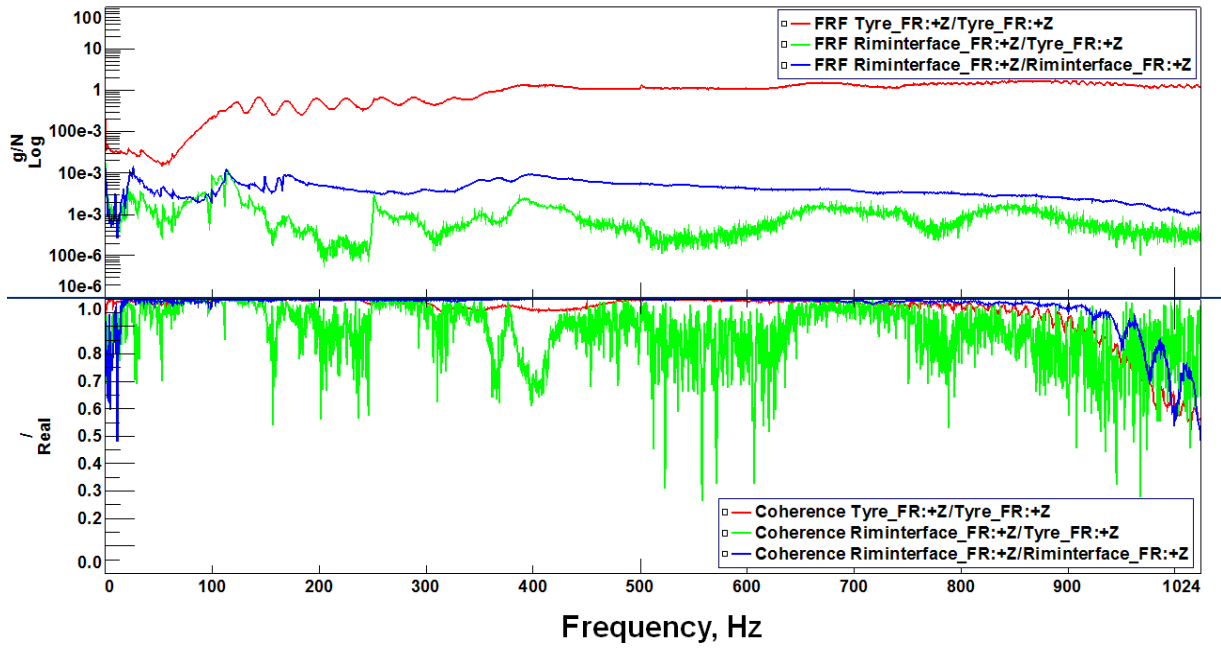


Figure 5.5c Front right wheel structural FRFs and Coherences in the vertical direction (in-situ method)

Equations 5.6 to 5.8 explain the determination of equivalent force that act at the interface point '2' for the full vehicle system (TV) and synthesize of structure borne vehicle interior noise at the target location.

$$f_2^{eq} = [Y_{22}^{TV}]^{-1}\{u_2\} \dots \dots \dots (5.6)$$

where,

u_2 represents the interface accelerations, determined by following equation

$$u_2 = Y_{21}^{TV}\{f_1\} \dots \dots \dots (5.7)$$

$$p = Y_{32}^B\{f_2^{eq}\} \dots \dots \dots (5.8)$$

5.4.3 Free velocity method

As the name suggests the method assumes free displacement at the interface point of the subsystem with no blocked forces at the interface. Tyre wheel subsystem (T) is removed from the vehicle and suspended freely using bungee cords as shown in Figure 5.6. Excitation in all

three directions at the contact patch is given using an aluminium cube fixed at the center of the contact patch and the acceleration responses are measured at a point near the rim spindle interface. Similarly excitation is given at rim spindle interface, at a point near the bolt hole and the responses are measured at the interface. $[Y_{21}^T]$ and $[Y_{22}^T]$ were estimated using these measurements. In addition, $[Y_{22}^V]$ is also determined by exciting the subsystem (V) near the interface at bolt head and measuring the responses close to this point. This is also shown in Figure 5.6



Figure 5.6 Position of accelerometers for free velocity method

$$f_2^{eq} = [Y_{22}^T]^{-1} \{u_2^{free}\} \dots \dots \dots (5.9)$$

where,

$$\{u_2^{free}\} = [Y_{21}^T]^{-1} f_1 \dots \dots \dots (5.10)$$

From equation 11 and 12 of the reference paper (van der Seijs et. al. 2016)

$$u_3 = Y_{32}^V (Y_{22}^T + Y_{22}^V)^{-1} Y_{22}^T f_2^{eq}$$

$$u_3 = Y_{32}^V (Y_{22}^T + Y_{22}^V)^{-1} Y_{22}^T (Y_{22}^T)^{-1} u_2^{free}$$

$$u_3 = Y_{32}^V (Y_{22}^T + Y_{22}^V)^{-1} u_2^{free}$$

$$u_3 = Y_{32}^V g_{2_free}^V \dots \dots \dots (5.11)$$

where,

$$g_{2_free}^V = (Y_{22}^T + Y_{22}^V)^{-1} u_2^{free} \dots \dots \dots (5.12)$$

Figure 5.7a to 5.7c show the structural FRFs of front right tyre wheel assembly for free condition. The drive point structural FRFs $[Y_{22}^T]$ (at Rim_sp_FR) and $[Y_{22}^V]$ (at Rim_ty_FR) and

the tyre structural FRFs between contact patch (Tyre_FR) and the rim spindle interface (Rim_sp_FR) $[Y_{21}^T]$ are shown in top half of the graph, represented by blue, red and green colors respectively and the corresponding coherence functions are given in the corresponding colors in the bottom half of the graph.

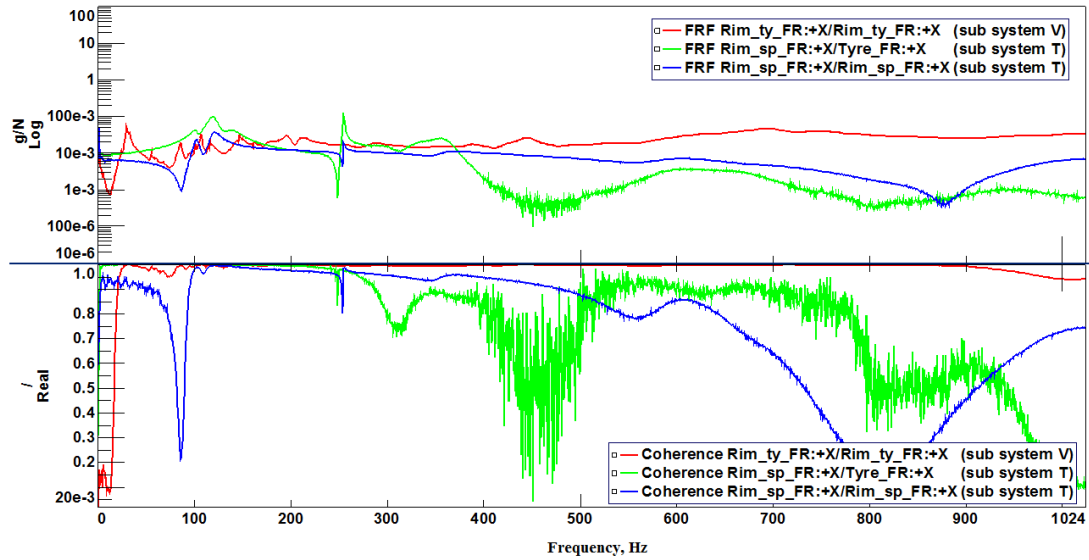


Figure 5.7a Front right wheel structural FRFs and Coherences in the longitudinal direction (free velocity method)

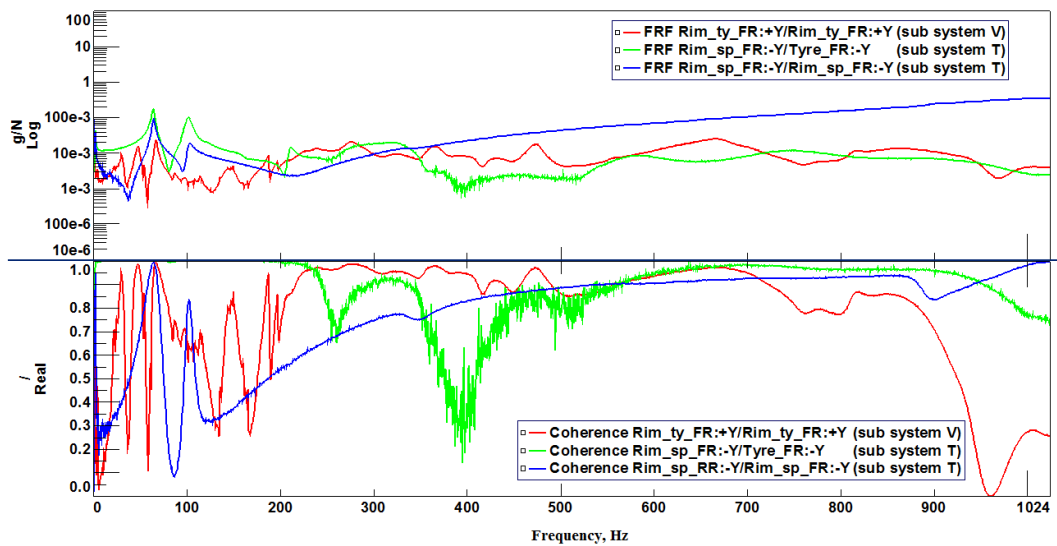


Figure 5.7b Front right wheel structural FRFs and Coherences in the lateral direction (free velocity method)

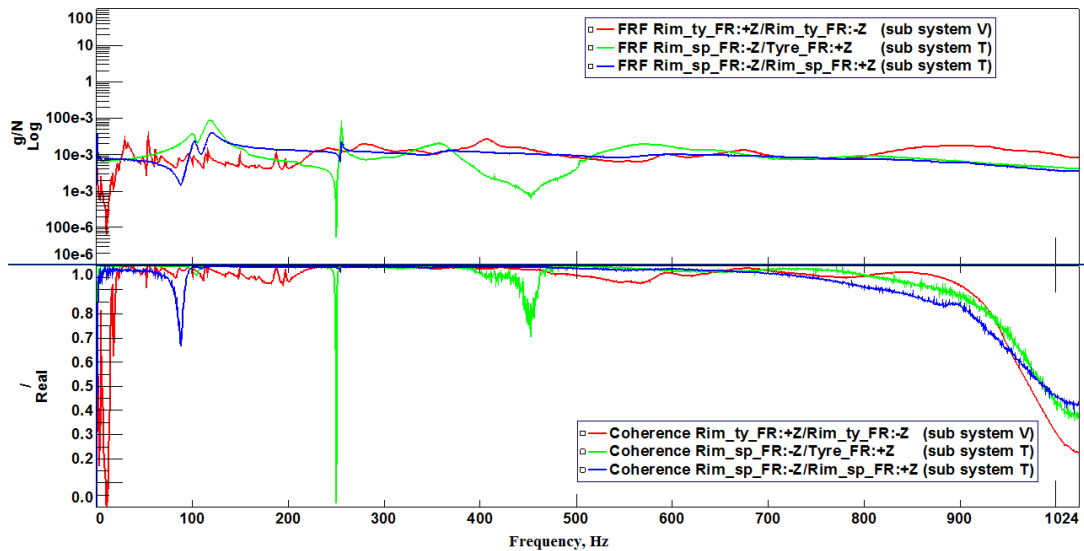


Figure 5.7c Front right wheel structural FRFs and Coherences in the vertical direction (free velocity method)

It is observed that the coherence value (green) beyond 300 Hz is poor for the structural FRFs between tyre contact patch and rim spindle interface for the excitation given in the longitudinal and lateral direction compared to the vertical direction. The drive point coherence at rim spindle interface on tyre wheel side (T) and vehicle side (V) is poor for the excitation in the lateral direction. This is due to the practical difficulty experienced while exciting in the lateral direction. Similarly, the structural FRFs for remaining wheels are determined and similar transfer characteristics are observed.

From equation 5.12 the equivalent excitation force at the rim spindle interface is estimated and then combined with NTFs to synthesize structure born vehicle interior noise. The following section discusses in detail the results of various TPA methods.

5.5 RESULTS AND DISCUSSIONS

The test run data corresponding to a speed of 30 kmph with engine off and free rolling condition for driver ear's target is considered for further discussion. The operational loads are estimated at rim spindle interface using the methods discussed in section 5.4.

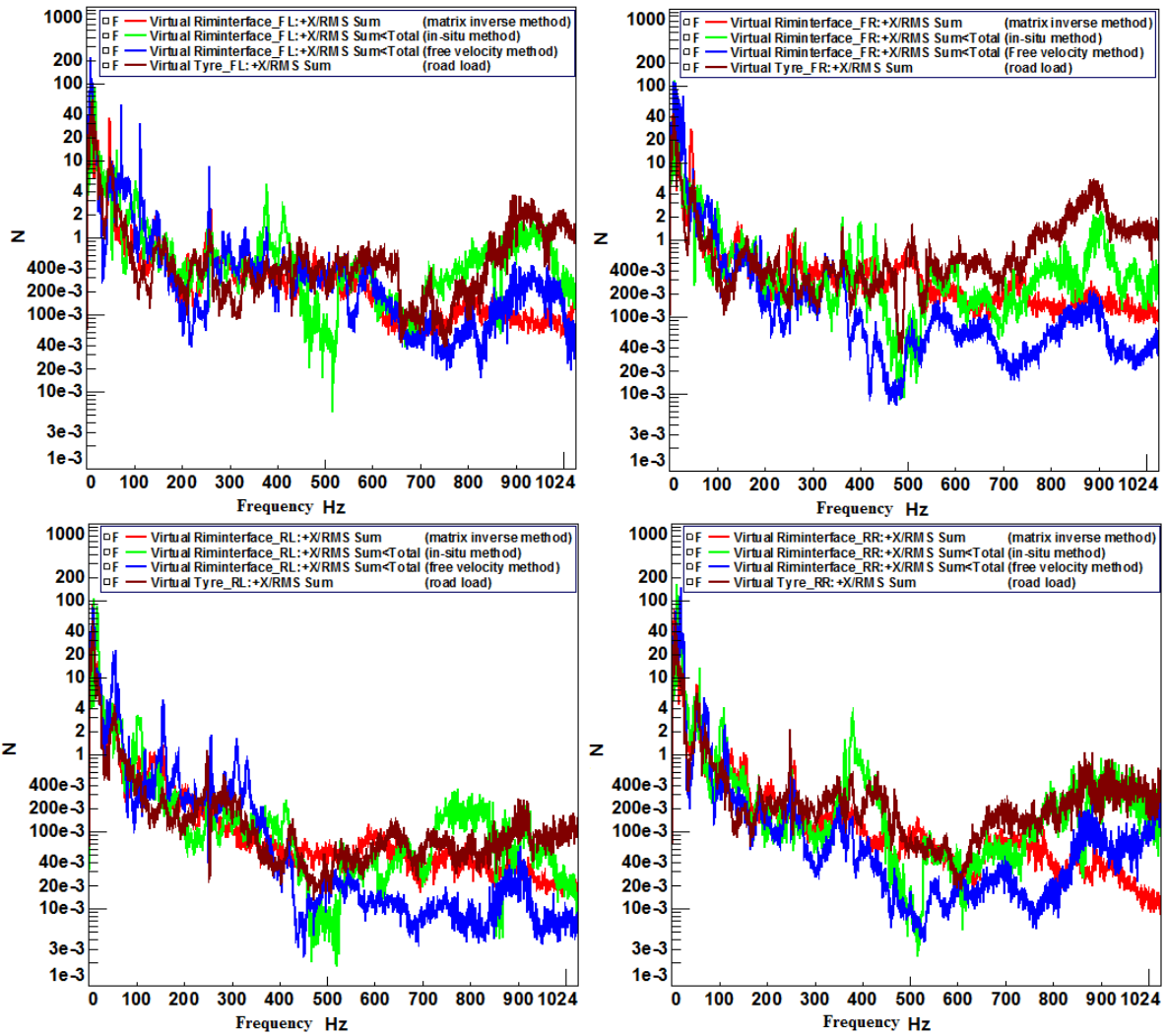


Figure 5.8a Comparison of operational loads in the longitudinal direction at rim spindle interface for all wheel from various methods

Figure 5.8a to 5.8c compares the estimated operational loads from matrix inverse (red) (method used in classical TPA and discussed in detail in chapter 4), in-situ (green), and free velocity methods (blue) as a function of frequency against the road load (brown) estimated as explained in section 5.3.

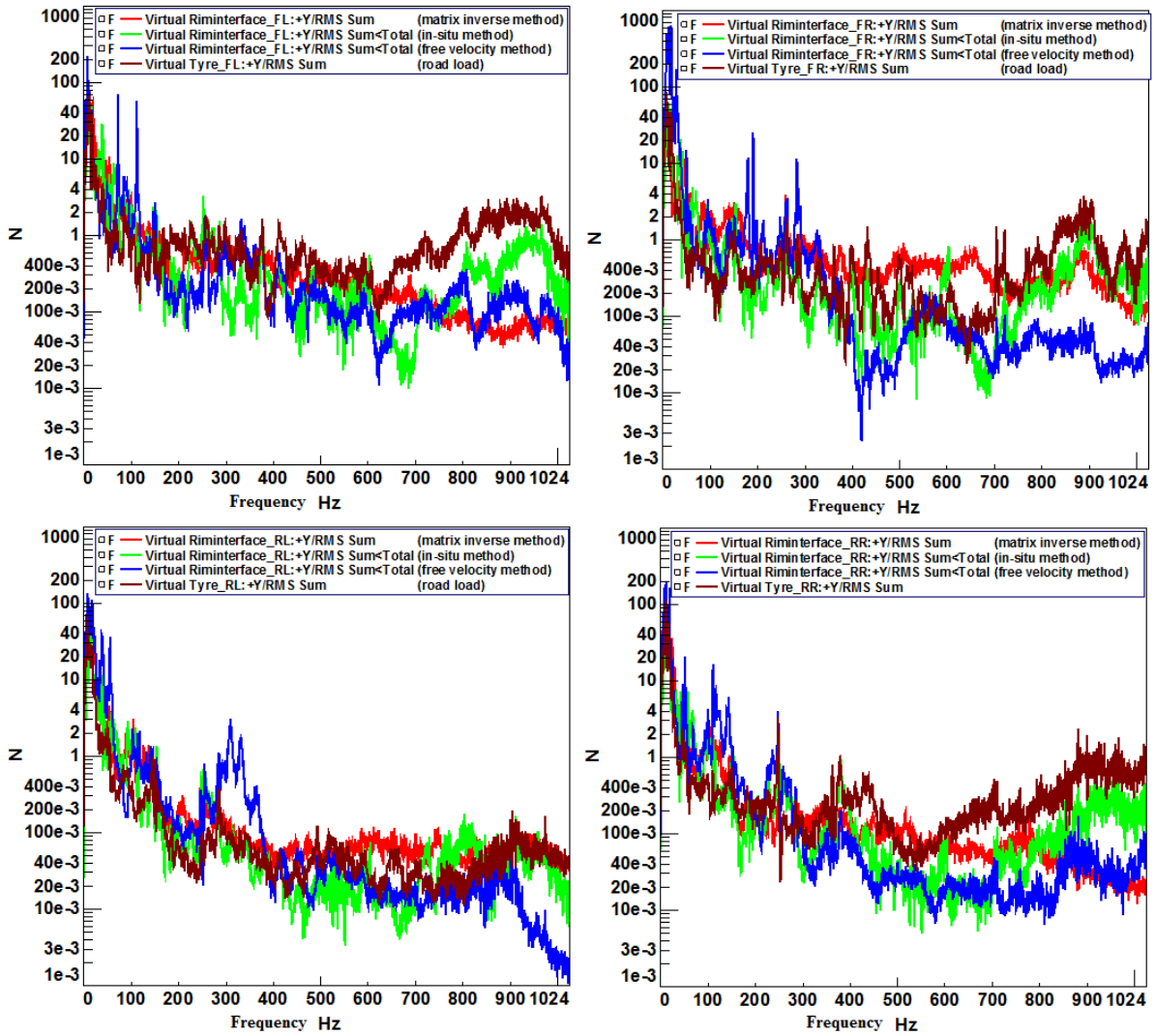


Figure 5.8b Comparison of operational loads in the lateral direction at rim spindle interface for all wheel from various methods

As can be seen from these figures, the estimated operational loads at rim spindle interface and the calculated road load, follow similar trend up to 400 Hz. However, in two paths shown in Figure 5.8b between 200 to 400 Hz (front right and rear left lateral directional paths in free velocity method) certain amount of deviation is observed and this is due to the poor coherence mentioned in the previous paragraph. This also manifests as an increase of the condition number for those FRFs of in-situ and free velocity method.

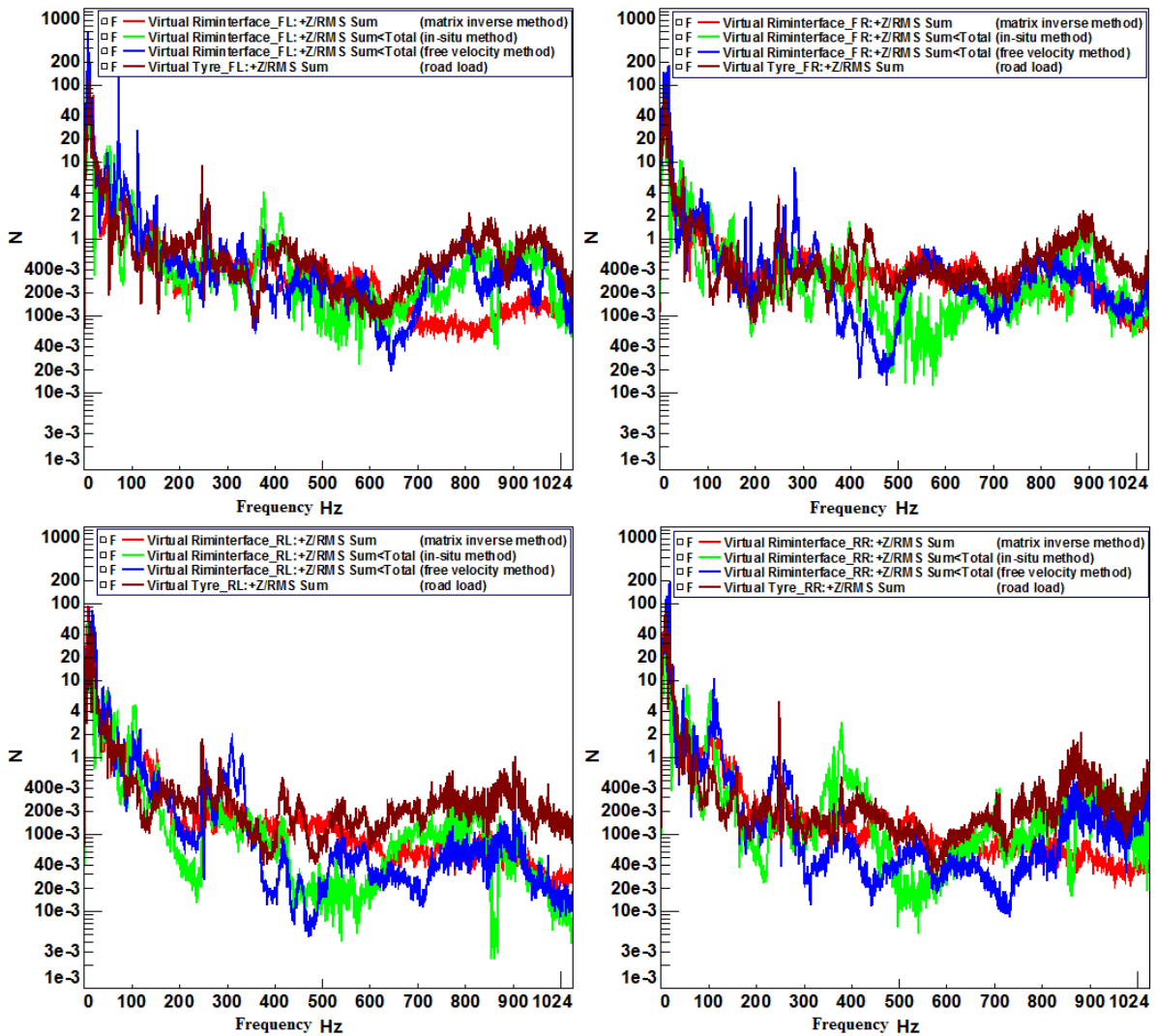


Figure 5.8c Comparison of operational loads in the vertical direction at rim spindle interface for all wheel from various methods

Figure 5.9a compares the variation of condition numbers of these three methods. It is evident that the condition number for in-situ method and free velocity method is high at frequencies where operational loads are high. The local structural FRFs used in matrix inverse method had additional indicators at suspension and lower arm and hence well conditioned. Hence relative percentage reduction in condition number is applied on the FRF matrix that was to be inverted for operational load estimation. These operational loads were further multiplied with respective NTFs to synthesize structure borne vehicle interior noise.

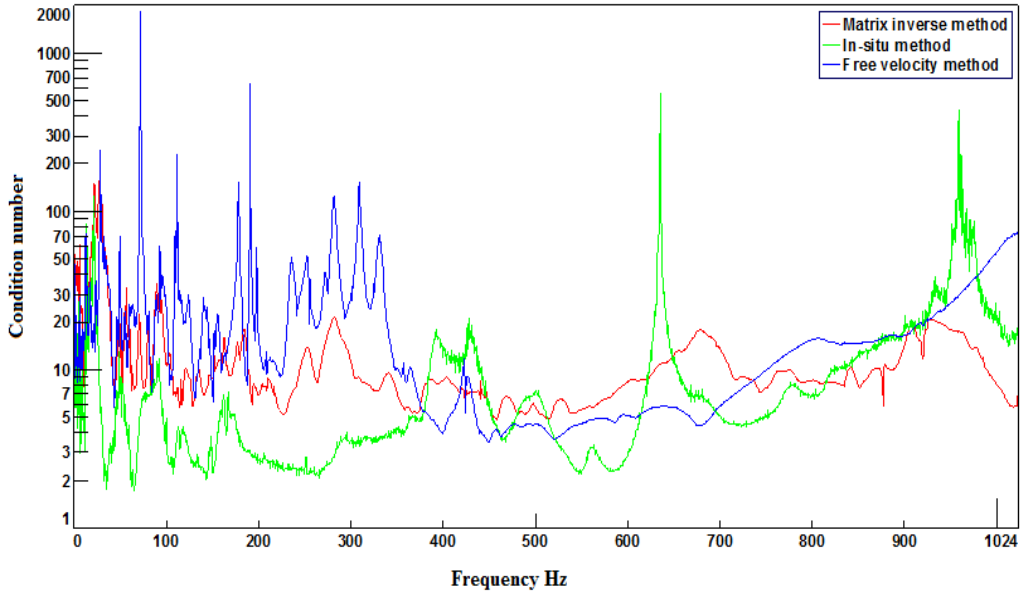


Figure 5.9a Variation of condition number of structural FRFs in different TPA methods

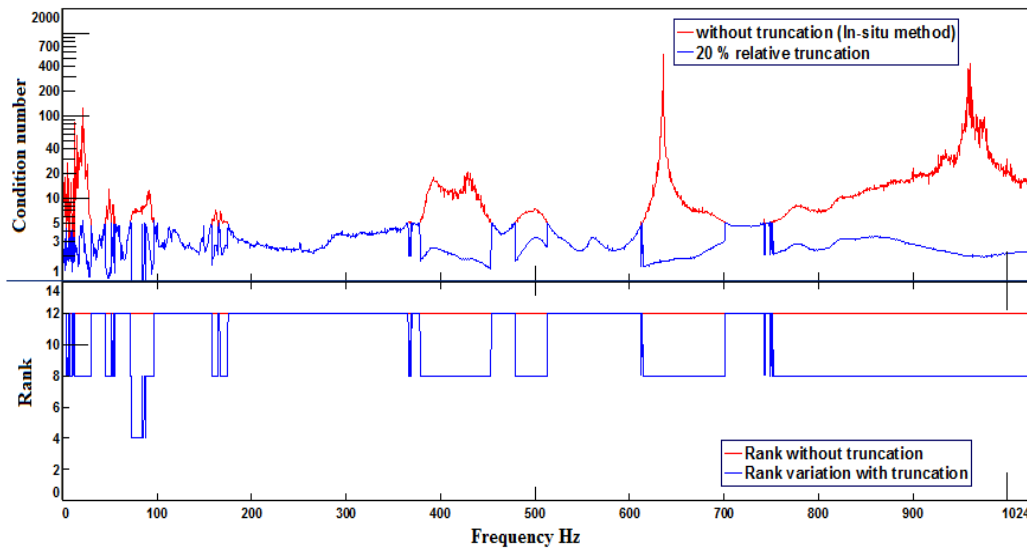


Figure 5.9b Truncation of condition number and the corresponding variation of rank of structural FRF matrix as function of frequency in 'in-situ' method

Figure 5.9b and 5.9c compare the condition number of structural FRFs obtained for in-situ method and free velocity method respectively, with and without truncation, as a function of frequency. The ensuing rank after correction is shown as rank-frequency plots in Figures 5.9b and 5.9c.

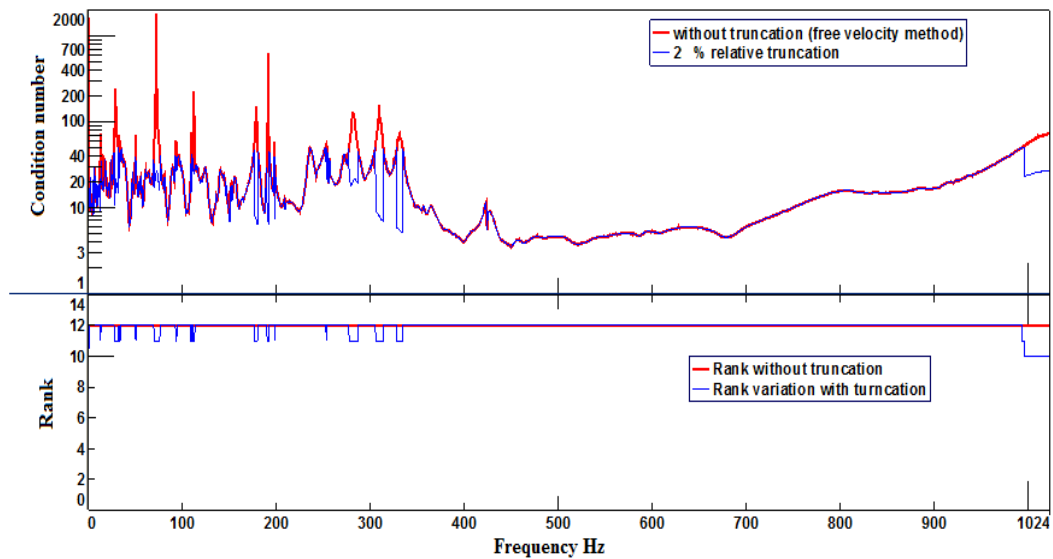


Figure 5.9c Truncation of condition number and the corresponding variation of rank of structural FRF matrix as function of frequency in 'in-situ' method

Figure 5.10a to 5.10c show the contribution of an individual path to the overall target response and this is shown in the third figures. Needless to say, these figures help one to identify the reasons for peak response. For example, in the matrix inverse method (subsystem V), (from Figure 5.10a) the peaks at the response for frequencies 122 Hz and 152 Hz is influenced by NTF rather than by the operational load. On the other hand, the peaks at 255 Hz and 377 Hz it is due to the operational loads. The same observations are also seen in in-situ and free velocity methods and are shown in Figure 5.10b and 5.10c. It should be noted that the data in these figures correspond to one path only and in total there are twelve paths which need to be taken into account for the full response analysis. But, they are not shown here.

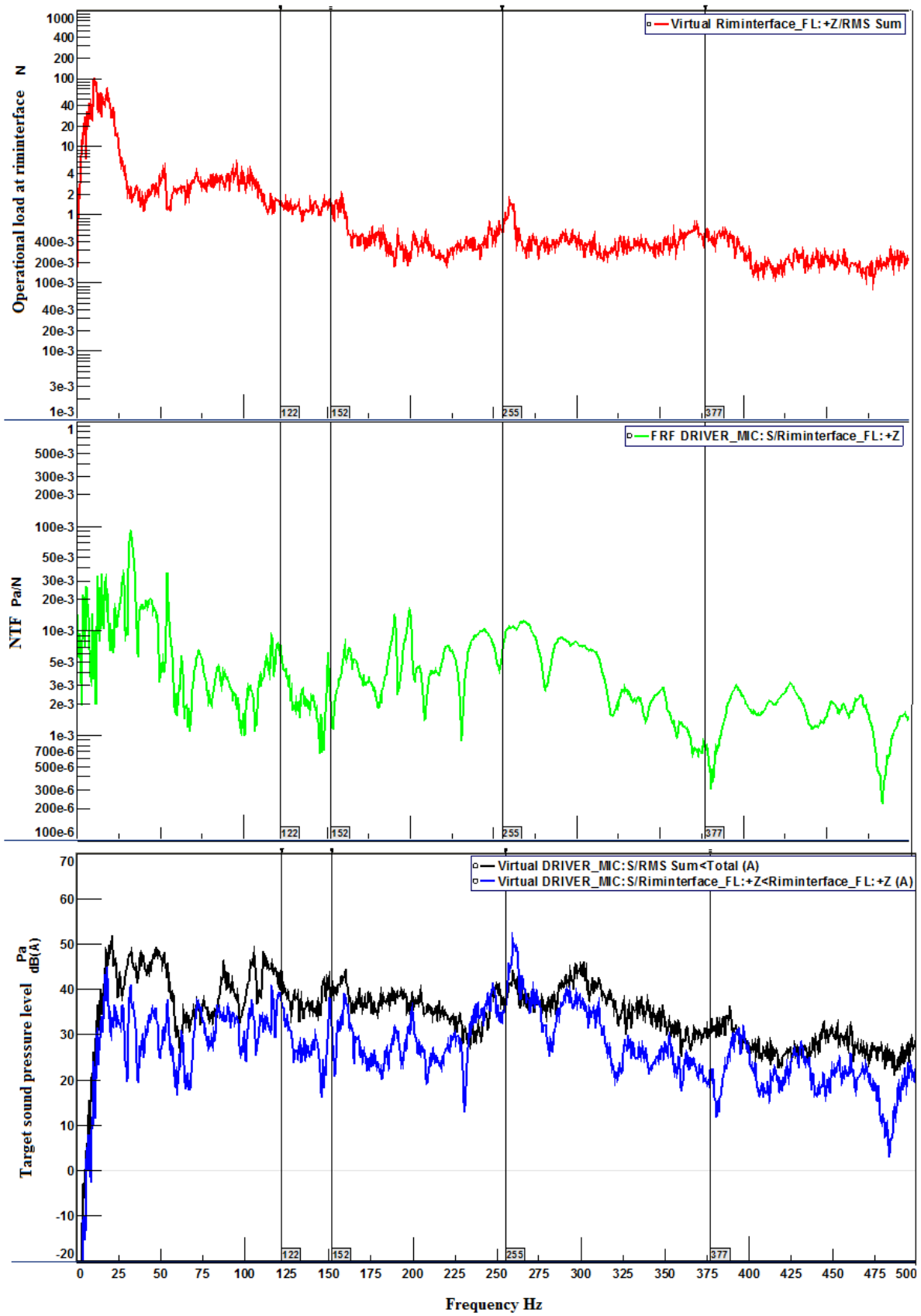


Figure 5.10a Individual path contribution analysis of Riminterface_FL:+Z to driver ear's target by matrix inverse method (subsystem V)

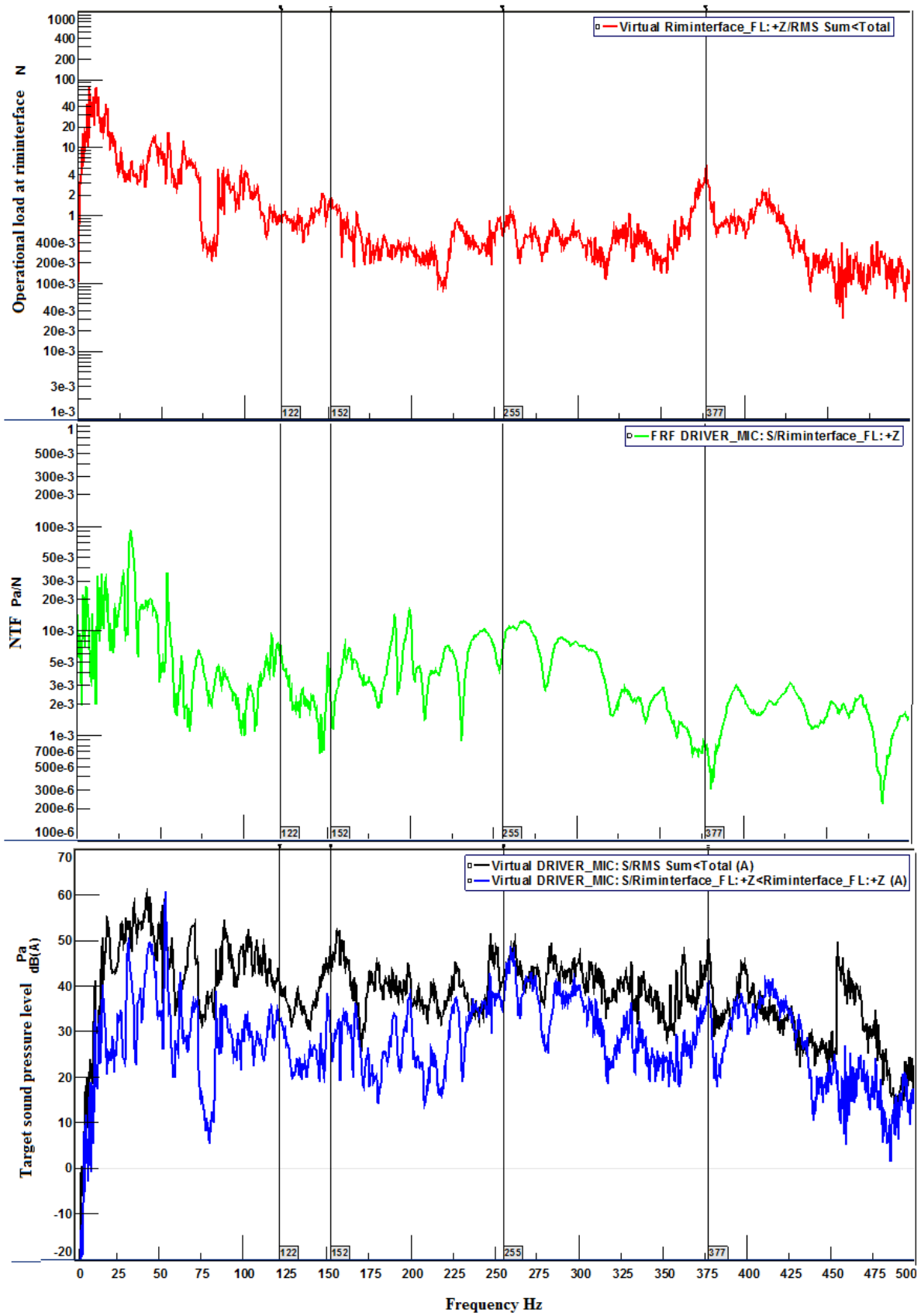


Figure 5.10b Individual path contribution analysis of Riminterface_FL:+Z to driver ear's target by in-situ method

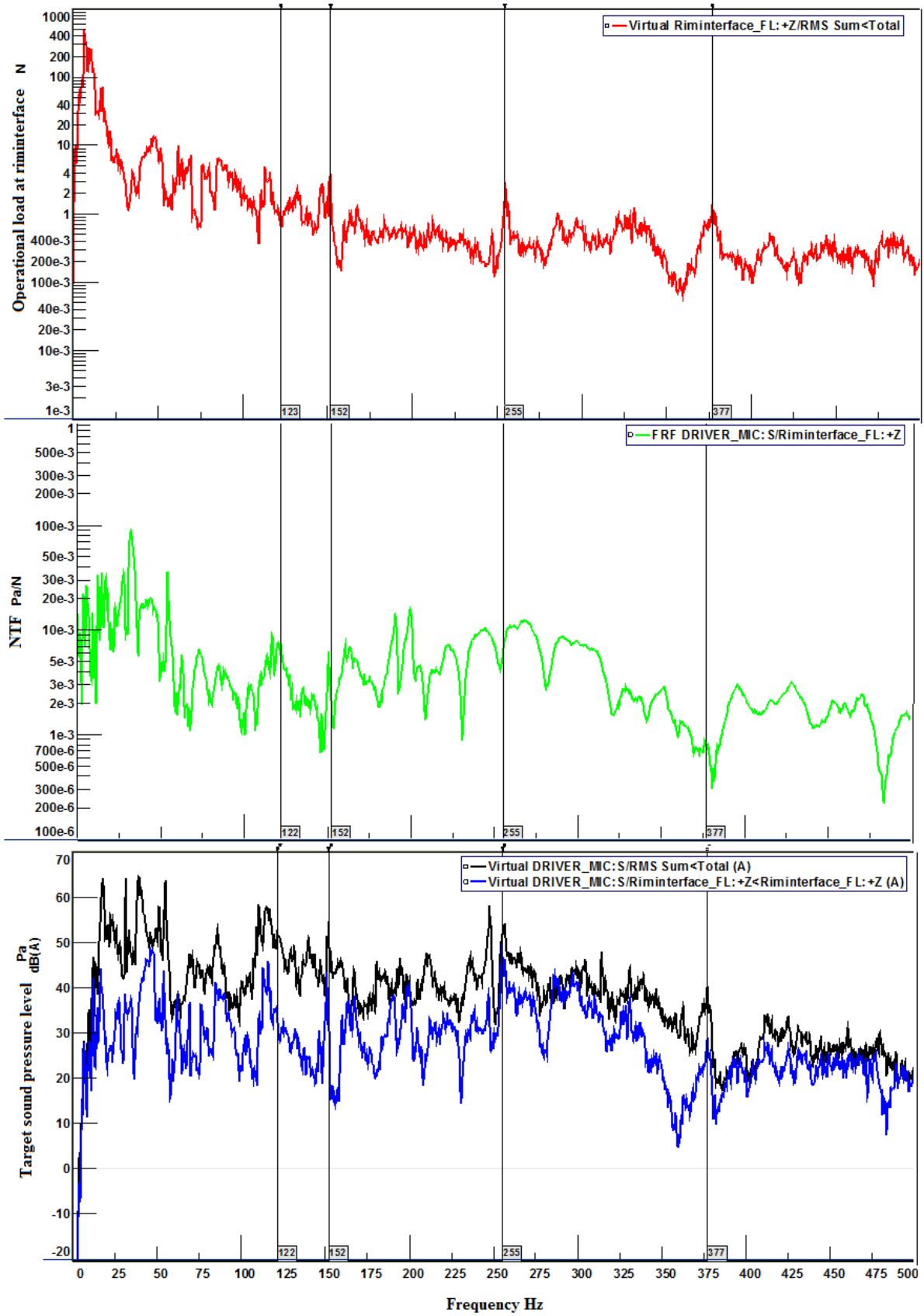


Figure 5.10c Individual path contribution analysis of Riminterface_FL:+Z to driver ear's target by free velocity method

The TPA results are interpreted using path and vector contribution analysis. Path contribution analysis gives the magnitude information of a particular path's (partial) contribution to the target microphone. This partial contribution of a single path also called 'partial path contribution plot' is obtained by multiplying the operational load estimated at the path by the corresponding NTF to the target and is shown in Figure 5.10a to 5.10c. The individual path contributions are shown by horizontal acoustic color bars as a function of frequency, while the contribution of the principal components and the overall RMS value of the target are shown by vertical bars. These plots do not give the phase information of different paths. Hence ranking of paths cannot be done by observing the partial path contribution plot alone. Vector contribution analysis is used to identify the phase information in an individual path with respect to the resulting target response. This plot helps to identify the actual dominating paths to the target.

Figures 5.11a and 5.11b, Figures 5.12a and 5.12b and Figure 5.13a and 5.13b compares the path contribution results of different methods with the one discussed in chapter 4 (Figure 4.13 and Figure 4.14), obtained from the classical experimental (matrix inverse method applied to subsystem V) TPA method.

The total structure borne interior noise obtained from matrix inverse method (assembly TV) is shown in Figure 5.11a. In Figure 5.11b the same is highlighted in the bar graph. The path contribution results shown in Figure 5.11a obtained from matrix inverse method applied to the assembly TV (Tyre Vehicle) show that the structure borne interior noise up to 400 Hz is similar to the one obtained without tyre wheel assembly (subsystem V) discussed in chapter 4 (Figure 4.13). The drop in coherence beyond 400 Hz (the NTFs shown in Figure 5.11c) precludes any reliable inferences in this data range. Figure 5.11b is an analogous plot of Figure 5.11a, where the contribution in terms of physical references are given in vertical bars and the contribution in terms of principal components for a chosen physical references are given in horizontal acoustic color maps.

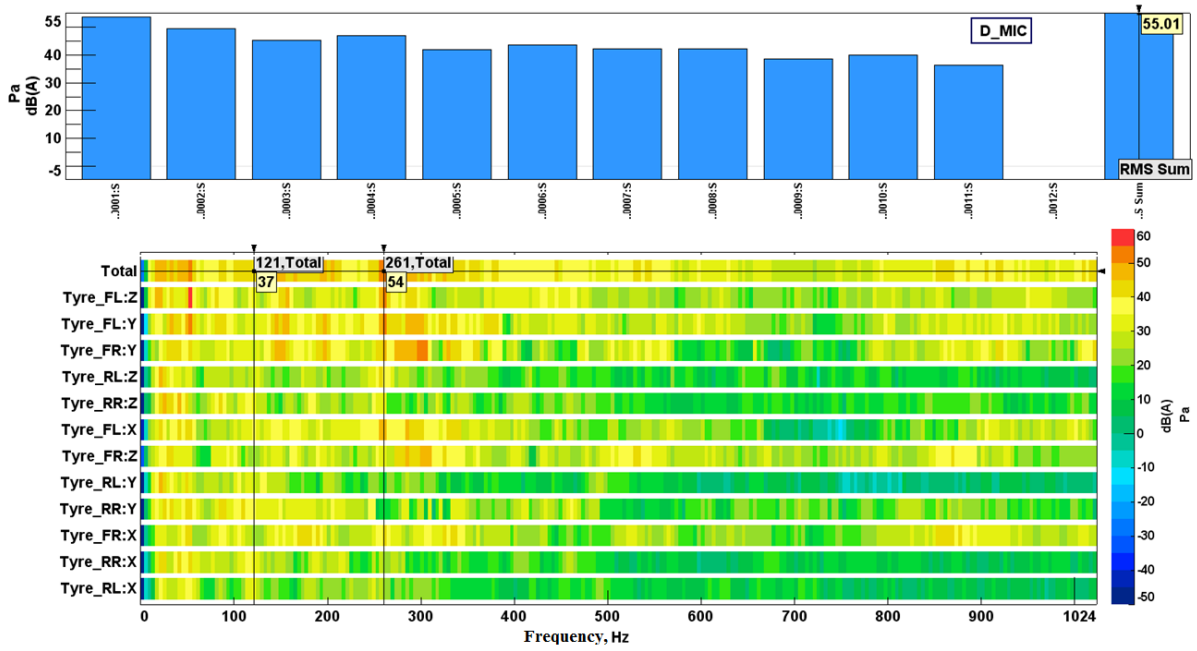


Figure 5.11a Path contribution results from matrix inverse method for assembly TV: vertical bars represents the contribution from principal components and horizontal acoustic color map represents the contribution from physical references

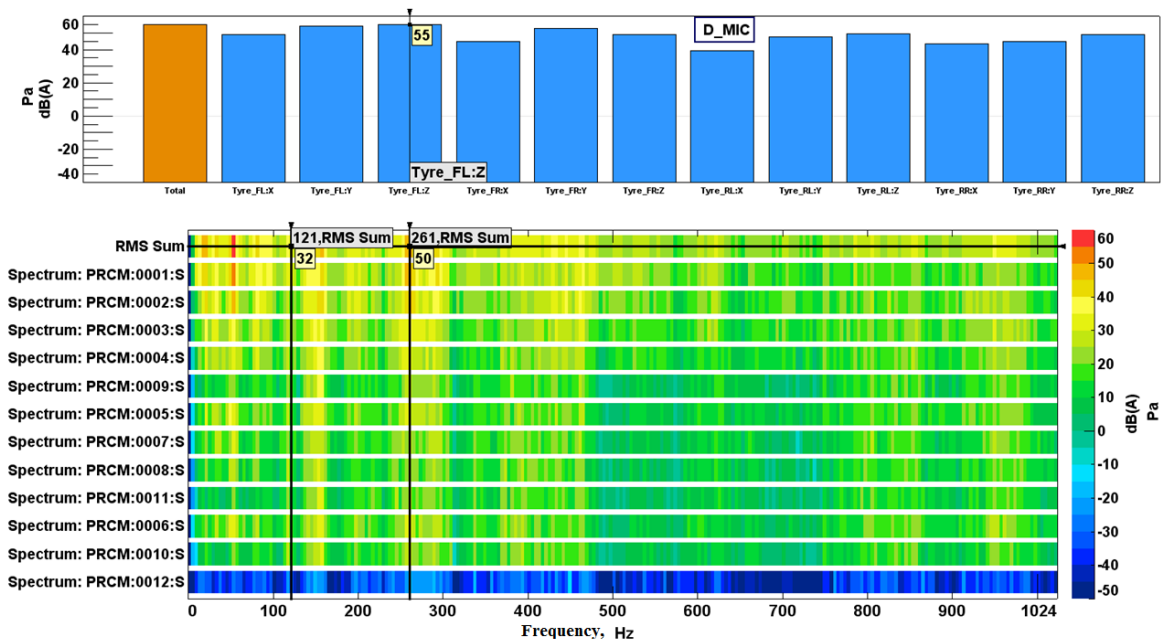


Figure 5.11b Contribution of principal components to the chosen critical path 'Tyre_FL:Z' from matrix inverse method for assembly TV: vertical bars at the top represents the contribution from physical references and horizontal acoustic color map represents the contribution of individual principal components.

The insignificant principal component (spectrum:PRCM:12:S) is observed in both the Figures (5.11a and 5.11b) which is conditioned during road load estimation as discussed earlier (Figure 5.9a - 5.9c).

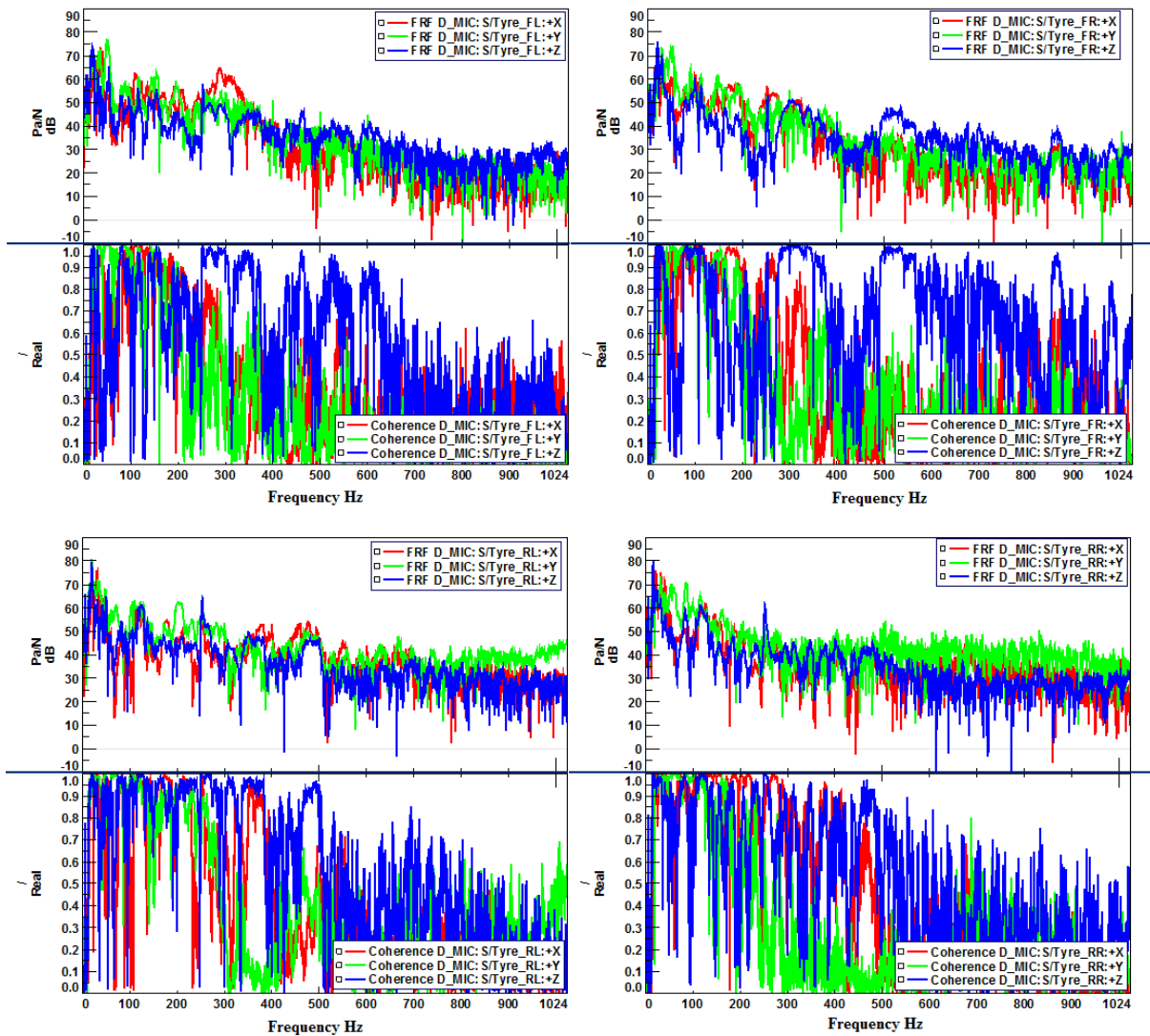


Figure 5.11c Variation of NTFs the between all tyre contact patch centre and driver's ear position and the corresponding coherence functions as function of frequency

Consider, Figures 5.11a (matrix inverse with tyre wheel assembly), 5.12a (in-situ method), 5.13a (free velocity method) and 5.11d (matrix inverse with only the vehicle and same as Figure 4.13 reproduced here for ease of comparison). From Figure 5.11a and Figure 5.11d it is observed that there is negligible difference in total RMS sound pressure level between the two cases (one is 54.3 and the other is 55.01dB(A)). A 4 dB(A) difference in RMS sound pressure level is observed between the matrix inverse methods and the component based TPA methods (in-situ and free velocity methods shown in Figure 5.12a and 5.13a. It can be noted that among the physical references, Riminterface_FL:Z shows higher contribution in terms of magnitude when compared to other paths. This can be seen from Figures 5.11a and 5.12a.

The vector contribution results are needed to conclude the dominance and is discussed in a later paragraph.

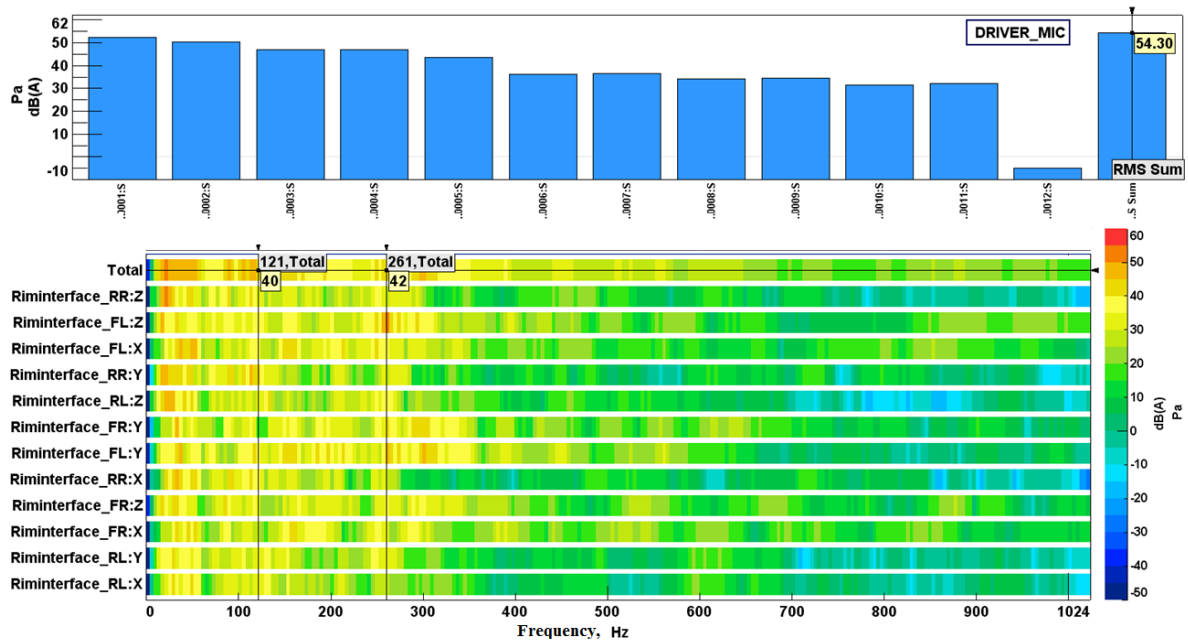


Figure. 5.11d Path contribution results from matrix inverse method for vehicle subsystem V: vertical bars represents the contribution from principal components and horizontal acoustic color map represents the contribution from physical references

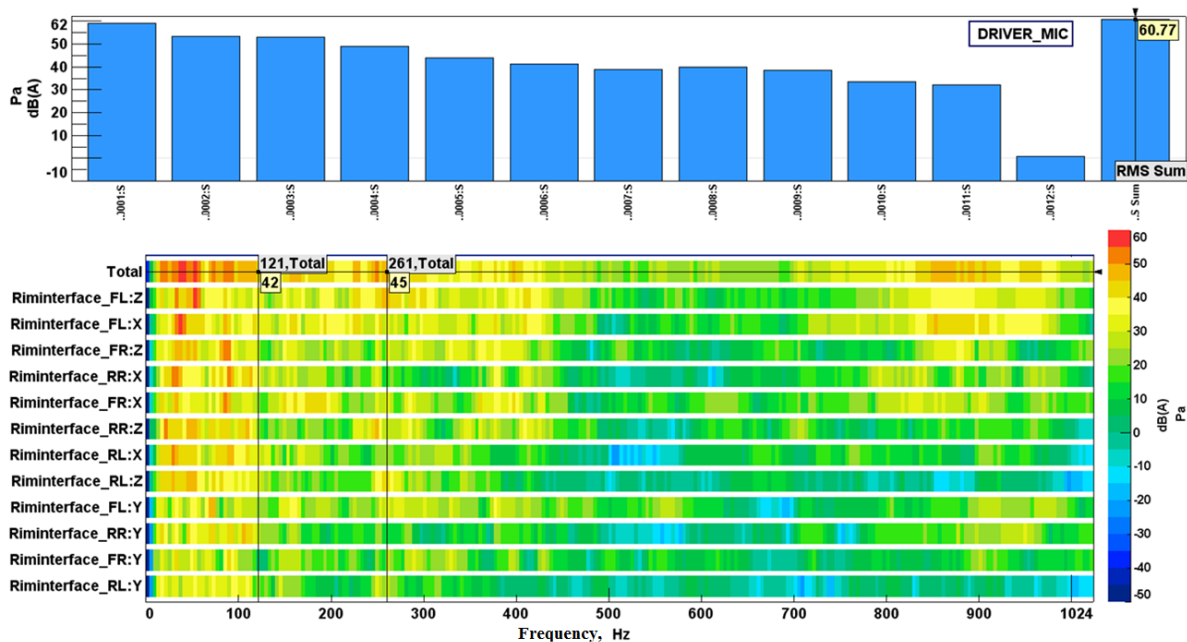


Figure 5.12a Path contribution results from in-situ method: vertical bars represents the contribution from principal components and horizontal acoustic color map represents the contribution from physical references

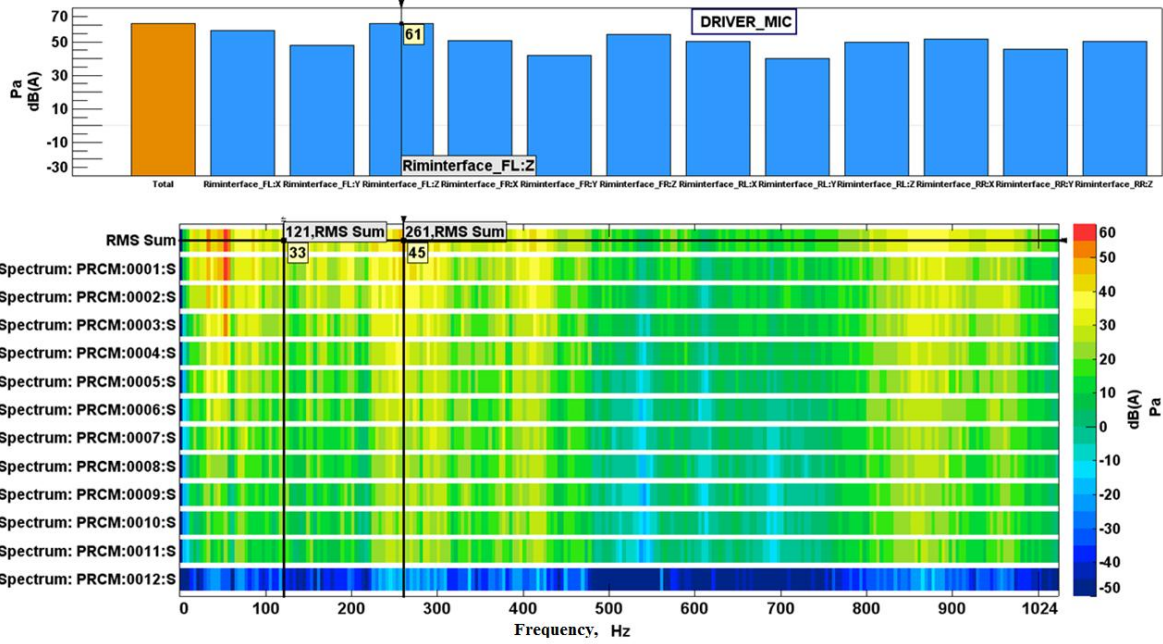


Figure 5.12b Contribution of principal components to the chosen critical path 'Riminterface_FL:Z' from in-situ method: vertical bars at the top represents the contribution from physical references and horizontal acoustic color map represents the contribution of individual principal components

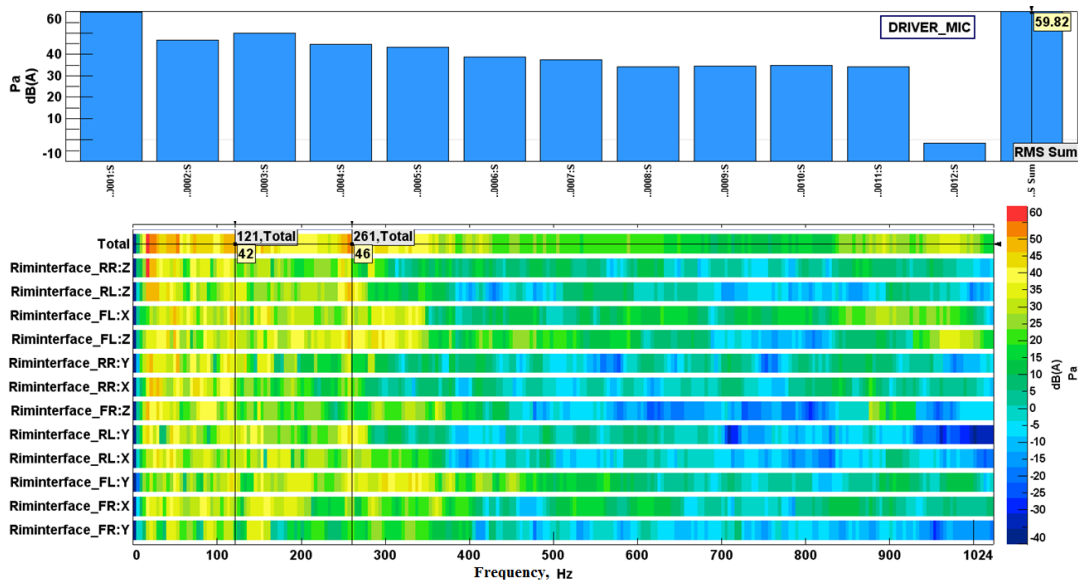


Figure 5.13a Path contribution results from free velocity method: vertical bars represents the contribution from principal components and horizontal acoustic color map represents the contribution from physical references

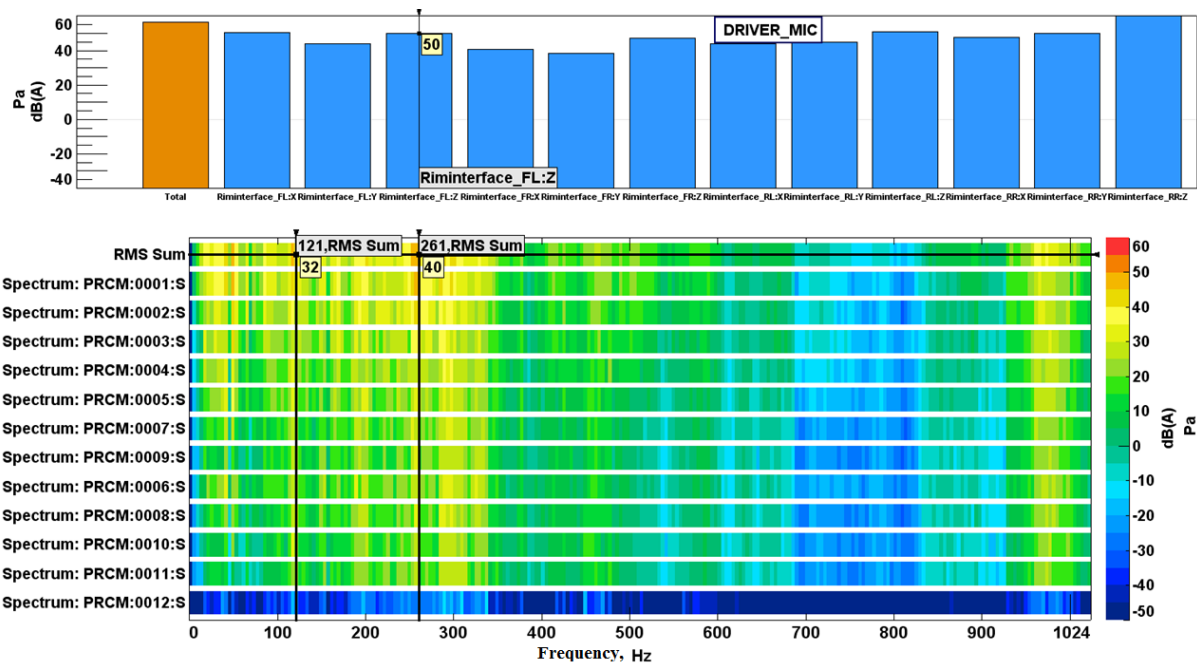


Figure 5.13b Contribution of principal components to the chosen critical path 'Riminterface_FL:Z' from free velocity method: vertical bars at the top represents the contribution from physical references and horizontal acoustic color map represents the contribution of individual principal components.

Similar to the matrix inverse method (applied to assembly TV), the in-situ and free velocity methods also identify the insignificant principal component (spectrum: PRCM:0012:S) as shown in their partial path contribution plots. This can be seen in Figure 5.12b and 5.13b. The path contributions are similar for the in-situ and free velocity methods. Figures 5.11b, 5.12b and 5.13b compare the contribution of the principal components to the chosen critical path 'Riminterface_FL:Z' for various methods. Similar discussions were presented in chapter 4 (Figure 4.14) for classical experimental TPA. Between 230 Hz to 320Hz all the PCs from 1 to 11 have equal contribution to the total RMS value of the path 'Riminterface_FL:Z'. However below 400 Hz, the first 3 PCs have a larger share to the total RMS value. First principal component is considered for vector contribution analysis.

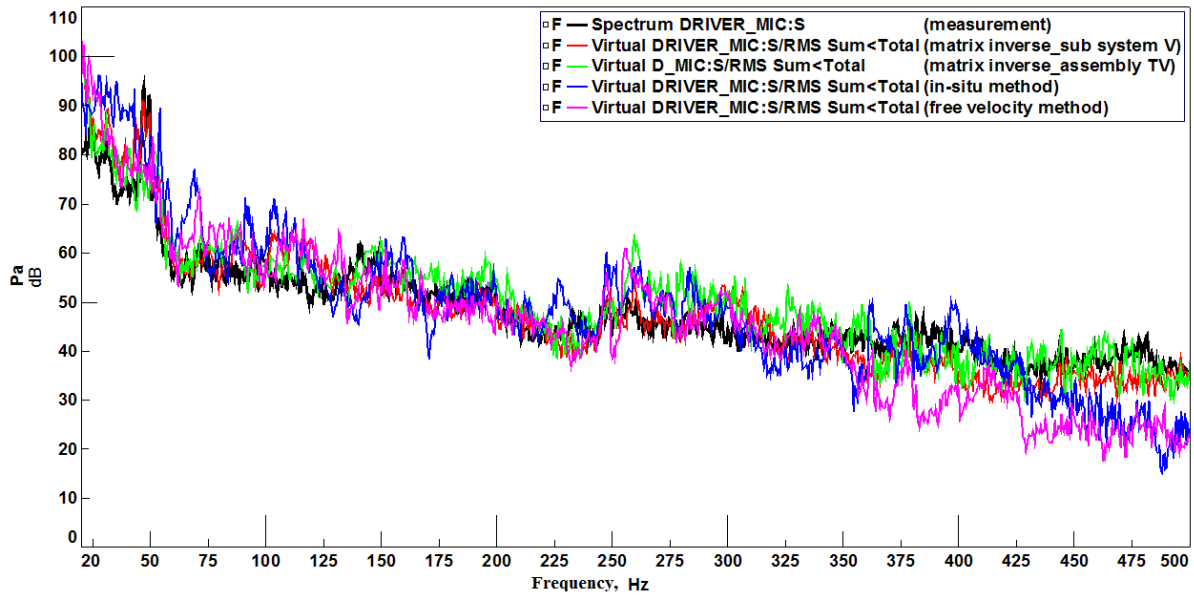


Figure 5.14 Comparison of total sound pressure levels obtained from various methods

Figure 5.14 compares the spectrum of sound pressure level synthesized at the target with the experimental data for all the techniques discussed. It is observed that the variation of sound pressure level by different methods fluctuate about the actual measurement spectrum. Two frequencies are chosen (121 Hz and 261 Hz) from this noise spectrum for further discussions based on the vector contribution analysis. The individual path's contribution for these two frequencies are represented in the partial path contribution plot. It is important to visualize the relative contributions of the paths. The earlier figures (5.11a, 5.12a, 5.13a, and 5.11d) can be used for this visualization.

Vector contribution plots for other methods are shown in Figure 5.15a to 5.15f to determine the dominant paths that contribute to the target. This is similar to the figs 4.15a and 4.15b shown for matrix inverse method with the vehicle subsystem alone. Figure 5.15a to 5.15c and Figure 5.15d to 5.15f compare the vector contribution results for two frequencies 121 Hz and 261 Hz respectively for all the methods. The results are further summarized in Table 5.2 and 5.3 respectively.

Table 5.2 Vector contribution analysis of Principal component no.1 (PRCM:0001:S) at 121 Hz

Paths	Matrix inverse (subsystem V)			Matrix inverse (assembly TV)			In-situ			Free velocity		
	Magnitude (dB(A))	Phase (degrees)	Magnitude (dB(A))	Phase (degrees)	Magnitude (dB(A))	Phase (degrees)	Magnitude (dB(A))	Phase (degrees)	Magnitude (dB(A))	Phase (degrees)	Magnitude (dB(A))	Phase (degrees)
FL_X	28.50	148.02	33.50	-41.21	29.89	-40.21	34.76	-333.38				
FL_Y	32.52	50.38	21.14	-1.15	19.55	104.91	33.41	1.10				
FL_Z	36.80	-53.15	31.09	98.90	32.24	-24.43	31.31	-9.53				
FR_X	21.43	-104.24	19.30	-103.96	10.99	51.54	23.06	-196.83				
FR_Y	15.65	-53.02	6.76	127.07	-5.59	-44.16	7.95	-170.9				
FR_Z	23.47	132.47	13.72	71.72	17.98	-80.25	10.74	-5.45				
RR_X	6.870	42.41	14.43	135.11	29.90	23.20	12.50	-36.80				
RR_Y	20.43	-95.23	27.15	129.29	22.38	120.99	23.25	-78.31				
RR_Z	22.37	198.74	26.16	-87.19	12.06	112.90	11.95	-200.94				
RL_X	10.59	86.95	15.87	-76.81	-0.48	131.78	9.60	-72.48				
RL_Y	23.12	63.39	19.60	51.20	2.44	-33.64	19.48	-220.09				
RL_Z	21.38	102.82	14.18	124.70	15.96	74.18	21.47	-117.07				
Total SPL	29.23	0	31.11	0	38.60	0	40.85	0				

Table 5.3 Vector contribution analysis of Principal component no.1 (PRCM:0001:S) at 261 Hz

Paths	Matrix inverse (subsystem V)		Matrix inverse (assembly TV)		In-situ		Free velocity	
	Magnitude (dB(A))	Phase (degrees)	Magnitude (dB(A))	Phase (degrees)	Magnitude (dB(A))	Phase (degrees)	Magnitude (dB(A))	Phase (degrees)
FL_X	32.96	-149.52	45.73	219.41	31	-204.05	28.43	334.6
FL_Y	39.32	-237.49	46.79	-6.86	41.05	41.06	37.41	205.21
FL_Z	42.91	-17.56	47.84	24.05	44.39	-18.08	35.79	12.31
FR_X	27.7	-16.17	40.82	314.79	32.13	-172.15	24.54	262.15
FR_Y	32.48	-154.15	41.36	96.7	29.52	-65.77	10.45	308.57
FR_Z	19.46	-290.37	25.3	-10.14	26.67	-50.1	13.49	63.8
RR_X	14.94	-28.34	12.19	261.72	6.83	23.94	9.52	19.51
RR_Y	14.15	-245.16	10.25	103.17	10.85	-178.32	-2.86	139.28
RR_Z	-0.59	-185.16	13.53	78.36	7.37	-103.09	3.05	36.39
RL_X	0.06	-251.26	7.01	149.14	17.16	-84.41	19.6	80.44
RL_Y	16.9	43.05	-0.41	205.33	32.65	-239.96	30.48	1.04
RL_Z	23.12	-160.51	26.89	156.2	25.28	-117.94	31.85	56.27
Total SPL	28.65	0	50.91	0	44.35	0	37.94	0

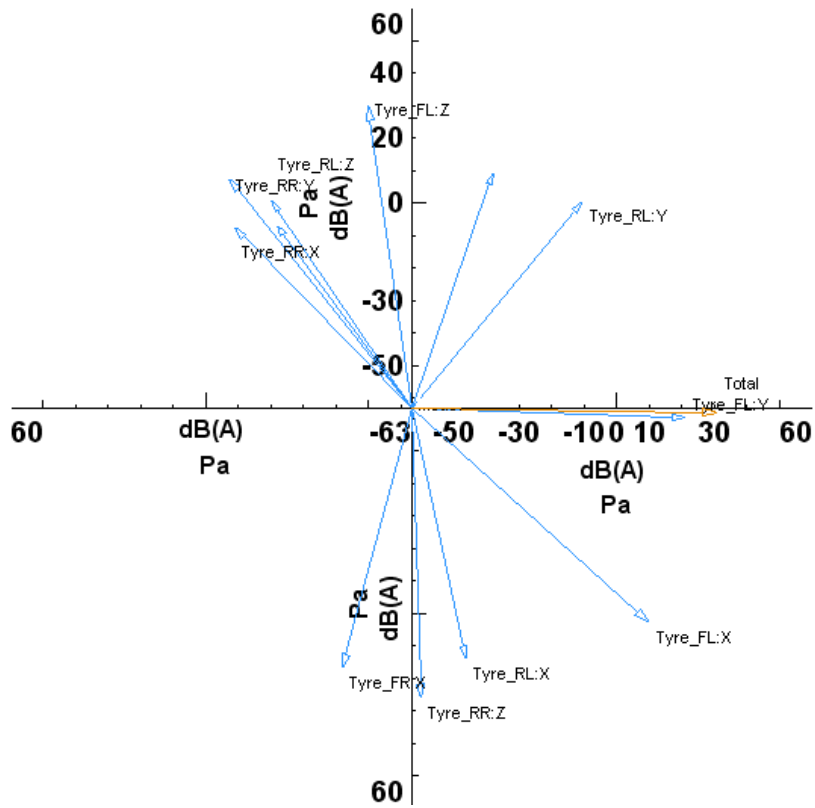


Figure 5.15a Vector contribution results at 121 Hz from matrix inverse for assembly TV

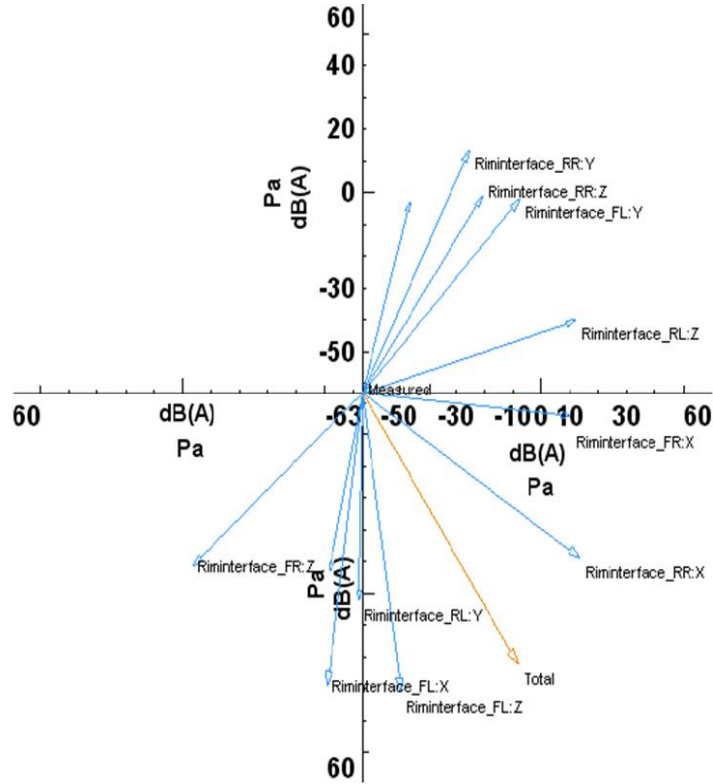


Figure 5.15b Vector contribution results at 121 Hz from in-situ method

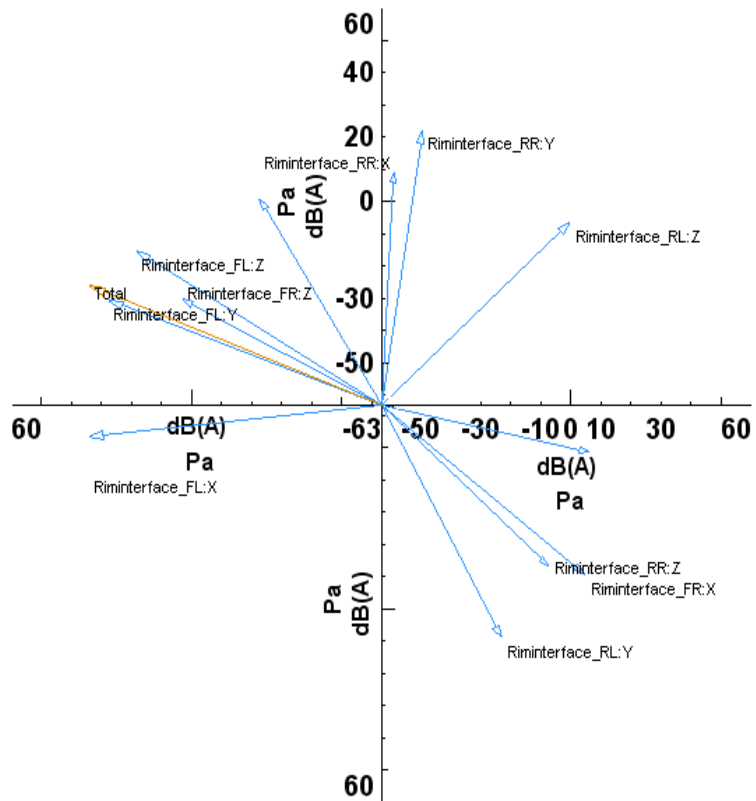


Figure 5.15c Vector contribution results at 121 Hz from free velocity method

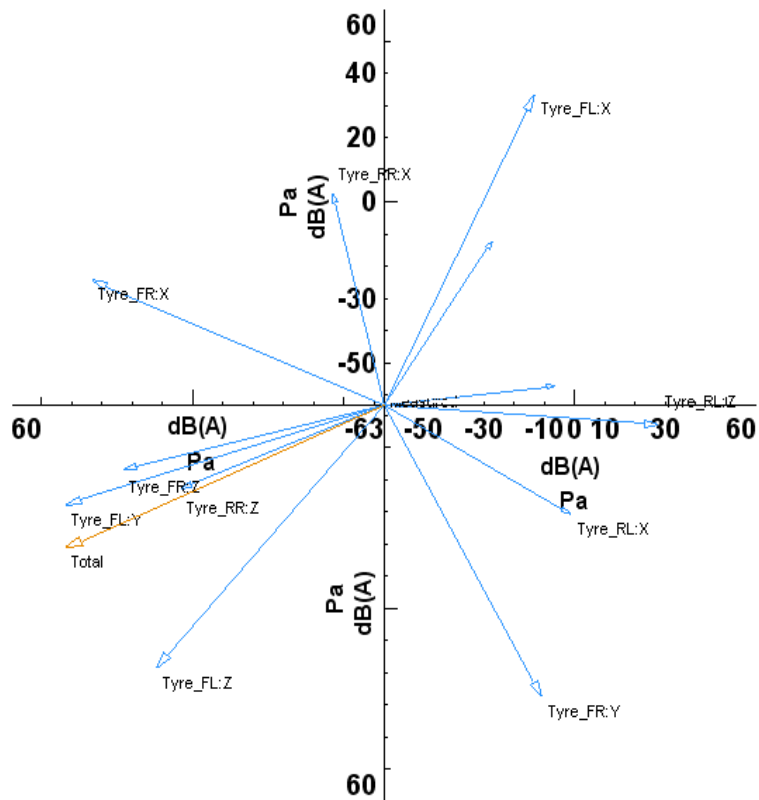


Figure 5.15d Vector contribution results at 261 Hz from matrix inverse for assembly TV

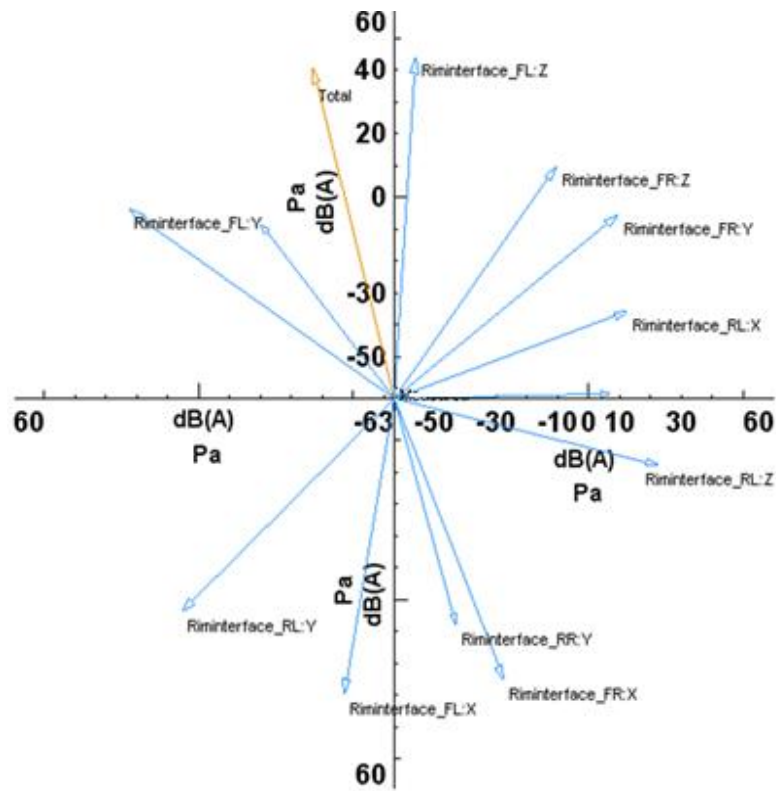


Figure 5.15e Vector contribution results at 261 Hz from in-situ method

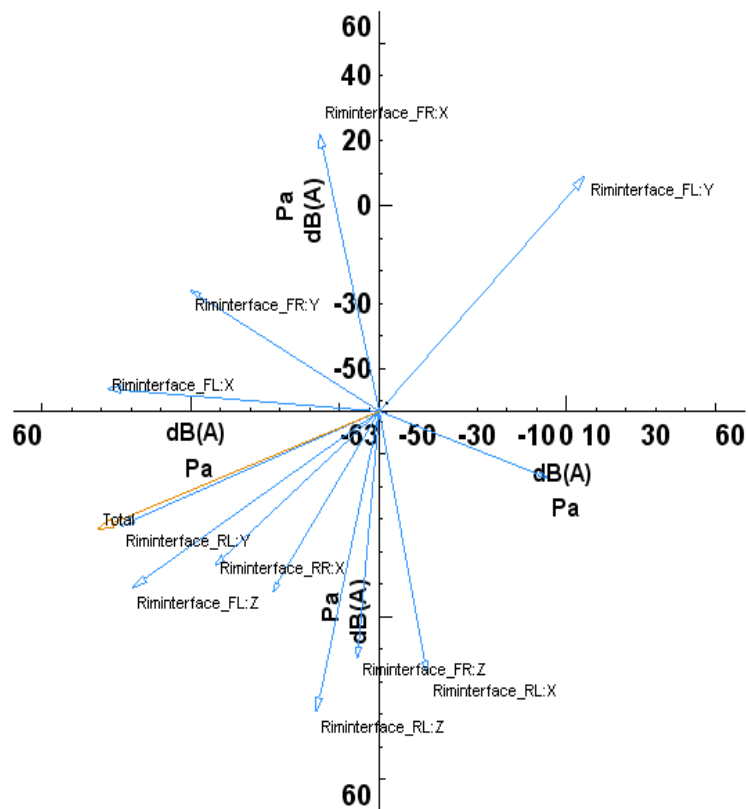


Figure 5.15f Vector contribution results at 261 Hz from free velocity method

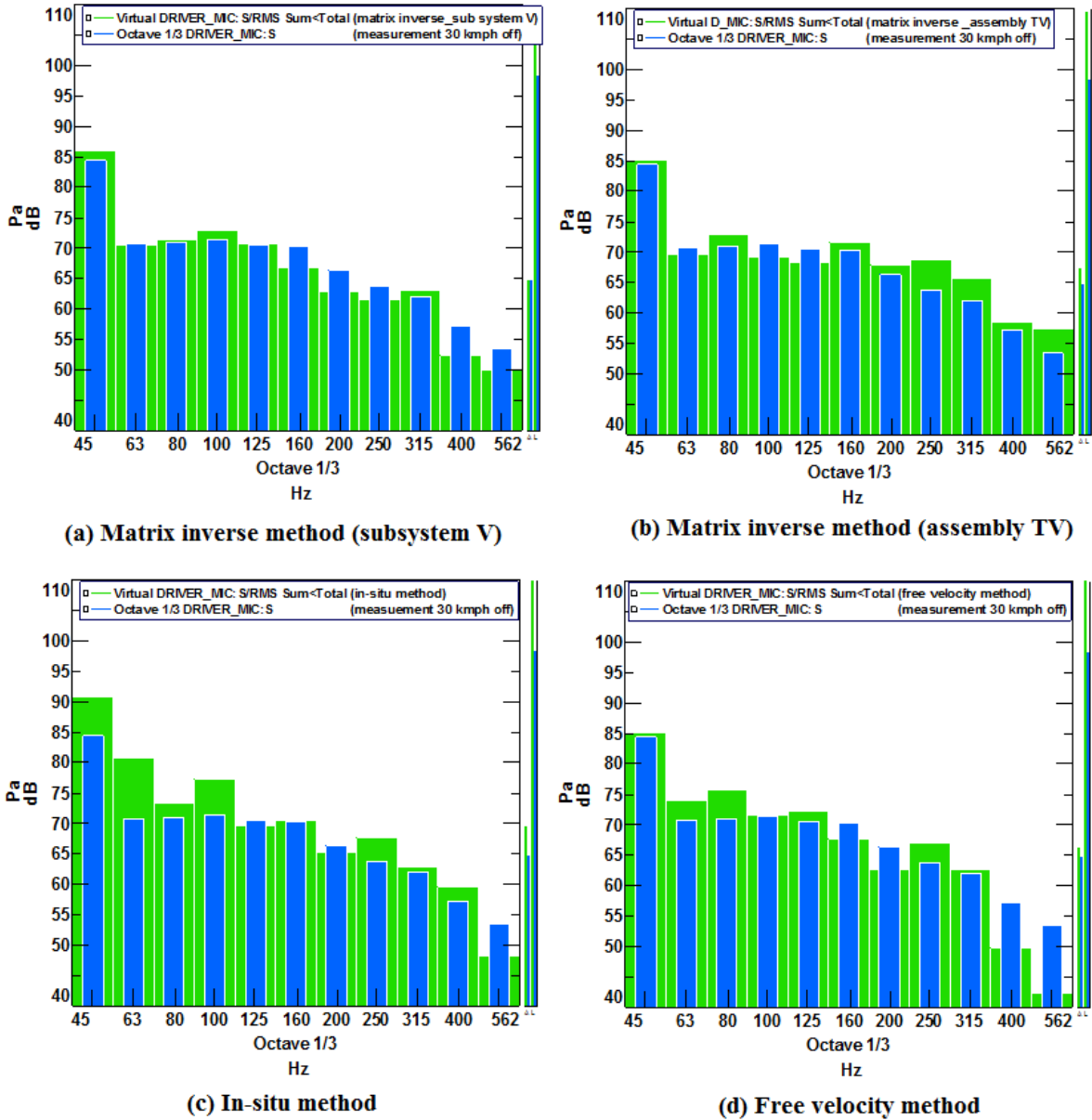


Figure 5.16 Comparison of sound pressure level obtained from different methods with measurements of driver's ear target

As far as the knowledge of the author, there has been no critical comparison of different TPA methods. The two Tables above (5.2 and 5.3) compare the methods at two different frequencies and one notices a big difference in phase and differences in magnitude as well. This fact has been lucidly presented by Juha Plunt (2005). Plunt observed a large change in phase for a very small change in frequency. As fig. 5 in this paper shows, there is also a large change in the magnitude. This is exactly what has been observed in this work, while comparing the magnitudes and phases at a particular frequency. Plunt recommends that for low frequency TPA (200-600 HZ), NTFs are 'smoothed' in frequency. In this work,

operational loads calculated also vary with frequency and this may also be a contributing factor. Figure 5.14, which compares the various sound pressure level also brings out a similar trend. In other words, what has been observed in this work has also been noted in other works reported in literature.

Hence, following the traditional method, Figure 5.16 compares the 1/3 octave sound pressure level (SPL) of these methods with actual measurements. It can be seen that the synthesized sound pressure levels by various TPA methods are very close to the actual measurement in the central frequency bands below 400 Hz. Most methods seem to agree closely with the measured data in the frequency range between 80 and 400 Hz. This is the frequency at which belt vibration is critical and the method for rolling modal analysis has been explained in the previous chapters. In the case of free velocity method, the error increases at 400 Hz. This is well correlated with a loss of coherence at this frequency. We conclude this chapter stating that there is a need to look at different methods more closely from the point of view of the phase.

5.6 SUMMARY

This chapter described in details the implementation aspects and the results comparisons of matrix inverse method (assembly TV), in-situ and free velocity methods. Importantly the matrix inverse method is used to quantify the road loads. Also, it is understood that once the laboratory and road tests for matrix inverse method, is performed repeating it for every new set of tyres is laborious and time consuming. Instead the in-situ or free velocity methods can be employed to study the influence of tyre design without conducting the road test. These two method belonging to the component based TPA family require only the individual tyre transfer characteristics. The tyre transfer function can be determined by a relatively simple experiment and can be combined with the vehicle characteristics. However, all these experiments require a reliable experimental data. Reliability can be checked by the repeatability of the data. The following chapter explains the repeatability of the experiments conducted.

CHAPTER 6

EXPERIMENTAL REPEATABILITY FOR MULTI REFERENCE TRANSFER PATH ANALYSIS

6.1 INTRODUCTION

The structural Frequency Response Functions (FRFs), Noise Transfer Functions (NTFs), operational accelerations and sound pressures are the main requirement for Transfer Path Analysis (TPA). Chapter 4 and Chapter 5 discussed about these measurements and the analysis. Figure 6.1 gives the aim of all the experiments conducted and the methodology for the conventional TPA and the component based TPA methods in the form of the flow chart. The reliability of the objective evaluation is mainly dependent on the quality of these measured data. Traditionally automotive industry conduct subjective evaluation with the help of trained juries to rate the NVH behaviour of the vehicle, on a relative basis, of different vehicles driven over a range of road surface. A well designed evaluation scheme is used by the juries. However, the degree of difference in ride quality among different vehicles cannot be quantitatively determined by subjective evaluation procedure (Wong, 2001). Hence the objective evaluation is very important to address the NVH issues correctly. This requires sophisticated experimental set up and an environment (anechoic chamber) where environmental noise can be fully isolated. However with limited facility in the absence of anechoic chamber the experiments were performed and multiple measurements made for TPA. Hence the repeatability check of all the measurements are necessary to ensure the reliable data. This chapter describes the optimum utility of minimum number of sensors and measuring channels.

6.2 PRINCIPAL COMPONENT ANALYSIS FOR TPA

Road noise TPA of a passenger car due to tyre/road interaction cannot be analyzed like an engine TPA, as there are four tyre wheel assemblies. The road loads are transferred through these wheel assemblies to the rim spindle interfaces. At the rim spindle interface these inputs

are called physical reference sources (responses at spindle indicators) and are partially correlated. Also they are partially correlated with the other indicator (responses at suspension and lower arm) measurements. Hence, they do not have fixed phase relationship. In case of engine TPA, the model has a single reference point that has a fixed phase relationship between fully coherent measured response points and a well defined Root Mean Square (RMS) sum can be obtained (Hendricx and Vandebroek, 1993). In case of road noise TPA, due to the partial coherence, the RMS sum of the responses is not well defined. In order to have well defined RMS sum, the physical references (path indicators) are to be converted into virtual references called independent phenomena or principal components (PCs) (LMS Test. Lab, 2009). The Principal Component Analysis (PCA) is used to convert the physical reference signals into an equivalent orthogonal PCs. This orthogonal transformation is further applied to all indicator response signals to get virtual referenced spectra as discussed in Chapter 4 & 5.

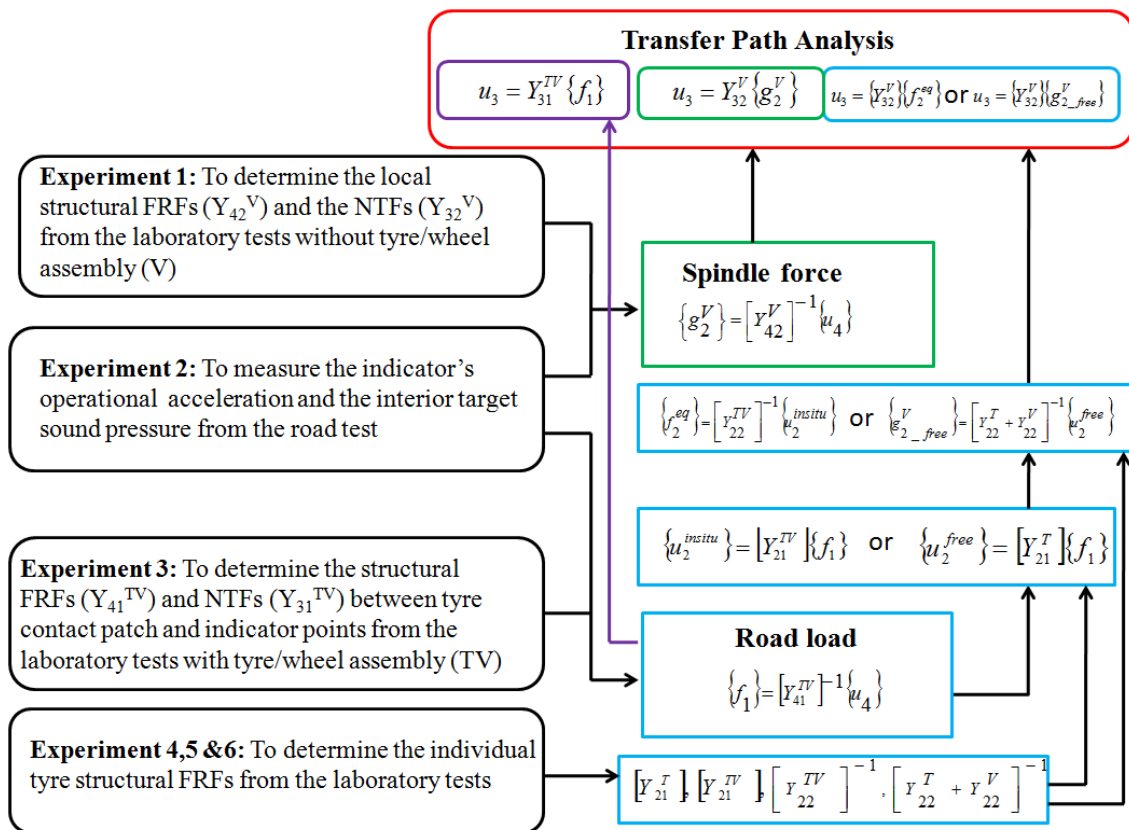


Figure 6.1 Details of experiments and methodology for various TPA methods

In Figure 6.1 $\{u_4\}$ refers to these virtual referenced spectra used for load estimation. Then, the TPA is carried out for each principal components like a single reference TPA. Finally

individual physical reference are given by the contribution of all principal components and hence, a well defined RMS sum is obtained. In order to qualify and quantify the contribution of individual paths (physical references), the ranking is done through path and vector contribution analysis discussed in previous chapter. The following section discusses the repeatability of laboratory experiments.

6.3 REPEATABILITY OF LABORATORY EXPERIMENTS

Laboratory experiments for the determination of local structural FRFs and NTFs were carried out using spectral testing software of LMS Test. Lab. Three tri-axial accelerometers and four microphones are used with the help of a 16 channel data acquisition system for all measurements. Figure 6.2 shows these accelerometers which are mounted on the indicator points and microphones fixed inside the vehicle at the target response positions. The data acquisition system (LMS Scadas mobile) collect and process the responses from these sensors during spectral testing and store in to the system.

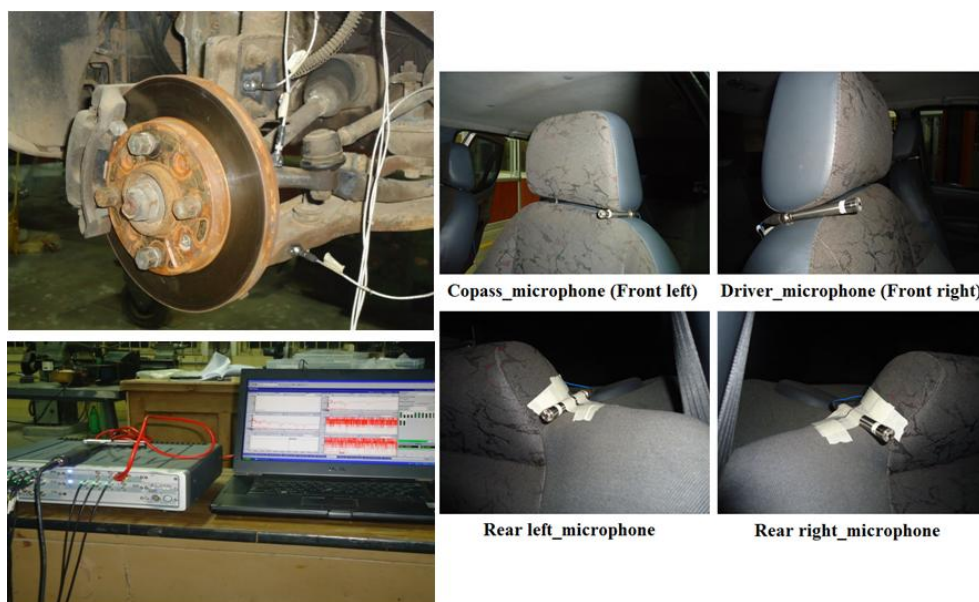


Figure 6.2 Measurement setup used for each run

The first channel is the reference channel used for impulse measurement using instrumented hammer; channels (2-5) are used for the interior target sound pressure response measurements using four microphones; and channels (6-14) are used for indicator acceleration response measurements using three tri-axial accelerometers. Thus 14 channels are used for each measurement run. The measured data from these channels are communicated to the spectral testing software from data acquisition system using a Local Area Network (LAN) chord. The test vehicle is described as follows: there are 12 path indicators (spindle) and 12x2 additional indicators (suspension and lower arm), in total 36 response measuring points, 9 per wheel. The excitation is given at the rim spindle interface of all the four wheels at the bolt head in all three translational directions, thus there are 12 (3x4) input locations.

During the first laboratory experiment (Experiment No.1) three tri-axial accelerometers were fixed at front right of the vehicle's indicator points and four microphones were fixed in the interior target locations as shown in figure 6.2. The responses were measured by exciting all 12 paths, there by finishing the first set of measurements. Then, the experiment was repeated without changing the microphone positions, with the accelerometer's position to be at the rear right, rear left and front left spindle locations. These additional 3 runs completed all the required measurements for the test vehicle. During these four measurement runs the microphones were kept at the same position, and thus four sets of NTFs were determined. These four sets of NTFs were compared for the experimental repeatability. Figure 6.3 shows the comparison of these four sets of NTFs and the corresponding coherence functions for the input excitation given in the vertical direction at the front right rim spindle interface. Similarly, all the NTFs for the remaining 11 paths were verified and no significant deviations were observed. The local structural FRFs are verified from the drive point coherence given in Chapter 4 (Figure 4.4). This repeatability check ensures the quality of the determined local structural FRFs and the NTFs for the TPA model. The same repeatability check was carried out for the third laboratory experiment for the proposed TPA method to determine road loads. Additional three experiments (4,5 & 6) as mentioned in Figure 6.1 are performed to determine structural FRFs for tyre/wheel assembly for the application of in-situ and free velocity methods those discussed in chapter 5. Multiple runs were conducted to confirm the repeatability for individual tyre transfer functions. As these experiments were not conducted

in a semi-anechoic chamber, a repeatability test has been conducted in order to ensure the validity of the obtained results.

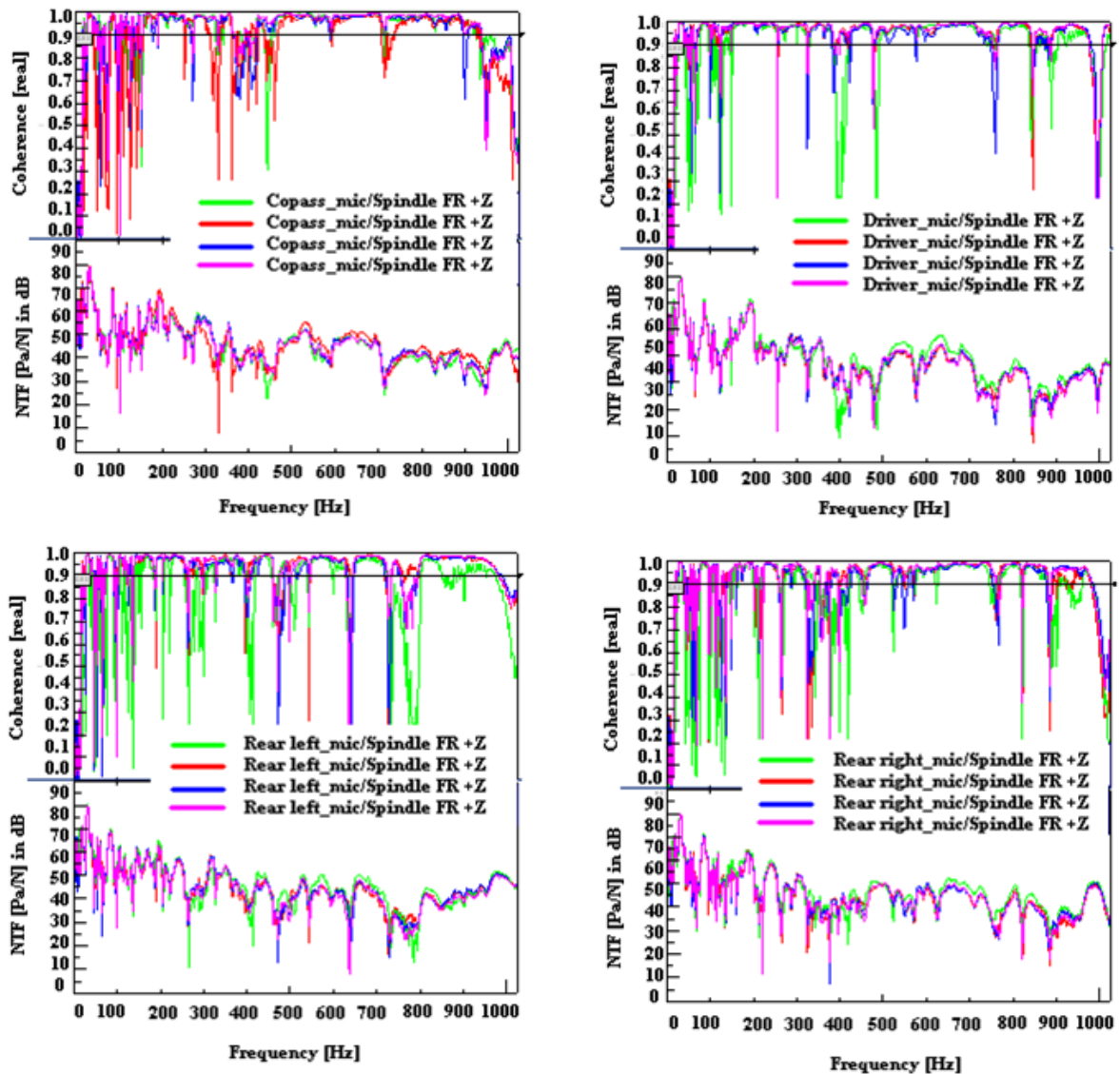


Figure 6.3 Repeatability of spectral testing

6.4 REPEATABILITY OF ROAD TESTS

Similar to the laboratory experiments, during road tests the operational accelerations and sound pressures are measured by relocating the accelerometers during each run; without changing the microphone positions. Figures 6.4-6.7 compare the spectra of measured interior

sound pressure level as a function of frequency obtained from these runs for the experimental repeatability.

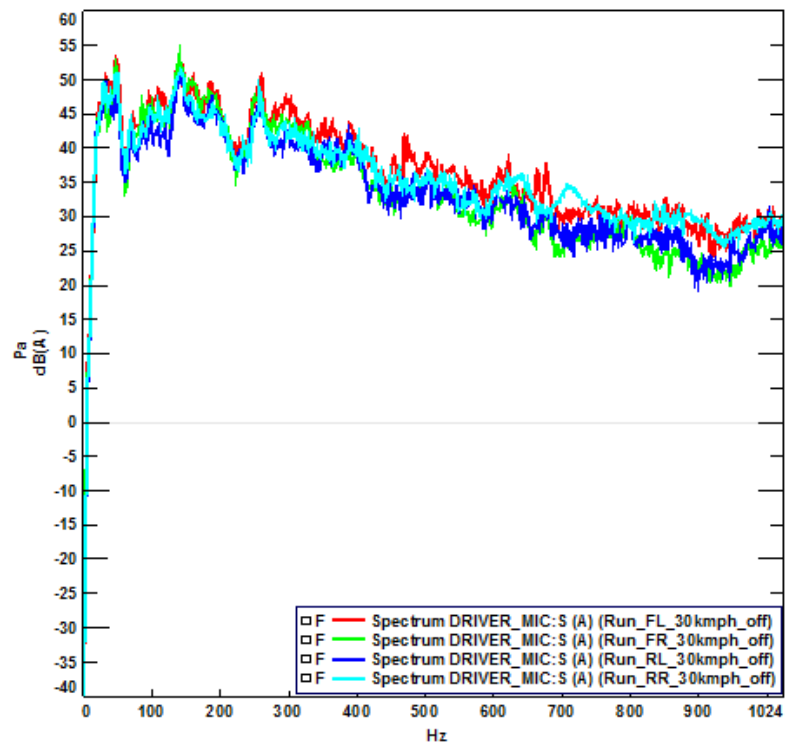


Figure 6.4 Repeatability of interior noise measurements: Driver ear's sound pressure level

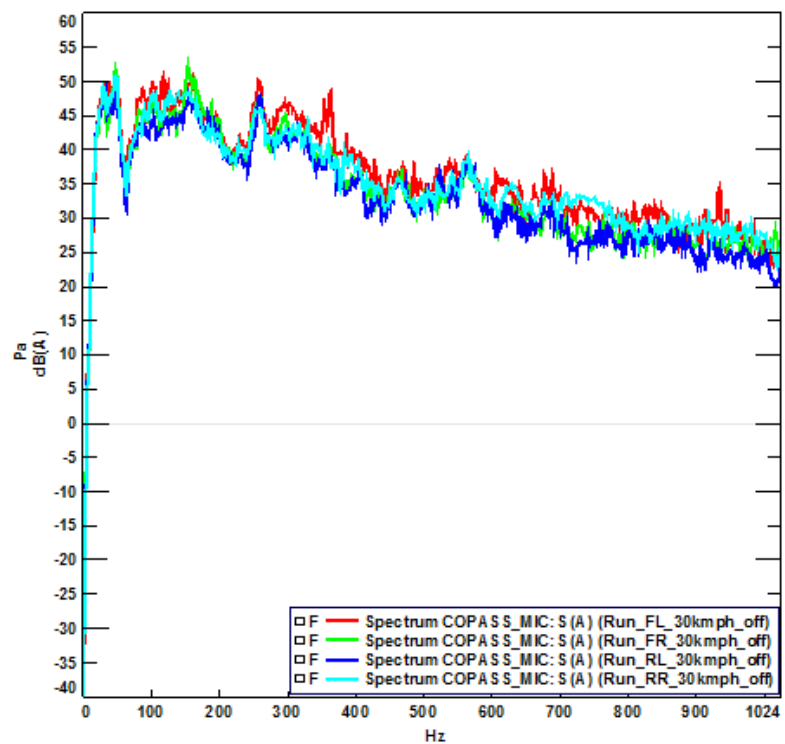


Figure 6.5 Repeatability of interior noise measurements:
Co-passenger ear's sound pressure level

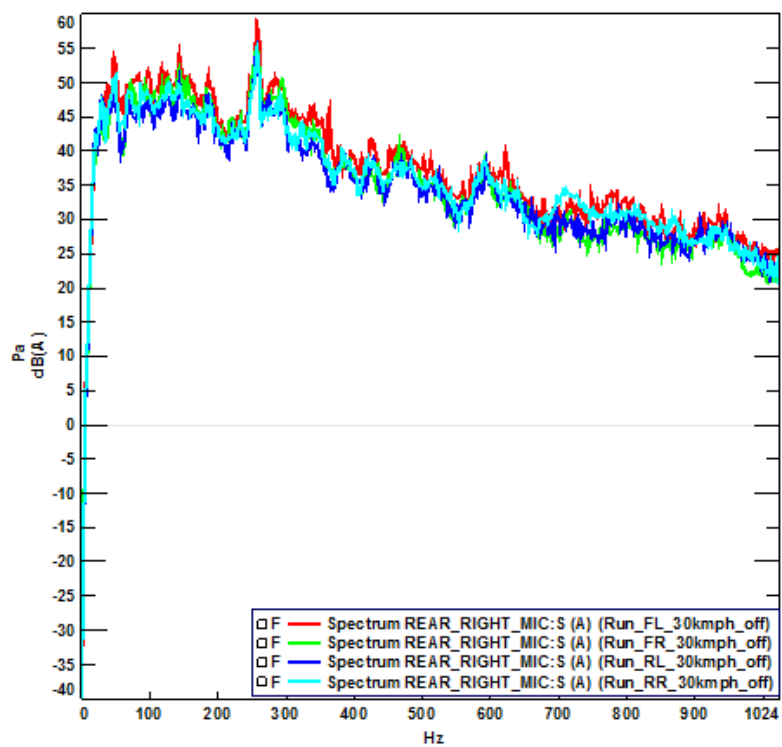


Figure 6.6 Repeatability of interior noise measurements:
Rear right microphone's sound pressure

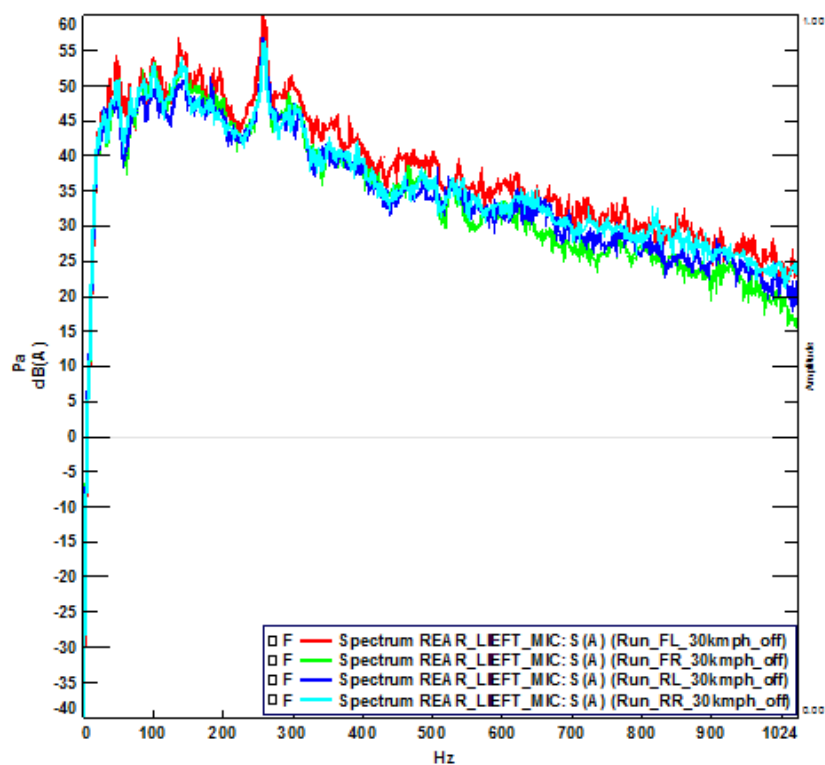


Figure 6.7 Repeatability of interior noise measurements:
Rear left microphone's sound pressure

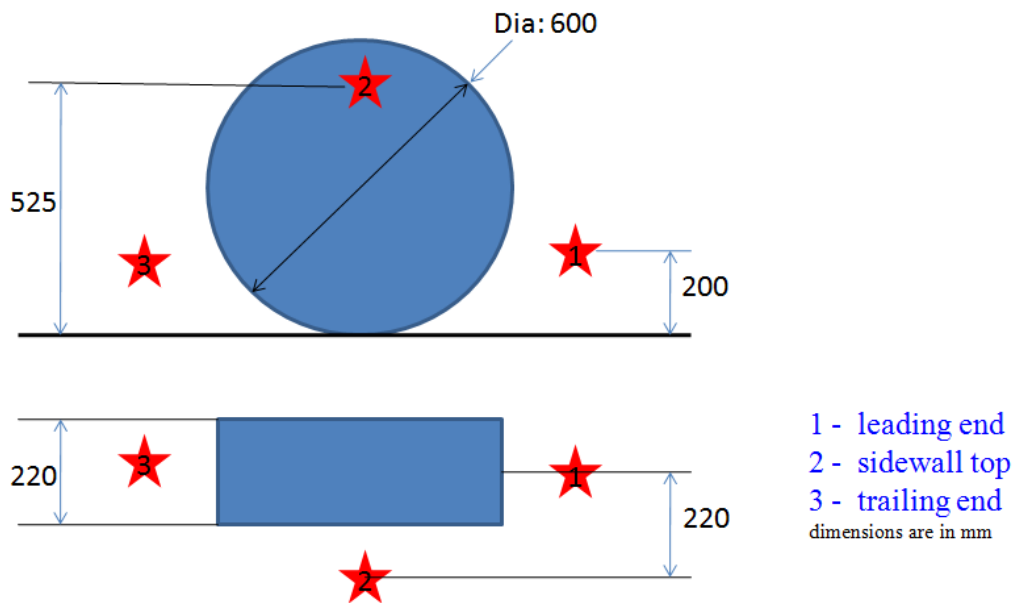


Figure 6.8 Microphone positions for near field exterior noise measurement

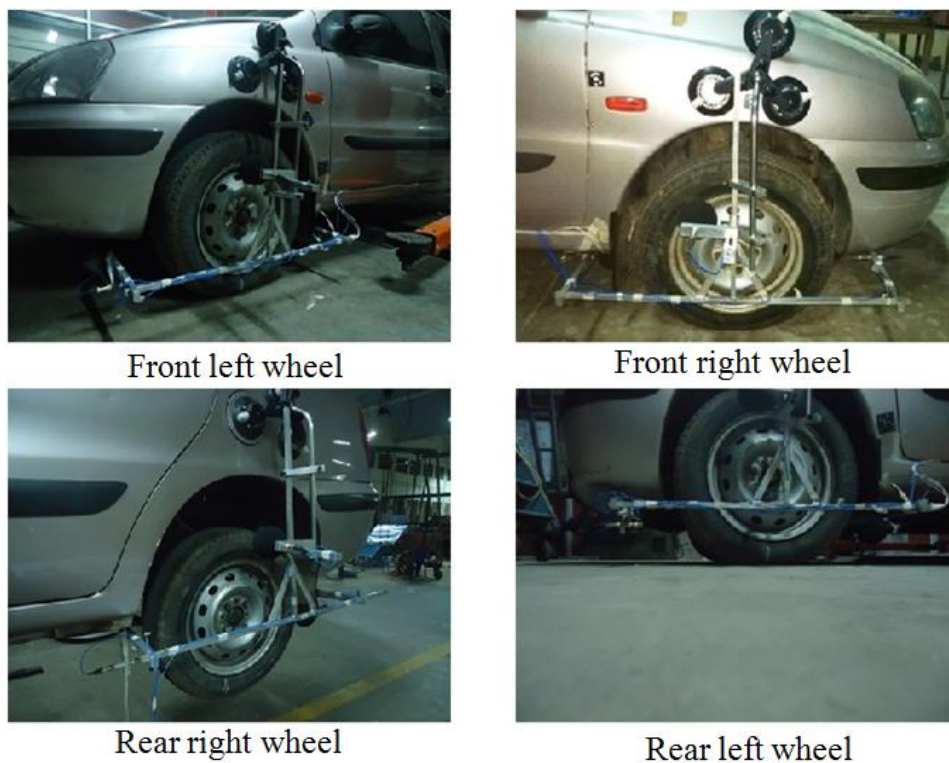


Figure 6.9 Test vehicle with operational measurement sensors

A second road test was conducted for the exterior near field sound pressure (acoustical path indicators) measurement for the proposed air-borne noise quantification which is one of the scope of present research work. During these test, the indicators' operational acceleration and interior noise were also measured at the same location considered during the first road test on the same road. During this road test thirteen channels were used; four measurement sets were made for front left, front right, rear right and rear left wheels. During the first set, three tri-axial accelerometers were mounted on front indicator points and those consumed nine channels and three microphones were fixed on the holder to measure exterior near field sound pressure at front left wheel leading, trailing and side wall positions as illustrated in Figure 6.8. Figure 6.9 shows the sensors that are mounted on the test vehicle. One microphone was mounted at the co-passenger left ear side.

Similarly three more sets of measurements were made for the remaining wheels and interior locations. These measurements were used to check the repeatability of operational acceleration responses of all indicators. Figure 6.10 compares the operational acceleration response spectra in the longitudinal directions for all spindle (one of the path indicators). The same comparison is made for the remaining 35 DOFs of indicators to ensure the repeatability of the road test measurements.

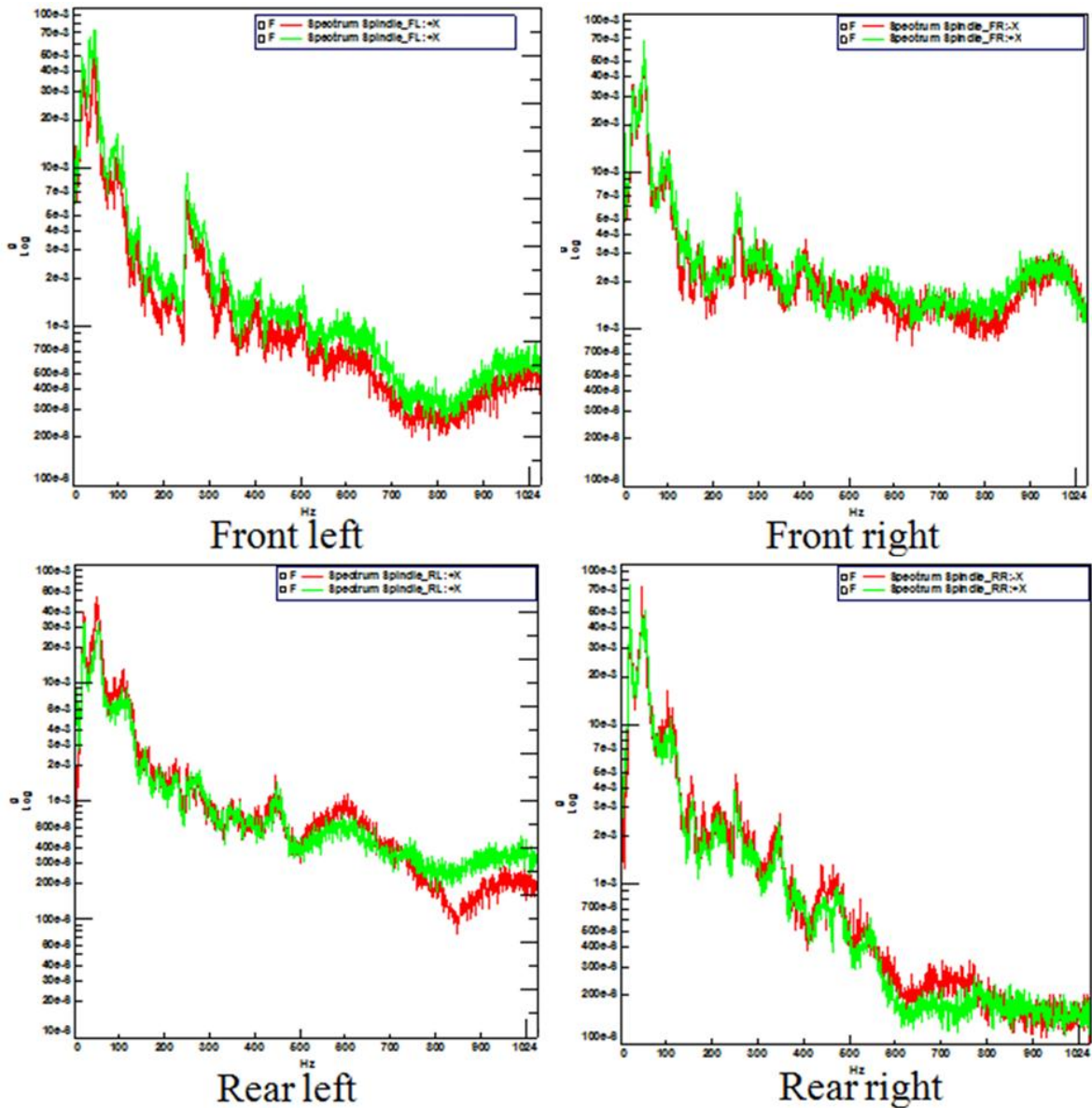


Figure 6.10 Repeatability of operational acceleration measurement

6.5 SUMMARY

In addition to the good coherence functions for drive points for local structural FRFs and NTFs, the repeatability check added credibility to the experiments. The following chapter enumerates the contribution, conclusion and the scope of future work.

CHAPTER 7

CONCLUSION AND FUTURE WORK

7.1 CONTRIBUTIONS

A procedure has been established to study rolling tyre characteristics using explicit Finite Element Analysis (FEA) and Operational Modal Analysis(OMA). This methodology offers an alternative way from the existing expensive experimental set up, to simulate the virtually the cleat impact experiment and determine rolling tyre modal frequencies and mode shapes. Subsequent to this procedure, experimental Transfer Path Analysis (TPA) is used to synthesis structure borne vehicle interior noise due to tyre road interaction. In a method which is first of its kind, TPA has been used to estimate excitation forces at contact patch during operating condition using matrix inverse method. Tyre/wheel assembly and the vehicle transfer characteristics are combined using component based TPA methods (in-situ and free velocity methods),in order to estimate the equivalent operational loads at the rim spindle interface. The merit of these methods is that they eliminate the conventional road test to determine operational responses at the path indicators virtually without conducting an actual road test. Moreover repeating the road test for the new set of tyres to study their influence over the structure borne vehicle interior noise is a time consuming and expensive task.

The salient points of overall contribution of the present work are given below.

- Virtual cleat test for a rolling tyre over straight and inclined cleat is carried out using explicit finite element analysis.
- The resulted acceleration responses of rolling tyre from the cleat test is integrated successfully with LMS Test. Lab software for operational modal analysis, thereby eliminating the need for a data acquisition system. The PolyMAX algorithm is used to determine the natural frequencies and mode shapes.

- This FEA-OMA based procedure is used to study the influence of inflation pressure and static preload over the modal parameters.
- Experimental modal analysis for the tyres of different sizes and of different boundary conditions are carried out to understand the behaviour of non rolling tyre.
- Various experimental Transfer Path Analysis (classical TPA) has been implemented on a complex noise source due to tyre/road interaction of a passenger car to determine the structure borne vehicle interior noise components. The central idea is to establish a procedure that will help the tyre manufacturer to derive the contribution from tyre to the interior noise, just from the tyre characteristics alone, for a given vehicle and road input data.
- Though there is an overall agreement of total magnitude of sound pressure levels when the frequency is ‘smoothed’, there are variations in phase data at fixed frequencies.

7.2 CONCLUSIONS

The following conclusions can be drawn based on the present research work.

- Explicit FEA is an efficient tool to handle large deformation, non linear problem such as a cleat impact simulation of a loaded and a rolling tyre over straight and inclined cleat. Frequency domain polyreference least square complex exponential algorithm is suitable to extract the rolling tyre modal frequencies and mode shapes through operational modal analysis.
- Experimental modal analysis is suitable for applying only to the Linear Time Invariant(LTI) systems and it requires known input excitation force, whereas the operational modal analysis requires only the responses and their cross correlation. Hence OMA is suitable for loaded rolling tyre modal analysis.

- The established FEA-OMA procedure of determining the rolling tyre modal frequencies and the mode shapes have an advantage over complex, costly and time consuming experimental procedures. Hence, it becomes a reliable tool to tyre manufacturer at the product development phase. This tool can be extensively used to carry out a parametric study, to address influence of tyre design, inflation pressure and static preload over the modal behaviour.
- The dispersion curves drawn for rolling tyre modal frequencies are the useful information to know the wave speed around the tyre structure. The effect of loading and rolling over natural frequencies corresponding to the real modes are captured in the dispersion curve for both circumferential and cross sectional modes.
- Multi reference Transfer Path Analysis handle a complex tyre/road interaction source to solve for structure borne vehicle interior noise.
- Matrix inverse method is suitable to estimate the operational loads at the paths when compared to mount stiffness and direct measurement method due to the fact that the connection points of wheel rim and spindle, spindle and suspension brackets and spindle and lower arm are rigid.
- Though path contribution analysis is good for visualizing the relative importance of the contributing paths and vector contribution analysis gives both magnitude and phase information of contributing paths with respect to the synthesized total noise for any frequency for a chosen principal component.
- The component based TPA methods used in the current work can eliminate the repetition of laboratory experiment (for vehicle characteristics) and the road test (for operational measurements) in order to study the influence of tyre design over structure borne vehicle interior noise.

7.3 SCOPE OF FUTURE WORK

The study of rolling tyre characteristics and vehicle interior noise can be extended to the following areas:

- Study of rolling tyre noise radiation with consideration of various noise generation mechanisms for the tread pattern tyres as described in chapter 2
- Modeling of visco-elastic materials to capture the actual damping characteristics of tyre in addition to modal frequencies and mode shapes obtained in the present study.
- The established procedure can be extended to study the effect of temperature over rolling tyre modal behaviour.
- Prediction of air borne vehicle interior noise components due to tyre road interaction, by using the operational near field pressure measurement reported in this thesis with appropriate acoustic-acoustic transfer functions. These transfer functions can be determined using a mid frequency volume source.
- The road input data estimated and the local structural FRFs and NTFs reported in this thesis can be further used to study the influence of new tyre design over structure borne vehicle interior noise using in-situ and/or free velocity method.
- The phase data and the magnitudes agree over a smoothed frequency, but do not agree at fixed frequencies. Large variations in phase and magnitude with respect to frequency have been observed in the literature as well. This requires further investigation

APPENDIX -I

Figure A1.1 to A1.4 show results that are similar to those in Figure 4.5 for co-passenger left, rear right passenger right and rear left passenger left ear's interior target response position.

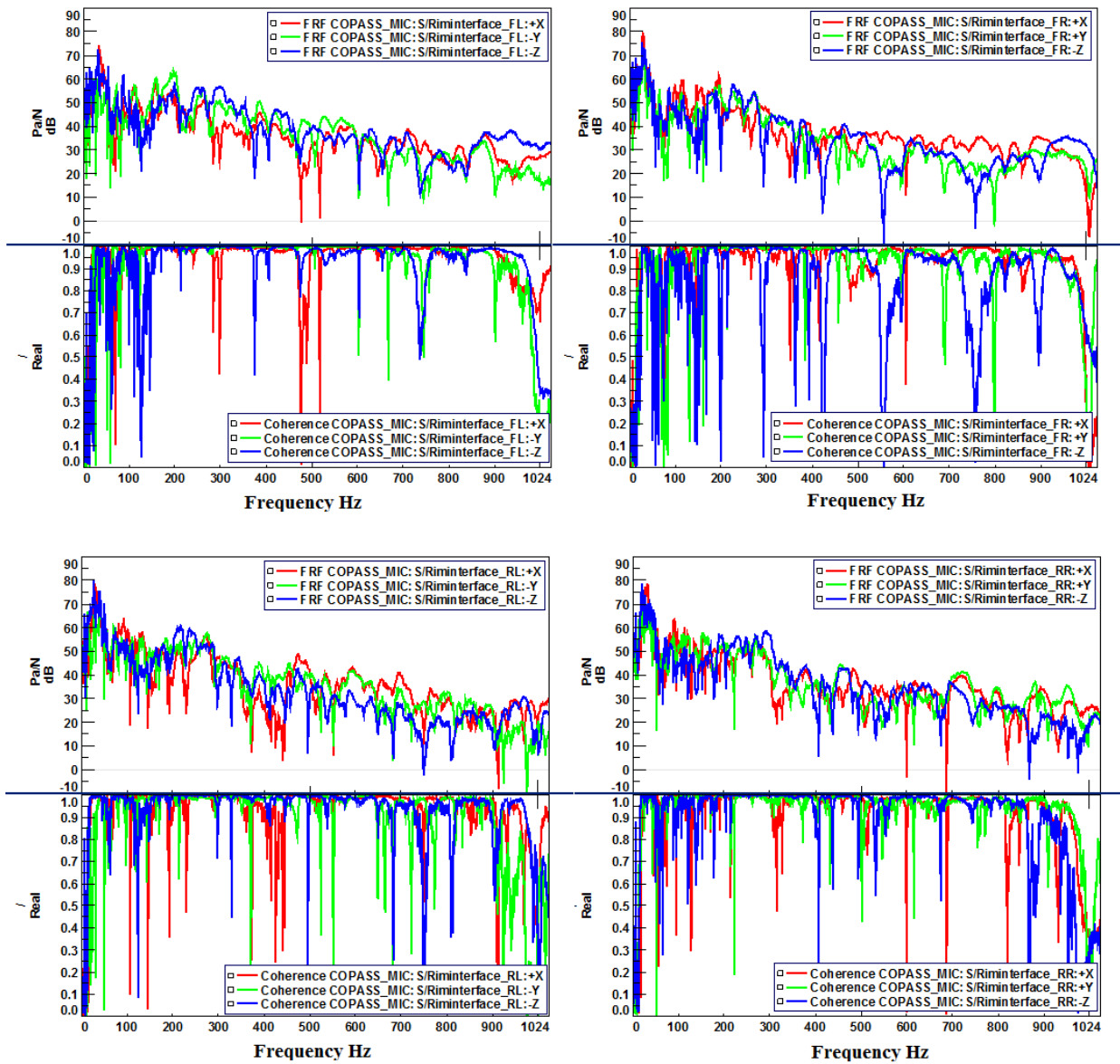


Figure A1.1 Variation of NTFs between all paths and co-passenger's left ear position and the corresponding coherence functions as function of frequency

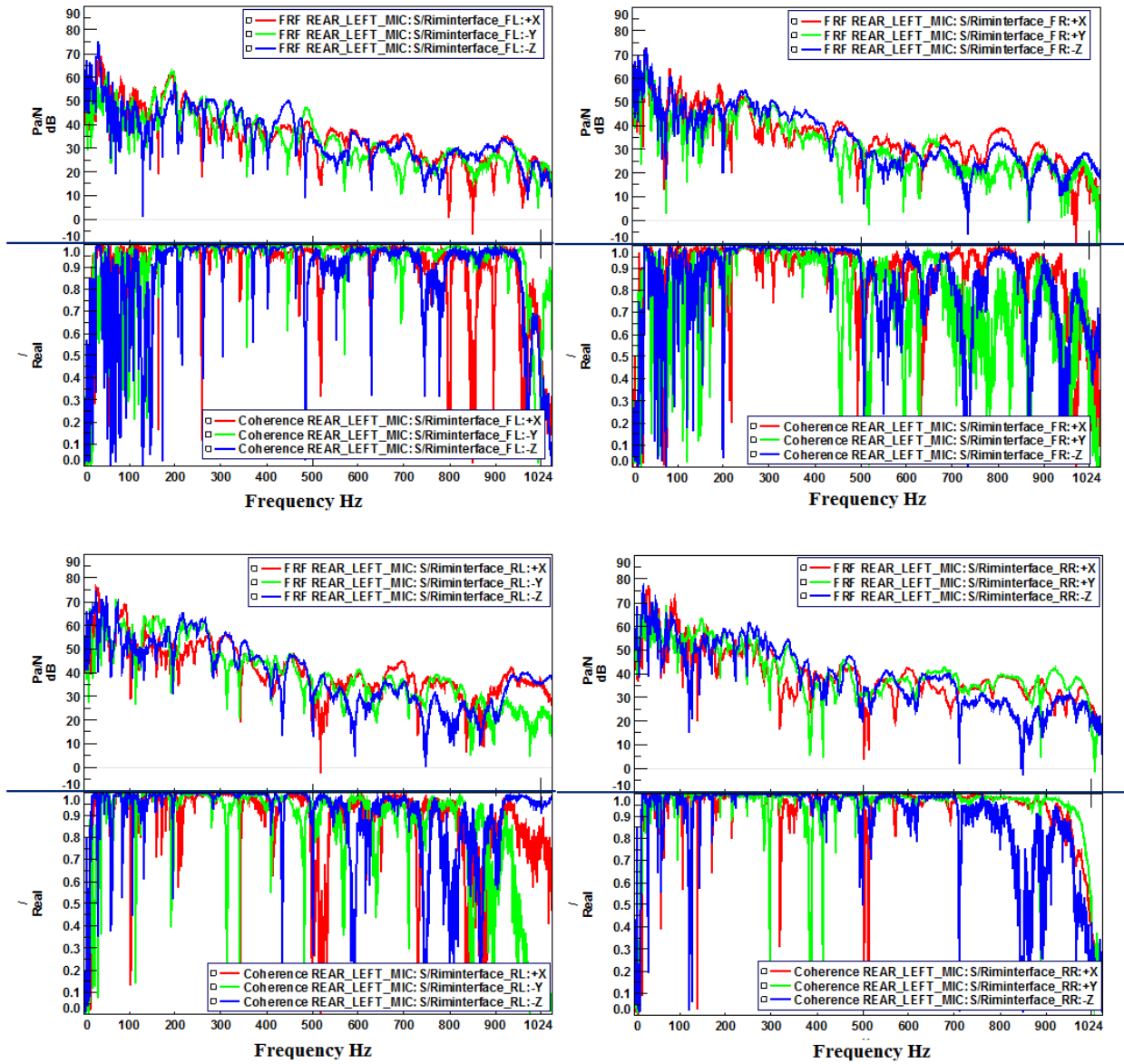


Figure A1.2 Variation of NTFs between all paths and rear left passenger's left ear position and the corresponding coherence functions as function of frequency

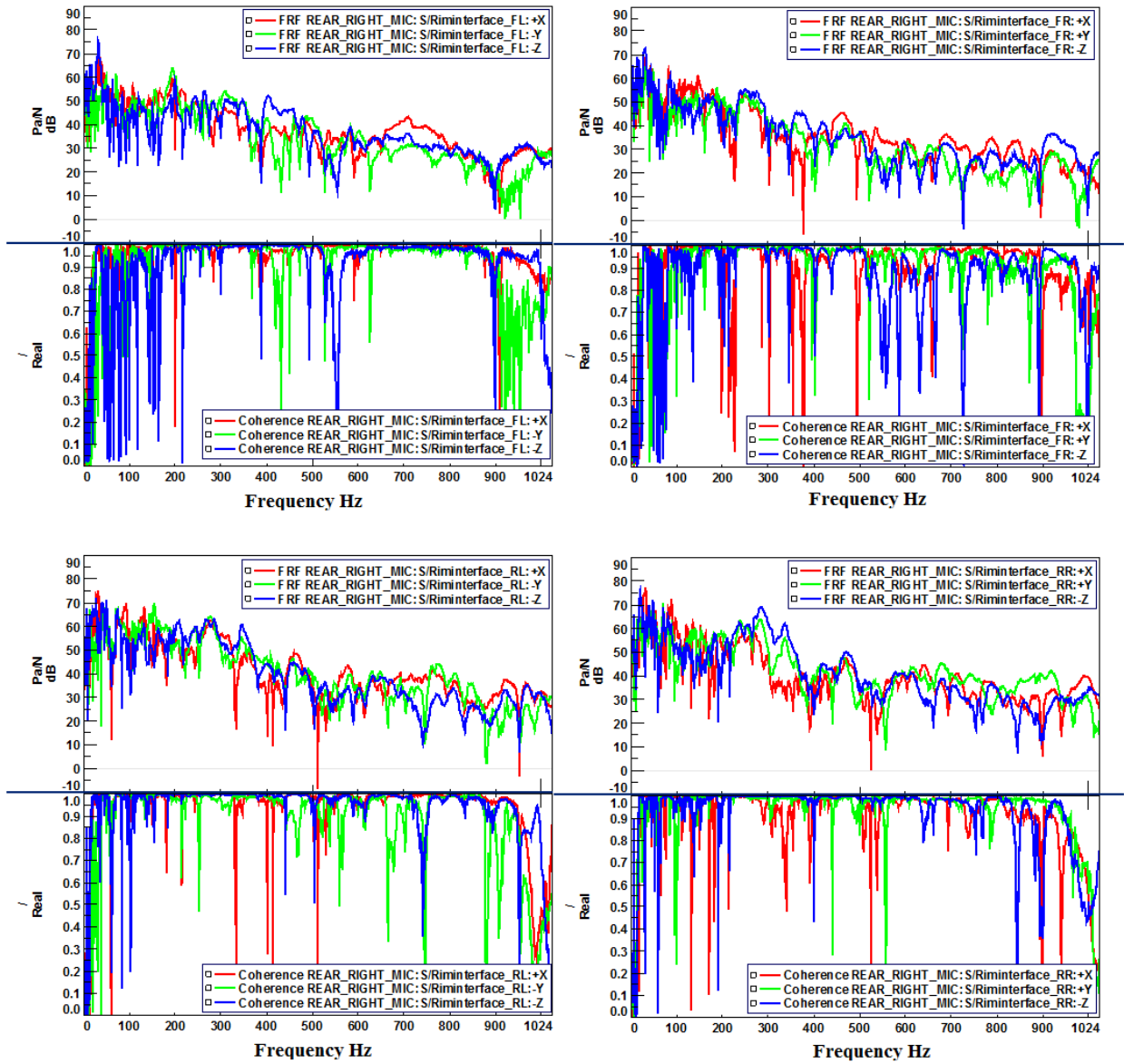


Figure A1.3 Variation of NTFs between all paths and rear right passenger's right ear position and the corresponding coherence functions as function of frequency

Figure A1.4 to A1.11 show results that are similar to those in Figure 4.6a - 4.6d for the remaining path excitation in lateral and vertical direction at front left, front right, rear right and rear left rim spindle interface points.

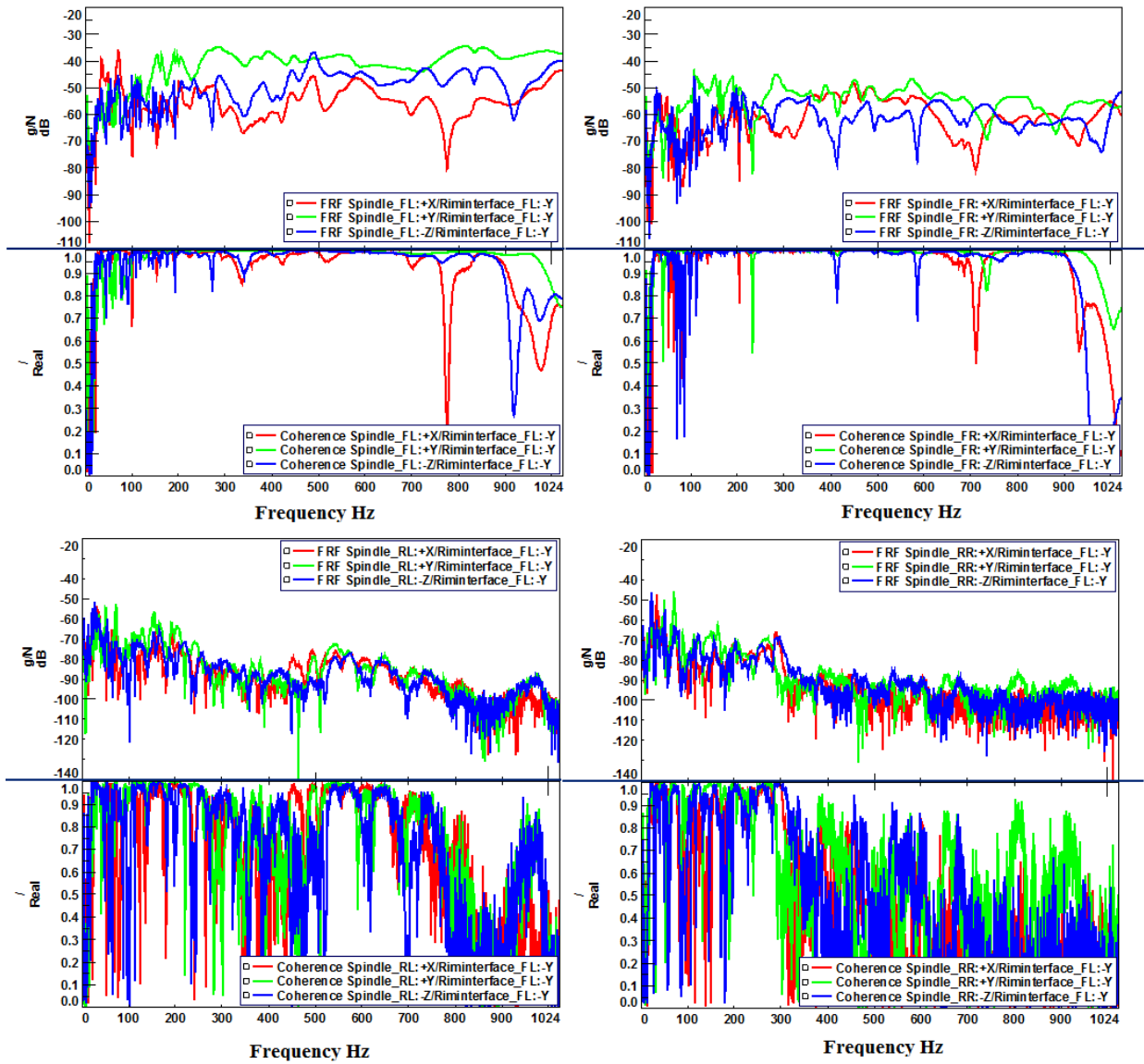


Figure A1.4 Variation of local structural FRFs between all path indicators and Riminterface_FL:Y and the corresponding coherence functions as function of frequency

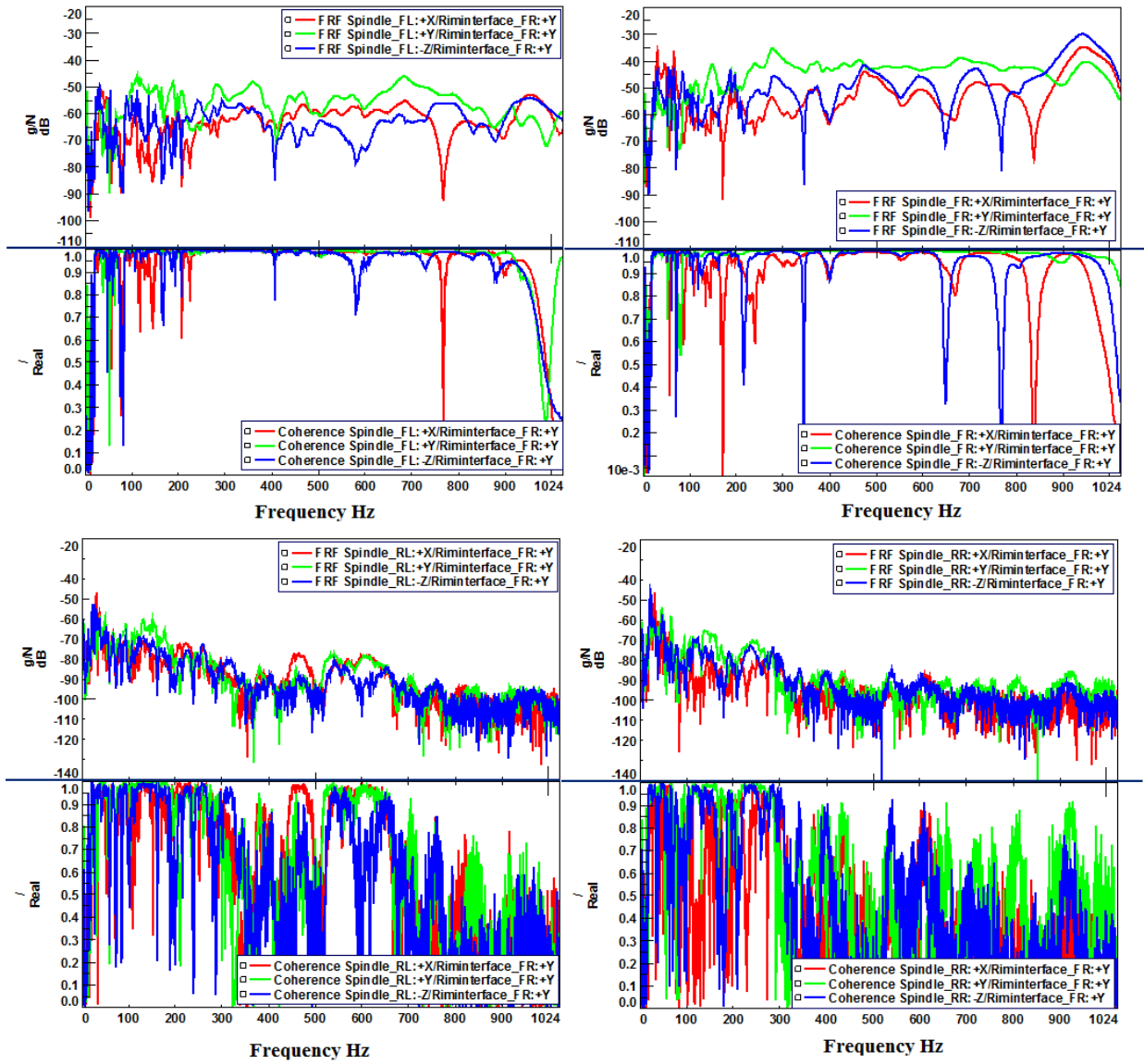


Figure A1.5 Variation of local structural FRFs between all path indicators and Riminterface_FR:Y and the corresponding coherence functions as function of frequency

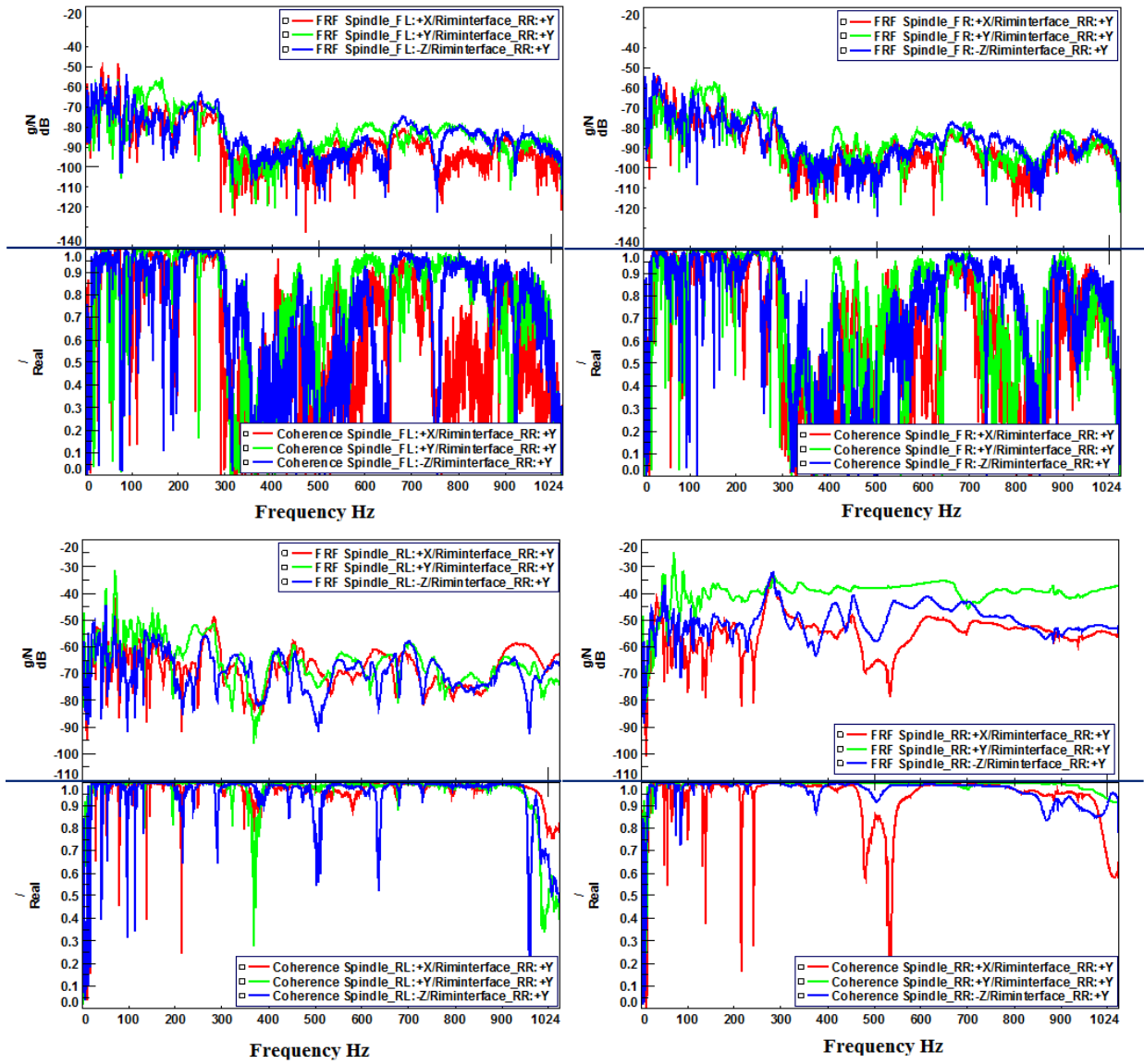


Figure A1.6 Variation of local structural FRFs between all path indicators and Riminterface_RR:Y and the corresponding coherence functions as function of frequency

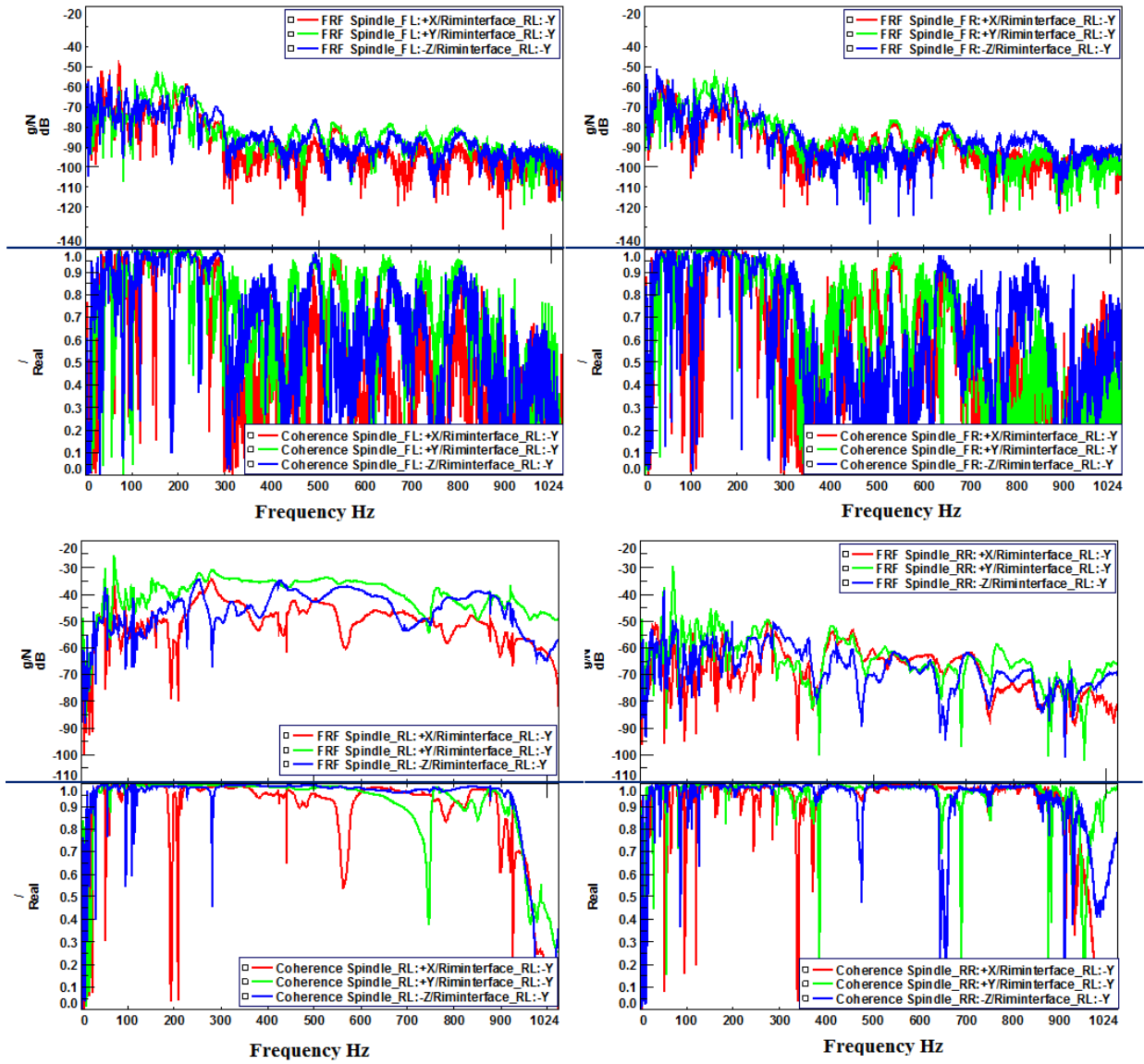


Figure A1.7 Variation of local structural FRFs between all path indicators and Riminterface_RL:Y and the corresponding coherence functions as function of frequency

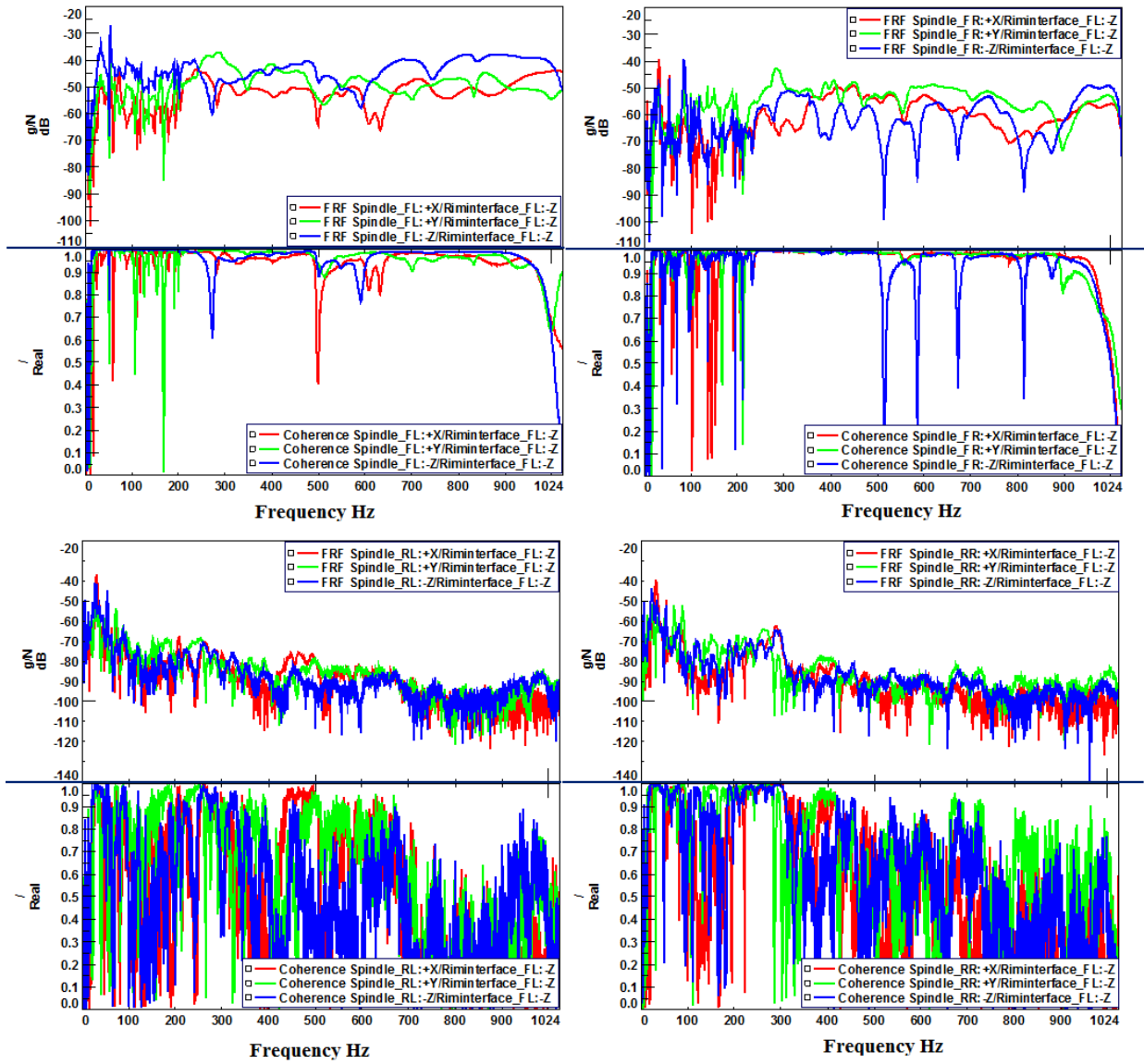


Figure A1.8 Variation of local structural FRFs between all path indicators and Riminterface_FL:Z and the corresponding coherence functions as function of frequency

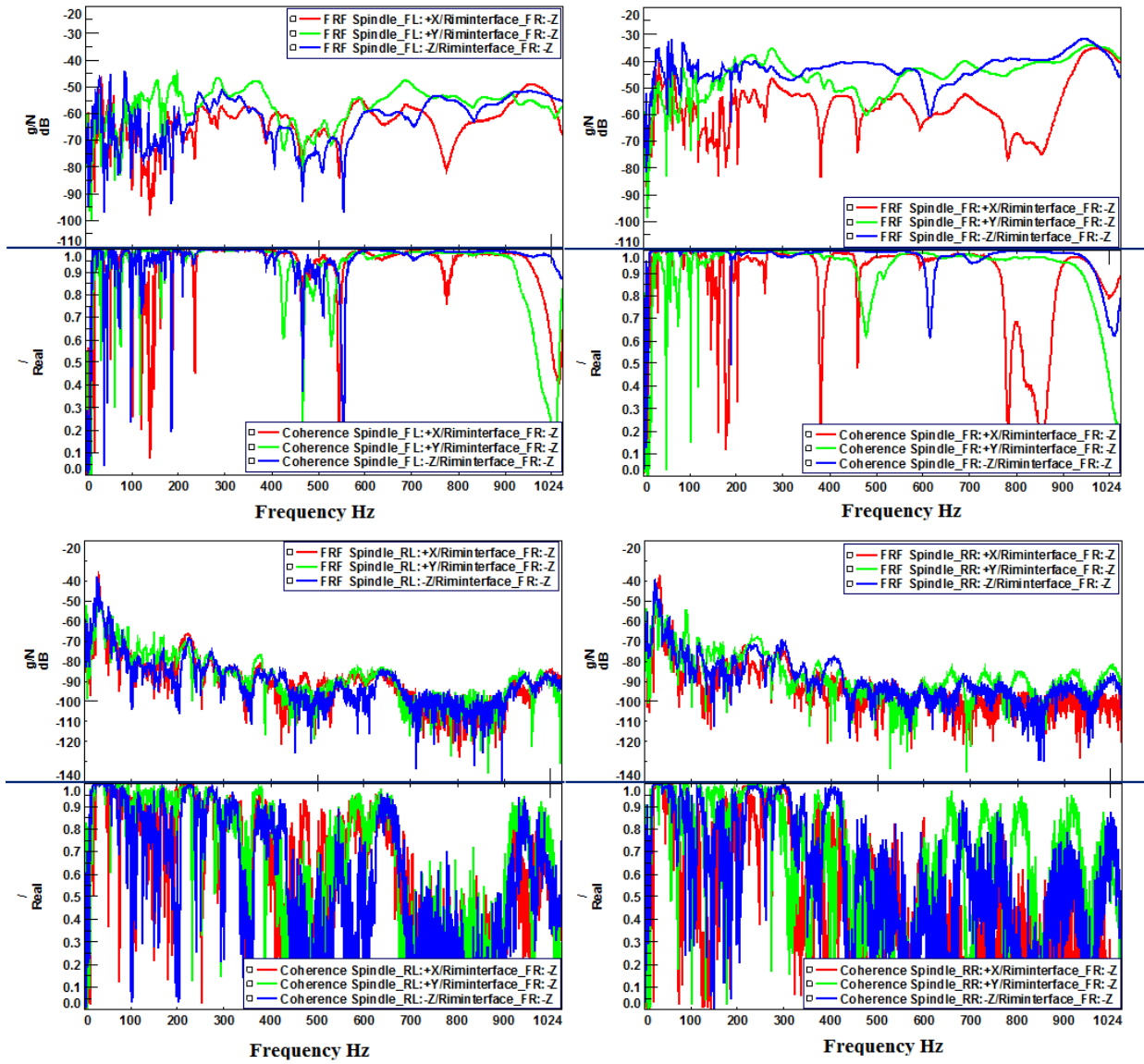


Figure A1.9 Variation of local structural FRFs between all path indicators and Riminterface_FR:Z and the corresponding coherence functions as function of frequency

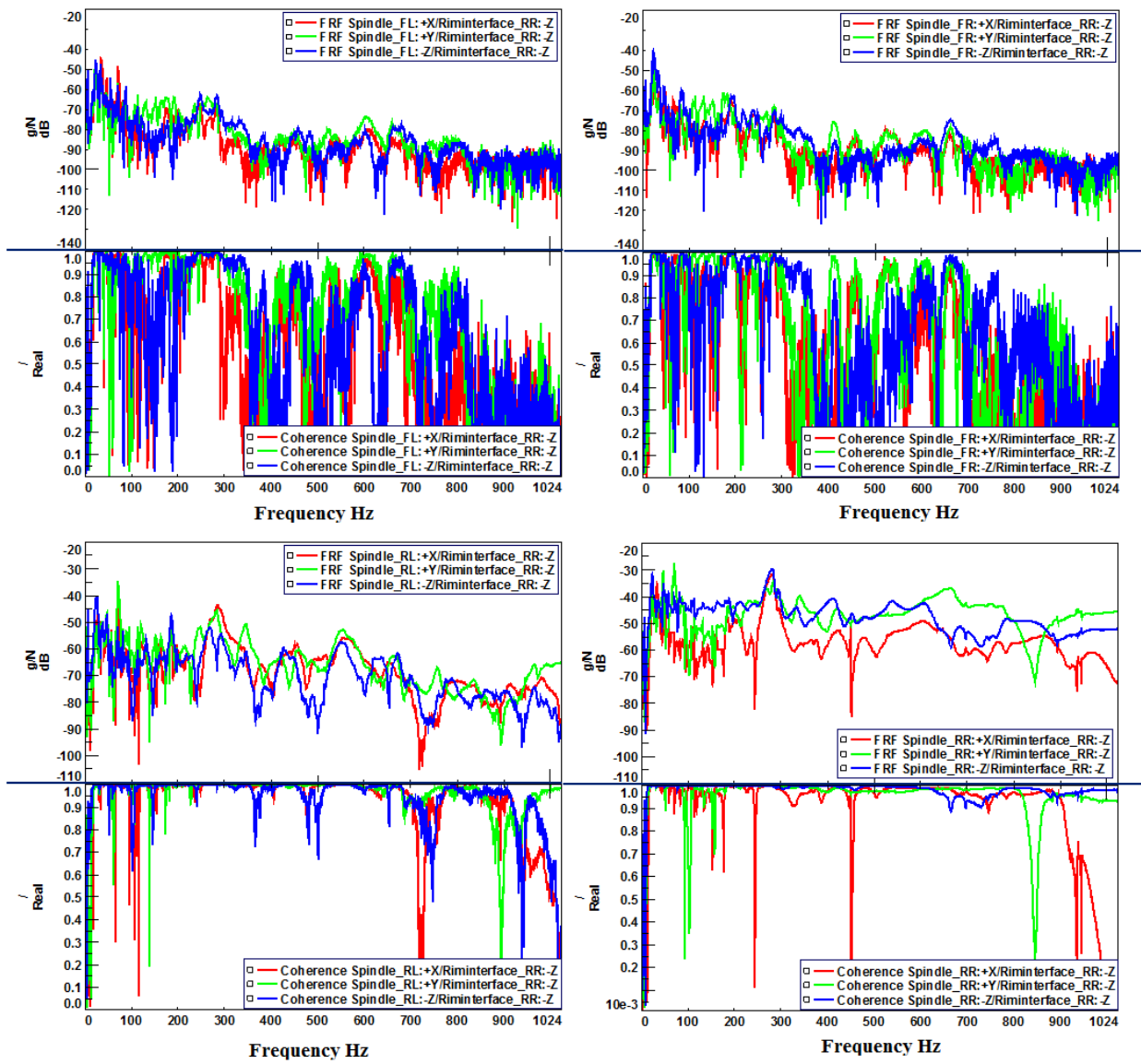


Figure A1.10 Variation of local structural FRFs between all path indicators and Riminterface_RR: Z and the corresponding coherence functions as function of frequency

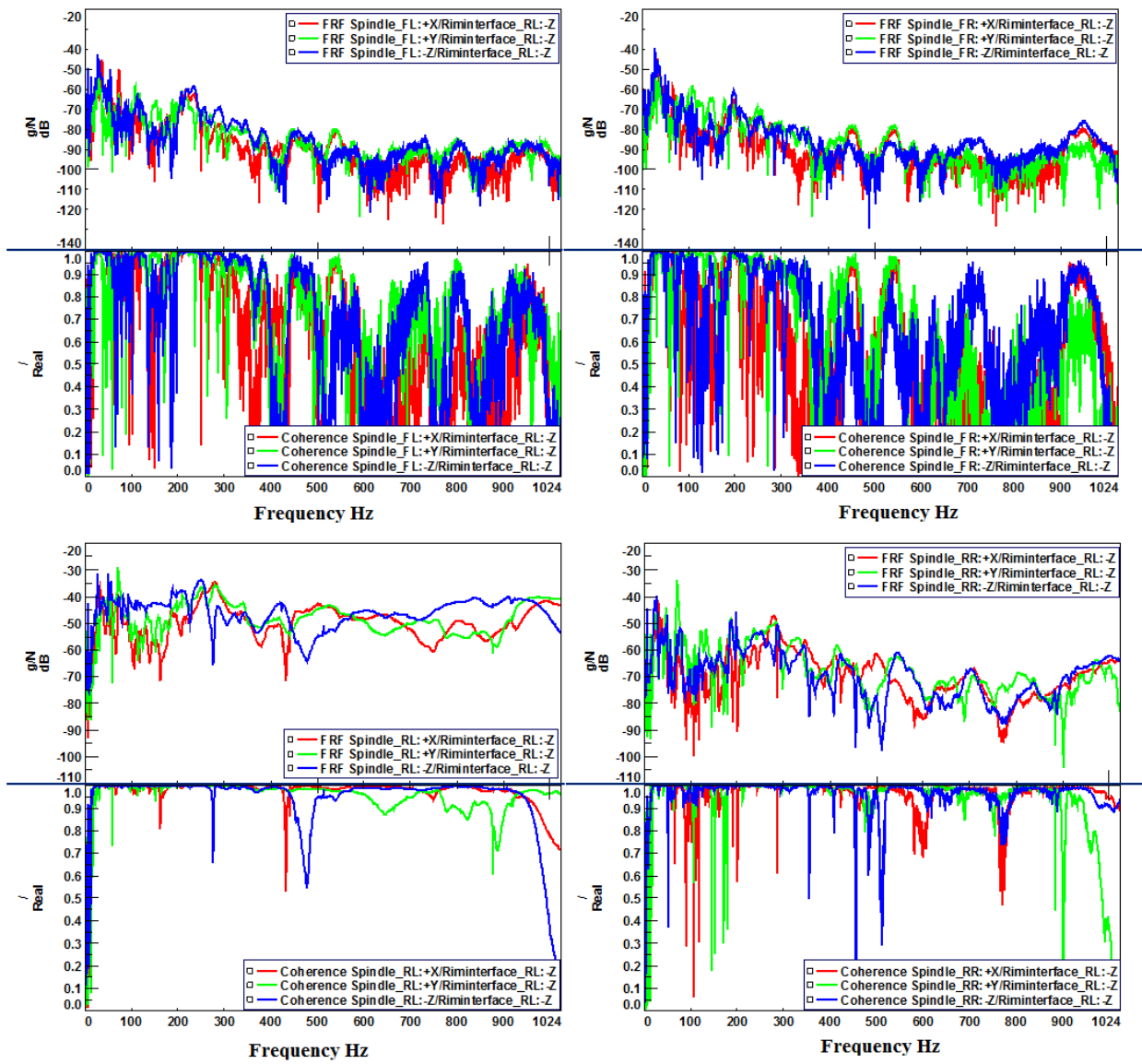


Figure A1.11 Variation of local structural FRFs between all path indicators and Riminterface_RL:Z and the corresponding coherence functions as function of frequency

Figure A1.12 to A1.14 show the results that are similar to those in Figure 4.10 for the remaining target interior positions at co-passenger's left ear, rear right passenger right ear and rear left passenger left ear position respectively for their individual path contribution.

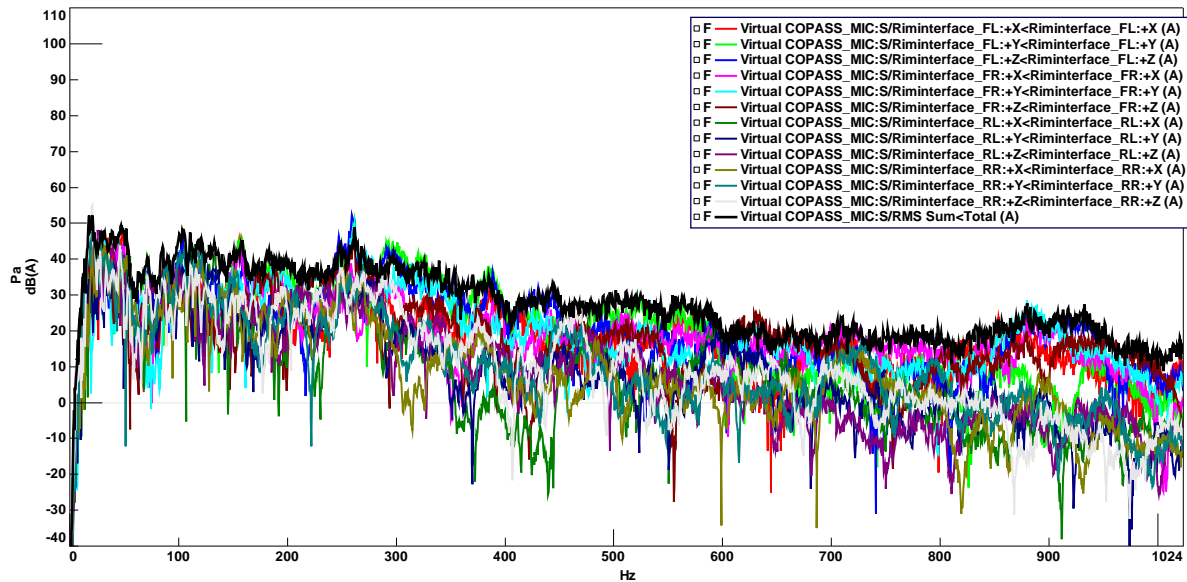


Figure A1.12: Individual path contribution to the total structure borne interior noise at copassenger's right ear position

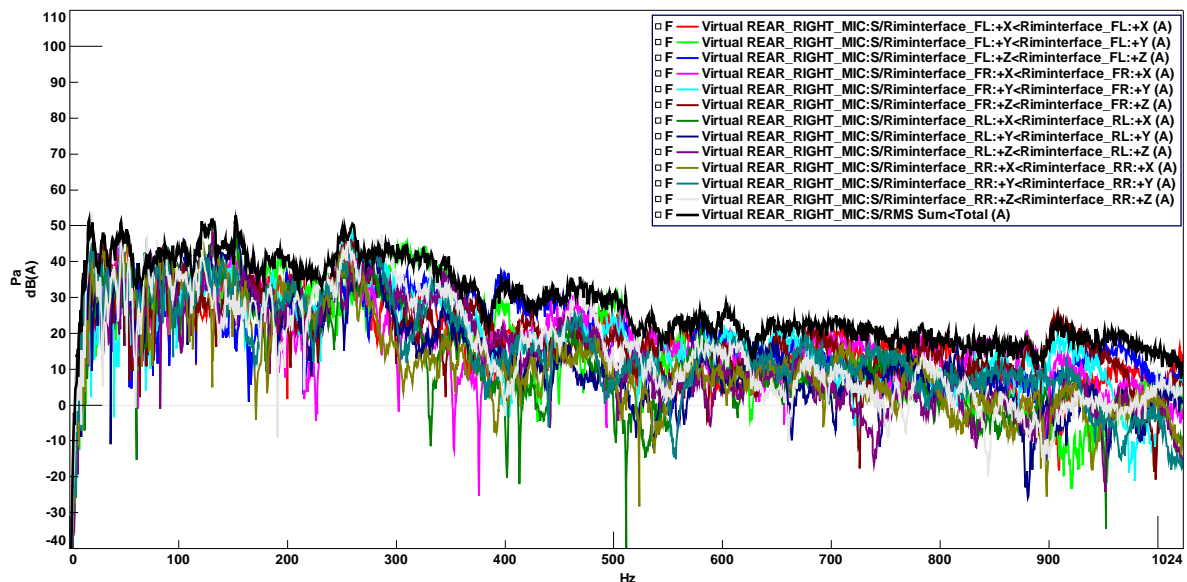


Figure A1.13: Individual path contribution to the total structure borne interior noise at rear right passenger's right ear position

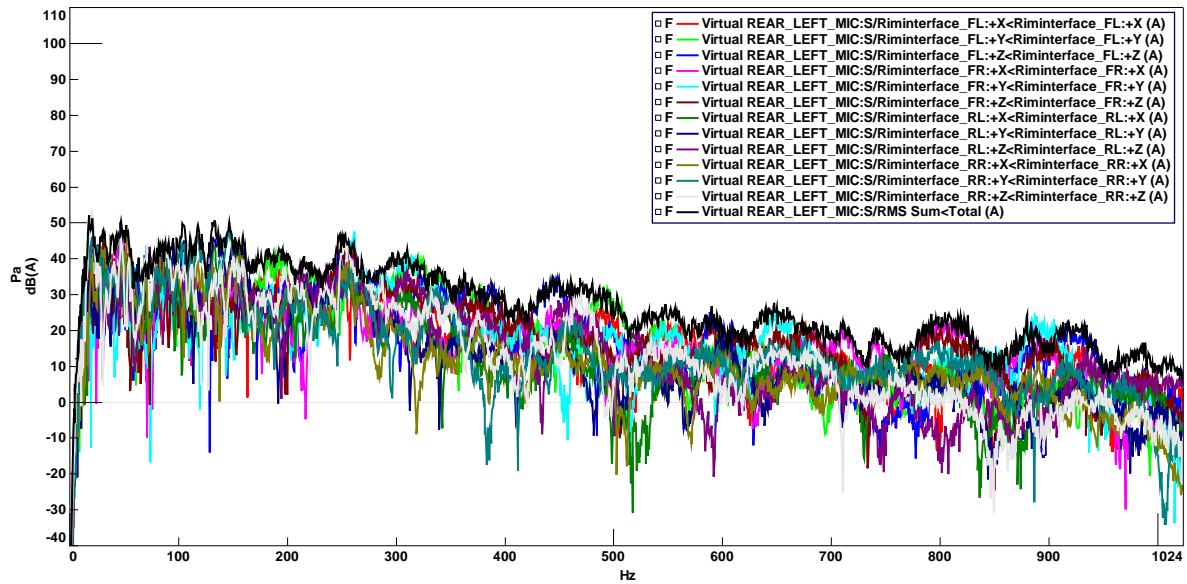


Figure A1.14: Individual path contribution to the total structure borne interior noise at rear left passenger's left ear position

Figure A1.15 to A1.17 show the results that are similar to those in Figure 4.11 for the remaining target interior positions at co-passenger's left ear, rear right passenger right ear and rear left passenger left ear position respectively that compares the TPA results for engine on and engine off condition with measurement separately.

Figure A1.18 to A1.20 show the results that are similar to those in Figure 4.12 for the remaining target interior positions at co-passenger's left ear, rear right passenger right ear and rear left passenger left ear position respectively that compares sound pressure level of engine 'on' and 'off' condition for the actual measurements and synthesized TPA results separately.

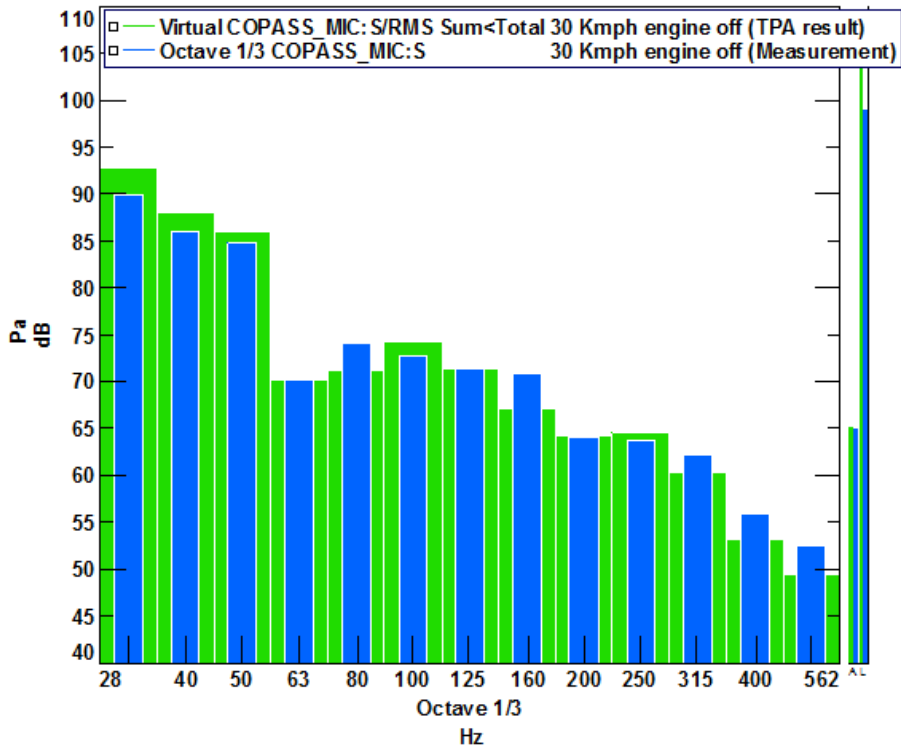
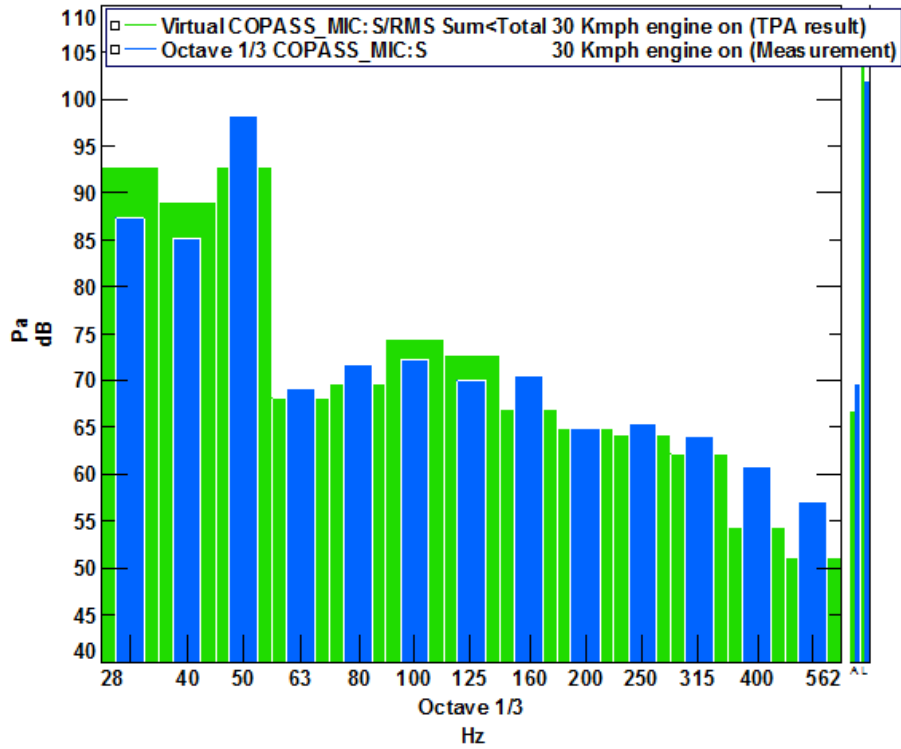


Figure A1.15 Comparison of TPA results with measurements of co-passenger's left ear target

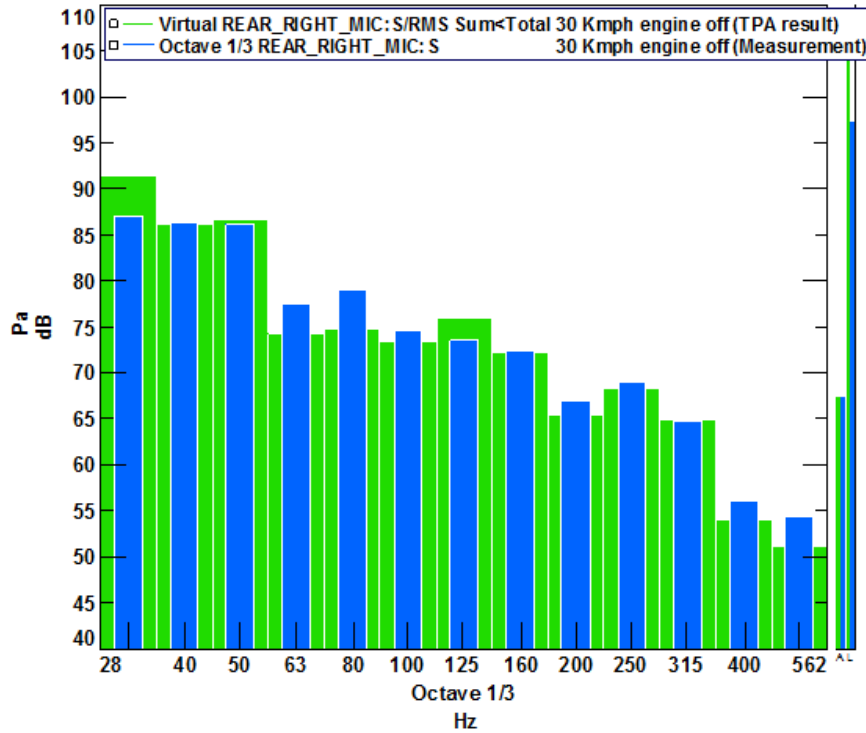
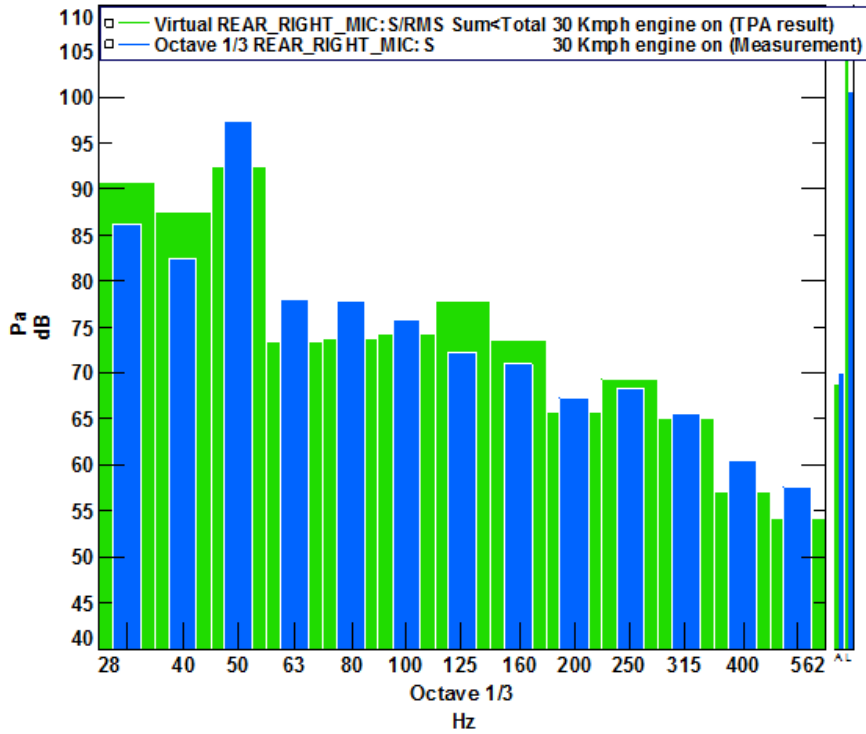


Figure A1.16 Comparison of TPA results with measurements of rear right passenger's right ear target

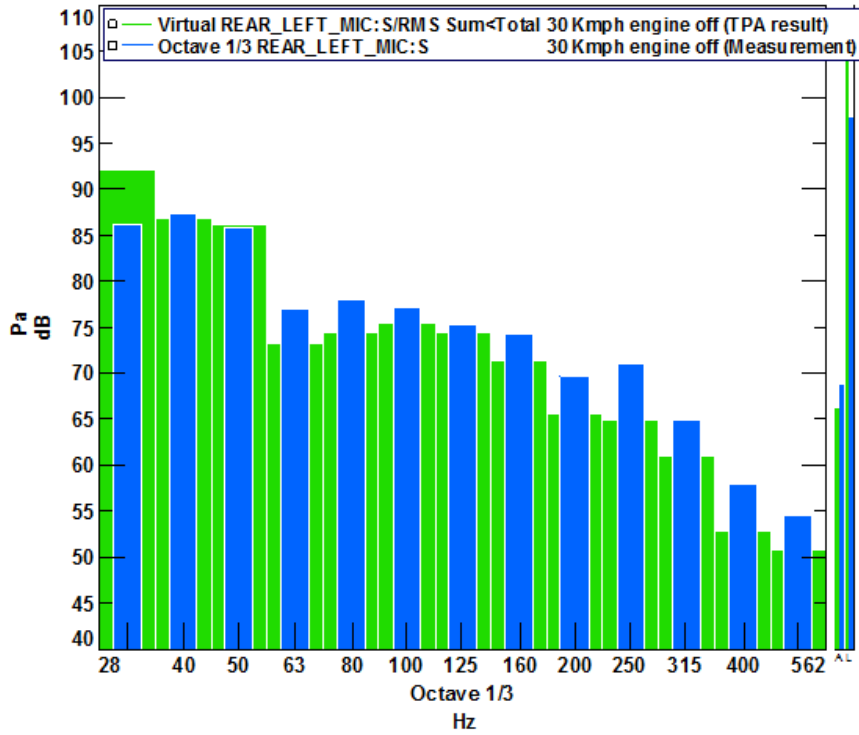
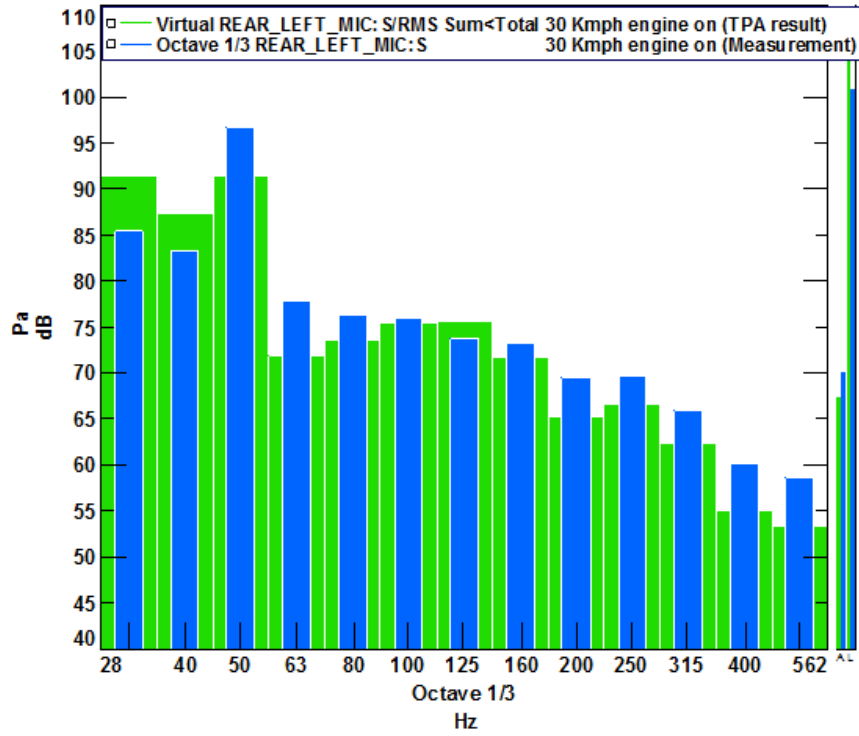


Figure A1.17 Comparison of TPA results with measurements of rear left passenger's left ear target

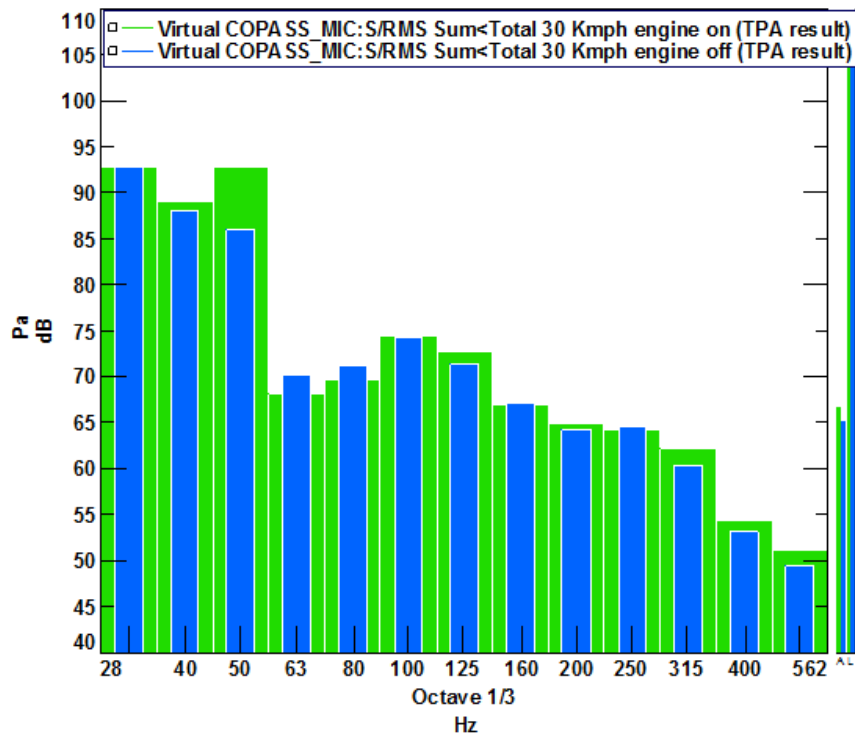
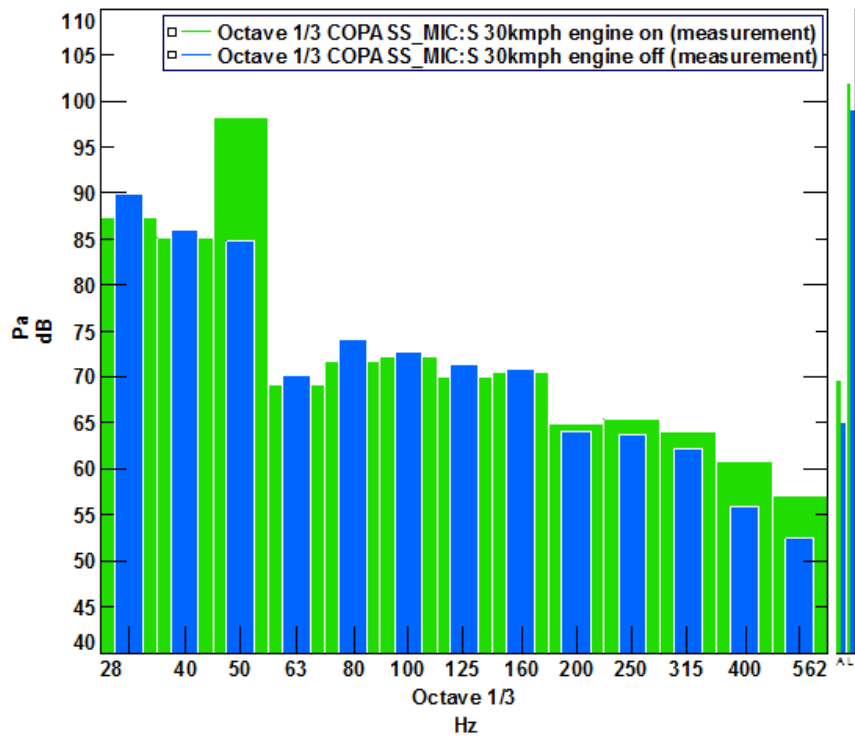


Figure A1.18 Comparison of 'engine on' and 'engine off' results of co-passenger's left ear target for measurements and TPA separately

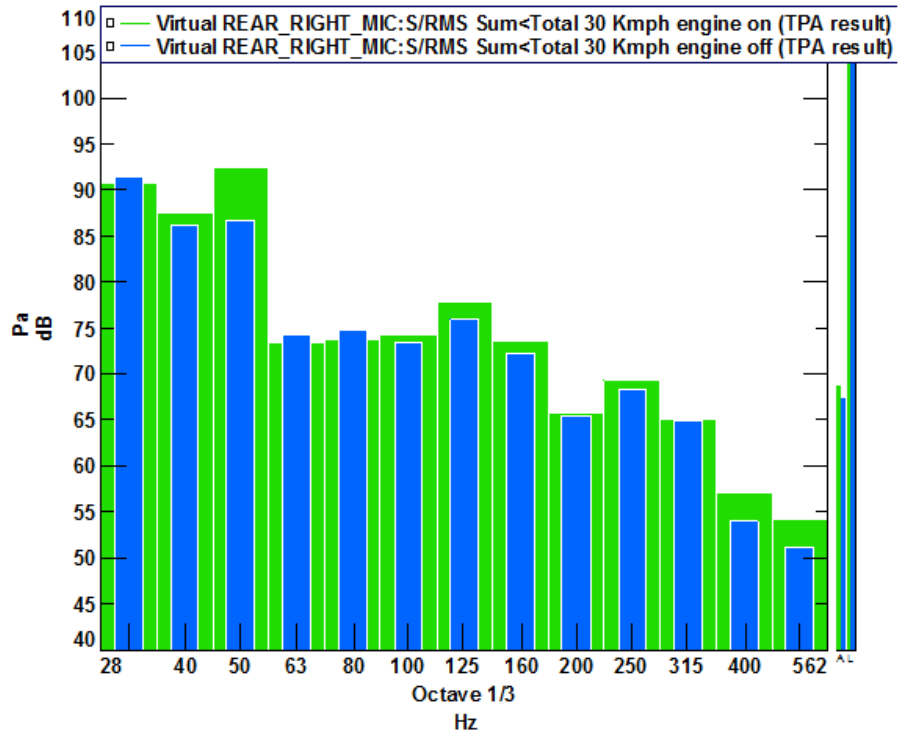
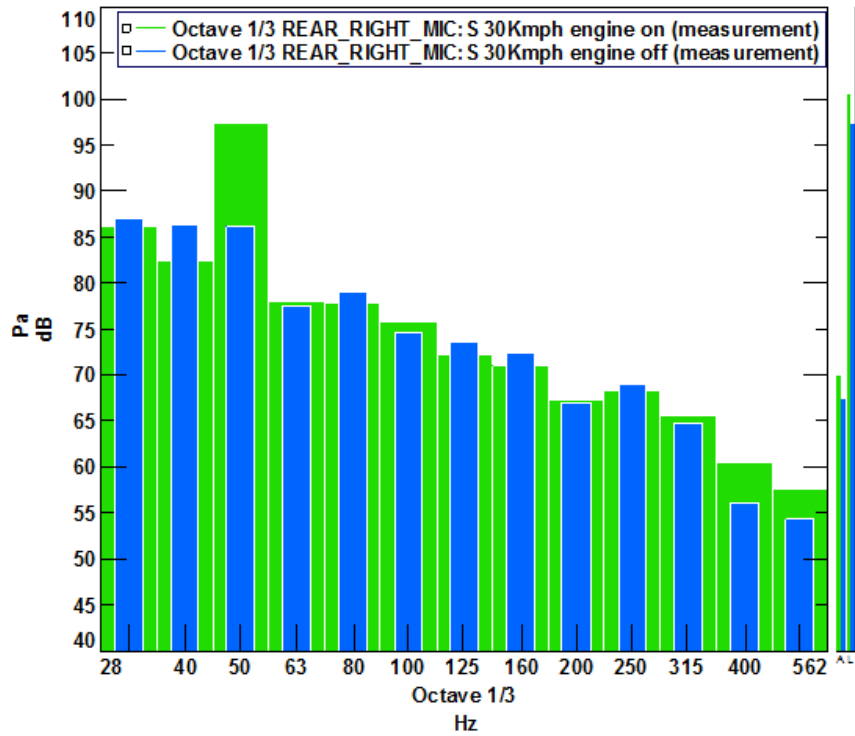


Figure A1.19 Comparison of 'engine on' and 'engine off' results of rear right passenger's right ear target for measurements and TPA separately

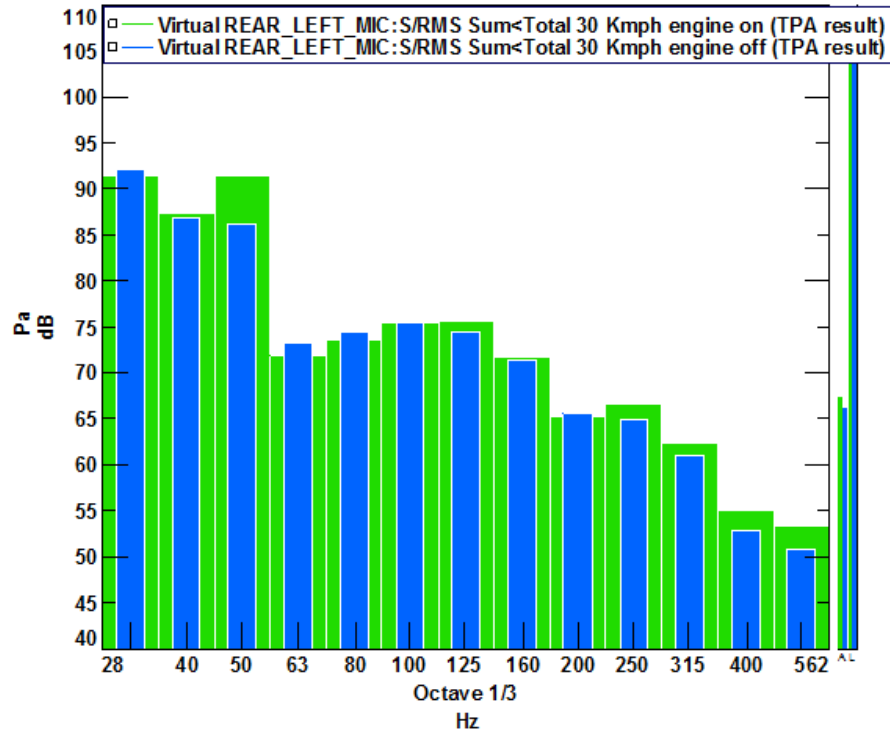
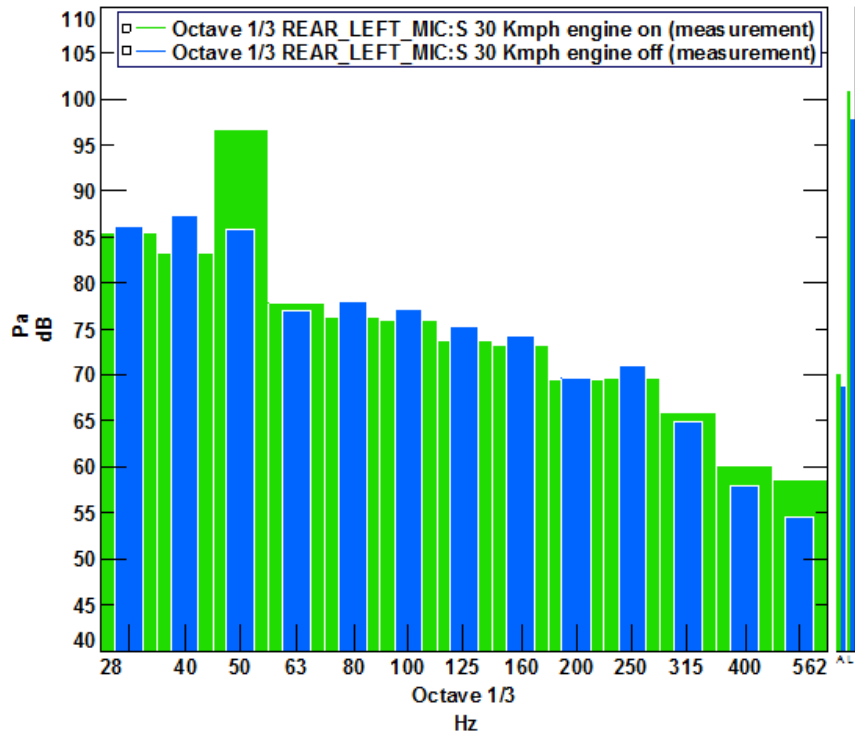


Figure A1.20 Comparison of 'engine on' and 'engine off' results of rear left passenger's left ear target for measurements and TPA separately

Appendix II

MATHEMATICAL BACKGROUND OF MULTI REFERENCE TRANSFER PATH ANALYSIS

The mathematical background of multi reference TPA is understood from the theoretical documentation of transfer path analysis given by LMS Test. Lab (LMS International, 2009) and explained as follows from the following equations. Also the paper published by Hendricx and Vandebroek, (1993) has been referred that dealt with the mathematical background of Principal Component Analysis (PCA) for the application of TPA on suspension analysis for road noise.

As discussed in Chapter 4, due to the existence of partial coherence among the twelve physical path references (represented at rim spindle interface in four tyre wheel assemblies), as well as among the indicator responses (spindle, suspension and lower arm), a multi reference TPA is performed. Initially, the required structural FRFs and NTFs are determined from laboratory experiments and in the subsequent step the operational loads are estimated. For this prediction, referenced virtual spectra, (Y') of all operational indicator signals (obtained from road test) are also needed. These referenced virtual spectra composed of the contribution of principal components (PCs) (X'). The PCs are obtained from the orthogonal transformation of the physical references (12 operational path indicators). Then the virtual crosspowers, [$G_{yx'}(f)$] between the PCs and the other indicator acceleration responses are obtained.

Let ' $X(f)$ ' in Equation A.2.1 be 'n' number of physical reference signals. In this case, $n = 12$, represents all path indicator signals. Equation A.2.2 represents the crosspower matrix $G_{xx}(f)$ of reference signals as they are partially correlated. Non-diagonal terms represents the cross coupling of the reference signals.

$$X(f) = \begin{bmatrix} x_1(f) \\ \vdots \\ x_n(f) \end{bmatrix} \dots\dots\dots (A.2.1)$$

$$[G_{xx}(f)] = [X(f)] \cdot [X(f)]^h \dots\dots\dots(A.2.2)$$

where, h represents the hermitian transpose that gives the following Equation A.2.3

$$[G_{xx}(f)] = \begin{bmatrix} X_1 X_1^h & X_1 X_2^h & \dots & X_1 X_n^h \\ X_2 X_1^h & X_2 X_2^h & \dots & X_2 X_n^h \\ \dots & \dots & \dots & \dots \\ X_n X_1^h & X_n X_2^h & \dots & X_n X_n^h \end{bmatrix} \dots\dots\dots(A.2.3)$$

This crosspower matrix is decomposed as follows:

$$[G_{xx}(f)] = [U(f)][G'_{xx}(f)][U(f)]^h \dots\dots\dots(A.2.4)$$

where, $[U(f)]$ is the eigenvector matrix of the crosspower matrix, $[G_{xx}(f)]$ and $[G'_{xx}(f)]$ is the eigenvalue diagonal matrix of crosspower matrix, $[G_{xx}(f)]$ which becomes the autopower matrix of virtual references, given by Equation A.2.5

$$[G'_{xx}(f)] = \begin{bmatrix} X'_1 X'^h_1 & 0 & \dots & 0 \\ 0 & X'_2 X'^h_2 & \dots & 0 \\ \dots & \dots & \dots & \dots \\ 0 & 0 & \dots & X'_n X'^h_n \end{bmatrix} \dots\dots\dots(A.2.5)$$

The crosspower matrix given in Equation A.2.2 and A.2.4 can also be written as follows:

$$[G_{xx}(f)] = X \cdot X^h = U \cdot (X' \cdot X'^h) \cdot U^h = (U \cdot X') \cdot (U \cdot X')^h \dots\dots\dots(A.2.6)$$

Therefore,

$$X = U \cdot X' \dots\dots\dots(A.2.7)$$

and

$$X' = U^h \cdot X \dots\dots\dots(A.2.8)$$

where, U is the matrix of eigen vectors and X' is the principal components matrix

After predicting the PCs from Equation A.2.8, this orthogonal transformation is applied to the response signals to get virtual crosspowers between the PCs and the response signals, given by Equation A.2.9.

$$[G_{yx'}(f)] = Y \cdot X'^h = Y \cdot (U^h \cdot X)^h = Y \cdot X^h \cdot U = G_{yx} \cdot U \dots\dots\dots(A.2.9)$$

where, $[G_{yx'}(f)]$ is the virtual crosspower matrix, Y is response signal spectra and G_{yx} is the crosspowers between response and reference signals.

Then the referenced virtual spectra (Y'), is obtained from the virtually referenced crosspower matrix $[G_{yx'}(f)]$ and the virtual autopower matrix of PCs $[G'_{xx}(f)]$ as given in Equation A.2.10.

$$Y'_{i,j} = \frac{G_{Y_i X'_j}}{\sqrt{G_{X'_j X'_j}}} \dots\dots\dots (A.2.10)$$

The contribution of a principal component to a response or reference signal is represented by the virtual coherence and given by Equation A.2.11.

$$\gamma'_{ij,2} = \frac{|G_{Y_i X'_j}|^2}{G_{Y_i Y_i} G_{X'_j X'_j}} \dots\dots\dots (A.2.11)$$

where, $G_{Y_i Y_i}$ is the crosspower matrix of physical response signals which are also partially correlated signals

Referenced virtual spectra obtained from Equation A.2.10 are used in the operational load estimation.

REFERENCES

1. **Abaqus**, (2011) Documentation-6.12, Abaqus analysis user's manual.
2. Abaqus Technology Brief, Full Vehicle NVH Analysis with Rolling Tires, TB-11-RT-1, Revised: March (2011).
3. Abaqus Technology Brief, An Integrated Approach for Transient Rolling of Tires, TB-03-TRT-1, Revised: January (2011).
4. **Allemang, Randall J.** (1999) Vibrations: Experimental Modal Analysis, UC-SDRL-CN-20-263-663/664.
5. **Anne and Russ Evans** (2006) The Composition of a Tyre: Typical Components, Project code: TYR0009-02, The Waste & Resources Action Programme, Banbury, Oxon OX16 0AH.
6. **Bangyi, D. Martin, G. Mark, V, Paul, B and Peter, K** (1995) Road noise modelling using Statistical Energy Analysis method, SAE paper No. 951327, pp.761-766.
7. **Bolton, J. S. and Kim, Y. J.** (2000) Wave number domain representation of tire vibration, *In proceedings of the Internoise 2000 conference*, Nice, France.
8. **Bolton, J. S. and Kim, Y. J.** (2003) Visualization of the tire vibration and sound radiation and modeling of tire vibration with an emphasis on wave propagation. Technical report, The Institute for safe, Quiet and Durable Highways.
9. **Brinkmeier, M. and Nackenhorst, U.** (2008) An approach for large-scale gyroscopic eigen value problems with application to high-frequency response of rolling tires. *Computational Mechanics*, 41(4) 503-515.
10. **Brinkmeier, M. Nackenhorst, U. Petersen, S and VonEstorff, O.** (2008) A finite element approach for the simulation of tire rolling noise, *Journal of Sound and Vibration*, 309,20-39.
11. **Byung, K. Y. and Kyoung, J. C.** (2005) Road Noise Reduction Using a Source Decomposition and Noise Path Analysis. SAE paper : 2005-01-2502.
12. **Burroughs, C.B. and Dugan, E. L.** (2003) Measurement and analysis of blank tire tread vibration and radiated noise. *The Institute for Safe, Quiet and Durable Highways*, Report no. SQDH 2003-3.
13. **Charles, G. Andrea, M. Jared, C. Kimberly, C. Francois, G. and Katleen, M.** (2005) A Hybrid Full Vehicle Model for Structure Borne Road Noise Prediction, SAE paper: 2005-01-2467.

14. **Clark Ed. S. M.** (2006) *Mechanics of Pneumatic Tires*, DOT HS 810 561, National Highway Traffic Safety Administration, Washington, D.C, February.
15. **Constant, M. Leyssens, J. Penne, F. and Freymann, R.** (2001) Tire and car contribution and interaction to low frequency interior noise, SAE 2001 Noise and vibration Conference, Traverse City, MI., SAE paper 2001-01-1528.
16. **D. de Klerk and Rixen, D. J.** (2010) Component transfer path analysis method with compensation for test bench dynamics, *Mechanical Systems and Signal Processing*, 24,1693-1710.
17. **Dorfi, H. R. Wheeler, R. L. and Keum, B. B.** (2005) Vibration modes of radial tires: Application to non-rolling and rolling events, In proceedings of the 2005 SAE Noise and Vibration Conference, Traverse City, USA, Paper 2005-01-2526.
18. **Filip DE Coninck.** (2007) Multi-axial road reproductions for non-linear road noise models, PhD Thesis, Katholieke Universiteit Leuven, Belgium.
19. **Gehring, M. A.** (2005) Application of experimental transfer path analysis and hybrid FRF based sub-structuring model to SUV axle noise, SAE paper 2005-01-1833.
20. **Gent A. N. and Walter J. D.** (2005) *The Pneumatic Tire*. National Highway Traffic Safety Administration, U. S. Department of Transportation, Washington DC 20590.
21. **Graf, R. A. G. Kuo, C. Y. and Dowling, A. P.** (1999) Horn Amplification at A Tyre/road Interface - Part I Experiment and computation. Proceedings of Inter Noise, Fort Lauderdale, Florida, USA.
22. **Guillaume, P. Verboven, P. VanLanduit, S. Van derAuweraer, H. and Peeteers, B.** (2013) A poly-reference implementation of the least squares complex frequency domain estimator, Proceedings of the IMAC 21, the International Modal Analysis Conference, Kissimmee (FL), USA.
23. **Hartleip, L.G. and Roggenkamp, T.J.** (2005) Case study - experimental determination of airborne and structure-borne road noise spectral content on passenger vehicles. *In proceedings of the 2005 SAE Noise and Vibration Conference*, Traverse City, USA, paper 2005-01-2522.
24. **Hendricx, W. and Vandenbroeck, D.** (1993) Suspension Analysis in View of Road Noise Optimization. SAE paper 931343.
25. **Hamet, J.H. Klein, P. and Lelong, J.** (2005) Applying tyre/road noise modelling for evaluation purposes, In Presentations from SILVIA Final Seminar, Brussels, Belgium.
26. **Ichiro Kido and Sagiri Ueyama,** (2005) Coupled Vibration Analysis of Tire and Wheel for Road Noise Improvement. SAE paper 2005-01-2525.
27. **Jin Chang, Wang Wan Ying and Jin Xiao Xiong,** (2010) Study of tire noise transfer path identification, ICSP 2010 Proceedings IEEE.

28. **Johan, G. and Luca, M.** (2009) Reciprocal Transfer Functions Synthesis Method for Rolling Noise and NVH Floor Treatment Investigations. SAE paper: 2009-01-2088.
29. **Juha Plunt,** (2005) Finding and Fixing Vehicle NVH Problems with Transfer Path Analysis, *Sound and Vibration*, Nov. 2005.
30. **Kiho Yum, Kwanwoo Hong and Stuart Bolton, J.** (2007) Influence of Tire Size and Shape on Sound Radiation from a Tire in the Mid-Frequency Region, SAE paper 2007-01-2251.
31. **Kim, K. S. and Kang, Y. J.** (2011) Local stiffness control for reducing vehicle interior noise by using FRF based synthesis method, *Journal of Mechanical Science and Technology*, 25(1) (2011) 81-88.
32. **Kindt, P. De Coninck, F Sas, P. and Desmet, W.** (2007) Analysis of tire/road noise caused by road impact excitations, *Noise and Vibration Conference and Exhibition* St. Charles, Illinois, SAE paper 2007-01-2248.
33. **Kindt, P. Berckmans, D. De Coninck, F Sas, P. and Desmet, W.** (2009) Experimental Analysis of the Structure-Borne Tyre/Road Noise due to Road Discontinuities, *Mechanical Systems and Signal Processing*, 23,2557-2574.
34. **Kindt, P. Sas, P. and Desmet, W.** (2009) Measurement and analysis of rolling tire vibrations, *Optics and Lasers in Engineering*, 47, 443-453.
35. **Kropp, W.** (1989) Structure-borne sound on a smooth tyre. *Applied Acoustics*, 26:181-192.
36. **Larrson, K. and Kropp, W.** (2002) A high-frequency three-dimensional tyre model based on two coupled elastic layers. *Journal of sound and Vibration*, 253(4) 889- 908.
37. **Lauwagie, T. Van Assche, R. Van derStraeten, J. and Heylen, W.** (2006) A Comparison of Experimental, Operational, and Combined Experimental-Operational Parameter Estimation Techniques, *Proceedings of the International Noise and Vibration Conference*, ISMA 2006, Leuven, Belgium, 2997-3006.
38. **Lee, D. H. and Hwang, W. S.** (2007) An identification method for joint structural parameters using an FRF based sub-structuring method and an optimization technique, *Journal of Mechanical Science and Technology*, 21(2007)2011-2022.
39. **Liu, W. and Ewins, D. J.** (2002) Substructure synthesis via elastic media, *Journal of Sound and Vibration*, 257(2)(2002) 361-379.
40. LMS International –Application Note Transfer path analysis – the qualification and quantification of vibro-acoustic transfer paths, LMS International, 1998.
41. LMS Test. Lab, Operational Modal Analysis Theory Documentation, LMS International (2009).

42. LMS Test, Lab, Transfer Path Analysis Theory Documentation, LMS International (2009).
43. **Luca, M. Philippe, G. and Jan, H** (2007) Reciprocal Power train Structure borne Transfer Functions Synthesis for Vehicle Benchmarking, SAE paper:2007-01-2354.
44. **Marten V. van der Seijs, Dennis de Klerk and Daniel J. Rixen.** (2016) General framework for transfer path analysis: History, theory and classification of techniques, *Mechanical Systems and Signal Processing*, 68-69, 217-244.
45. **Mark, J. E. Erman, B and Roland, C. M.** (2013) The Science and Technology of Rubber, Fourth Edition, Elsevier Academic Press 2013.
46. **Mehdi Batel,** (2002) Operational Modal Analysis - Another way of doing modal testing, *Sound and Vibration*, 22-27.
47. **Nakajima, Y. Inouc, Y. and Ogawa, H.** (1993) Application of the Boundary Element Method and modal Analysis to Tire Acoustics Problems. *Tire Science and Technology*, TSTCA, Vol. 21 (2), 66-90.
48. **Nackenhorst, U.**(1993) On the finite element analysis of steady state rolling contact, *Transactions on Engineering Sciences*, Vol. 1, , WIT Press, www.witpress.com, ISSN 1743-3533.
49. **Nachenhorst, U.** (2004) The ALE formulation of bodies in rolling contact - theoretical foundations and finite element approach, *Computer Methods in Applied Mechanics and Engineering*. 193, 4299 - 4322.
50. **Nackenhorst, U. and Brinkmeier, M.**(2008) On the dynamics of rotating and rolling structures, *Archive of Applied Mechanics*, 78 (6)477-488.
51. **Nicolas, M. and Jean, L. W.** (2007) FEA Design of a Vibration Barrier to Reduce Structure Borne Noise, SAE paper: 2007-01-2164.
52. **Peeteers, B. Guillaume, P. Van derAuweraer, H. Cauberghe, H. Verboven, P. and Leuridan, J.** (2004) Automotive and aerospace applications of LMS PolyMAX modal parameter estimation method, Proceedings of the IMAC 22, the International Modal Analysis Conference, Dearborn (MI), USA.
53. **Peter Kindt,** (2009) Structure-Borne Tyre/Road Noise due to Road Surface Discontinuities, PhD Thesis, Katholieke Universiteit Leuven, Belgium.
54. **Peter Willem Anton Zegelaar,** (1998) The dynamic response of tyres to brake torque variations and road unevennesses, PhD Thesis, Delft University of Technology, The Netherlands.
55. **Pinnington, R. J. and Briscoe, A. R.** (2002) A wave model for a pneumatic tyre belt. *Journal of Sound and Vibration*, 253(5) 941-959.

56. **Pottinger, M. G.** (1992) The three-dimensional contact patch stress field of solid and pneumatic tires, *Tire Science and Technology*, TSTCA,20 (1) 3-32.
57. **Rao, K.V.N. Kumar, R. K. and Bohara, P. C.** (2003) Transient Finite Element Analysis of Tire Dynamic Behaviour, *Tire Science and Technology*, TSTCA, Vol.31, No.2, 104-127.
58. **Ren, Y. and Beard, C. F.** (2001) On substructure synthesis with FRF data, *Journal of Sound and Vibration*, 185(5) (2001)845-866.
59. **Renata, G. S. and Paulo, J. P. G** (2003) Investigation of Sub-System Contribution to a Pickup Truck Boom Noise using a Hybrid Method Based on Noise Path Analysis to Simulate Interior Noise. SAE paper: 2003-01-3677, E series.
60. **Riegel. M and Wiedemann. J** (2008) A test stand method to determine tyre-road noise in the interior of passenger vehicles, *In the proceedings of the 5th International Styrian Noise, Vibration & Harshness Congress*, Graz, Austria, pages 135-142.
61. **Sakata, T., Morimura, H., and Ide, H.** (1990) Effects of Tire Cavity Resonance on Vehicle Road Noise, *Tire Science and Technology*, TSTCA, Vol.18,No.2,pp.68-79.
62. **Sandberg, U and Ejsmont, J.A.** (2002) *Tyre/road noise reference book*, Informex, Kisa, Sweden, (2002). ISBN 91-631-2610-9.
63. **Scott, D. O. and Robert, J. B.** (1993) Automotive suspension models using component mobility methodology, SAE paper: 931298,pp.299-310.
64. **Tsai, J. S. and Chou, Y. F.** (1988) The identification of dynamic characteristics of a single bolt joint, *Journal of Sound and Vibration*, 125(3) (1988) 487-502.
65. **Wong, J. Y.** (2001) *Theory of Ground Vehicles (Third edition)*, John Wiley & Sons, Inc., 2001.
66. **Yam, L. H. Guan, D. H. and Zhang, A. Q.** (2000) Three dimensional mode shapes of a tire using experimental modal analysis, *Experimental Mechanics*, Vol.40(2000) 369-375.
67. **Yeoh, O.H.** (1993) Some Forms of the Strain Energy Function for rubber, *Rubber Chemistry and Technology*, 66,754-771.

LIST OF PUBLICATIONS BASED ON THE RESEARCH WORK

I. REFEREED JOURNALS

- 1. Sakthivel, P., Narasimha Rao, K.V., and Krishna Kumar, R.,** Determination of Rolling Tyre Modal Parameters using Finite Element Techniques and Operational Modal Analysis, *Mechanical Systems and Signal Processing*, 64-65(2015)385-402.

- 2. P. Sakthivel and R. Krishna Kumar,** '*Determination of road input excitation and structure borne vehicle interior noise using Transfer Path Analysis*', The Journal of Automobile Engineering, Part D of the Proceedings of the Institution of Mechanical Engineers (to be communicated)

II. CONFERENCES

- 1. Sakthivel, P., Narasimha Rao, K.V., and Krishna Kumar, R.,** Operational Modal Analysis of tyre road interaction using Abaqus Explicit and Operational Modal Analysis. *In proceedings of the ISMA 2012 International Conference on Noise and Vibration Engineering*, Leuven, Belgium. September 17-19, (2012) 1603-1616.

- 2. Sakthivel, P. and Krishna Kumar, R.,** Synthesis of Structure Borne Vehicle Interior Noise Due to Tire/Road Interaction, *Proceedings of ASME 2015 International Design Engineering Technical Conferences and Computers & Information in Engineering Conference*, Boston, Massachusetts, August 2-5, 2015

CURRICULUM VITAE

1. Name : **P. Sakthivel**

2. Date of Birth : 4th June 1976

3. Educational Qualifications

1997 Bachelor of Engineering

Institution : Alagappa Chettiar College of Engineering and
Technology, Madurai Kamaraj University,
Karaikudi, Tamil Nadu, India

Specialization : Mechanical Engineering

2004 Master of Technology

Institution : Indian Institute of Technology Bombay
Powai, Mumbai, Maharashtra, India

Doctor of Philosophy

Institution : Indian Institute of Technology Madras
Chennai, Tamil Nadu, India

Registration Date : 23-07-2010

DOCTORAL COMMITTEE

- Chairperson : **Dr. Nilesh Jayantilal Vasa**
Professor & Head
Department of Engineering Design
- Guide : **Dr. R. Krishna Kumar**
Professor
Department of Engineering Design
- Members : **Dr. Meher Prasad A**
Professor & Head
Department of Civil Engineering
- Dr. Sujatha C**
Professor
Department of Mechanical Engineering
- Dr. Shankar Ram C S**
Associate Professor
Department of Engineering Design
- Dr. Sankara J Subramanian**
Associate Professor
Department of Engineering Design